# UC Irvine

## UC Irvine Electronic Theses and Dissertations

### Title

Investigating the Impacts of Climate, Hydrology, and Asian Monsoon Intensity on a 13 kyr Speleothem Record from Laos

### Permalink

https://escholarship.org/uc/item/1cp3q8j9

### Author

Yang, Hongying

### Publication Date

2016

Peer reviewed|Thesis/dissertation

eScholarship.org Powered by the California Digital Library
University of California

UNIVERSITY OF CALIFORNIA,
IRVINE

# Investigating the Impacts of Climate, Hydrology, and Asian Monsoon Intensity on a 13 kyr Speleothem Record from Laos

DISSERTATION

submitted in partial satisfaction of the requirements
for the degree of

DOCTOR OF PHILOSOPHY

in Earth System Science

by

Hongying Yang

Dissertation Committee:
Associate Professor Kathleen Johnson, Chair
Professor Jin-Yi Yu
Researcher John Southon

2016

All materials © 2016 Hongying Yang

# TABLE OF CONTENTS

# LIST OF FIGURES



**Page**

# LIST OF TABLES

**Page**

# ACKNOWLEDGMENTS

Chapter3:, is being prepared for publication. Yang, Hongying; Johnson, Kathleen R.; Griffiths, Michael L.; LeGrande, Allegra N.; Ersek, Vasile; Henderson, Gideon M.; The dissertation author is the primary investigator and author of this paper.

Chapter 4:, in part, is being prepared for publication. Yang, Hongying; Johnson, Kathleen R.; Griffiths, Michael L., The dissertation author is the primary investigator and author of this paper.

Chapter 5:, is an article submitted to Journal of Geophysical Research, Atmosphere, 2016. Yang, Hongying; Johnson, Kathleen R.; Griffiths, Michael L.; Yoshimura, Kei, American Geophysical Union, 2016. The dissertation author is the primary investigator and author of this paper.

This thesis would not have been possible without the support of many great people that surrounded me. First of all, I gratefully thank my advisor, Prof. Kathleen Johnson for accepting me as one of her graduate students and financially supporting me over the past few years. I thank her for believing in me and giving me the chance to pursue a PhD. The past five years are the most influential time period of my life. She triggered my passion and opened my eyes to this scientific world. I thank her for her patient on my awkward english especially during my first year. I thank her for teaching me how to reconstruct climate from speleothem with such a huge passion. She is an extremely supportive advisor. She kindly supported me for traveling, field work, conference, summer school and so on. She gave me the chance to learn and to meet great people. She generously offered her time, advice, and endless patient for my research. Every single word of this thesis comes with her support. I really enjoyed working with her and I appreciated the way she supported me. I am certain that I will miss her.

I thank my committee members, Prof. Jin-Yi Yu and Dr. John Southon for their advice, encouragement, suggestions on interpretation of my results and further research directions. I thank Prof. Jin-Yi Yu for his endless patient on my climatology questions and useful

discussions regarding interpretation of some of my results. I also appreciate John's advice on my thesis and I have no doubt that these advice improved this thesis.

I would like to thank my research group. I am extremely luck to work with these kind and talented people. I would like to thank Michael Griffiths. He gave me a lot hands-on help when he was a postdoc in our research group. He guided me through this whole project. I thank him for many hours he has put in discussing my results and proofreading my paper. I thank Julie Ferguson for taking an interest in my research and providing countless suggestions on my presentations. I thank Dachun Zhang for taking care of Kiel Device and helping me a lot on isotope measurements. I also would like to thank Staryl Mccabe-Glynn, Alexandra Noronha, Jessica Wang, and Christopher wood. I've had the pleasure of getting to know them and work with them. I also thank several undergraduate students I have worked with, Natasha Sekhon, Christopher Glynn, Jane Liu and Danielle Sison for their help in Johnson's lab.

I thanks my many collaborators. I thank Gideon Henderson, Vasile Ersek, Alex Thomas and Andrew Mason for help with U-Th dating at Oxford University, England. I thank Silvia Frisia for her help on thin sections and suggestions on my research direction. I thank Andrea Borsato for taking care us in Tham Mai cave during 2013 field trip. I thank Sengphone Keophanhya, Norseng Sayvongdouane, and Khamsouk Souksome for their help during 2013 Laos field trip. I thank Benjamin Cook for his hands-on teaching on modeling and program technics. I thank Kei Yoshimura and Allegra Legrand for their technique and knowledge supports on my isotope model data studies.

I would like to thank all the faculty members who have taught me during my first year. I thank my first year class graduate students. They walked me through the most painful and memorable year. I thank Morgan Sibley not only for her wonderful work as ESS student affairs manager, but also for her numerous help on my oral english. She helped practice my oral english during my second year until I pass the TOEP oral english test.

I would like to thank my parents for always supporting me in my decision. I could not reached this far without their support. I thank my friends for their encouragement and mentally support.

Finally, a big "Thank you" to my significant other Qiang Xu. I am lucky to meet him and have his encouragements on finishing this thesis. He also spent countless time and patiently helped me with several graphs. I am looking forward to heading out our next life chapter and adventure.

# CURRICULUM VITAE

## Hongying Yang

### EDUCATION

**Doctor of Philosophy in Earth System Science** **2016**

University of California Irvine *Irvine, CA*

**Master of Science in Statistics** **2015**

University of California Irvine *Irvine, CA*

**Master of Science in Earth System Science** **2012**

University of California Irvine *Irvine, CA*

**Bachelor of Science in Geographical Sciences** **2010**

Southwest University *Chongqing, China*

**Bachelor of Science in Applied Psychology(Minor)** **2010**

Southwest University *Chongqing, China*

### RESEARCH EXPERIENCE

**Research Assistant** **2010–2015**

**Project: Investigating the impacts of Climate, Hydrology,and**

**Asian Monsoon Intensity on a 13 kyr Speleothem Record from Laos**

University of California, Irvine *Irvine, CA*

### TEACHING EXPERIENCE

**Teaching Assistant** **2011–2014**

**Six quarters experiences of TA.**

**Geology, The atmosphere, Intro. to earth science, Oceanography**

University of California, Irvine *Irvine, CA*

**Teaching Assistant** **2012–2014**

**AISESS(American Indian Summer Earth System Science) program**

University of California, Irvine *Irvine, CA*

## SUMMER SCHOOL

**S4 (Summer School on Speleothem Science)** **2013**

University of Heidelberg *Heidelberg, Germany*

## CONFERENCE EXPERIENCE

**Holocene Shifts in Southeast Asian Hydrology Recorded in Speleothems from Laos** **Dec 2012**

American Geographical Union

**Climatic controls of Holocene shift of Indo-pacific precipitation: speleothems from Laos and isoGCM GISS simulations** **June 2014**

Goldschmidt

**Tropical Indo-pacific modern and paleo-hydrology : comparison of paleoclimate modeling and speleothems data** **AUG 2014**

Karst Record International Conference

**Hydrologic variability during the Younger Dryas and Holocene based on speleothems from Laos** **AUG 2014**

Karst Record International Conference

**Inter-annual controls on oxygen isotopes of precipitation in the Asian Monsoon Region** **DEC 2015**

American Geographical Union

## REFEREED JOURNAL PUBLICATIONS

**Inter-annual controls on oxygen isotopes of precipitation in the Asian Monsoon region** **2016**

Journal of Geophysical Research

# ABSTRACT OF THE DISSERTATION

Investigating the Impacts of Climate, Hydrology, and Asian Monsoon Intensity on a 13 kyr Speleothem Record from Laos

By

Hongying Yang

Doctor of Philosophy in Earth System Science

University of California, Irvine, 2016

Associate Professor Kathleen Johnson, Chair

I present a high-resolution record of Southeast Asian Monsoon (SEAM) evolution compiled from $\delta^{18}$O measurements conducted on five U-Th dated speleothems from Tham Mai Cave in northern Laos (20.75N, 102.65E), a key site at the interface between the Indian and East Asian monsoon systems. The speleothem oxygen isotope records are tied to robust uranium-series dates and indicate the records span from 0.79 to 13 kyr BP with sub-decadal resolution. During the Holocene, the Tham Mai speleothem $\delta^{18}$O records are characterized by lower values during the early to mid-Holocene with increasing values towards the late Holocene. This is similar to trends seen throughout the Asian monsoon region, reflecting the strong insolation control on monsoon strength and ITCZ position. The Younger Dryas is characterized by an abrupt $\delta^{18}$O increase and is synchronous with the even observed in Chinese speleothem records and Greenland ice cores within age uncertainties. This suggests that the SEAM weakened in sync with high-latitude abrupt cooling events.

Four speleothems from Tham Mai cave grew contemporaneously from 4,300 years BP to 9,000 years BP. These four samples show a similar $\delta^{18}$O pattern, despite a 1.2‰ between

sample $\delta^{18}$O variability is observed. A lumped parameter forward model method (KarstFor model) is used to assess to which extent this 1.2 ‰ discrepancy can be attributed to hydrological variability. Results suggested that this 1.2 ‰ discrepancy can be generated due to hydrological variability within one cave.

To better interpret interannual $\delta^{18}$O variability in high-resolution oxygen isotope records in the Asian Monsoon region, I utilize existing simulations from a spectrally nudged isotope-enabled general circulation model (IsoGSM) to investigate the climatic controls on $\delta^{18}O_p$ at four cave locations along the Asian monsoon region. Results show that $\delta^{18}O_p$ at the four cave sites reflects large-scale ocean-atmosphere processes, instead of local precipitation amount. Spatial correlation with vertical wind shear indicates that $\delta^{18}O_p$ at all sites is significantly related to monsoon strength and Walker circulation. The spatial correlations with SST and precipitation, suggest that the ENSO likely does play a role and that central Pacific type El Niño events influence precipitation $\delta^{18}$O in Oman and northern Laos, in particular.

# Chapter 1

# Introduction

## 1.1 Background

The tropics play an important role in the study of global climate change because they transport energy and moisture from low latitude to high latitudes through the global atmospheric general circulation. Rainfall in the tropical Indian and Pacific Ocean regions is controlled by complex atmospheric mechanisms such as the migration of the Intertropical Convergence Zone (ITCZ), the Asian-Australian monsoon system, the El Niño Southern Oscillation (ENSO), and the Indian Ocean Dipole (IOD). These systems are closely coupled with one another and are known to be sensitive to external forcing, such as seasonal and orbital scale variations in solar insolation, and to internal forcing, such as changes in Atlantic Meridional Overturning Circulation (AMOC), that occur during abrupt climate changes (*Chiang*, 2009). Convection over the Indo-Pacific warm pool (IPWP) region provides the largest source of heat and moisture to the global climate system. The seasonal and orbital change of the ITCZ migration influences the onset, duration, strength and termination of the rainfall season in the tropical and subtropical areas. ENSO variability, which

is connected to the Pacific Walker Circulation, also profoundly influences tropical Pacific hydrology. Furthermore, the Asian monsoon (AM) is an important climate system that affects more than half of the world's population and has been shown to be influenced by ITCZ and ENSO. The AM region has been further divided into several sub-domains, which display more coherent precipitation variability, including the East Asian monsoon (EAM), the Indian Summer monsoon (ISM; or the India-China monsoon;) and the Southeast Asian monsoon (SEAM) (*Conroy and Overpeck*, 2011a; *Dayem et al.*, 2010). Almost two-thirds of the global population lives in the AM domain (*P. D. and R. A*, 2008). Any small changes in these systems can impact global climate, and the reorganization of these systems may play a major role in abrupt climate transitions. Even small variations in the strength and timing of seasonal rainfall can have significant impacts on the billions of people living within tropical and the AM domain.

An ensemble of of climate models has agreed that future temperature will increase with increasing greenhouse gases in the atmosphere (IPCC,2013). However, model projections on regional precipitation still have large uncertainties, especially on precipitation over tropical and AM regions (IPCC, 2013)(Fig.1.1). CMIP3 and CMIP5 models do not agree well regarding the sign of AM region precipitation prejection at the end of 21 century. Due to the scarce knowledge of the dynamical processes that control temporal and spatial monsoon rainfall variability, it is hard to model and predict precipitation patterns in these regions (*Cook et al.*, 2010). The atmosphere-ocean coupled general circulation models have failed to correctly interpret the climatology in the tropical Pacific. For instance, numerical climate models give variable results when predicting future ENSO change in a warming world (*Merryfield and Boer*, 2005; *Guilyardi*, 2006; *Hwang et al.*, 2011; *Yancheva et al.*, 2007; *Paeth et al.*, 2008). In addition, the spatial heterogeneity of precipitation over AM region hampers predictive efforts since rainfall in different AM sub-domains does not covary or respond co-herently to changes in forcing factors (*Zhou et al.*, 2009).

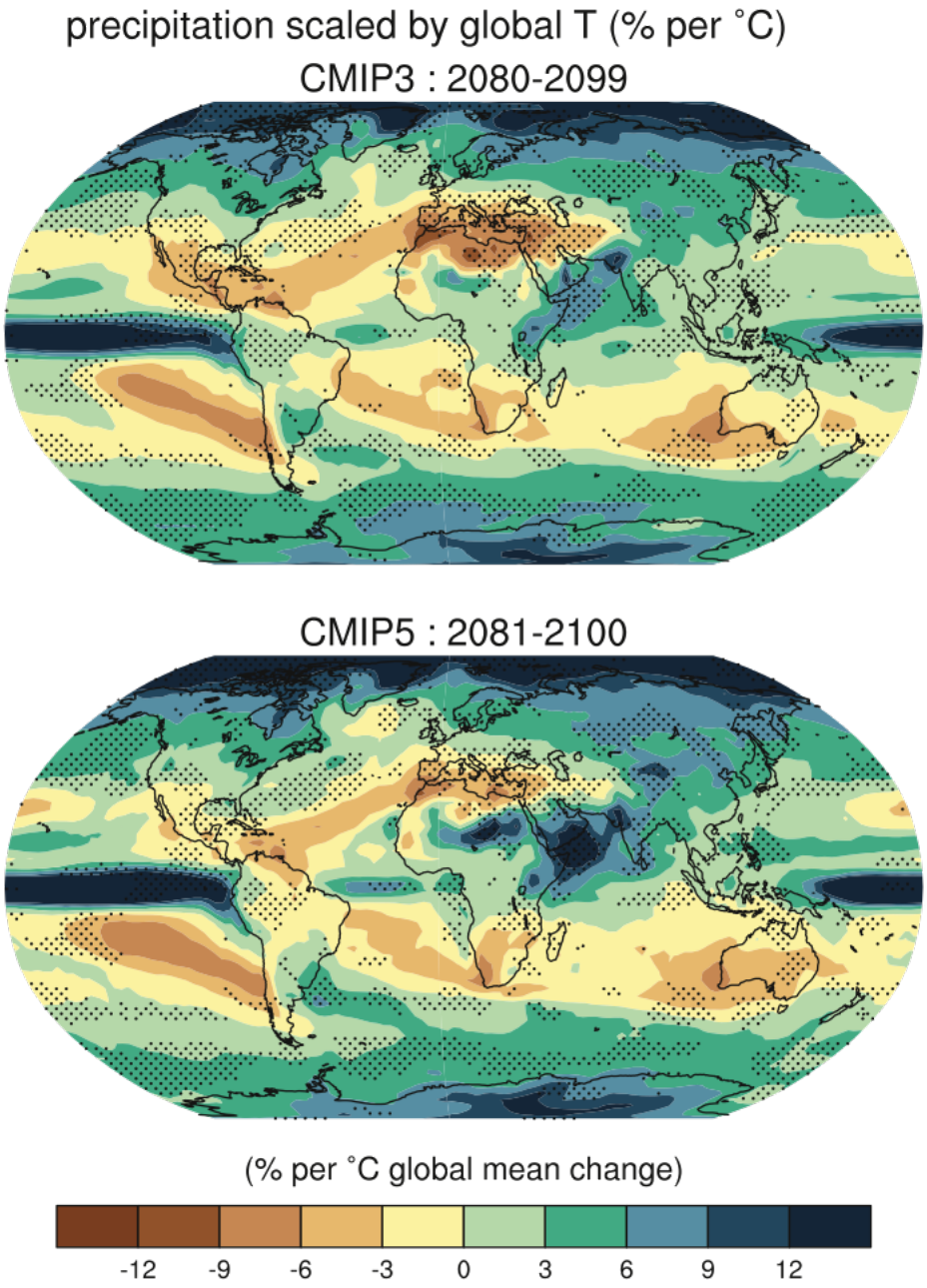


Figure 1.1: CMIP3(a) and CMIP5(b) models average prediction on present precipitation change, scaled by the corresponding global average temperature changes (adapted from IPCC Fifth Assessment Report, 2013). Stippled indicates 90% model agreement on sign of change and changes is more than two standard deviations away from the model's internal variability.

How will the tropics and AM respond in a warming world? Will the ongoing global warming cause more extreme summer rainfall? Can we predict future tropical monsoon region

precipitation with a higher confidence in the future? To answer these questions and to help refine climates models, we need more knowledge about the factors that influence tropical climate variations and coupled climate modes over a range of time scales. Successful long-term climate prediction depends on a robust understanding of the mechanisms that control how these climate systems work together, the relative importance of these climate systems, the controlling factors, and the natural range of their variability. Gaining a clearer understanding of how climate in these densely populated regions has varied over inter-annual to millennial timescales is critical to improve monsoon predictions and to implement timely adaptation measures, especially given the uncertainties still evident in climate model projections under enhanced greenhouse-gas forcing (*Solomon et al.*, 2007). In order to achieve a better understanding of ENSO, ITCZ and monsoon dynamics, specific mechanisms that control their intensities and geographical positions, and their interaction with global climate, we need to examine how they have changed through time. Due to the limited instrumental records, paleoclimate records are necessary to solve this problem.

### 1.1.1 Paleoclimate records in tropical and Asian monsoon domain

The development of paleoclimate reconstructions broadens our knowledge of natural climate variability on various timescales and underpins our understanding of the response of the climate system to forcing mechanisms. A number of researchers have reconstructed the orbital and millennial scale rainfall variability in tropical and the AM region using different types of proxies, e.g. sediments, tree-ring records, ice core, and speleothems (Fig.1.2) (*Conroy and Overpeck*, 2011a).

Despite significant advances in our understanding of tropical and monsoon climate variability on orbital to millenial timescales (*Cruz et al.*, 2005; *Wang et al.*, 2008), we still know very little about the range and mechanisms of variability in the Southeast Asian Monsoon (SEAM)

region (red box in Fig 1.2). This highly populated region sits at the interface of the East Asian and Indian monsoon systems and exhibits natural hydrologic variability related to changing monsoon strength, ENSO, and the IOD (*Conroy and Overpeck*, 2011a; *Buckley et al.*, 2010, 2007). High-resolution and continuous paleoclimate records of the Late Pleistocene and Holocene are desperately needed to determine the natural mechanisms of climate variability in the SEAM region and improve predictions of future hydrologic change.

Previous studies of paleoclimate in tropical regions are primarily limited to coral (*Gagan et al.*, 2004; *McGregor and Gagan*, 2004; *Abram et al.*, 2007), lake (*Magee et al.*, 2004) and deep-sea sediment records (*Stott et al.*, 2007), tree rings(*Li et al.*, 2011), and pollen (*van der Kaars*, 2001; *Hope*, 2001), which provide limited information of paleoclimate change due to their short duration or low resolution. In recent years, stable isotopes ratios ($\delta^{18}$O and $\delta^{13}$C and trace elements of speleothems have been used as important proxies to reconstruct paleoclimate especially paleo-rainfall variability at different time scales (*Burns et al.*, 1998; *Wang et al.*, 2005), but very few stalagmite climate reconstructions have focused on the SEAM region.

In this PhD thesis, speleothems from Tham Mai cave, northern Laos are studied. New decadal resolution speleothem records from Laos for the last 13 kyrs are provided. Speleothems from Tham Mai cave are uniquely situated to fill in the spatial and temporal gaps in the paleo-hydrologic record of continental Southeast Asia. Our high resolution record from Tham Mai cave will fill in the spatial gap of paleoclimate records in the SEAM region and provide insights into the parameters and mechanisms that control variations of rainfall variability over decadal to centennial time scales.

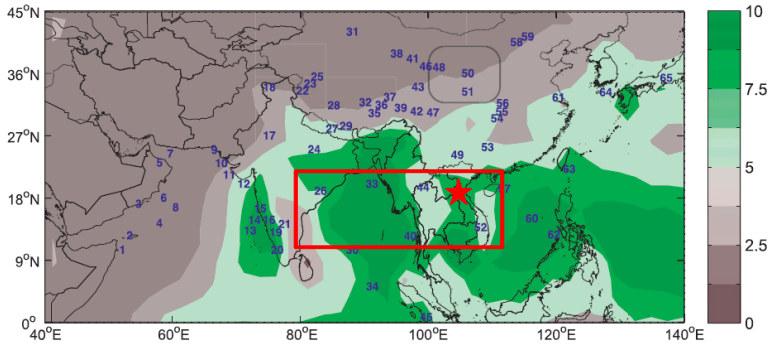


Figure 1.2: Map showing the mean summer (JJAS) CMAP precipitation (mm/day) from 1979 to 2009 and locations of select paleoclimate records of Asian monsoon variability. Note the low density of records in the Indo-China peninsula near the location of our study site, Tham Mai cave (red star), in northern Laos. Modified from *Conroy and Overpeck* (2011a)

## 1.2 Speleothems as high resolution climate archives

### 1.2.1 Formation of speleothems

Spelothems are calcite deposits formed in limestone caves, including stalagmite, stalactites, and flowstones. Surface water (normally from rainfall) reacts with soil $CO_2$ forming carbonic acid ($H_2CO_3$). Carbonic acid dissolves cave limestone bedrock when water moves through fissures. The deposition of speleothems results either from the evaporation of the cave drip water or the degassing of carbon dioxide (Fig.1.3). Speleothems near cave entrances are affected by evaporation due to low relative humidity at these sites. For those speleothems growing in deep caves, due to the high relative humidity and lower $pCO_2$ of cave air relative to the drip water, speleothem precipitation is driven primarily by degassing of $CO_2$ (*Fairchild et al.*, 2006).

The chemical reactions that describe these processes are:

$$CO_2 + H_2O \longrightarrow H_2CO_3$$
$$H_2CO_3{}^{+} + CaCO_3 \longrightarrow Ca^{2+} + 2\,HCO_3{}^{-}$$
$$Ca^{2+} + 2\,HCO_3{}^{-} \longrightarrow CO_2 + CaCO_3 + H_2O$$

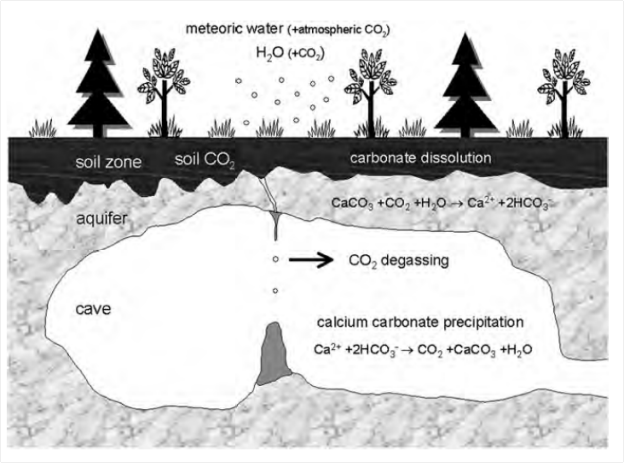


Figure 1.3: Schematic representation of the karst processes and speleothem formation. Adapted from *Frisia, S. and Borsato, A.* (2010)

Through these processes, the oxygen and carbon isotopes in speleothems incorporate the isotopic signal from rainfall, the soil zone, and the epikarst. The variations of oxygen isotopes in speleothem calcite precipitated under isotopic equilibrium conditions refect the oxygen isotope signal of precipitation above the cave and cave temperature. Carbon isotope variation in speleothem calcite is mainly influenced by overlying vegetation change above the cave,degassing, prior calcite precipitation, and kinetic effects (*Baker et al.*, 1997; *Rudzka et al.*, 2011; *Frisia et al.*, 2011). In general, speleothems in deep caves are advantageous over those growing at the entrance, because these tend to precipitate in isotopic equilibrium, with less influence from rapid $CO_2$ degassing, evaporation, and seasonal temperature change.

Speleothem records from tropical areas have proven to be particularly useful archives of rainfall oxygen isotopes ( *Yadava et al.*, 2004), due to the relatively small temperature change

in the tropics. In addition, several other geochemical proxies, including $\delta^{13}$C and trace elements, in speleothem calcite are proven to be good recorders of past climate.

### 1.2.2 The Delta ($\delta$) notation

Stable oxygen and carbon isotope ratios are commonly expressed in $\delta$ notation and in units of ‰ relative to international reference standards.

$\delta_{\text{sample}}=(\text{R}_{sample}/\text{R}_{standard}-1)\cdot 1000$
where $R$ is the isotope ratio: $R=\frac{Rare_Isotope}{Common_Isotope}$
$e.g. R=\frac{^{18}O}{^{16}O}$

Conventional and commonly used standards are Vienna Standard Mean Ocean Water (VSMOW) for water samples and Vienna Pee Dee Belemnite (VPDB) for carbonate samples.

### 1.2.3 Speleothem paleoclimate proxies

Speleothems have the potential to provide high-resolution paleoclimate evolution information needed to refine the climate models from inter-annual to orbital scales. Speleothems provide excellent paleoclimate proxies because they are often continuously growing, well-preserved, contain clear visible growth banding, can be precisely dated by U-Th dating, and contain several types of physical and geochemical proxy data.

Stable oxygen isotope ratios ($\delta^{18}$O) are the most commonly used paleoclimate proxy in speleothems, and these records have advanced our knowledge of continental temperature and precipitation variability over the past 500 kyr BP (*McDermott*, 2004). A number of speleothem $\delta^{18}$O records and other paleo-records have been published recently from the

monsoon regions, such as China, Oman, Yemen, and India (*Wang et al.*, 2001; *Fleitmann et al.*, 2007; *Hu et al.*, 2008; *Zhang et al.*, 2008; *Berkelhammer et al.*, 2013) for the sake of understanding the mechanisms of AM precipitation variation (Fig 1.4). These records display a coherent variability within East Asia monsoon region and also with those in India monsoon region, following the change of summer (JJA) mean insolation at $65^oN$, which is a reflection of precession influences. The strong similarity between orbital to millennial scale speleothem $\delta^{18}$O variability across the broad Asian monsoon region (e.g *Wang et al.*, 2008; **?**; *Liu et al.*, 2014) is suggestive of a large-scale monsoon control rather than a local precipitation amount control, especially given that precipitation in these disparate locations does not vary coherently, at least over the instrumental period (*Dayem et al.*, 2010; *Conroy and Overpeck*, 2011a).

Speleothem records from China show that the AM was weaker during cold phases in the Northern Hemisphere (*Wang et al.*, 2001; *Yuan et al.*, 2004; *Dykoski et al.*, 2005), when the ITCZ tends to move southward (*Hughen et al.*, 1996; *Haug et al.*, 2001; *Wang et al.*, 2005) on an orbital scale. *Wang et al.* (2001), provided a continuous record of monsoon changes from Hulu cave in China, which covers between 11 kyr years BP to 75 kyr BP using 5 overlapping stalagmites from that cave. This study shows that the changes in East Asian monsoon strength are mainly controlled by summer isolation, suggesting that periods of increasing summer isolation result in a higher land-ocean temperature gradient, which enhances the strength of the summer monsoon. Similar to Chinese cave records, speleothem records from southern Oman indicate a decrease in the Indian monsoon rainfall after 8 kyr BP (*Fleitmann et al.*, 2003), consistent with northern hemisphere insolation forcing. *Fleitmann et al.* (2003) suggested the connection between ITCZ and Indian ocean monsoon and hypothesized a mechanism that a more northward ITCZ lifts the height of the tropic ocean inversion, leading to stronger convection and higher monsoon precipitation over southern Oman (*Fleitmann et al.*, 2003). Both Chinese and Oman records suggest that

southern shift of ITCZ is driven by a decrease in summer insolation (*Fleitmann et al.*, 2003; *Dykoski et al.*, 2005; *Wang et al.*, 2005).

Instead of summer insolation, *Berkelhammer et al.* (2010), investigated a record from Dandak Cave in east-central India. This study shows a dominant mode of multidecadal variability of Indian monsoon and interprets this variability as the influence of multidecadal sea surface temperature variability in the Atlantic. *Griffiths et al.* (2009) shows the southward displacement of the austral-summer ITCZ, which was driven by reduced north Atlantic overturning circulation is the most important driver of Australian-Indonesian summer monsoon rainfall in southeast Indonesia during the late glacial. In addition, the timing of maximum AM intensity and several abrupt events (e.g 8.2 and 9.2 event) during the early Holocene period varies slightly over AM region (*Ruddiman*, 2006; *Clemens and Prell*, 2007). There is still a lack of consensus on the controlling factors of AM over different time scales. It is not clear if paleo-records from the different AM domains should be expected to covary with each other as a function of climate forcing over inter-decadal to millennial time scales (*Conroy and Overpeck*, 2011b).

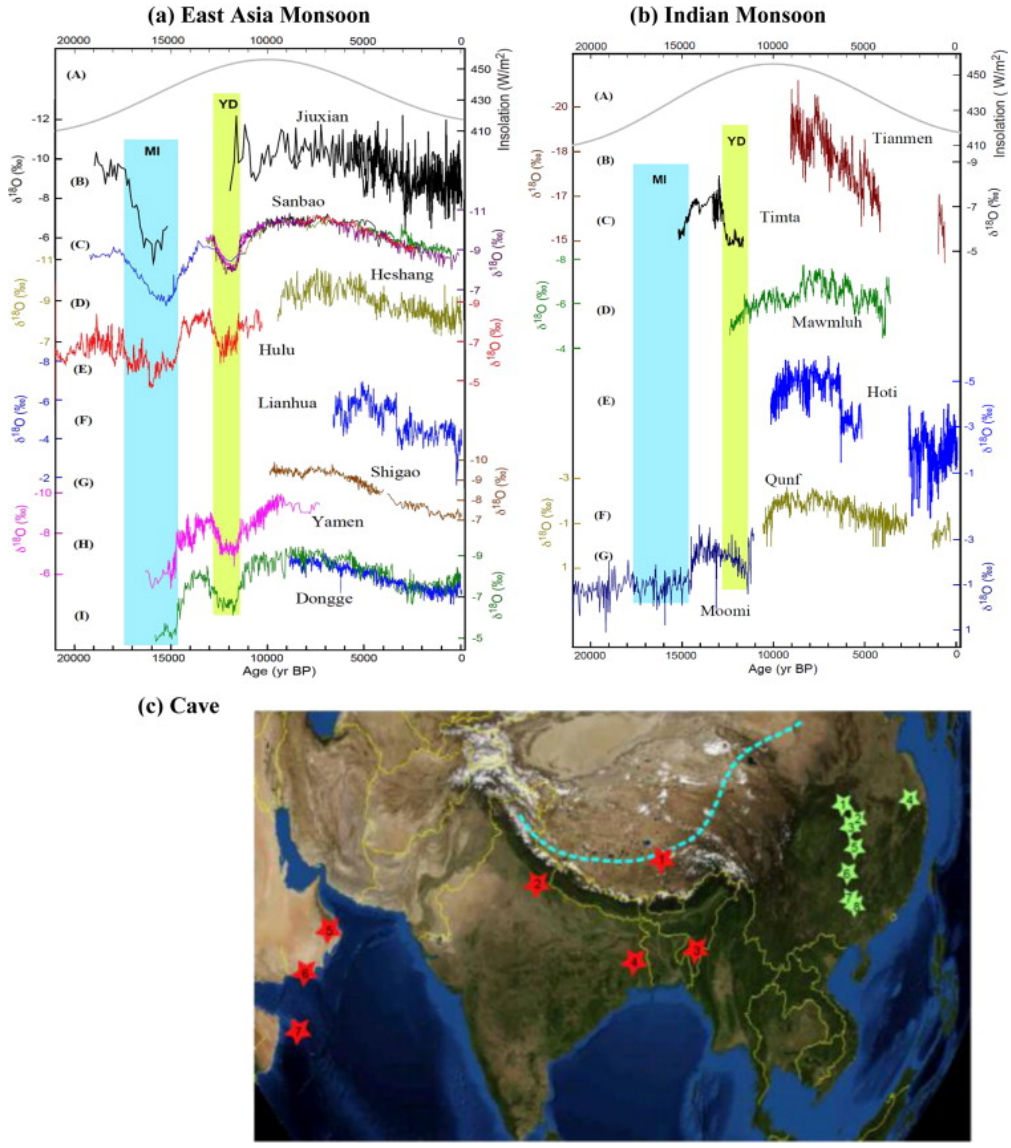


Figure 1.4: Comparison of different speleothem $\delta^{18}$O records from a) the East Asia monsoon region and b) the Indian monsoon region. These speleothem records show a coherent variability within East Asia monsoon region and also with those in India monsoon region over orbital scale. Cave locations are marked in c). Green stars show cave locations in Indian monsoon region. Red stars show cave locations in the East Asia monsoon region. The blue dashed line is the approximate fringe of modern summer Asian monsoon. Adapted from (*Liu et al.*, 2014)

## 1.3 Speleothems as high resolution records

### 1.3.1 Advantages of speleothems as high-resolution climate archives

Speleothems have significant advantages over other paleo-records, such as tree rings, lake sediments, and marine records, since:

1. They can be precisely and absolutely dated using U-series dating techniques (*Edwards et al.*, 1987; *Richards and Dorale*, 2003)
2. They are widely spread over continents
3. They are often continuously and fast-growing over thousands of years, well-preserved, and contain clear visible growth band
4. They contain several types of physical and geochemical proxy data, such as $\delta^{18}$O, $\delta^{13}$C, and trace elements

Although speleothems have a number of advantages in paleoclimate reconstruction, a considerable weakness of speleothems is our limited knowledge of the true sensitivity of measured proxies (e.g. $\delta^{18}$O, $\delta^{13}$C) to climate variables (*Fleitmann et al.*, 2008) and uncertainties in uranium-series dating.

### 1.3.2 Uranium-series dating

Uranium-series (U-series hereinafter) dating is based on the decay of the parent isotope $^{234}U$ to daughter isotope $^{230}Th$. Under the assumption that speleothem calcite contains no initial $Th$, U-series ages are absolute ages and no correction is needed. Under this condition, relative age uncertainties are small and typically vary between 0.5 to 2% of the absolute

age, depending on the uranium concentration (*Fleitmann et al.*, 2008). However, large uncertainties in speleothem U-series ages can be generated due to:

1. For younger speleothems, $Th$ concentration is usually low and close to the detection limit of mass spectrometers. Thus, for young speleothems with low uranium concentration, age uncertainties can range from 5% to 10% of the absolute age.

2. Large age uncertainties are also associated with the presence of so-called "initial" $Th$. At the time of speleothem formation, incorporation of impurities can lead to artificially old U-series ages, due to incorporation of excess $^{230}Th$.

3. Presence of hiatuses and/or non-linear growth rate can introduce significant chronological error into speleothem proxy records. The undetected hiatus and/or changes in growth rate between $U - Th$ dates can introduce significant error in age modeling.

### 1.3.3 Speleothem age modeling

$U - Th$ dating has been used in paleoclimatology to construct age-depth relationships, especially for speleothems. However, due to the expensive cost and time-consuming nature of doing U-series dating, it is generally not possible to date as many samples as we would prefer. An age-depth model based on $U - Th$ dates is therefore needed since the measured climate proxies have a higher resolution than the age points. Hiatuses and changes in growth rate between two consecutive dating points can induce significant chronological errors into the age model. Thus, to construct a better age model, which can relate the sediments depth and its age, becomes important.

Age modelling is a challenge for all climate archives, and a variety of approaches has been used. The most frequently used method is linear point-to-point interpolation between dated sub-sample distances. However, the linear interpolation model is only based on two adjacent

data points, not able to detect hiatus, and usually has no quantification of the age error between two data points. Other models, such as least-squares polynomial fits,and various kinds of splines have also been used. Least-squares polynomial fits have the tendency to display large curving and can creat overshoots (*Scholz et al.*, 2012). Recently, (*Scholz and Hoffmann*, 2011) have presented an algorithm (StalAge) specifically developed for speleothem age modeling. The StalAge age model delivers an easy to use algorithm that allows robust uncertainty estimation throughout the length of the record. StalAge can be applied to problematic datasets that include age inversions, outliers, hiatuses and large changes in growth rate (*Scholz and Hoffmann*, 2011). StalAge is also the method we used to contruct our age models in this dissertation.

### 1.3.4 Controls on speleothem $\delta^{18}$O

The interpretation of $\delta^{18}$O in speleothems is complicated due to since various competing factors that can influence $\delta^{18}$O in speleothem calcite. Variations of speleothem $\delta^{18}$O reflect either variations of seepage water $\delta^{18}$O and/or cave air temperature variations, if speleothem calcite is deposited under isotopic equilibrium conditions (*Hendy*, 1971). On seasonal time scales, variations of $\delta^{18}$O in precipitation arises from variations in the rainfall source and its characteristics (e.g., frequency, duration, intensity) and surface air temperature. On decadal to millennial timescales, additional factors such as changes in the $\delta^{18}$O in the ocean ("ice volume" effect), changes in the seasonality of precipitation (change in the proportion of winter and summer precipitation) and shifts in the source of moisture and/or storm tracks must be taken into account (e.g. *Bar-Matthews et al.*, 1999; *Fleitmann et al.*, 2003)

In tropical regions, which is the focus region of this dissertation, on a millennial scale, $\delta^{18}$O of speleothem can be influenced by several factors: 1) global ice-volume effect; 2) temperature change; 3) variations in rainfall amount related to intensity and/or position of the ITCZ;

4) changes in the seasonal balance of summer and winter rainfall; and 5) changes in the frequency and/or intensity of ENSO events (*Griffiths et al.*, 2009). Despite these factors, speleothem $\delta^{18}O$ is primarily used as an indicator of monsoon strength or rainfall amount in tropical areas, with low $\delta^{18}O$ values reflecting wet conditions and/or stronger monsoon)and high values reflecting dry conditions and/or weaker monsoon.

Currently, $\delta^{18}O$ of speleothem calcite is the most frequently used speleothem-based proxy. It can provide information on the $\delta^{18}O$ of precipitation from annual to millennial time scales. Data from on-site rainfall and drip water $\delta^{18}O$ monitoring programs can be combined with atmospheric general circulation models equipped with water isotopes to unravel the complexities associated with speleothem $\delta^{18}O$ record interpretation.

### 1.3.5 Controls on speleothem $\delta^{13}C$

Spleleothem $\delta^{13}C$ is another important environmental proxy, although the interpretation of $\delta^{13}C$ of speleothem remains unclear (*Baker et al.*, 1997).

The complexity of the interpretation of $\delta^{13}C$ is due to multiple carbon sources of speleothem calcite and the fact that several climatic and non-climatic factors can influence the carbon isotopic composition of calcite. Nevertheless, the $\delta^{13}C$ of speleothems has increasingly become an important tool with which to track past changes in environmental and climatic conditions above and within cave systems, especially when combined with othe proxies.

Specifically, the $\delta^{13}C$ of the carbonate should reflect that of the dissolved inorganic carbon (DIC) of the parent solution, which may be influenced by a number of climate-related factors including: 1) shifts in the $\delta^{13}C$ of soil $CO_2$ due to changes in the ratio of C3:C4 plants in the overlying vegetation cover (*Dorale et al.*, 1998), changes in soil respiration rates, and/or contributions from atmospheric $CO_2$ (*Genty et al.*, 2003); 2) relative contribution of bedrock

carbon due to changes in open- versus closed-system dissolution conditions (*Hendy*, 1971) or the degree of water-rock interaction (*Oster et al.*, 2010); 3) $CO_2$ degassing and prior calcite precipitation upstream of the stalactite drip site (*Johnson et al.*, 2006); and iv) kinetic fractionation during $CO_2$ degassing (*Frisia et al.*, 2011).

Despite the potential for kinetic effects to corrupt the environmental $\delta^{13}C$ signal within the speleothem calcite, many studies have demonstrated that speleothem $\delta^{13}C$ shifts often reflect changes in vegetation cover, the degree of microbial activity in the soil, and/or the effective water balance within the karst system (*Griffiths et al.*, 2010b; *Genty et al.*, 2003; *Oster et al.*, 2010), which are related to climate in such a way that higher $\delta^{13}C$ values are indicative of drier conditions at the study site and vice versa.

### 1.3.6 Controls on speleothem trace element proxies

Trace elements of speleothems have become important proxies for paleostudies due to their ability to record annual to interannual cave and local environmental factor changes. Speleothem calcite incorporates trace elements (e.g. Mg, Sr, Ba, Ca, U, P) into its molecular structure as it is forming. The ratios of these elements can be used as indicators of cave and local environmental condition variations at the time of deposition. However, the relationship between trace element content in speleothems and climatic conditions can vary between caves due to differences in their general setting, such as thickness and chemical composition of bedrock, groundwater movement, soil thickness and climatic conditions. Despite these difficulties there is fast growing interest in speleothem-based trace elements time-series. Trace elements of speleothem is not a focus of this thesis, but will certainly be an interesting further study direction.

### 1.3.7 Cave monitoring for proxy calibration

Although speleothem proxies have great potential as high resolution paleoclimate records, an important prerequisite in using the stable isotopes ($\delta^{18}$O and $\delta^{13}$C) as climate indicators is that the carbonate deposition occurred at or close to isotopic equilibrium with the cave drip water. It has been demonstrated that the proxies in stalagmites from different cave systems may respond differently to surface climate and environmental changes (*Baker et al.*, 1997). Understanding the modern water-carbonate geochemistry mechanisms at the study site, is an essential prerequisite for the interpretation of these geochemical proxies. In some cases, the cave environment, such as cave $CO_2$ concentration, humidity, drip rate and soil zone, may influence the isotope signals in speleothems when they were forming (*Fairchild et al.*, 2006), which may change the key climatic signal preserved in speleothem calcite. In order to obtain robust paleoclimate records, detailed studies of modern cave systems are required to determine the modern environmental controls on speleothem geochemistry (*Fairchild et al.*, 2006).

Cave monitoring allows for a better understanding of the variables, such as temperature, relative humidity, and $CO_2$ concentration, all of which control the growth rate and geochemistry of modern water-carbonate systems. In order to understand how different caves record modern climate process and also accurately interpret stable isotope and trace element variations, the relationship between cave environment, modern rainfall and isotope signals needs to be understood.

### 1.3.8 Forward modeling of stalagmite $\delta^{18}$O

The interpretation of stalagmite $\delta^{18}$O proxies as climate records requires a stationary quantitative relationship between stalagmite $\delta^{18}$O and climate parameters, such as precipitation (*Bowen and Wilkinson*, 2002a; *Fischer and Treble*, 2008; *Jones*, 2009). However, processes

that transform $\delta^{18}$O of rainfall, in the soil, ground water and within the cave are very complex (*Fairchild et al.*, 2006). Water infiltrating the soil zone and permeable epikarst eventually reaches karst aquifers (cave cavities). Once within the karst aquifer, various flow paths deliver karst water to drip sites in cave. The storage capacity, outflow rates of karst aquifers, and different flow paths determine the response of those drip sites to rainfall events. The geochemical climate signal (e.g. $\delta^{18}$O) is thus transformed from the surface to stalagmites (*Fairchild et al.*, 2006), and the factors controlling this transformation process are site specific. Researchers therefore calibrate high-resolution stalagmite proxy data against instrumental data using regression approaches (*Baker and Bradley*, 2010). However, this approach is limited to study sites where modern annual resolution stalagmite records are available.

*Baker and Bradley* (2010) developed a forward modeling based approach (KarstFor model) to investigate the role of karst hydrology process quantitatively (Fig.1.5). For the study sites, where $\delta^{18}$O of precipitation is available, the KarstFor model uses conceptual models of karst hydrology to forward model the $\delta^{18}$O from rainfall to stalagmite (*Baker and Bradley*, 2010). This forward modeling method has progressed to be driven by Global Climate Model (GCM) output to provide constraints on the climate proxy calibrations (*Baker et al.*, 2012, 2013; *Lohmann et al.*, 2013). This forward modeling approach will not only provide a method to access the stationarity between stalagmite $\delta^{18}$O and climate parameters, but also allow one to quantify possible between-sample variabilities in $\delta^{18}$O associated with hydrological variability within one cave and/or under similar climate regions.

## 1.4 Study site

In this dissertation, I utilize five speleothems from Tham Mai cave, Laos, to construct decadal resolution stable isotope records ($\delta^{18}$O and $\delta^{13}$C) to provide a history of the SEAM

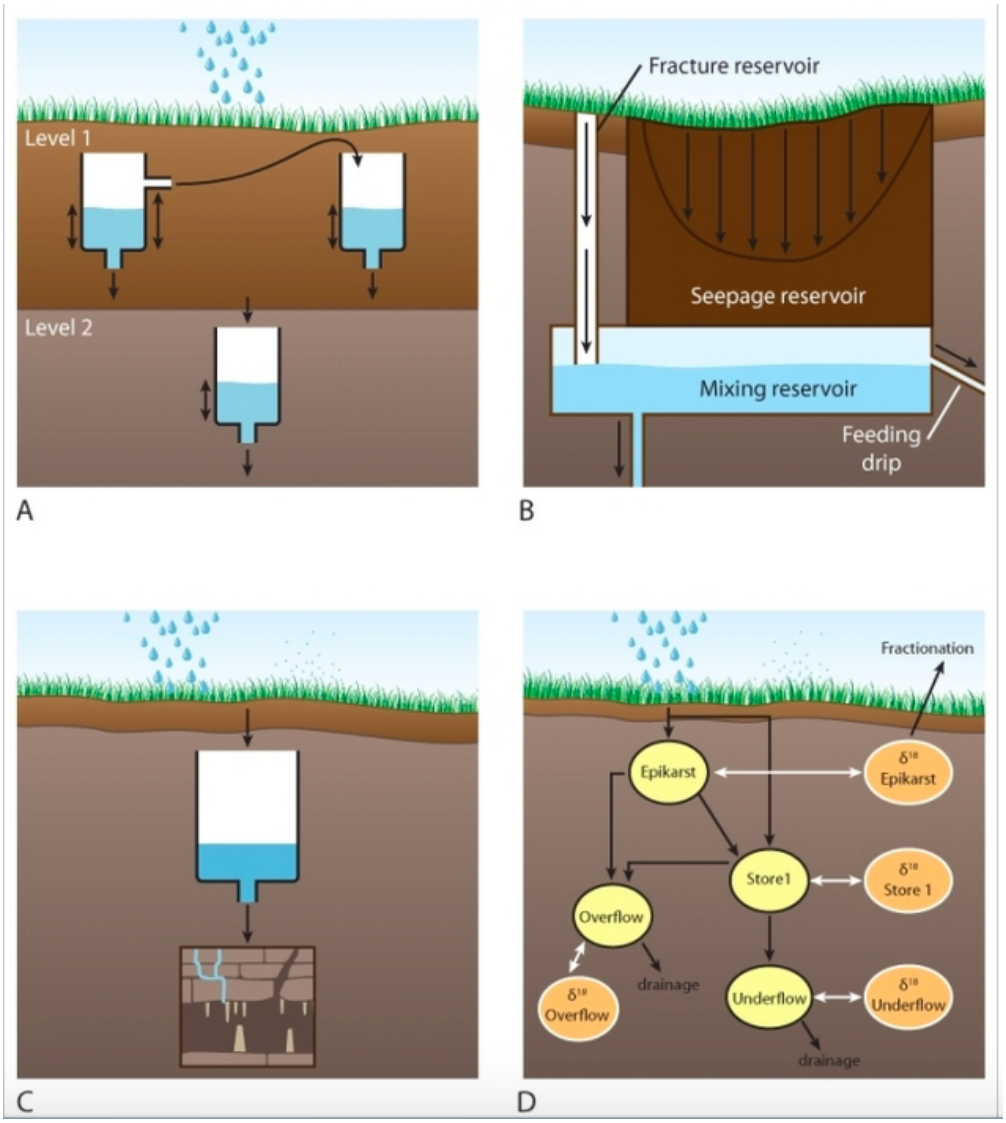


Figure 1.5: Conceptual diagrams of numeric models of karst water movement to stalagmites. a) Two-layer model of (*Fairchild et al.*, 2006). (b) Single reservoir with overflow feed model of (*Baker et al.*, 2010) (c) Single reservoir model with underflow feed of (*Baker and Bradley*, 2010) and (d) lumped parameter model of (*Chris Bradley and Andy Baker and Catherine N. Jex and Melanie J. Leng*, 2010; *Baker et al.*, 2013). Adapted from *Baker and Fairchild* (2012).

hydroclimate variations over past 13 kyr BP. The speleothem records are tied to 63 $U-Th$ ages in total. Age models are constructed for each stalagmite. I compare the geochemical time-series with numerous paleoclimate records across the AM region, Greenland, and South America to investigate regional coherence and tele-connections in the paleoclimate records. This study site sits at the interface of East Asian monsoon and Indian monsoon systems and

is ideally located to capture substantial hydrologic variability related to changing monsoon strength and coupled climate modes such as the ENSO and IOD.

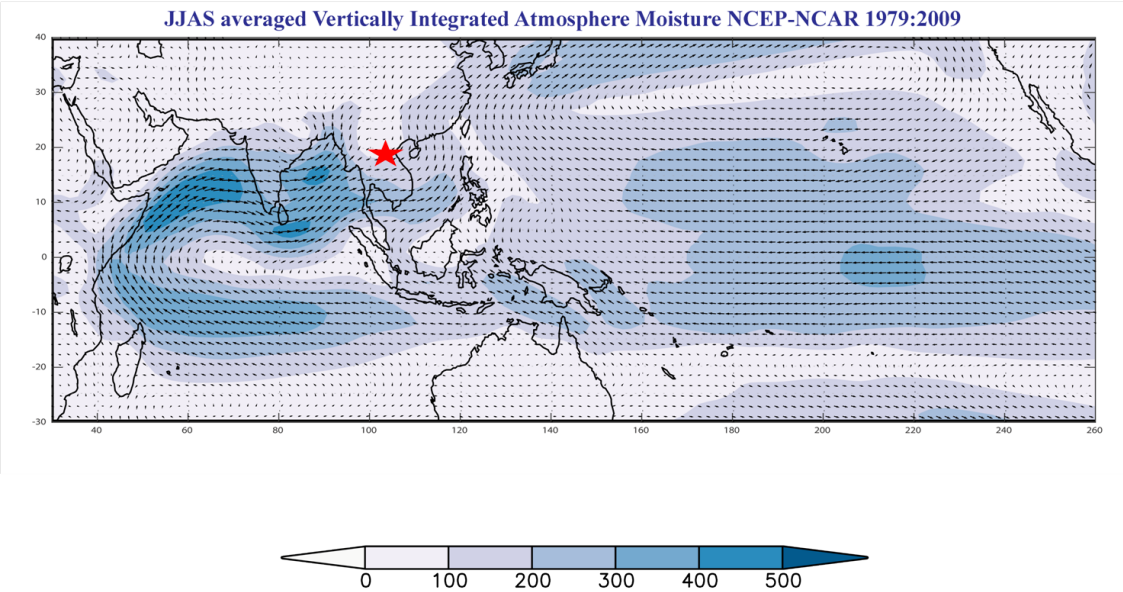


Figure 1.6: Average vertical integrated atmospheric water vapor flux for JJAS of 1979-2009 based on the reanalysis monthly data from the NCEP-NCAR. The color indicates the intensity of water vapor flux (kg/m/s). The arrows indicate direction of moisture flux transport. Red star is the location of Tham Mai cave, Laos, 20.75$^o$ N, 102.65$^o$ E.

## 1.5 Research objectives

My main research objectives are to use Tham Mai cave speleothems and a spectrally nudged isotope-enabled general circulation model (IsoGSM) coupled with instrumental climate data to address:

1. How has regional climate of Southeast Asia varied over the past 13 kyrs on decadal to orbital timescales?

2. What are the mechanisms that control precipitation and speleothem $\delta^{18}$O on orbital to seasonal timescales in Laos, in the tropical Indo-Pacific, and in the broad Asian Monsoon region?

3. Can we quantify the noise from cave hydrological processes on speleothem $\delta^{18}$O signatures?

4. What are the dominant mechanisms of interannual to multi-decadal hydrologic variability in Southeast Asia over the last 13 kyrs?

5. What is the relationship between Southeast Asian Monsoon strength and mid-to-high latitude climate over the last 13 kyrs years? For example, what were the impacts of the Younger Dryas, and the 8.2 kyr event?

## 1.6 Chapter outline

To address these research questions, I developed well-calibrated and replicated stable isotope ($\delta^{18}$O and $\delta^{13}$C) records from precisely-dated Laos speleothems covering at least the last 13 kyrs at decadal resolution. I conducted intensive statistical analysis on instrumental/reanalysis/climate model data.

Chapter 1 of this dissertation introduces central aspects of speleothem paleoclimatology. This chapter first introduces the karst hydrology, deposition of speleothems, dating techniques and application of stable isotope ratios as paleoclimate proxies.

Chapter 2 of this dissertation presents the result of $U-Th$ dating for 7 speleothems. A total of 83 dates are presented in this chapter. In this chapter, I first introduce $U-Th$ dating technique, sample preparation and column chemistry protocol. I then present our $U-Th$

dating results. Mean $^{238}U$ concentration, ($^{230}Th/^{232}Th$), and detailed age results for each speleothem are presented.

Chapter 3 of this dissertation presents a high-resolution late Pleistocene to Holocene record of Southeast Asian Monsoon (SEAM) evolution compiled from five speleothems (TM4, TM5, TM9, TM11, and TM13) collected from Tham Mai Cave in northern Laos (20.75$^o$ N, 102.65$^o$ E). Speleothems from Laos can provide ideal paleorecords for the study of the variation of the monsoon system and help unravel the controlling mechanisms.The stable isotope($\delta^{18}$O and $\delta^{13}$C) records are tied to a chronology constructed from a total of 63 U-Th dates, which indicate the records extend from 0.79±0.13 to 13.01±0.81 kyr BP with sub-decadal resolution.

In Chapter 4, I utilize a previously developed speleothem proxy forward model, Karst-For model (*Baker et al.*, 2013), to quantify the noise of stalagmite $\delta^{18}$O signiature associated with cave hydrological process. I use existing IsoGSM output(temperature, precipitation,eveporation and $\delta^{18}O_p$) as input data for KarstFor model. I generate six pseudo stalagmite $\delta^{18}$O proxies. The absolute differences among these six pseudo-proxes is 1.2 ‰, consistent with the observed offset between Holocene speleothem records from Tham Mai cave.

In Chapter 5, I utilize existing simulations from a spectrally nudged isotope-enabled general circulation model (IsoGSM) (*Yoshimura et al.*, 2008) coupled with instrumental climate data to investigate the climatic controls on $\delta^{18}O_p$ at four key cave locations affected by the Asian monsoon: Qunf cave, Oman; Mawmluh cave, India; Tham Mai cave, Laos; and Dongge cave, China. I first correlate IsoGSM $\delta^{18}O_p$ data from the closest grid point of each cave site spatially with instrumental climate data (e.g. precipitation, SST, SLP, wind stress) from 1979-2010. I find that $\delta^{18}$O at the four cave sites is unrelated to local precipitation amount, but instead reflects large-scale ocean-atmosphere processes, such as ENSO. To further investigate how ENSO, IOD and AM affect $\delta^{18}O_p$, I composite JJAS $\delta^{18}$O during strong El

Niño years, La Niña and IOD years. Through the composite maps, I find that the association between AM and ENSO is probably manifested through the change of moisture source. The positive anomalies over Southeast Asia during El Niño events may reflect increased contribution of high $\delta^{18}$O precipitation from the Bay of Bengal.

Chapter 6 is the final chapter of this dissertation. I discuss areas where future research is needed, i.e. the AM region paleo-climate reconstruction and controlling mechanism of the AM region $\delta^{18}O_p$.

# Chapter 2

# Speleothem Age Determination

## 2.1 Introduction

A unique advantage of using speleothems to reconstruct paleoclimate is that they can be precisely and accurately dated.The development of uranium-thorium ($U-Th$) dating techniques with small calcite samples, enabled by the development of TIMS (Thermal Ionization Mass Spectrometer) and ICP-MS (Inductively Coupled Plasma Mass Spectrometer), has allowed speleothems to become prominent geological archives for paleoclimate. The initial attempts to apply the $U-Th$ method to speleothem (e.g. *Rosholt and PS*, 1962; *Cherdyntsev et al.*, 1965) were not well constrained, however, better understanding of $U-Th$ chronological techniques on carbonate samples were obtained in early 1970s (e.g. *DUPLESSY et al.*, 1970; *Harmon et al.*, 1977). In a condition of $U-Th$ disequilibrium in systems and given the rates of ingrowth of daughter isotopes $^{230}Th$ from parent isotopes $^{238}U$ and $^{234}U$, recently $U-Th$ methods allows precise and reliable dating of speleothem samples back to 0.6 Ma (e.g. *Edwards et al.*, 1987; *Cheng et al.*, 2000). MC-ICP-MS (Multi-Collector Inductively Coupled Plasma Mass Spectrometer) is the most widely used dating techniques to deter-

mine speleothem $U-Th$ ages, though TIMS and sector field ICP-MS are also utilized (e.g. *Shen et al.*, 2006; *Fairchild and Baker*, 2012).

The $U-Th$ dating techniques is based on the decay of the parent isotope to daughter isotope ($^{238}U$- $^{234}U$- $^{230}Th$)(Fig.2.1). The radioactive decay law was defined *Cosma and Jurcuţ* (1996); *Ivanovich, M.* (1982):

$$N = N_0 e^{-\lambda t} \tag{2.1}$$

where:

- $N$ is the number of radioactive nuclei remaining after time t;

-$N_0$ is the initial radioactive nuclei number.

-$\lambda$ is radioactive constant

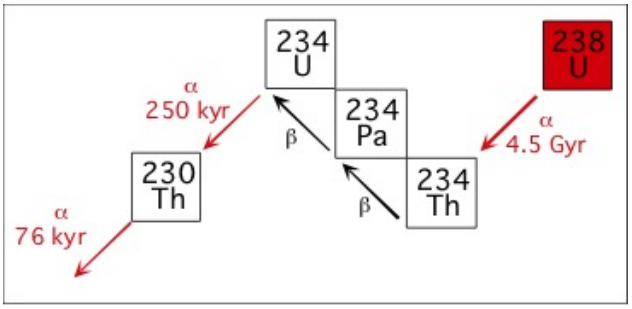


Figure 2.1: The parent isotope $^{238}U$ undergoes alpha decay to form the daughter isotope $^{234}U$, which decays further to form $^{230}Th$. The sample age is based on the difference between the initial ratio of $^{230}Th/^{234}U$ and the one in the sample being dated

The carbonate bedrock normally contains both uranium and thorium. Uranium isotopes are leached from the carbonate bedrock and precipitated as uranyl carbonate with calcite during speleothem formation. Normally, the precipitating solution does not contain $^{230}Th$ since uranium is soluble in water under oxidizing conditions, while thorium is not. Thorium ions are either absorbed into clay minerals or remain in place as insoluble hydrolysates (*Richards and Dorale*, 2003). From there, $^{238}U$ decays radioactively through a series of intermediate

daughter products until stable isotope $^{206}Pb$ is produced. This method is based on the natural separation of $U$ from $Th$. For $U-Th$ dating, only the decay from $^{234}U$ to $^{230}Th$ (Fig. 2.1) is used. Thus, the amount of $^{230}Th$ measured in the speleothem is an indicator of the age of the calcite based on the balance between parent $^{234}U$ and it's radioactive daughter $^{230}Th$. Provided that the speleothem calcite contains no initial $^{230}Th$, $U-Th$ dating can give accurate absolute ages that don't require a correction factor (*Richards and Dorale*, 2003). Using the $U-Th$ dating method, age uncertainties are small and typically vary between 0.5% and 2% of the absolute age, depending on the Uranium content of speleothem calcite.

However, initial $^{230}Th$ can be incorporated into speleothem calcite during deposition process causing artificial older $U-Th$ ages. The contribution of initial $^{230}Th$ can be monitored by measuring the amount of $^{232}Th$ in the speleothem calcite samples. The measured $U-Th$ ages then can be corrected for initial $^{230}Th$ based on an estimation of the $^{230}Th/^{232}Th$ ratio of the detrital phase. The estimation of $^{230}Th/^{232}Th$ can be obtained by using isochron techniques or by measuring the ratio directly in the chemically separated detrital phase or by using the bulk earth value. While the estimation of $^{230}Th/^{232}Th$ likely varies site by site and through time at a given site, the isochron $^{232}Th$ corrected ages can be associated with large errors.

The initial $^{230}Th$ problem is especially the case for younger speleothems with low uranium concentration where little $^{230}Th$ is produced from the decay of uranium. Age uncertainties for younger stalagmites with low uranium concentrations can be within a range of 5% to 10% of the absolute age (*Shen et al.*, 2006). Although initial $^{230}Th$ may present in some speleothems, most speleothem are less contaminated and can be precisely dated with $U-Th$ methods. Moreover, high confidence of dating precision can be achieved by $U-Th$ dating if consistent timing is observed between climate events recorded by trace elements or stable isotopes in a speleothem and that observed in other archives, such as ice cores (*Richards and Dorale*, 2003).

## 2.2 Cave and sample description

During 2010 fieldwork, we collected over 15 speleothems from three caves in central and northern Laos. We split each sample in half and conducted XRD (X-ray powder diffraction) analyses, which showed that all of the samples are composed of 100% calcite. In 2011, we conducted 120 U-Th dates at the University of Oxford, UK on 10 different stalagmite samples. 7 samples (TD1,TM4, TM5, TM6, TM9, TM11, and TM13), that cover from 0.08±0.00 to 15.53±0.12 kyr BP are finally chosen for this Ph.D project. TD1 from Tham Duk Cave(19.72 N,102.07 E; 165 m long; elevation 779 m), and TM4, TM5, TM9, TM11,TM13 from Tham Mai Cave(20.75 N, 102.65 E; 2010 m long; elevation 360 m). A map of Tham Mai cave with sample locations is shown in Fig 2.2. These stalagmites all have visible annual lamina, high uranium concentration and low initial $Th$ correction, though initial $Th$ correction for some samples is large. The uranium concentration of most samples ranges from 100-800 ppb, though the one from Tham Duk contains 8-20 ppm. Having several samples with age overlaps allows us to replicate our time series, hence gives a high confidence for our climate reconstruction (presented in chapter 3).

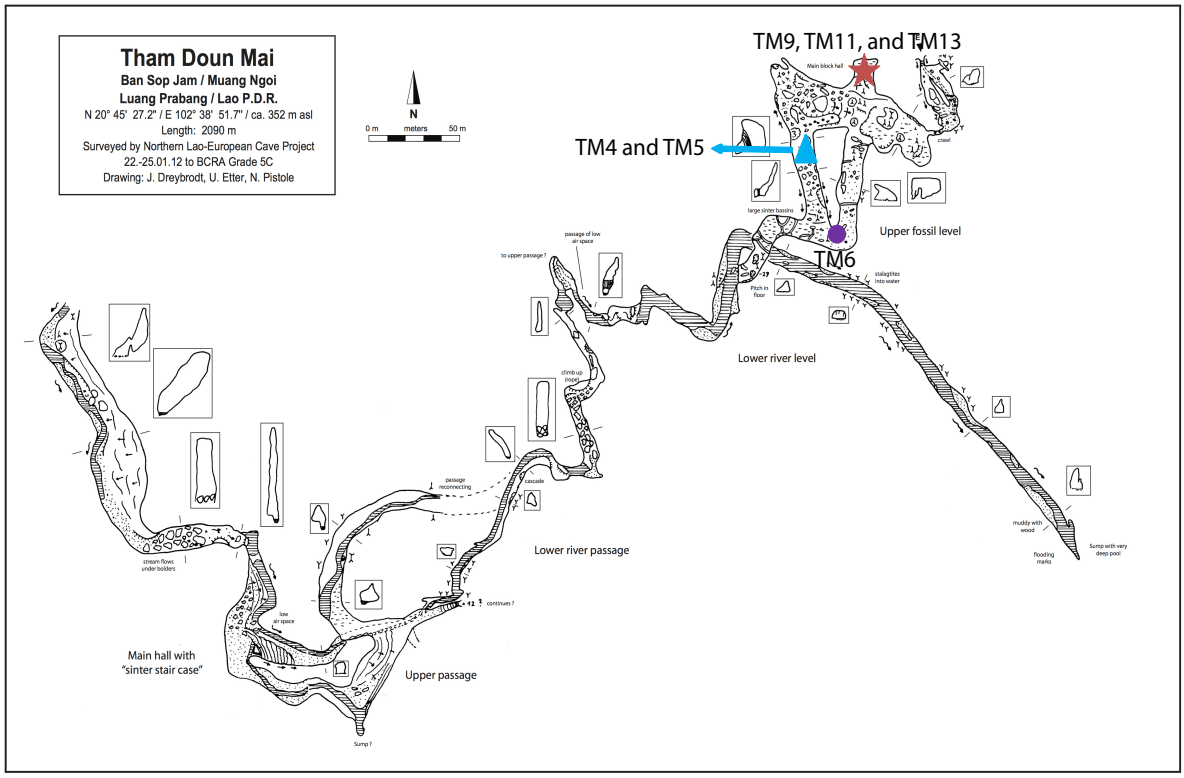


Figure 2.2: Map of Tham Mai cave with stalagmite samples locations, red star is location of TM9, TM11 and TM13, blue triangle is location of TM4 and TM5, Purple circle is the location of TM6

## 2.3 Chronology and analytical techniques

$U-Th$ dating is the most widely used dating method applied to speleothems and is the main dating method that I use to get absolute ages for Laos speleothem samples. Stalagmite calcite samples were prepared in a class-1000 clean lab and measured via MC-ICP-MS (Fig.2.3) at the Department of Earth Science, University of Oxford, England, in 2011.

Figure 2.3: Multi-Collector Inductively Coupled Plasma Mass Spectrometer(MC-ICP-MS) is used to determine Tham Mai cave speleothems $U-Th$ ages

### 2.3.1 Sampling

Sub-samples for dating were obtained by milling out solid chunks, parallel to speleothem growth bands, using the "moat-and-spall" method. I drilled samples from polished stalagmite section surfaces using a hand-held dental drill. For $U-Th$ analysis, 0.1-0.2 g samples were taken every 1-2 cm along growth axes for each stalagmites,including above and below any suspected hiatus. I then cleaned samples with ultrasonic bath in isopropanol and Milli-Q water, dried in oven on foil, and stored samples in clean $1.5ml$ eppendorf tubes.

### 2.3.2 Chemical separation of uranium and thorium

The chemical procedure and U-series dating methods are similar to those demonstrated in *Edwards et al.* (1987), although smaller stalagmite calcite sample sizes are used compared to that described in the reference. Samples were transferred to pre-weighed 30 $ml$ Teflon vials and were re-weighed using a Sartorius balance. The samples were dissolved following the procedure described below. Most of our samples were dissolved completely without any acid-insoluble residue. Few samples had some residue after nitric acid dissolution, which may indicate detrital impurities and organic matter contaminations.

Sample preparation:

1. Samples heated in $HNO_3$ overnight
2. Samples heated to incipient dryness
3. Samples converted to nitrate form
4. Samples dissolved in 4 $ml$ 7.5 N $HNO_3$
5. Clean 2 $ml$ columns in 7 N $HNO_3$ and rinse with Milli-Q water

Once dissolved, the samples were spiked with a mixed $^{229}U$ - $^{236}U$ tracer of known concentration and isotopic composition. The solution was loaded on an anion exchange column, purified by ion-exchange chemistry, and analyzed via Nu Instruments MC-ICP-MS. The ion-exchange chemistry aims to isolate $U$ and $Th$ elements from calcite samples. $U$ and $Th$ then were separated following the procedure described below. All acids were double distilled TM (TraceMetal) grade.

Column protocol:

1. 2 $ml$ Biorad columns filled with 2 $ml$ new resin slurry (washed 1*8 anion-exchange resin 100-200 mesh)
2. Washed with 10 $ml$ $H_2O$, 10 $ml$ 6 M $HCl$, 10 $ml$ $H_2O$
3. Conditioned with 2*5 $ml$ 7.5 M $HNO_3$
4. Load samples directly from sample beaker
5. Wash columns with 2*2 $ml$ 7.5 M $HNO_3$, adding the first 2 $ml$ to the sample beaker and adding it directly to the column
6. Convert the column with 4*0.25 $ml$, 1*0.5 $ml$ 6M $HCl$
7. Collect $Th$: elute $Th$ out with 2*1 $ml$, 2*2 $ml$ 6 M $HCl$
8. Collect $U$: elute $U$ out with 2*1 $ml$, 2*4 $ml$ $H_2O$
9. Dry down each cut (without boiling)
10. Add 0.2 $ml$ of conc $HNO_3$ to each cut and dry down
11. Dissolve in 42 $\mu l$ of 7.5 N $HNO_3$ to store for mass spec (add 958 $\mu l$ Milli-Q water to male 1 $ml$ 2% $HNO_3$)

### 2.3.3 $U-Th$ chronology

The prepared samples were measured at University of Oxford, England, by MC-ICP-MS. Ages are calculated using half lives from *Cheng et al.* (2000) and reported relative to 1950. The uncertainties incorporate mass spectrometric analytic uncertainty, weighing uncertainty,

and spike uncertainty. The raw $U-Th$ ages were calculated under the assumption that the initial contents of $^{230}Th$ is zero. The equation is given by *Ivanovich, M.* (1982):

$$^{230}Th/^{234}U = \frac{1-e^{-\lambda_{230}t}}{^{234}U/^{238}U} + (1-\frac{1}{^{234}U/^{238}U})\frac{\lambda_{230}}{\lambda_{230}-\lambda_{234}}(1-e^{-(\lambda_{230}-\lambda_{234})t}) \tag{2.2}$$

Where:

$\lambda_{230} = 8.77401 * 10^{-5}$ yr$^{-1}$

$\lambda_{234} = 2.82629 * 10^{-6}$ yr$^{-1}$

### 2.3.4 Initial $Th$ concentration correction

The impact of detrital contamination is crucial for speleothem age determination. Because the source of initial $Th$ materials varies considerably, it is likely that the estimation of $^{230}Th/^{232}Th$ varies site by site.

The presence of initial $Th$ can be corrected by a priori estimation of initial ($^{230}Th/^{232}Th$) (e.g. *Ivanovich and Harmon*; *Hellstrom*, 2006). These assumed values are utilized in conjunction with the measured $^{232}Th$ content of each sample to subtract the initial $Th$ from the measured $^{238}U$, $^{234}U$ and $^{230}Th$ (e.g. *Ivanovich and Harmon*; *Dorale et al.*, 1998; *Hopley et al.*, 2011). The predominant current practice in correction for speleothem initial $Th$ is to assume a detrital phase of crustal equilibrium composition at the time of deposition, usually a $\sim 50\%$ uncertainty is assigned to this (*Hellstrom*, 2006). A choice of ($^{230}Th/^{232}Th$) = 1 $\pm$ 0.5 ($\pm$ 50%) is widely used (*Richards and Dorale*, 2003). However, the reported range of initial ($^{230}Th/^{232}Th$) in speleothem is much larger than 1 $\pm$ 0.5, and can range from $\sim$0.2 (*Drysdale*

*et al.*, 2006) to ∼18 (*Beck et al.*, 2001), although a median initial $(^{230}Th/^{232}Th)$ ∼1 is an appropriate default assumption for most speleothems.

In our study, the raw ages of TM4, TM5, TM9, and TM11 were corrected for the presence of initial $Th$ utilizing the average crustal $(^{230}Th/^{232}Th)$ value of 1.21±50%. The uncertainties corresponding to this initial $Th$ correction are assigned to be 50% of the $(^{230}Th/^{232}Th)$.

The raw ages of TM13 is first corrected with initial $(^{230}Th/^{232}Th)$ value of 1.21±50%, which is the same as other speleothems from Tham Mai cave. Fig.2.4.a shows a StalAge model of TM13 with $U-Th$ dates that corrected by the initial value of 1.21±50%. The StalAge model indicates that TM13 was growing during Younger Dryas. TM13 $\delta^{18}$O indicates that the onset of Younger Dryas is ∼ 14 kyr BP, which is off by ∼ 1 kyr compared with other existing paleo-records(e.g. *Wang et al.*, 2001; *Ayliffe et al.*, 2013; *Griffiths et al.*, 2009; *GISP2*; *Haug et al.*, 2001). Regardless the possibility that this recorded earlier onset of Younger Dryas on our site, it is more likely that the assumed initial $Th$ concentration value is not suitable for TM13. We further compared TM13 $\delta^{18}$O result with Hulu cave $\delta^{18}$O result (*Wang et al.*, 2001; *Southon et al.*, 2012). We manually tuned TM13 initial $(^{230}Th/^{232}Th)$ value until the timing of Younger Dryas recorded in TM13 is close to that of Hulu cave. An initial initial $(^{230}Th/^{232}Th)$ value of 3.7±50% is chosen for TM13 final age model. Fig.2.5.a shows a StalAge model of TM13 with $U-Th$ dates that corrected by the initial value of 3.7±50%. All TM13 ages reported hereafter are corrected with an initial $(^{230}Th/^{232}Th)$ value of 3.7±50%.

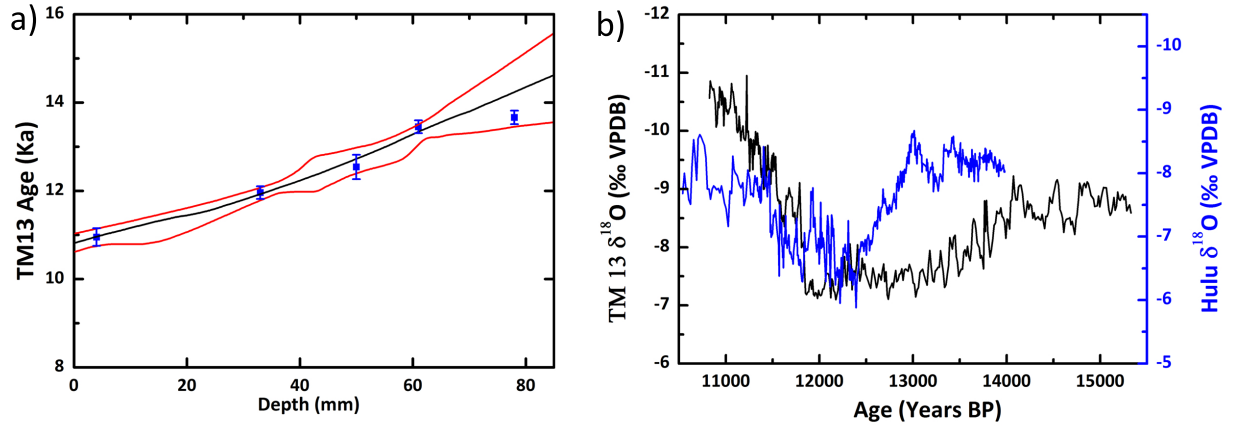


Figure 2.4: a)StalAge model of TM13 with $U-Th$ dates corrected with initial $(^{230}Th/^{232}Th)$ value of 1.21±50%. b)Comparison of TM13 $\delta^{18}$O with Hulu cave $\delta^{18}$O, black: TM13 $\delta^{18}$O record, blue: Hulu cave $\delta^{18}$O record

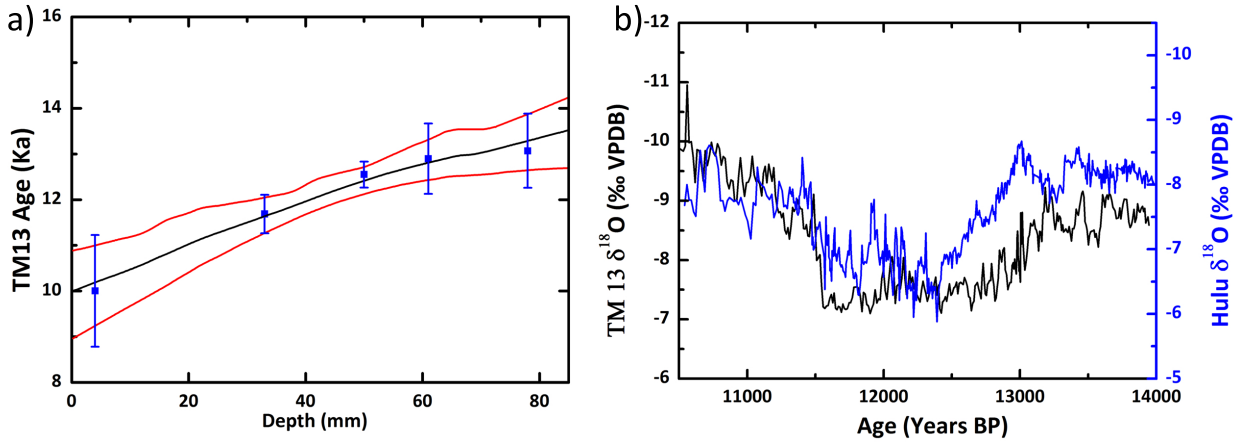


Figure 2.5: a)StalAge model of TM13 with $U-Th$ dates corrected with initial $(^{230}Th/^{232}Th)$ value of 3.7±50%. b)Comparison of TM13 $\delta^{18}$O with Hulu cave $\delta^{18}$O, black: TM13 $\delta^{18}$O record, blue: Hulu cave $\delta^{18}$O record

## 2.4 Results

Seven stalagmites (TD1,TM4, TM5, TM6, TM9, TM11, and TM13) from northern Laos are dated. Results show that these seven stalagmites span the period since the Younger Dryas, with sufficient overlap between samples to allow replication of much of the Holocene time period (Table2.1 and Fig.2.6). Growth rates of these stalagmites range from 21 to 389 $\mu m/yr$. $^{238}U$ concentration ranges from 0.12 to 10.35 ppm, with average $^{238}U$ equal to 2.32±3.02.

Our $U-Th$ results show that our samples cover the period from 0.08 kyr BP to 13.01 kyr BP. Results show that detrital correction ($^{230}$Th Correction) has some effect on several ages, especially for younger ages. For samples TM4, TM5, TM9 and TM11, detrital corrections range from 4 years to 358 years (average = 118±120 years). Detrital correction for TM13 is larger than other samples, with an average = 687±163 years.

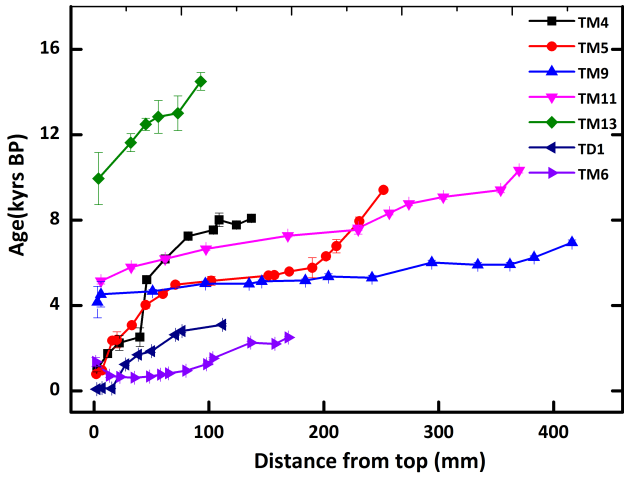


Figure 2.6: Tham Mai cave stalagmites (that ones we propose to use in this research) $U-Th$ age-depth summary plot. The color-coded shapes represent individual $U-Th$ ages for each specimen along with their uncertainty.

Table 2.1: Summary of Laos speleothems $U$ and $Th$ concentration, $U-Th$ age results, growth rate

| Sample name | Length (cm) | of dates | Mean $^{238}U$ conc (ppm) | Mean ($^{230}Th/^{232}Th$) | Top age (kyr BP) | Basal age (kyr BP) | Mean growth rate ($\mu m/yr$) |
|---|---|---|---|---|---|---|---|
| TD1 | 11.2 | 7 | 10.35±6.10 | 1038.65 ±1429.25 | 0.08 ±0.00 | 3.09 ±0.06 | 42 |
| TM4 | 14 | 11 | 0.22±0.04 | 353.82±526.57 | 1.01 ± 0.11 | 8.08 ± 0.18 | 35 |
| TM5 | 22 | 17 | 0.24 ± 0.08 | 197.74±199.90 | 0.79 ± 0.09 | 9.42 ± 0.13 | 68 |
| TM6 | 17 | 13 | 6.44± 6.39 | 75.01 ± 77.01 | 0.7 ± 0.07 | 2.50 ± 0.03 | 101 |
| TM9 | 45 | 14 | 0.5 ± 0.08 | 523.44±591.86 | 4.16 ± 0.59 | 6.95 ± 0.12 | 390 |
| TM11 | 33 | 12 | 0.32 ± 0.04 | 255.73±205.05 | 5.14 ± 0.08 | 10.33 ±0.12 | 79 |
| TM13 | 22 | 9 | 0.32 ± 0.15 | 129.59±174.76 | 9.94 ±1.22 | 13.01 ± 0.81 | 22 |

### 2.4.1 $U-Th$ age results for the last two millennia

TD1 and TM6 are two stalagmites covering the last two millennia. TM4 and TM5 also have younger sections that cover the last two millennia. I will discuss TD1 and TM6 in this section, and TM4 and TM5 will be discussed in next section. Age uncertainties for TD1 and TM6 are ranging from 1% to 15% with detrital correction average equals to 72 years.

TD1 is 11.2 cm long with average growth rate of 42 $\mu m/yr$. TD1 has high uranium concentration (average = 10.35±6.1 ppm), and was growing from 0.08±0.00 to 3.09±0.06 kyr BP, with a possible hiatus after 0.13±0.01 kyr BP. Detrital correction for TD1 is very low, ranging from 1 year to 16 years with average equals to 4 years.

TM6 is 16.9 cm long with average growth rate of 43.49 $\mu m/yr$. TM6 also has a high uranium concentration (average = 6.44±6.39 ppm), and was growing from 1.35±0.2 kyr BP to 2.5±0.03 kyr BP.

Table 2.2: $U$ and $Th$ concentration and isotope ratios with resulting $U$-$Th$ ages for stalagmites covering last two millennia

| Sampel name | Distance (cm) | $^{238}U$ conc (ppm) | $^{232}Th$ conc (ppb) | $\delta^{234}$U [a] | $(^{230}Th/^{232}Th)$b | $(^{230}Th/^{238}U)^b$ | Age(raw)[b] (kyrs BP) | age(corr)[c] (kyrs BP) |
|---|---|---|---|---|---|---|---|---|
| | 0.25 | ± | ± | ± | 24.98 ± 0.00 | 0.00 ± 0.0000 | 0.09 ± 0.00 | 0.08 ± 0.00 |
| | 0.7 | 9.17 ± 0.43877 | 336.78 ± 1.05 | 2.19 ± 0.042 | 32.00 ± 0.00 | 0.00 ± 0.0001 | 0.14 ± 0.01 | 0.13 ± 0.01 |
| | 1.55 | 8.41 ± 0.10599 | 331.27 ± 1.04 | 0.71 ± 0.043 | 80.26 ± 0.00 | 0.00 ± 0.0001 | 0.11 ± 0.01 | 0.11 ± 0.01 |
| | 2.75 | 9.03 ± 0.01618 | 339.45 ± 2.41 | 0.75 ± 0.072 | 499.88 ± 0.00 | 0.02 ± 0.0004 | 1.24 ± 0.03 | 1.23 ± 0.03 |
| TD1 | 3.85 | 8.75 ± 0.00387 | 351.49 ± 1.13 | 6.61 ± 0.094 | 87.80 ± 0.00 | 0.02 ± 0.0003 | 1.71 ± 0.03 | 1.69 ± 0.03 |
| | 5 | 7.00 ± 0.01191 | 351.06 ± 2.35 | 0.27 ± 0.037 | 1483.42 ± 0.00 | 0.02 ± 0.0008 | 1.86 ± 0.07 | 1.86 ± 0.07 |
| | 7.1 | 4.91 ± 0.00202 | 349.70 ± 1.13 | 0.24 ± 0.044 | 1499.36 ± 0.00 | 0.03 ± 0.0003 | 2.63 ± 0.02 | 2.63 ± 0.02 |
| | 7.65 | 10.72 ± 0.00475 | 354.99 ± 1.13 | 0.92 ± 0.041 | 1172.15 ± 0.00 | 0.04 ± 0.0007 | 2.80 ± 0.06 | 2.80 ± 0.06 |
| | 11.2 | 24.85 ± 0.04129 | 336.91 ± 2.34 | 0.58 ± 0.039 | 4468.00 ± 0.00 | 0.04 ± 0.0007 | 3.09 ± 0.06 | 3.09 ± 0.06 |
| | 0.15 | 0.44 ± 0.00112 | 1372.50 ± 7.37 | 13.09 ± 0.258 | 5.22 ± 0.00 | 0.04 ± 0.0004 | 1.72 ± 0.02 | 1.35 ± 0.20 |
| | 1.35 | 0.39 ± 0.00062 | 1437.12 ± 2.41 | 3.70 ± 0.112 | 7.24 ± 0.01 | 0.02 ± 0.0004 | 0.82 ± 0.02 | 0.70 ± 0.07 |
| | 2.25 | 0.49 ± 0.00131 | 1452.70 ± 7.36 | 4.08 ± 0.080 | 8.19 ± 0.01 | 0.02 ± 0.0003 | 0.75 ± 0.01 | 0.65 ± 0.06 |
| | 3.5 | 0.55 ± 0.01113 | 1452.32 ± 2.41 | 1.73 ± 0.052 | 16.77 ± 0.04 | 0.02 ± 0.0004 | 0.65 ± 0.02 | 0.61 ± 0.03 |
| | 4.85 | 5.32 ± 0.01117 | 1453.35 ± 2.42 | 1.56 ± 0.026 | 173.53 ± 1.62 | 0.02 ± 0.0001 | 0.67 ± 0.01 | 0.67 ± 0.01 |
| | 5.8 | 2.66 ± 0.00482 | 1456.04 ± 2.20 | 0.82 ± 0.016 | 187.52 ± 3.85 | 0.02 ± 0.0001 | 0.76 ± 0.01 | 0.76 ± 0.01 |
| TM6 | 6.5 | 21.57 ± 0.09833 | 1458.03 ± 2.44 | 9.51 ± 0.160 | 138.90 ± 0.99 | 0.02 ± 0.0002 | 0.83 ± 0.01 | 0.82 ± 0.01 |
| | 8 | 7.21 ± 0.02234 | 1461.06 ± 2.43 | 4.40 ± 0.073 | 114.76 ± 0.65 | 0.02 ± 0.0002 | 0.95 ± 0.01 | 0.94 ± 0.01 |
| | 9.8 | 10.81 ± 0.02373 | 1468.34 ± 2.22 | 27.76 ± 0.213 | 36.94 ± 0.06 | 0.03 ± 0.0002 | 1.28 ± 0.01 | 1.25 ± 0.02 |
| | 10.35 | 12.19 ± 0.03536 | 1457.36 ± 2.43 | 59.10 ± 0.982 | 24.12 ± 0.03 | 0.04 ± 0.0004 | 1.58 ± 0.02 | 1.52 ± 0.04 |
| | 13.65 | 12.97 ± 0.06447 | 1447.66 ± 2.21 | 132.16 ± 1.054 | 17.18 ± 0.01 | 0.05 ± 0.0004 | 2.38 ± 0.02 | 2.26 ± 0.07 |
| | 15.75 | 4.43 ± 0.01140 | 1441.51 ± 2.42 | 3.33 ± 0.056 | 205.88 ± 2.13 | 0.05 ± 0.0004 | 2.21 ± 0.02 | 2.20 ± 0.02 |
| | 16.9 | 4.75 ± 0.01709 | 1443.99 ± 2.21 | 22.27 ± 0.167 | 38.85 ± 0.06 | 0.06 ± 0.0003 | 2.55 ± 0.01 | 2.50 ± 0.03 |

All errors are $2\sigma$. Distance is from top of each stalagmite
a. $\delta^{234}\text{U} = [(^{234}U/^{238}U)\text{-}1]*1000$ where $(^{234}U/^{238}U)$ is the measured activity ratio
b. Round brackets signify activity ratios
All errors are $2\sigma$. Distance is from top of each stalagmite
c. Age is calculated using half lives from (*Cheng et al.*, 2000) and is relative to 1950
Raw ages are corrected for inital $^{230}Th$ content by assuming $(^{230}Th/^{232}Th) = 1.21$
Uncertainties in inital correction is assumed to be 50% of the size of the correction
Uncertainties incorporates mass spectrometric,weighing and spike uncertainties

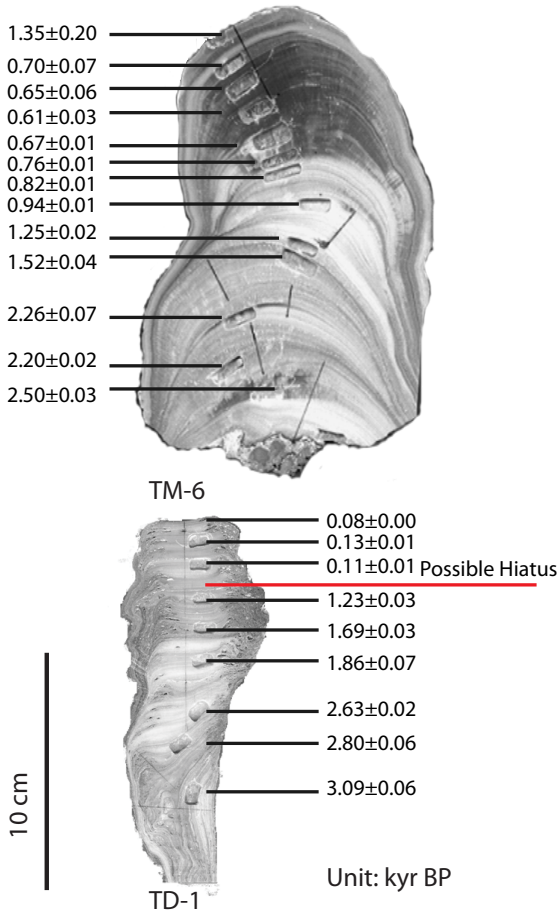


Figure 2.7: Scanned image of TD1 and TM6 with drilling holes for $U-Th$ dating, showing $U-Th$ dating results with 2 $\sigma$ error and the location of the possible major depositional hiatus.

### 2.4.2 $U-Th$ age results for Holocene and Younger Dryas

TM4, TM5, TM9, TM11 are four stalagmites coving Holocene, and TM13 is the one covering Younger Dryas. Age uncertainties for these samples are ranging from 1% to 18% with detrital correction range of 38 year to 357 years (average = 136±120 years). These samples have relative lower uranium concentration compared with TD1 and TM6. Uranium concentration of these samples ranges from 0.22 to 0.5 ppm (average = 0.32 ±0.11 ppm).

TM4 is 14 cm long with average growth rate of 35 $\mu m/yr$. TM4 has mean uranium concentration of 0.22±0.04 ppm, and was growing from 1.01±0.11 to 8.08±0.18 kyr BP, with a possible hiatus after 2.52±0.44 Kyrs BP. Detrital correction for TM4 is ranging from 8 to 217 years (average = 83 years).

TM5 is 22 cm long with average growth rate of 68 $\mu m/yr$. TM5 has mean uranium concentration of 0.24±0.08 ppm, and was growing from 0.79±0.09 to 9.42±0.13 kyr BP. Detrital correction for TM4 is ranging from 0 to 208 years (average = 48 years).

TM9 is 45 cm long with average growth rate of 390 $\mu m/yr$. TM9 has mean uranium concentration of 0.5±0.08 ppm, and was growing from 4.16±0.59 to 6.95±0.12 kyr BP. Detrital correction for TM4 is ranging from 1 to 828 years (average = 111 years). The consecutive two ages obtained from the top of TM9 have relatively large detrital correction, with 828 years and 286 years respectively.

TM11 is 33 cm long with average growth rate of 79 $\mu m/yr$. TM11 has mean uranium concentration of 0.32±0.04 ppm, and was growing from 5.14±0.08 to 10.33±0.12 kyr BP. Detrital correction for TM11 is ranging from 15 to 80 years (average = 38 years).

TM13 is 22 cm long with average growth rate of 22 $\mu m/yr$. TM13 has mean uranium concentration of 0.32±0.25 ppm, and was growing from 10.95±0.2 to 15.53±0.12 kyr BP. Detrital correction for TM13 is ranging from 12 to 81 years (average = 22 years).

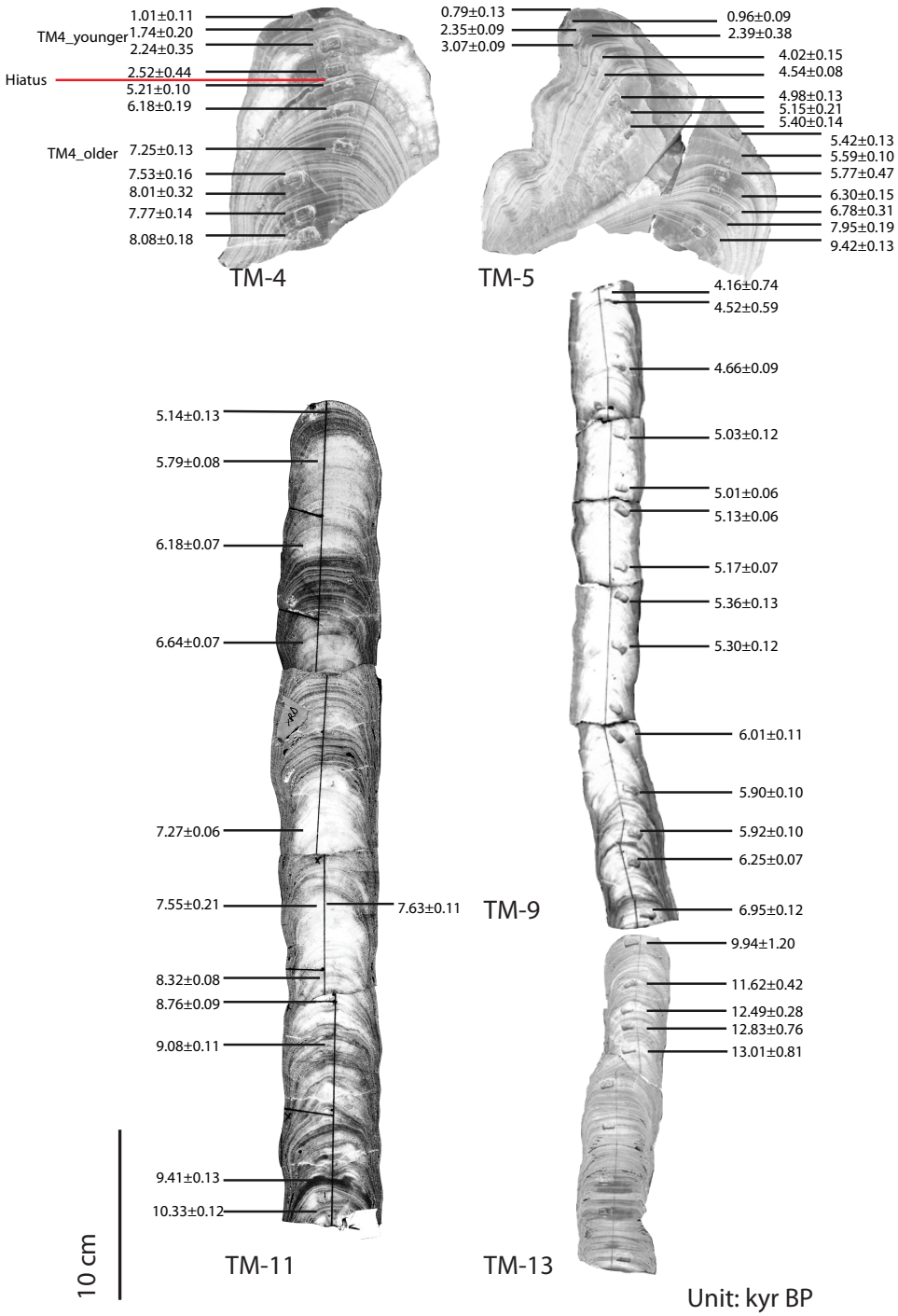


Figure 2.8: Scanned image of TM4, TM5, TM9,TM11 and TM13, with drilling holes for $U-Th$ dating, showing $U-Th$ dating results with $2\sigma$ error and the location of the possible major depositional hiatus.

Table 2.3: $U$ and $Th$ concentration and isotope ratios with resulting $U$-$Th$ ages for stalagmites covering Holocene and Younger Dryas

| Sampel name | Distance (cm) | $^{238}U$ conc (ppm) | $^{232}Th$ conc (ppb) | $\delta^{234}$U [a] | $(^{230}Th/^{232}Th)$[b] | $(^{230}Th/^{238}U)$[b] | Age(raw) (kyrs BP) | age(corr)[c] (kyrs BP) |
|---|---|---|---|---|---|---|---|---|
| | 0.25 | 0.12 ± 0.00022 | 492.59 ± 2.37 | 0.05 ± 0.009 | 78.54 ± 1.71 | 0.01 ± 0.0016 | 1.02 ± 0.11 | 1.01 ± 0.11 |
| | 1.2 | 0.25 ± 0.00077 | 460.11 ± 5.81 | 0.63 ± 0.065 | 29.36 ± 7.55 | 0.02 ± 0.0025 | 1.81 ± 1.11 | 1.74 ± 0.20 |
| | 2.2 | 0.27 ± 0.00046 | 456.15 ± 1.67 | -0.01 ± -0.004 | 1013.62 ± 606.08 | 0.03 ± 0.0046 | 2.24 ± 0.35 | 2.24 ± 0.35 |
| | 4 | 0.23 ± 0.00458 | 460.05 ± 2.35 | 0.00 ± -0.001 | 1548.19 ± 1934.27 | 0.03 ± 0.0058 | 2.51 ± 0.44 | 2.52 ± 0.44 |
| | 4.6 | 0.20 ± 0.00000 | 438.30 ± 2.53 | 0.02 ± 0.007 | 824.58 ± 209.28 | 0.07 ± 0.0012 | 5.21 ± 0.10 | 5.21 ± 0.10 |
| TM4 | 6.2 | 0.22 ± 0.00592 | 467.75 ± 1.95 | 0.34 ± 0.014 | 156.82 ± 1.28 | 0.08 ± 0.0025 | 6.21 ± 0.19 | 6.18 ± 0.19 |
| | 8.2 | 0.28 ± 0.00033 | 475.39 ± 1.56 | 2.29 ± 0.020 | 35.92 ± 0.06 | 0.10 ± 0.0011 | 7.41 ± 0.09 | 7.25 ± 0.13 |
| | 10.4 | 0.23 ± 0.00179 | 465.14 ± 2.26 | 1.41 ± 0.027 | 49.50 ± 0.14 | 0.10 ± 0.0018 | 7.65 ± 0.15 | 7.53 ± 0.16 |
| | 10.9 | 0.21 ± 0.00069 | 502.02 ± 5.99 | 1.88 ± 0.053 | 38.19 ± 8.86 | 0.11 ± 0.0031 | 8.23 ± 1.15 | 8.01 ± 0.32 |
| | 12.4 | 0.22 ± 0.00040 | 443.65 ± 2.53 | 0.73 ± 0.020 | 89.40 ± 0.54 | 0.10 ± 0.0017 | 7.84 ± 0.14 | 7.77 ± 0.14 |
| | 13.7 | 0.23 ± 0.00088 | 460.18 ± 3.61 | 2.77 ± 0.025 | 27.92 ± 0.04 | 0.11 ± 0.0015 | 8.32 ± 0.12 | 8.08 ± 0.18 |
| | 0.2 | 0.21 ± 0.00053 | 471.40 ± 6.11 | 0.19 ± 0.017 | 39.58 ± 153.69 | 0.01 ± 0.0117 | 0.81 ± 0.08 | 0.79 ± 0.13 |
| | 0.7 | 0.18 ± 0.00031 | 470.52 ± 2.35 | 0.24 ± 0.014 | 30.23 ± 0.19 | 0.01 ± 0.0011 | 0.99 ± 0.08 | 0.96 ± 0.09 |
| | 1.6 | 0.21 ± 0.00054 | 443.94 ± 6.13 | 0.08 ± 0.002 | 263.69 ± 207.90 | 0.03 ± 0.0012 | 2.36 ± 1.08 | 2.35 ± 0.09 |
| | 2 | 0.21 ± 0.00051 | 446.53 ± 2.64 | 0.00 ± 0.002 | 717.13 ± 317.65 | 0.03 ± 0.0049 | 2.39 ± 0.38 | 2.39 ± 0.38 |
| | 3.3 | 0.23 ± 0.00448 | 454.96 ± 4.37 | 0.77 ± 0.012 | 38.40 ± 0.09 | 0.04 ± 0.0011 | 3.14 ± 0.09 | 3.07 ± 0.09 |
| | 4.5 | 0.25 ± 0.00080 | 471.71 ± 2.40 | 0.84 ± 0.022 | 49.04 ± 0.36 | 0.06 ± 0.0019 | 4.09 ± 0.15 | 4.02 ± 0.15 |
| | 6 | 0.36 ± 0.00060 | 473.29 ± 2.38 | 0.60 ± 0.017 | 107.36 ± 0.74 | 0.06 ± 0.0010 | 4.57 ± 0.08 | 4.54 ± 0.08 |
| | 7.1 | 0.26 ± 0.00029 | 454.91 ± 1.58 | 0.22 ± 0.015 | 213.77 ± 4.31 | 0.07 ± 0.0017 | 5.00 ± 0.13 | 4.98 ± 0.13 |
| TM5 | 10.2 | 0.34 ± 0.01062 | 455.82 ± 1.93 | 0.17 ± 0.016 | 350.52 ± 14.22 | 0.07 ± 0.0027 | 5.16 ± 0.21 | 5.15 ± 0.21 |
| | 15.2 | 0.20 ± 0.00024 | 443.05 ± 1.58 | 0.37 ± 0.015 | 111.42 ± 1.35 | 0.07 ± 0.0018 | 5.43 ± 0.14 | 5.40 ± 0.14 |
| | 15.7 | 0.28 ± 0.00025 | 451.28 ± 1.47 | 0.74 ± 0.018 | 79.42 ± 0.62 | 0.07 ± 0.0016 | 5.47 ± 0.13 | 5.42 ± 0.13 |
| | 17 | 0.18 ± 0.00046 | 445.53 ± 6.01 | 0.12 ± 0.203 | 330.00 ± 241.76 | 0.07 ± 0.0013 | 5.61 ± 1.13 | 5.59 ± 0.10 |
| | 19 | 0.19 ± 0.00060 | 436.98 ± 2.71 | 0.07 ± 0.015 | 392.59 ± 42.21 | 0.08 ± 0.0059 | 5.77 ± 0.47 | 5.77 ± 0.47 |
| | 20.2 | 0.22 ± 0.00035 | 454.33 ± 1.67 | 2.23 ± 0.021 | 25.89 ± 0.03 | 0.09 ± 0.0012 | 6.50 ± 0.09 | 6.30 ± 0.15 |
| | 21.1 | 0.17 ± 0.00037 | 464.57 ± 3.36 | 0.16 ± 0.021 | 79.18 ± 3.55 | 0.09 ± 0.0040 | 6.80 ± 0.31 | 6.78 ± 0.31 |
| | 23.1 | 0.45 ± 0.00106 | 476.77 ± 6.15 | 3.69 ± 0.483 | 39.94 ± 61.96 | 0.11 ± 0.0007 | 8.16 ± 1.31 | 7.95 ± 0.19 |
| | 25.2 | 0.20 ± 0.00049 | 429.98 ± 6.06 | 0.15 ± 0.000 | 493.49 ± 318.75 | 0.12 ± 0.0015 | 9.43 ± 2.31 | 9.42 ± 0.13 |
| | 0.3 | 0.44 ± 0.00130 | 336.91 ± 5.03 | 12.93 ± 0.377 | 6.25 ± 8.39 | 8.39 ± 0.0018 | 4.99 ± 0.57 | 4.16 ± 0.74 |
| | 0.6 | 0.46 ± 0.00037 | 339.18 ± 1.41 | 6.06 ± 0.044 | 13.80 ± 0.12 | 0.06 ± 0.0068 | 4.81 ± 0.57 | 4.52 ± 0.59 |
| | 5.1 | 0.51 ± 0.00088 | 352.41 ± 2.35 | 0.49 ± 0.021 | 170.76 ± 2.17 | 0.06 ± 0.0010 | 4.68 ± 0.09 | 4.66 ± 0.09 |
| | 9.7 | 0.44 ± 0.00032 | 331.99 ± 1.34 | 0.02 ± 0.008 | 1412.70 ± 2248.45 | 0.06 ± 0.0014 | 5.03 ± 0.12 | 5.03 ± 0.12 |
| | 13.5 | 0.62 ± 0.00066 | 330.57 ± 1.54 | 0.01 ± 0.006 | 2068.04 ± 1433.29 | 0.06 ± 0.0007 | 5.01 ± 0.06 | 5.01 ± 0.06 |
| | 14.6 | 0.53 ± 0.00025 | 334.68 ± 1.14 | 0.11 ± 0.025 | 698.09 ± 243.62 | 0.06 ± 0.0007 | 5.13 ± 0.06 | 5.13 ± 0.06 |
| | 18.4 | 0.67 ± 0.00112 | 336.11 ± 1.69 | 0.15 ± 0.019 | 669.23 ± 72.31 | 0.06 ± 0.0009 | 5.17 ± 0.07 | 5.17 ± 0.07 |
| TM9 | 20.4 | 0.49 ± 0.00092 | 333.07 ± 2.34 | 0.18 ± 0.021 | 433.88 ± 32.24 | 0.06 ± 0.0016 | 5.36 ± 0.13 | 5.36 ± 0.13 |
| | 24.2 | 0.56 ± 0.00083 | 352.10 ± 2.37 | 0.12 ± 0.014 | 724.30 ± 53.11 | 0.07 ± 0.0015 | 5.30 ± 0.12 | 5.30 ± 0.12 |
| | 29.4 | 0.41 ± 0.00065 | 372.35 ± 1.73 | 1.62 ± 0.022 | 58.05 ± 0.23 | 0.08 ± 0.0011 | 6.10 ± 0.09 | 6.01 ± 0.11 |
| | 33.4 | 0.40 ± 0.00069 | 398.42 ± 1.73 | 0.12 ± 0.020 | 539.01 ± 40.71 | 0.07 ± 0.0013 | 5.91 ± 0.10 | 5.90 ± 0.10 |
| | 36.2 | 0.46 ± 0.00074 | 373.47 ± 2.37 | 2.07 ± 0.021 | 347.41 ± 9.75 | 0.07 ± 0.0011 | 6.01 ± 0.09 | 5.92 ± 0.10 |
| | 38.3 | 0.51 ± 0.00085 | 380.09 ± 1.67 | 0.76 ± 0.019 | 155.55 ± 1.17 | 0.08 ± 0.0009 | 6.28 ± 0.07 | 6.25 ± 0.07 |
| | 41.6 | 0.46 ± 0.00077 | 375.87 ± 1.68 | 4.01 ± 0.022 | 31.09 ± 0.03 | 0.09 ± 0.0007 | 7.13 ± 0.06 | 6.95 ± 0.12 |
| | 0.6 | 0.24 ± 0.00060 | 667.43 ± 6.76 | 0.86 ± 0.026 | 66.53 ± 157.69 | 0.08 ± 0.0015 | 5.22 ± 0.08 | 5.14 ± 0.13 |
| | 3.25 | 0.28 ± 0.00048 | 748.33 ± 1.67 | 1.00 ± 0.014 | 77.37 ± 0.36 | 0.09 ± 0.0012 | 5.85 ± 0.08 | 5.79 ± 0.08 |
| | 6.2 | 0.35 ± 0.00059 | 665.24 ± 1.65 | 0.32 ± 0.013 | 295.12 ± 3.32 | 0.09 ± 0.0009 | 6.20 ± 0.07 | 6.18 ± 0.07 |
| | 9.75 | 0.28 ± 0.00051 | 677.56 ± 1.65 | 0.82 ± 0.013 | 104.11 ± 0.39 | 0.10 ± 0.0009 | 6.69 ± 0.06 | 6.64 ± 0.07 |
| | 16.875 | 0.28 ± 0.00052 | 602.90 ± 1.67 | 0.59 ± 0.011 | 150.67 ± 0.74 | 0.11 ± 0.0008 | 7.31 ± 0.06 | 7.27 ± 0.06 |
| TM11 | 23 | 0.34 ± 0.00057 | 620.12 ± 1.73 | 0.45 ± 0.030 | 227.76 ± 5.60 | 0.11 ± 0.0029 | 7.57 ± 0.21 | 7.55 ± 0.21 |
| | 23 | 0.33 ± 0.16663 | 875.54 ± 7.30 | 0.31 ± 0.034 | 571.18 ± 38.05 | 0.15 ± 0.0017 | 7.65 ± 0.08 | 7.63 ± 0.11 |
| | 25.7 | 0.32 ± 0.00054 | 658.01 ± 1.70 | 0.77 ± 0.016 | 151.87 ± 0.84 | 0.12 ± 0.0010 | 8.36 ± 0.07 | 8.32 ± 0.08 |
| | 27.4 | 0.35 ± 0.00087 | 653.95 ± 6.77 | 0.54 ± 0.001 | 493.49 ± 318.75 | 0.12 ± 0.0015 | 8.80 ± 1.07 | 8.76 ± 0.09 |
| | 30.4 | 0.28 ± 0.14165 | 643.41 ± 6.24 | 0.23 ± 0.038 | 633.12 ± 52.60 | 0.14 ± 0.0018 | 9.10 ± 2.07 | 9.08 ± 0.11 |
| | 35.4 | 0.35 ± 0.17412 | 1093.81 ± 8.10 | 0.23 ± 0.036 | 33.86 ± 38.98 | 0.23 ± 0.0027 | 9.43 ± 1.45 | 9.41 ± 0.13 |
| | 37 | 0.39 ± 0.00093 | 635.63 ± 6.87 | 0.94 ± 0.945 | 263.69 ± 207.90 | 0.03 ± 0.0012 | 10.38 ± 2.45 | 10.33 ± 0.12 |
| | 0.4 | 0.16 ± 0.00019 | 1194.79 ± 1.68 | 3.40 ± 0.024 | 30.41 ± 0.04 | 0.22 ± 0.0024 | 11.24 ± 0.13 | 9.94 ± 1.2 |
| | 3.3 | 0.21 ± 0.00023 | 1075.41 ± 1.57 | 1.41 ± 0.023 | 95.93 ± 0.41 | 0.22 ± 0.0023 | 12.06 ± 0.14 | 11.62 ± 0.42 |
| | 5 | 0.25 ± 0.00041 | 632.64 ± 1.67 | 0.20 ± 0.017 | 574.07 ± 21.97 | 0.18 ± 0.0038 | 12.56 ± 0.28 | 12.49 ± 0.28 |
| | 6.1 | 0.25 ± 0.00030 | 697.78 ± 1.58 | 2.60 ± 0.021 | 59.19 ± 0.11 | 0.20 ± 0.0015 | 13.63 ± 0.11 | 12.83 ± 0.76 |
| TM13 | 7.8 | 0.24 ± 0.00045 | 734.75 ± 2.34 | 2.68 ± 0.021 | 56.79 ± 0.11 | 0.21 ± 0.0016 | 13.85 ± 0.12 | 13.01 ± 0.81 |

All errors are $2\sigma$. *Distance is from top of each stalagmite*

a. $\delta^{234}U = [(^{234}U/^{238}U)\text{-}1]*1000$ where $(^{234}U/^{238}U)$ is the measured activity ratio

b. Round brackets signify activity ratios

All errors are $2\sigma$. Distance is from top of each stalagmite

c. Age is calculated using half lives from (*Cheng et al.*, 2000) and is relative to 1950

Raw ages are corrected for inital $^{230}Th$ content by assuming $(^{230}Th/^{232}Th) = 1.21$ for TM4, TM5, TM9,and TM11

Raw ages are corrected for inital $^{230}Th$ content by assuming $(^{230}Th/^{232}Th) = 3.7$ for TM13

Uncertainties incorporates mass spectrometric,weighing and spike uncertainties

# Chapter 3

# Hydrologic variability during the Younger Dryas and Holocene based on speleothems from Laos

## 3.1 Introduction

The Asian monsoon (AM) transports heat and moisture from the tropics to higher latitudes and generates intense seasonal precipitation in AM region, therefore affecting the livelihood of the world's most populous regions. Yet general circulation model (GCM) projections of future regional-scale hydrologic change still remain uncertain (*Bollasina and Nigam*, 2009), hampering efforts to conduct appropriate planning. Recent analyses of instrumental data show pronounced spatial variability in regional precipitation patterns in the Asian monsoon region (*Conroy and Overpeck*, 2011a; *Dayem et al.*, 2010), with the identification of several sub-domains which display more coherent precipitation variability, including the East Asian monsoon (EAM), the Indian Summer monsoon (ISM; or the India-China monsoon) and

the Southeast Asian monsoon (SEAM). Due to the short instrumental record and a sparse paleoclimate record within certain regions, it is unclear whether precipitation changes across the broad AM region behaved in a similarly incoherent manner over decadal to orbital timescales, in response to larger forcings, and/or under different background climates. To address this issue, it is necessary to: i) fill gaps in the paleoclimate record of the AM region; ii) investigate spatial and temporal patterns in these records; iii) use this data to investigate mechanisms of AM variability on a range of timescales, and thus provide a valuable test for GCM simulations.

Paleoclimate records have significantly advanced our understanding of EAM and ISM variability on orbital to multidecadal timescales (e.g. *Wang et al.*, 2008; *Berkelhammer et al.*, 2010). Over the last decade, a large network of paleoclimate records from regions affected by the Asian monsoon have begun to emerge. Most notably, speleothem records from China, Oman, Yemen, and India have provided remarkable insight into the behavior of the Asian monsoon through the Late Pleistocene and Holocene (e.g. *Wang et al.*, 2008; *Sinha et al.*, 2007; *Fleitmann et al.*, 2007; *Shakun et al.*, 2007). Moreover, in recent years, speleothem records from the tropical and southern sector of the greater Asian-Australian monsoon have filled in the broader picture of Indo-Pacific paleoclimate (e.g. *Partin et al.*, 2007; *Meckler et al.*, 2012; *Griffiths et al.*, 2009, 2010,b). However, despite this increased level of interest in tropical Indo-Pacific and monsoonal climates in recent years, there is still a need for well-dated high-resolution paleoclimate records from this region, particularly over the Indochina peninsula where there is an obvious gap in the proxy network.

Gaining a clearer understanding of the spatial behavior of the Asian monsoon is of critical importance given that the region has played a role in transmitting climate signals from the North Atlantic to the southern latitudes during the deglacial stadial events, namely Heinrich Stadial 1 (HS1) and the Younger Dryas (YD). Specifically, Denton (Denton et al., 2010) and others (Skinner et al., 2010; Anderson et al., 2009; Cheng et al., 2009) have proposed

that meltwater entering the North Atlantic during HS1 and the YD reduced the formation of North Atlantic Deep Water, causing marked diminution of the Atlantic meridional overturning circulation (AMOC), and an expansion in Northern Hemisphere sea-ice. The resultant steepened thermal gradients in the Northern Hemisphere are thought to have led to southward shifts of the ITCZ and Southern Hemisphere westerly wind belts, producing Southern Hemisphere warming (Blunier and Brook. 2001) and increased release of $CO_2$ from the southern ocean. A strengthened Australian-Indonesian monsoon during the YD (Griffiths et al., 2009; Muller et al., 2008) has added considerable weight to this hypothesis. However, there is still some uncertainty as to exactly how this signal was propagated southward across the equator from China to Indonesia/northern Australia because, hitherto, lake (Maxwell, 2001), pollen (Penny, 2001; White et al., 2004), and freshwater bivalve (Marwick and Gagan, 2011) records provide only low-resolution and/or fragmentary information on monsoon behavior over the Indochina region during the deglaciation and Holocene. For instance, the HS1 and YD signals preserved in the Chinese cave records (e.g. Wang et al., 2008) were not clearly reflected in a recent synthesis (Cook and Jones, 2012). Tierney et al. (2012) recently noted, using a Holocene marine $\delta D$ plant leaf-wax record off of Sulawesi and a series of GCM simulations, that orbital forcing caused heterogeneous changes in precipitation across the IPWP during the Holocene. Given the above mentioned heterogeneity of published records from SE Asia and similar observations in the instrumental record (Conroy and Overpeck, 2011), it is highly likely that the greater Asian monsoon behaved in a similar fashion to its Southern Hemisphere counterpart, whereby changing climate forcings produced markedly different rainfall patterns over SE Asia during the deglaciation and Holocene.

Laos speleothems are uniquely situated to fill in the spatial and temporal gaps in the paleohydrologic record of continental Southeast Asia, yet are thus far underutilized, despite the fact that limestone caves are widespread throughout the Indochina peninsula. Speleothems are well-suited for terrestrial climate reconstruction because: (i) they tend to be very pure and well-preserved; (ii) they usually contain clear visible growth banding which, like tree

rings, is often annual in nature; (iii) they can be very precisely dated using U-Th dating; and (iv) they contain numerous types of physical and geochemical climate proxy data (*Fairchild et al.*, 2006). Here we present new stable isotopes based ($\delta^{18}$O and $\delta^{13}$C) speleothem records of SEAM variability from Tham Mai cave in northern Laos(20.75N, 102.65E, elevation 360 m) for the last $\sim$ 13 kyr Bp. We developed decadal resolution stable isotope records, spanning the Younger Dryas and Holocene, to investigate orbital to decadal scale climate variability in the region. Furthermore, we combined a detailed modern calibration study, analysis of isotope-enabled General Circulation Model (GCM) simulations, and forward-modeling of speleothem $\delta^{18}$O to robustly interpret the new speleothem records. Through rigorous chronological control, replication, proxy calibration, and data-model synthesis, these new records from Laos represent the first high-resolution records from SEAM region that span from the Holocene to the Younger Dryas.

## 3.2 Cave location and sample description

Tham Mai cave is located in NE Laos, near the Vietnamese border. This 2010 m long cave is extremely well-suited for paleoclimate reconstruction as it is hydrologically active, contains numerous actively forming stalagmites, and has only one known entrance. Five speleothems(TM4, TM5, TM9, TM11, and TM13) were collected from Tham Mai cave(Fig.3.2). TM9, TM11 and TM13 were collected from the same location in the upper level of the cave. TM4 and TM5 were collected from the same location, deeper inside the cave. TM4 is 14 cm long with an average growth rate of 35 $\mu$m/yr. Growth of TM4 occurred in two intervals: 1.01 $\pm$ 0.11 to 2.52 $\pm$ 0.44 kyr BP and 5.21 $\pm$ 0.10 to 8.08 $\pm$ 0.18 kyr BP. TM5 is 22 cm long with average growth rate of 68 $\mu$m/yr. Growth of TM5 occurred from 0.79 $\pm$ 0.09 to 9.42 $\pm$ 0.13 kyr BP. TM9 is 45 cm long with an high average growth rate of 390 $\mu$m/yr. Growth of TM9 occurred from 4.16 $\pm$ 0.59 to 6.95 $\pm$ 0.12 kyr BP. TM11 is 33 cm long with

an average growth rate of 79 $\mu$m/yr. Growth of TM11 occurred from 5.14 $\pm$ 0.08 to 10.33 $\pm$ 0.12 kyr BP. TM13 is 22 cm long with average growth rate of 22 $\mu$m/yr. Growth of TM13 occurred from 9.94 $\pm$ 1.22 to 13.01 $\pm$ 0.81 kyr BP.

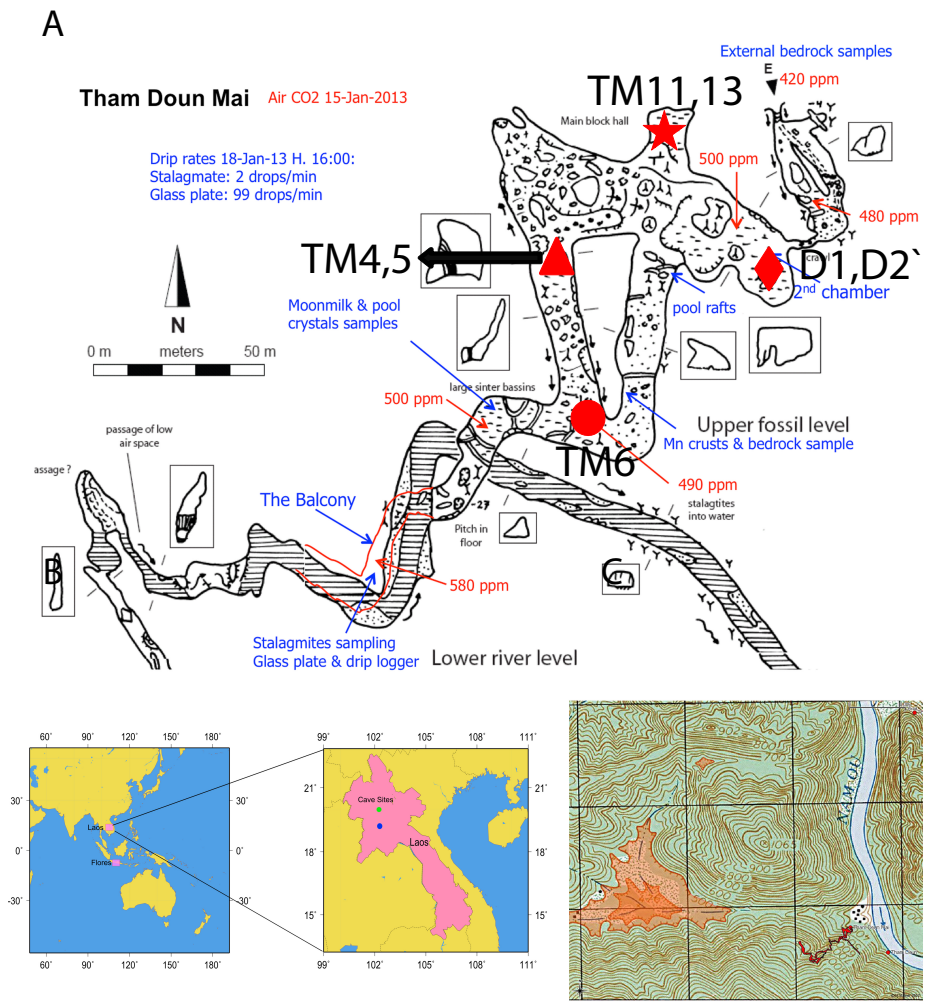


Figure 3.1: A) Map of Tham Mai cave with stalagmite samples locations, red star is location of TM9, TM11 and TM13, red triangle is location of TM4 and TM5, red circle is TM6, red diamond is drip water collection locations D1 and D2. Blue text is cave interior description, red text is cave $CO_2$ measurement from from January 15th 2013 filed trip (courtesy of Northern Lao- European Cave Project and And Andrea Borsato); B) Location map of Tham Mai cave (green dot) in Luang Phrabang province, Laos (20.75 N, 102.65 E,elevation 360 m); C) Contour map of Tham Mai cave (red)

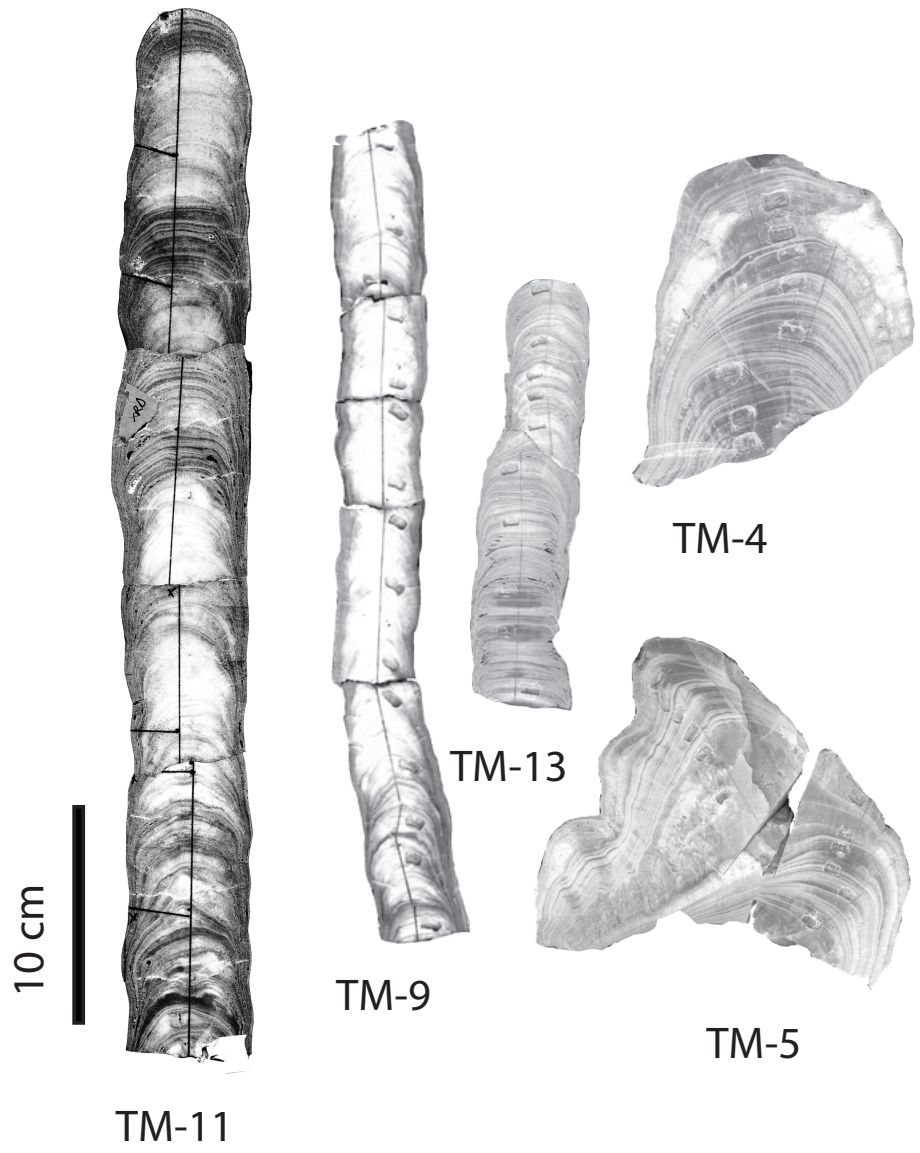


Figure 3.2: Tham Mai cave stalagmites used for reconstructing SEAM hydroclimate variability over past 13 kyr BP, collected during field work in 2010

## 3.3 Modern climatology

The mean annual precipitation near the cave site is 1195 mm, and 67 % of rain falls during the summer monsoon season from June to September. The modern climate of our study site in northern Laos is dominated by the SEAM, and is thus characterized by a highly seasonal rainfall regime. During the Northern Hemisphere winter (Dec-Mar) the study site is exceptionally dry with very little precipitation. The onset of the SEAM generally occurs in May, as increased continental heating enhances the land-sea thermal contrast, resulting in a complete reversal in the surface winds from the northeast to the southwest. These stronger summer monsoonal winds carry with them moisture-laden air masses sourced primarily from the Indian Ocean.

We utilize interpolated data calculated from raw GNIP data (*Bowen and Wilkinson*, 2002b; *Bowen and Revenaugh*, 2003) to estimate the monthly mean oxygen isotope composition of precipitation at Tham Mai cave. Instrumental precipitation data from the Global Precipitation Climatology Project (GPCP) data version 2.2 is used to estimate the monthly mean precipitation at Tham Mai cave. Fig.3.1 shows that Laos precipitation peaks during May, and precipitation $\delta^{18}$O has the lowest values during August.

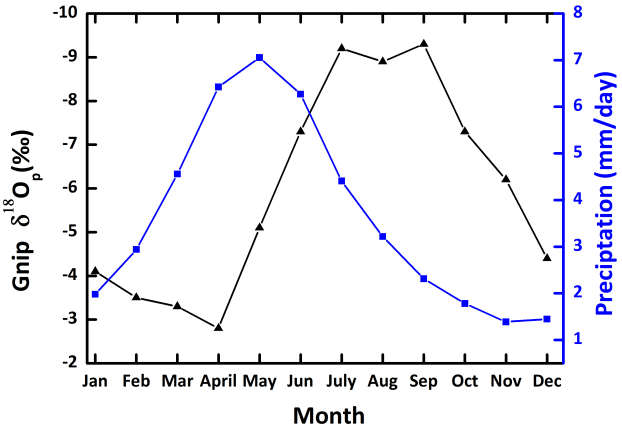


Figure 3.3: Comparison of interpolated GNIP $\delta^{18}$O and GPCP precipitation from the grid point closest to Tham Mai cave

The Global Network for Isotopes in Precipitation (GNIP) contains only a few incomplete years of data for Luang Prabang, Laos, so to investigate the climatic controls on precipitation $\delta^{18}$O at our site we also conducted analyses on more complete GNIP data from Hanoi ($\sim$300 km to the E), Kunming ($\sim$450 km to the N), and Bangkok ($\sim$850 km to the S). All sites show a strong seasonality in rainfall amount and $\delta^{18}$O values, with summer monsoon moisture being significantly depleted in $\delta^{18}$O with respect to boreal winter rainfall (Fig.3.4). Furthermore, each site shows a significant negative correlation between monthly precipitation amounts and $\delta^{18}$O values, though unfortunately the datasets are too short to assess this relationship on the annual or longer timescales that are more relevant for speleothem records. To investigate controls on longer timescales, we must utilize either model-based or reconstructed precipitation $\delta^{18}$O time series, which is discussed in section 3.10.

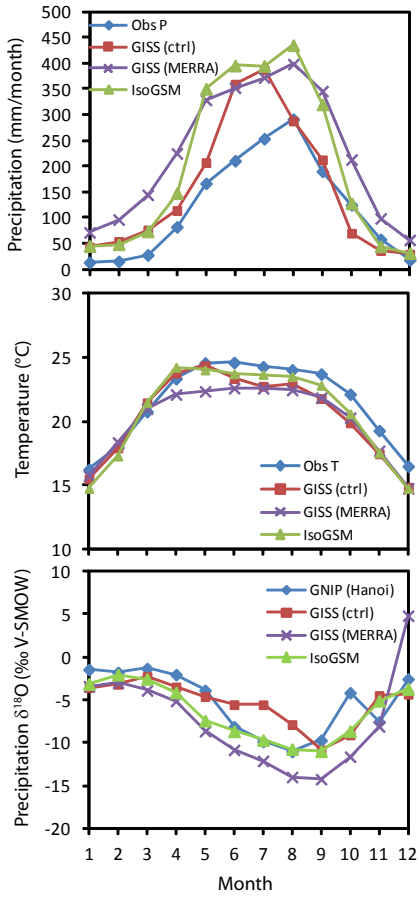


Figure 3.4: Monthly averages of precipitation (top), temperature (middle), and $\delta^{18}O_p$ (bottom) for our study site from observations (blue curves; temperature and precipitation: CRU TS 3.21 data, 1901-2012;$\delta^{18}O_p$: Hanoi, GNIP, 2004-2007) and climate model output (red curve: GISS ModelE2-R time-slice control run; purple curve: ModelE2 MERRA nudged run (1979-2009); green curve: 20th century IsoGSM (1871-2010))

## 3.4 Analytical Methods

### 3.4.1 Cave monitoring

The measured speleothem calcite $\delta^{18}$O ($\delta^{18}O_c$) value is a function of the $\delta^{18}$O value of the drip water($\delta^{18}$O $_{water}$), and cave mean annual temperature (Equations below). The $\delta^{18}$O value of cave drip water is a reflection of the precipitation above the cave site (*Matthew S. Lachniet*,

2009), which is influenced by regional and global water cycle. For tropical speleothems, the variations of measured calcite $\delta^{18}$O generated by the fractionation between the water and calcite is negligible in caves with a relatively constant temperature. Therefore, variations in $\delta^{18}$O values of precipitation are usually larger than the fractionation between the water and calcite (*Rozanski et al.*, 1993; *Gat*, 1996). Thus, in caves with a relatively constant temperature, variations in the drip water $\delta^{18}$O are primarily a reflection of the precipitation $\delta^{18}$O above the cave. Other in-cave processes that can lead to isotopic variations in the drip water and eventually speleothems, include changes in drip rate (*Scholz et al.*, 2009, e.g.), water evaporation (e.g *Hendy*, 1971; *Deininger et al.*, 2012), and kinetic isotopic fractionation (*Hendy*, 1971; *Mickler, Patrick J. and Banner, Jay L. and Stern, Libby and Asmerom, Yemane and Edwards, R. Lawrence and Ito, Emi*, 2004, e.g.).

While speleothem calcite $\delta^{18}$O values can be affected by kinetic fractionation, under equilibrium conditions, speleothem calcite $\delta^{18}$O value is only affected by the $\delta^{18}$O value of the drip water and the cave temperature (*Kim, Sang-Tae and O'Neil, James R.*, 1997). Assuming equilibrium deposition, the measured $\delta^{18}O_c$ depends only on the $\delta^{18}$O of cave drip water and cave temperature.

Equations:

$10001\,\mathrm{n}\alpha = 18.03\,(10^{3}\mathrm{T}^{-1}) - 32.42$

$\delta^{18}O_c$ (SMOW)$= (\alpha(\delta^{18}\mathrm{O}_{\,water} + _{1000})) - 1000$

$\delta^{18}O_c$ (PDB)$= (\alpha(\delta^{18}O_c\ (\mathrm{SMOW}) + _{1000})) - 1000$

where:

-$\alpha$ is calcite-water fractionation factor

-$\delta^{18}O_c$ is measured speleothem calcite $\delta^{18}$O;

-$\delta^{18}\mathrm{O}_{\,water}$ is drip water $\delta^{18}$O

In order to better understand site-specific speleothem formation, such as the hydrological and geochemical behavior of cave drip water and other environmental variables in the cave, and to access if a specific speleothem is formed under equilibrium conditions, a detailed and continuous monitoring program is needed. Intensive cave monitoring studies are a prerequisite to develop well-dated, high resolution records of past climate change using speleothem samples.

During the December 2010 and January 2013 fieldwork, we collected speleothems and cave drip water; conducted a suite of hydro-geochemical measurements (alkalinity, pH, conductivity); installed and maintained data loggers to continuously monitor cave temperature, relative humidity(RH), and drip rate; and trained a local contact (Mr.Sai, head of the nearest village) to collect monthly drip water samples and count drip rates for our collection sites.

Cave temperature and RH were measured by HOBO U23 Pro v2 Temperature/Relative Humidity Data Logger. Cave $pCO_2$ was measured with a Telaire 7001 portable $pCO_2$ monitor. Drip water $\delta^{18}O$ and $\delta D$ were analyzed on a Temperature Conversion Elemental Analyzer (TC/EA) coupled to a Thermofinnigan Delta Plus XP isotope ratio mass spectrometer(IRMS) instrument.

Cave monitoring programs were conducted in three caves in Laos, two adjacent caves(19.72N,102.07E), Tham Duk (165 m long, elevation 779 m), Tham Loum(1.6 km long) , and Tham Mai(20.75 N, 102.65 E,elevation 360 m), although only speleothems collected from Tham Mai cave are presented for the purpose of reconstructing the Holocene hydrological cycles in this thesis. Speleothems from Tham Duk and Tham Loum are not the major focus of this thesis. However, since these cave are not far from each other, cave monitoring results from Tham Duk and Tham Loum are also presented. Drip water samples from Tham Duk and Tham Loum were collected from 01/2010 to 12/2011. Drip water samples from Tham Mai were collected from 01/2011 to 12/2011.

### 3.4.2 Sample sectioning and microsampling

The five stalagmite samples, TM4, TM5, TM9, TM11 and TM13, were sectioned in half parallel to their growth axis and then polished. XRD analyses showed that all of the samples are composed of 100% calcite. Samples for isotopic ratio measurements were drilled along the stalagmite's central axis. Stalagmite surfaces and drill bit were cleaned with Ethanol prior to sampling. The older portion (pre-hiatus, ∼5.21 kyr BP to 8.08 kyr BP ) of TM-4 was sampled at 250 $\mu$m resolution (∼8-10 years) using a Sherline micromill and the younger portion was sampled at 50 $\mu$m resolution (∼5years) using a New Wave MicroMill drill. The younger portion (∼0.479 kyr BP to 5.02 kyr BP ) of TM-5 was sampled at 500 $\mu$m resolution (∼20-30 years) , and the older portion (∼5.02 kyr BP to 7.38 kyr BP) was sampled at 1 mm resolution (∼5-10years) using a Sherline micromill. TM11, and TM13 are sampled at 500 $\mu$m resolution using a Sherline micromill, which is equivalent to approximately 5-7 years resolution. TM9 was sampled at 1mm resolution, which is approximately 4-6 years resolution.

### 3.4.3 Hendy test

Under isotopic equilibrium conditions, $\delta^{18}$O variations along speleothem growth axes reflect changes in drip water $\delta^{18}$O composition and/or cave temperature. Under kinetic fractionation due to rapid $CO_2$ degassing and/or evaporation, a significant variation in $\delta^{18}$O along a growth band and a correlation between $\delta^{18}$O and $\delta^{13}$C would be observed (*Hendy*, 1971).

To determine whether isotopic equilibrium was consistent within each stalagmite, we conducted Hendy tests on TM4 and TM11 (*Hendy*, 1971). The Hendy test measures the multiple $\delta^{18}$O and $\delta^{13}$C values from a single growth lamina (Fig.3.5 solid squares) and along the growth axis (Fig.3.5 open circles) of a stalagmite. Samples were taken by a Dremel Drill with a diamond dental drill bit to collect calcite powder (∼50 $\mu$g per each sample). Three

growth layers and 21 samples in total were measured for TM4; two growth layers and 12 samples in total were measured for TM11.

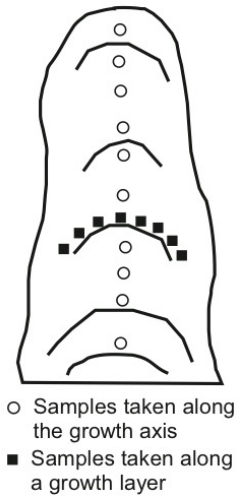


Figure 3.5: Schematic diagram of a stalagmite, showing samples taken along a growth layer(solid square) for Hendy test, and samples taken along growth axis(open circles) for isotopic ratios analysis (adapted from (*Mickler et al.*, 2006))

### 3.4.4 $U - Th$ dating

The chronology of Tham Mai cave stalagmites have been established by $U - Th$ dating. The $U - Th$ dating was conducted at the University of Oxford via MC-ICP-MS methods. 0.1-0.2 g samples were taken every 1-2 cm along growth axes. Stalagmite calcite samples were dissolved, spiked with a mixed $^{229}Th/^{236}U$ spike, purified by ion-exchange chemistry, and analysed by multi-collector ICP mass spectrometer(Nu Instruments). Techniques broadly followed those used for other carbonate samples at Oxford (*Robinson et al.*, 2002). U/Th ages are corrected for the presence of small amounts of initial Th using a ($^{230}Th/^{232}Th$) ratio of 1.21 ± 50% for TM4, TM5, TM9,and TM11. An initial ($^{230}Th/^{232}Th$) ratio of 3.7±50% is used for TM13. 68 $U - Th$ dates in total have been utilized for final age models.

### 3.4.5 Stable isotopes

Powdered calcite samples were analyzed for stable isotope composition utilizing a Kiel IV-carbonate device coupled with a Thermofinnigan Delta V Plus isotope ratio mass spectrometer at UC Irvine. A total of 16 standards (NBS-19, NBS-18, and OX, an in-house quality control standard) were analyzed during each run of 30 unknown samples. The results of isotopic analysis are presented in conventional delta ($\delta$) notation, defined as:

$$\delta^{18}\mathrm{O} = (^{18}\mathrm{O}/\ ^{16}\mathrm{O})_{sample}/(^{18}\mathrm{O}/\ ^{16}\mathrm{O})_{standard} - 1] * 1000$$

The standard deviation of repeated NBS-19 measurements is $\sim$0.06‰ for $\delta^{18}$O. Values are reported with respect to Vienna Pee Dee Belemnite (VPDB) standard.

A total of 2967 samples were measured for stable isotopic ratios of oxygen ($\delta^{18}$O) and carbon ($\delta^{13}$C). 1022 samples have been measured from TM4, 388 samples have been measured from TM5, 423 samples have been measured from TM9, 742 samples have been measured from TM11, and 392 samples have been measured from TM13.

## 3.5 Chronology and age models

$U - Th$ ages increases systematically with depth for each stalagmites (all ages are reported relative to 1950, years BP). TM5, TM9, TM11 and TM13 grew continuously throughout the dating period. TM4 grew from $\sim$1.01 - 8.08 kyr BP with a hiatus at $\sim$2.5kyr BP to $\sim$5.21 kyr BP, TM5 grew from $\sim$0.79 - 9.43 kyr BP, TM9 grew from $\sim$4.16 - 6.95 kyr BP, TM11 grew from $\sim$5.14 - 10.33 kyr BP, TM13 grew from $\sim$9.94 - 13.01 kyr BP. Detailed $U - Th$ results are reported in Chapter 2. Age models were developed using the StalAge algorithm, which takes into account dating errors throughout the length of the record (*Scholz and Hoffmann*, 2011).

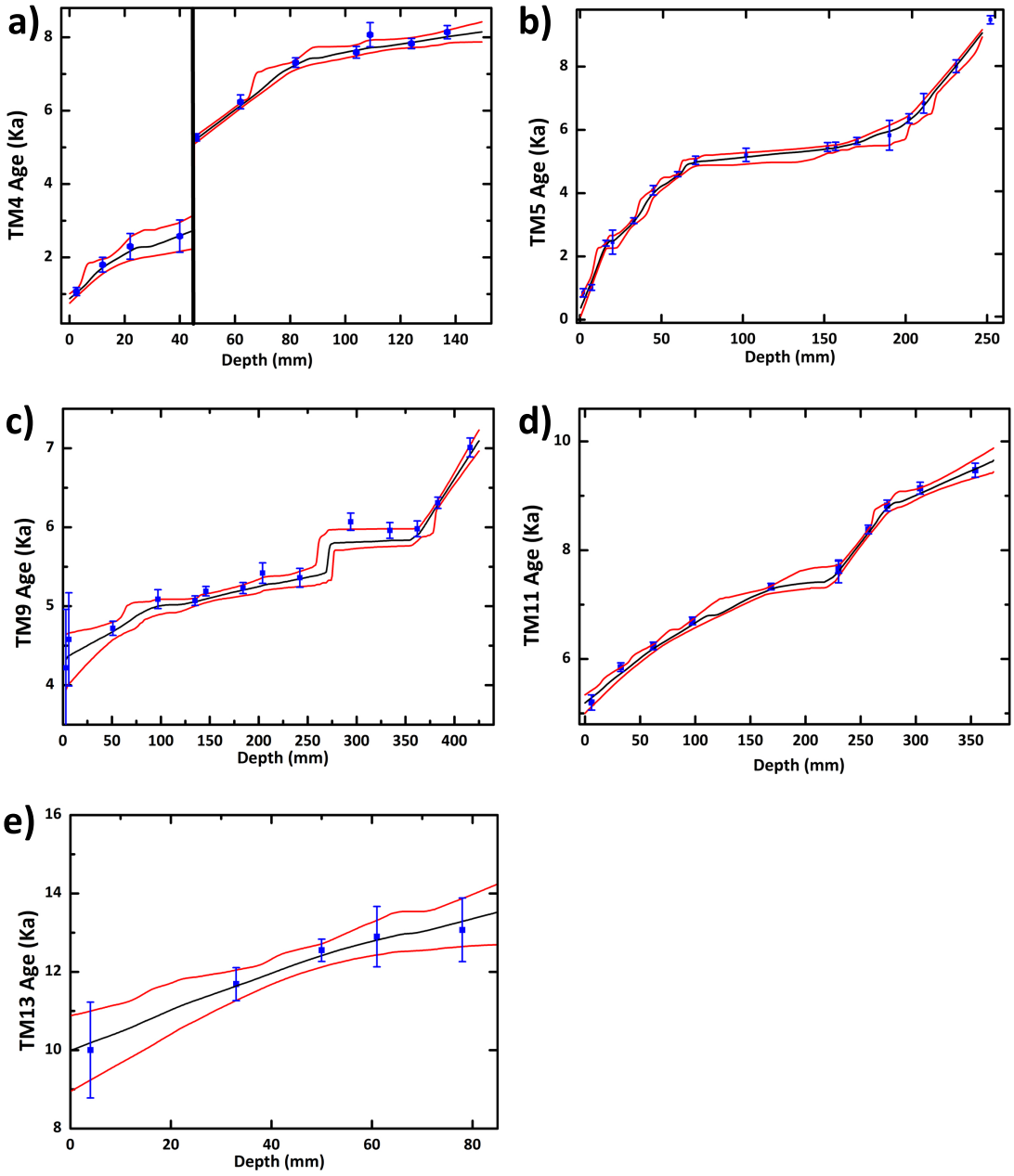


Figure 3.6: Plot of the age versus depth for stalagmites a)TM4, b)TM5, c)TM9, d)TM11, and e)TM13. All ages are reported as year before the present (1950 AD), years BP. The age error indicated in the plots are $2\sigma$ error. Age model results are produced using StalAge *Scholz and Hoffmann* (2011)

## 3.6 Results

### 3.6.1 Cave monitoring

Cave monitoring results show that the average temperature in Tham Mai cave was 21.98 ± 0.38 $^{o}$C and cave air relative humidity is greater than 95%, indicating that speleothem calcite $\delta^{18}$O is not likely influenced by large kinetic effects or seasonal temperature swings. Cave air $pCO_2$ in 2013 measured 580 ppm and indicates that the cave is well ventilated. Monthly drip rates measured in 2011 at one location show an increase from minimum values (6/min) beginning around the start of the summer monsoon to a maximum of (20 drips/min) in October.

Thirty-one dripwater samples collected in December during 2010-2013 from several locations (D1 and D2) in the Tham Mai cave, including from some stalagmite sampling locations, have an average $\delta^{18}$O (reported relative to Vienna Standard Mean Ocean Water(VSMOW)) of -8.4±0.23‰, very close to GNIP precipitation(JJAS) weighted average $\delta^{18}$O of -8.3‰. The seasonal cycle does not match with GNIP $\delta^{18}$O data, which is probably due to mixing within different reserviors within the epikarst(Fig.3.7 and Fig.3.8).

Drip rates of Tham Mai cave are collected in two ways: installed drip loggers and manually counted drip rate by us and also our collaborator Sai. The manually counted drip rate peaks around October(20 drips/min), which is about 1 month lag off of the GNIP precipitation $\delta^{18}$O peak(Fig.3.9). The second smaller peak is in January. These two peaks, 01/2011 and 10/2011 drip rate peak, are also indicated in drip logger output(Fig.3.10).

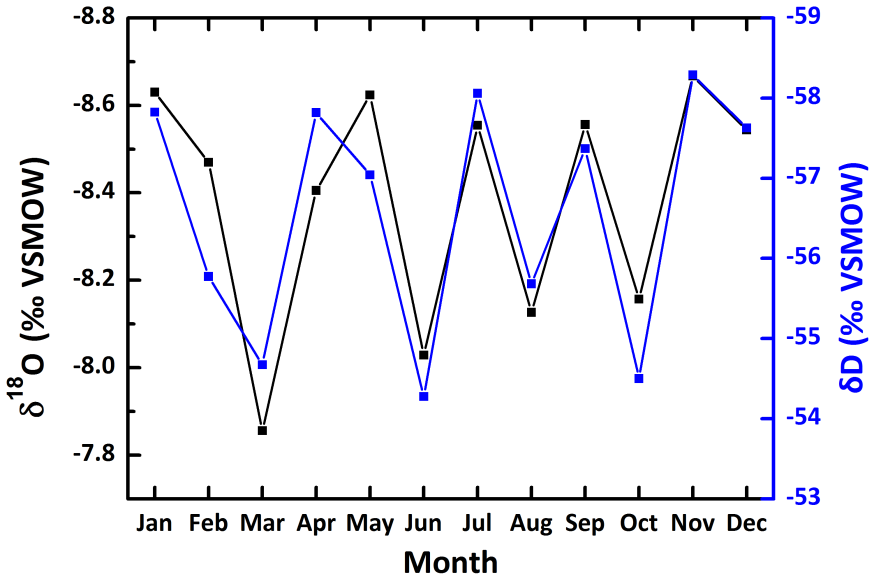


Figure 3.7: Tham Mai cave monthly drip water D1 $\delta^{18}$O from 01/2011 to 12/2012, location of D1 is shown in Fig.1.1

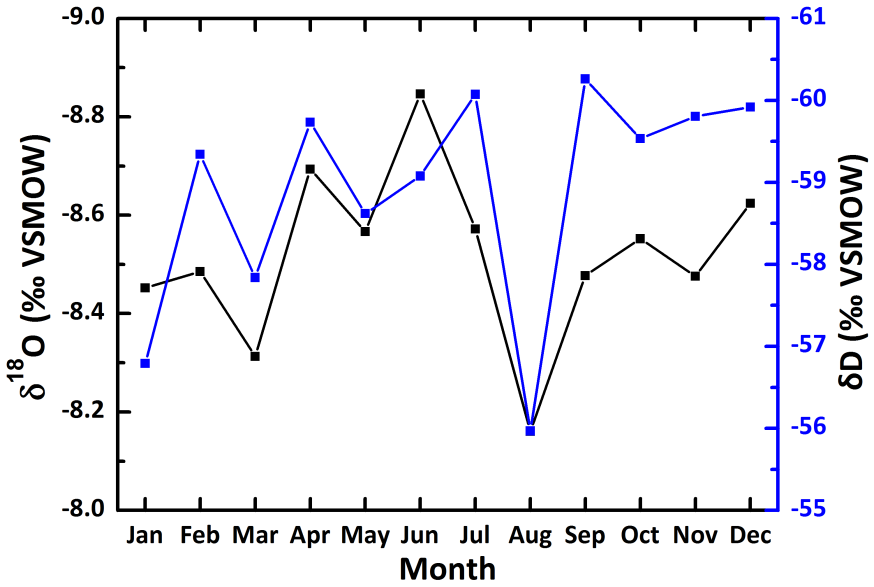


Figure 3.8: Tham Mai cave monthly drip water D2 $\delta^{18}$O from 01/2011 to 12/2012, location of D2 is shown in Fig.1.1

Table 3.1: Tham Mai cave drip water isotopic from 12/09/10 to 12/03/11

| TM drip water location 1 | | | TM drip water location 2 | | |
|---|---|---|---|---|---|
| Sample Date | $\delta$D (‰ VSMOW) | $\delta^{18}$O (‰ VSMOW) | Sample Date | $\delta$D (‰ VSMOW) | $\delta^{18}$O (‰ VSMOW) |
| 1/3/11 | -57.82 | -8.63 | 1/3/11 | -56.79 | -8.45 |
| 2/2/11 | -55.77 | -8.47 | 2/2/11 | -59.34 | -8.49 |
| 3/4/11 | -54.67 | -7.86 | 3/4/11 | -57.84 | -8.31 |
| 4/2/11 | -57.82 | -8.41 | 4/2/11 | -59.73 | -8.69 |
| 5/2/11 | -57.04 | -8.62 | 5/2/11 | -58.62 | -8.57 |
| 6/3/11 | -54.28 | -8.03 | 6/3/11 | -59.08 | -8.85 |
| 7/2/11 | -58.06 | -8.55 | 7/2/11 | -60.07 | -8.57 |
| 8/4/11 | -55.68 | -8.13 | 8/4/11 | -55.97 | -8.16 |
| 9/3/11 | -57.37 | -8.56 | 9/3/11 | -60.26 | -8.48 |
| 10/2/11 | -54.50 | -8.16 | 10/2/11 | -59.53 | -8.55 |
| 11/4/11 | -58.29 | -8.67 | 11/4/11 | -59.80 | -8.48 |
| 12/3/11 | -57.63 | -8.54 | 12/3/11 | -59.92 | -8.62 |
| Average: $\delta$D is -57.75±1.84; $\delta^{18}$O is -8.45±0.23<br>T = 23.11$^o$C, RH=95% | | | | | |

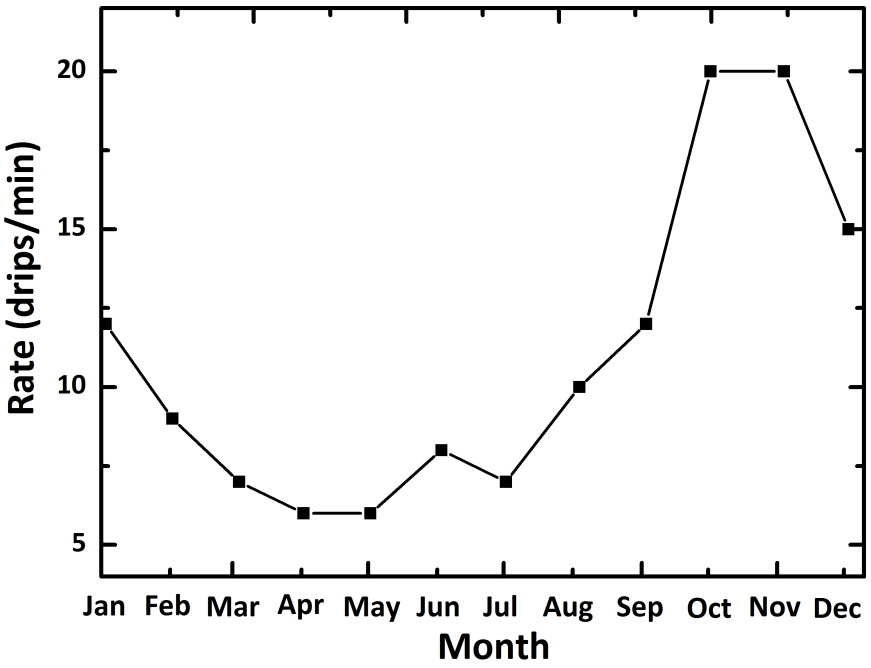


Figure 3.9: Tham Mai cave drip rate of drip water collection site 1 (D1) from 01/2011 to 12/2011

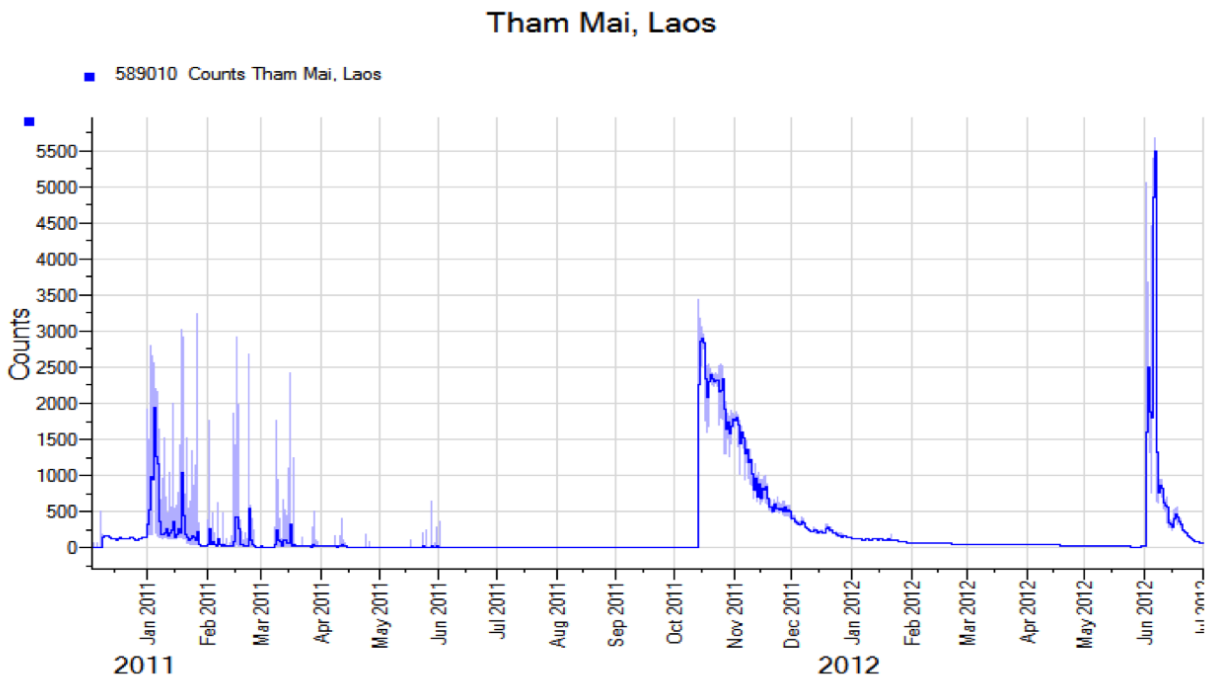


Figure 3.10: Tham Mai cave drip logger results from 2011 to 2012

We also conducted cave monitoring program in two other adjacent caves: Tham Duk and Tham Loum cave, from 2010 to 2011. Although these two caves are not the major focus of this thesis, the cave monitoring results from these two caves is still usuful since these three caves are not far from each other.

During our trip in 2010, the mean temperature of Tham Duk cave was 19.8 $^{o}$C, with relative humidity around 78.55%. The relatively small relative humidity introduce enhanced evaporation which will increase $\delta^{18}$O values of both drip-water and calcite (*Hendy*, 1971). The mean temperature of Tham Loum cave is 19.6$^{o}$C, with relative humidity greater than 95%. 12 drip water samples were collected monthly for Tham Duk cave and Tham Loum cave respectively.

The average drip water $\delta^{18}$O of Tham Duk cave is -8.10±0.59‰. The average drip water $\delta^{18}$O of Tham Loum cave is -7.79±0.87‰. Drip water samples collected from Tham Duk cave and Tham Loum cave are both characterized by a strong seasonal cycle with a peak

around August and September(Fig.3.11). This is consistent with the seasonal peak of GNIP precipitation $\delta^{18}$O (Fig. 3.1).

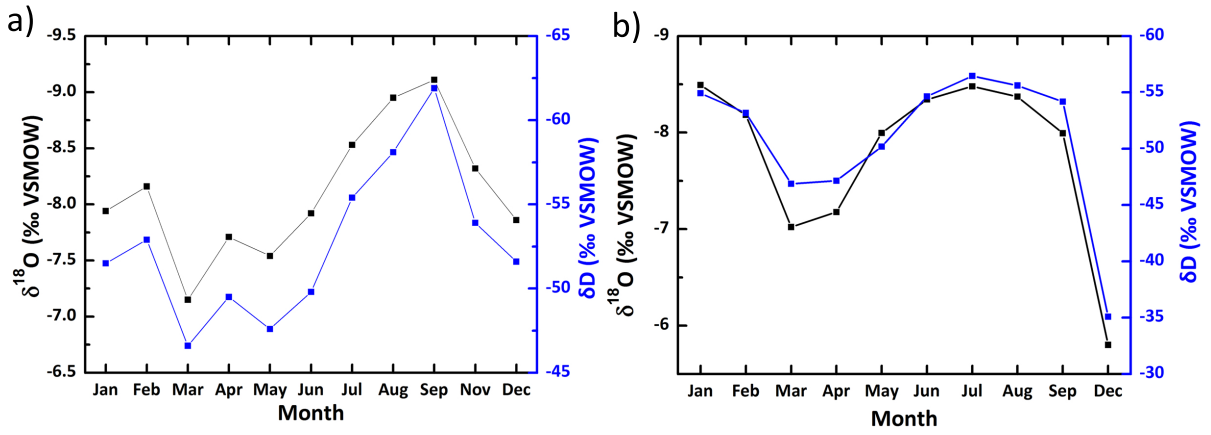


Figure 3.11: a)Tham Duk cave and b)Tham Loum cave drip water $\delta^{18}$O from 01/2010 to 12/2010

Table 3.2: Tham Duk cave drip water isotopic from 12/09/10 to 12/03/11

| Sample Date | $\delta$D (‰ VSMOW) | $\delta^{18}$O (‰ VSMOW) | Sample Date | $\delta$D (‰ VSMOW) | $\delta^{18}$O (‰ VSMOW) |
|---|---|---|---|---|---|
| 1/15/10 | -51.5 | -7.94 | 7/5/10 | -55.4 | -8.53 |
| 2/14/10 | -52.9 | -8.16 | 8/14/10 | -58.1 | -8.95 |
| 3/14/10 | -46.6 | -7.15 | 9/14/10 | -61.9 | -9.11 |
| 4/14/10 | -49.5 | -7.71 | / | / | / |
| 5/16/10 | -47.6 | -7.54 | 11/10/10 | -53.9 | -8.32 |
| 6/3/10 | -49.8 | -7.92 | 12/11/10 | -51.6 | -7.86 |
| Average: $\delta$D is -52.60±4.53; $\delta^{18}$O is -8.10±0.59<br>T = 19.8$^o$C, RH = 78.55% | | | | | |

Table 3.3: Tham Loum cave drip water isotopic from 12/09/10 to 12/03/11

| Sample Date | $\delta$D (‰ VSMOW) | $\delta^{18}$O (‰ VSMOW) | Sample Date | $\delta$D (‰ VSMOW) | $\delta^{18}$O (‰ VSMOW) |
|---|---|---|---|---|---|
| 1/15/10 | -54.93 | -8.49 | 6/3/10 | -54.64 | -8.34 |
| 2/14/10 | -53.16 | -8.18 | 7/5/10 | -56.46 | -8.48 |
| 3/15/10 | -46.88 | -7.02 | 8/14/10 | -55.61 | -8.37 |
| 4/15/10 | -47.15 | -7.18 | 9/1/10 | -54.18 | -7.99 |
| 5/16/10 | -50.18 | -8.00 | 12/11/10 | -35.08 | -5.80 |
| Average: $\delta$D is -50.83±6.5; $\delta^{18}$O is -7.79±0.87<br>T = 19.6$^o$C, RH = 95% | | | | | |

### 3.6.2 Hendy test

*Hendy* (1971) revealed that under equilibrium conditions, $\delta^{18}$O and $\delta^{13}$C values of samples along a single growth layer of a stalagmite should have no progressive increase away from the center of the growth axis. We conducted Hendy tests on TM4 and TM6. We found no significant correlation between $\delta^{13}$C and $\delta^{18}$O and no significant variability along individual growth layers (Fig. 3.12), indicating that the calcite was precipitated under isotopic equilibrium conditions(*Hendy*, 1971).

Another check for equilibrium condition is to test for correlation between $\delta^{18}$O and $\delta^{13}$C (*Hendy*, 1971). We correlate $\delta^{18}$O with $\delta^{13}$C for each stalagmite(Fig. 3.13). $R^2$ values are relatively low for TM4, TM5, TM9 and TM11 ($R^2$ range from 0.0-0.3) suggesting little kinetic fractionation effect and the $\delta^{18}$O signal is primarily dominated by climatic factors. $R^2$ value for TM13 is slightly higher than other stalagmite samples. TM13 was growing through the Younger Dryas, which is an extreme event, and thus this high correlation ($R^2$ = 0.59)is probably indicating a local climatic contribution to the isotopic signals.

Although the Hendy test is not the most reliable test of equilibrium, the fact that little variation in $\delta^{18}$O along a single growth layer of stalagmite and that no signigicant correlation between $\delta^{18}$O and $\delta^{13}$C is consistant with a lack of kinetic fractionation effects. Thus, we

assumed that speleothems from Tham Mai cave formed in isotopic equilibrium with drip water.

Table 3.4: Summary of Laos speleothems Hendy test $\delta^{18}O$ (‰) results

| sample name | Distance from center(cm) | Layer1 $\delta^{18}O$ | Layer2 $\delta^{18}O$ | Layer3 $\delta^{18}O$ |
|---|---|---|---|---|
| TM4 | -3 | -10.78 | -10.54 | -10.35 |
| | -2 | -10.68 | -10.60 | -10.32 |
| | -1 | -10.56 | -10.48 | -10.45 |
| | 0 | -10.53 | -10.47 | -10.49 |
| | 1 | -10.51 | -10.48 | -10.37 |
| | 2 | -10.39 | -10.31 | -10.50 |
| | 3 | -10.40 | -10.46 | -10.33 |
| TM11 | -1.8 | -10.38 | -10.06 | / |
| | -1.2 | -10.35 | -9.91 | / |
| | -0.6 | -10.15 | -9.99 | / |
| | 0.6 | -10.16 | -10.00 | / |
| | 1.2 | -10.24 | -10.03 | / |
| | 1.8 | -10.16 | / | / |

Table 3.5: Summary of Laos speleothems Hendy test $\delta^{13}C$ (‰) results

| sample name | Distance from center(cm) | Layer1 $\delta^{13}C$ | Layer2 $\delta^{13}C$ | Layer3 $\delta^{13}C$ |
|---|---|---|---|---|
| TM4 | -3 | -11.28 | -9.78 | -11.28 |
| | -2 | -11.43 | -10.01 | -11.37 |
| | -1 | -11.03 | -10.17 | -11.53 |
| | 0 | -10.97 | -10.48 | -11.46 |
| | 1 | -10.95 | -10.21 | -11.37 |
| | 2 | -10.88 | -10.29 | -11.46 |
| | 3 | -10.43 | -10.34 | -11.42 |
| TM11 | -1.8 | -11.03 | -10.48 | / |
| | -1.2 | -11.28 | -10.57 | / |
| | -0.6 | -11.22 | -10.52 | / |
| | 0.6 | -11.07 | -10.42 | / |
| | 1.2 | -11.17 | -10.52 | / |
| | 1.8 | -11.01 | / | / |

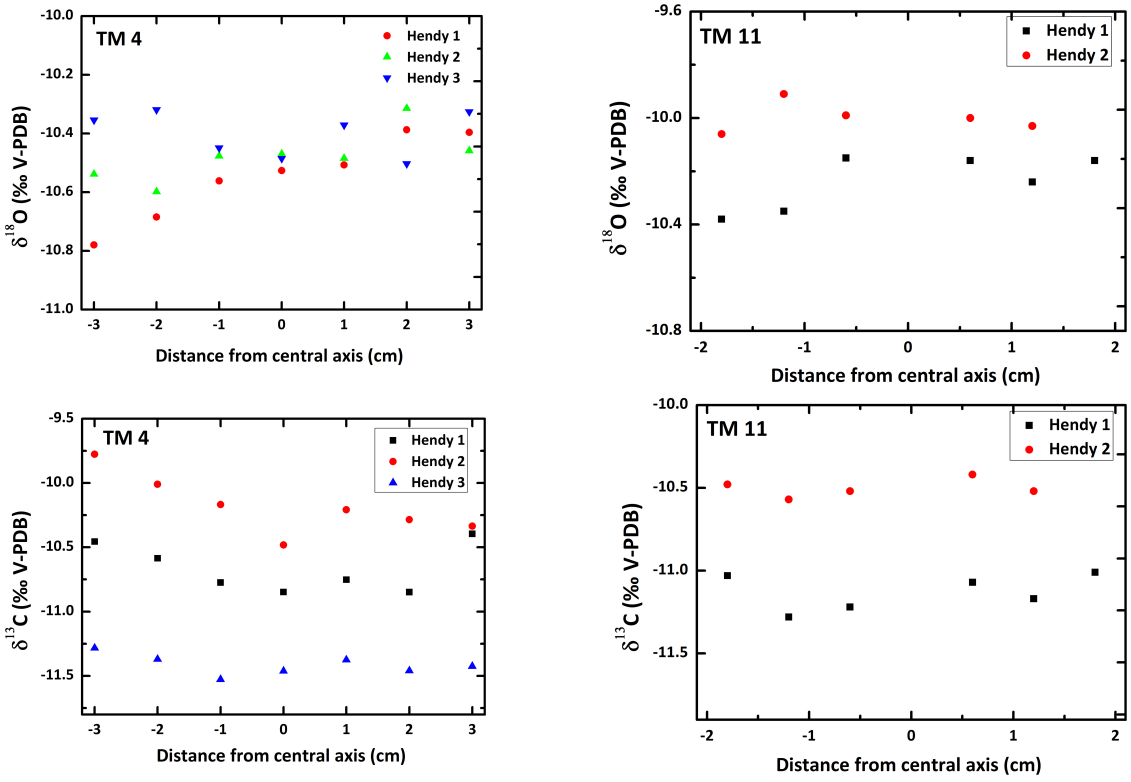


(a) (b)

Figure 3.12: Hendy test results for $\delta^{18}$O and $\delta^{13}$C from different layers of stalagmites TM4 and TM11, with different color representing different layers. $\delta^{18}$O of TM4 and TM 11 within individual horizons varies by less than 0.5 ‰, indicating the lack of significant kinetic effects related to evaporation. $\delta^{13}$C of TM4 and TM11 of varies by less than 1‰

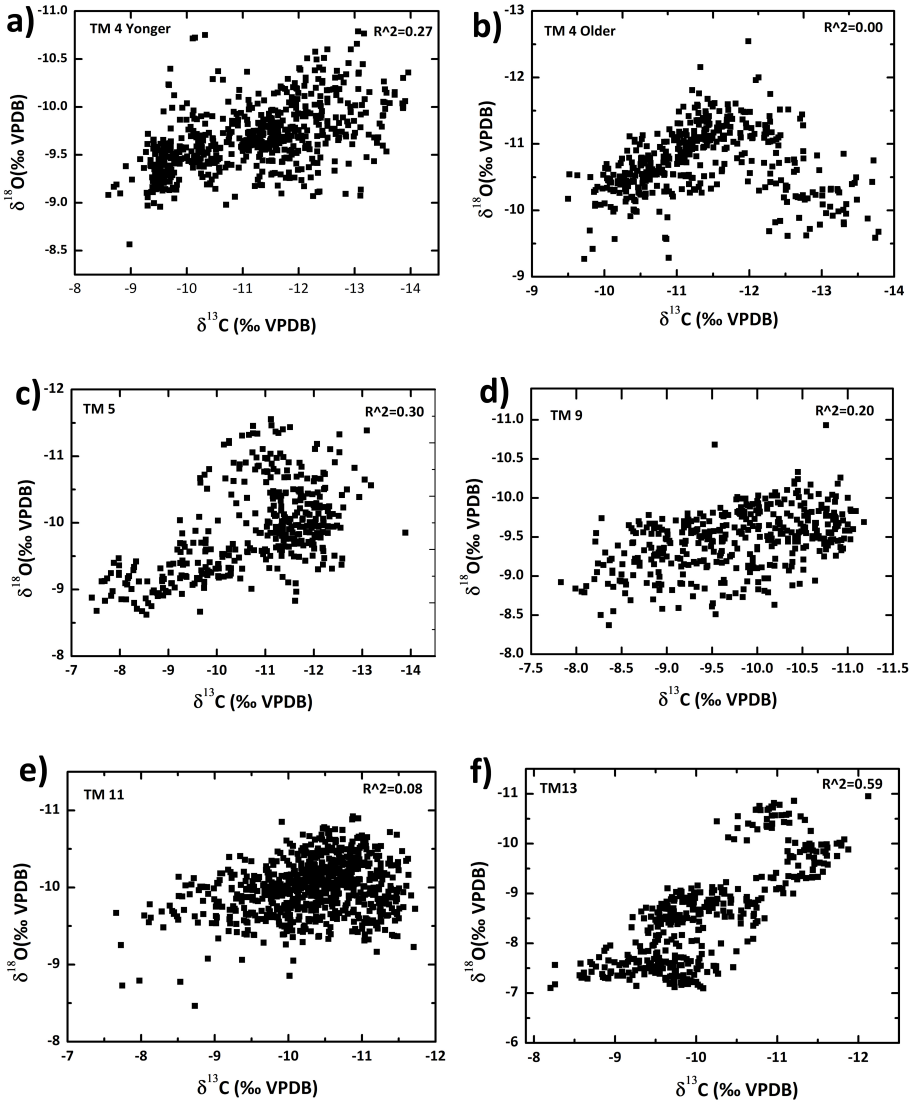


]

Figure 3.13: $\delta^{18}$O versus $\delta^{13}$C from slaglamite TM4 younger portion, TM4 older portion, TM5, TM9, TM11, and TM13. The low $R^2$ between $\delta^{13}$C and $\delta^{18}$O for TM4, TM5, TM9 and TM11 indicates that the speleothem was likely deposited under equilibrium conditions. The relatively high $R^2$ value between $\delta^{13}$C and $\delta^{18}$O for TM13 probably indicating extreme climate events on stalagmite isotopic ratios.

### 3.6.3 Replication

The isotopic signals in stalagmite are controlled by many factors. Many processes other than climate may be contributing the $\delta^{18}$O signals measured in speleothems. Kinetic fractiona-

tion, mixing of water within the epikarst, degassing history and dissolution-reprecipitation can be involved in producing the $\delta^{18}$O signal, leading to shifts of the climate signal. Replication of isotopic records from multiple stalagmites in same cave is the best method to test the suitability of utilizing these speleothems proxies for climate reconstructions. Four speleothems (TM4, TM5, TM9, TM11) grew contemporaneously (∼4300 years BP to ∼ 9000 years BP ), and are used to do a replication test. TM4 and TM5 are from the same location, while TM9 and TM11 are from another location within the same cave (Fig.3.2). Although a ∼1‰ absolute discrepancy is observed, the strong similarity among these four stalagmites $\delta^{18}$O record (Fig.3.14) provides further evidence for precipitation of speleothem calcite under isotopic equilibrium conditions indicating that speleothem $\delta^{18}$O should provide a useful paleoclimate proxy.

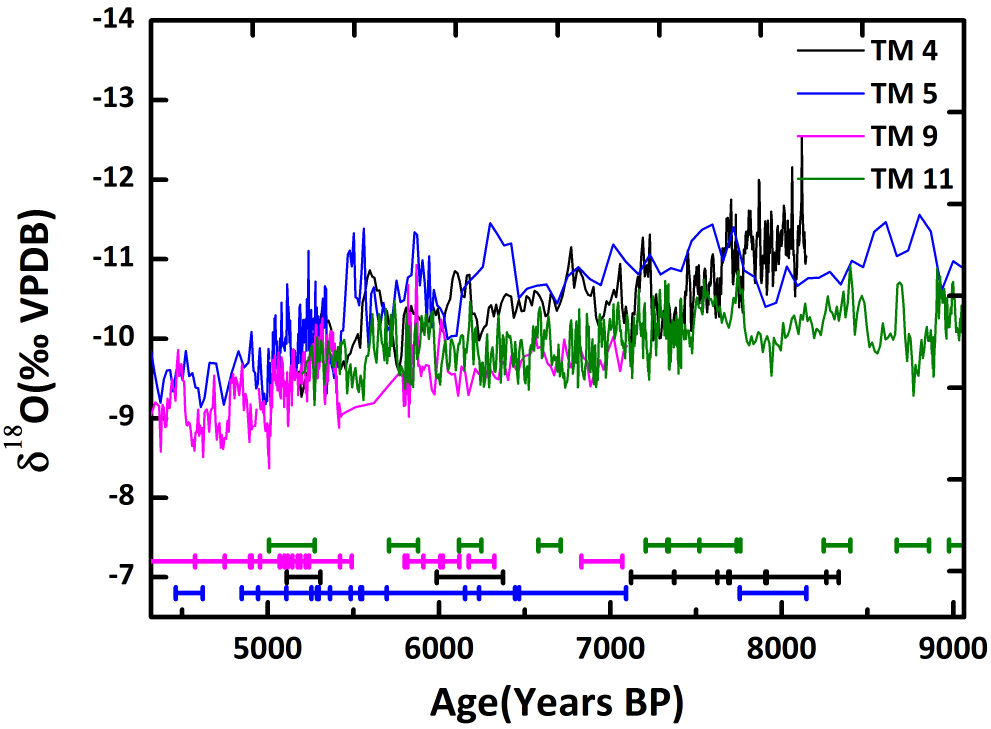


Figure 3.14: The $\delta^{18}$O records of TM4, TM5, TM9 and TM11 from 4300 years BP to 9000 years BP. Though a 1‰ absolute discrepancy is observed, these four stalagmites show a remarkably similar $\delta^{18}$O pattern suggesting climatic variations are recorded in these four stalagmites. The color-coded circles represent individual U-Th ages for each specimen along with their $2\sigma$ uncertainty.

### 3.6.4 Growth rate

Speleothem growth rates vary by several factors, such as drip water flux and drip water calcium ion concentration, discharge amounts, drip rate, temperature and the $pCO_2$ gradient between the drip water and cave air (*Genty and Quinif*, 1996; *Baker et al.*, 1998; *Genty et al.*, 2001). The drip water calcium ion concentration can affect growth rate, with higher calcium ion concentration in drip water causing higher growth rate. The drip water calcium ion concentration can increase with longer water residence time in the epikarst (*Genty et al.*, 2001). Discharge changes may affect growth rate, with higher discharge causing faster calcite deposition and thus higher growth rate. A stronger $pCO_2$ gradient between the drip water and the cave air will cause stronger $CO_2$ degassing of the drip water when entering the cave, which causes higher calcite supersaturation of the drip water and thus higher growth rate. In general, speleothems growth rates can vary in a range 10-1000 $\mu m$/yr (*McDermott*, 2004). Speleothems collected from sub-tropical climates are considered to grow at 300- 500 $\mu m$/yr (*Fairchild et al.*, 2006). However, growth rate of speleothem could be higher than expected due to high $CO_2$ and high drip water calcium ion concentration, or source of strong acid, particularly sulphuric acid from pyrite oxidation (*Atkinson*, 1977, 1983; *Sasowsky et al.*, 2004).

Laos speleothem growth rate varied from 2 to 960 $\mu m$/yr with an average of 105 $\mu m$/yr. TM4 younger portion has a relatively low and constant growth rate(15 to 100 $\mu m$/yr) from ∼880 to ∼2200 years BP, with a sharp transition into high growth rate (∼ 500 $\mu m$/yr) ∼2300 years BP. This sharp tradition could be generated by the age model artificially due to the hiatus effect. TM4 older portion growth rate stays relatively constant (∼15 to 50 $\mu m$/yr ) from ∼5200 years BP to ∼7400 years BP. TM4 older portion growth rate peaks during 7500 years BP to 8000 years BP (∼80 $\mu m$/yr). Between 5000 years BP to 5500 years BP, growth rates of TM5(∼200 $\mu m$/yr) and TM9 (∼350 $\mu m$/yr) reaches their peaks. TM11 growth rate peaks between 7200 years BP to 7500 years BP. These periods of high growth

rate correspond to the period of lightest $\delta^{18}$O between 7500 years BP to 8500 years BP, although some is slightly lagged within age uncertainties. *Dykoski et al.* (2005) observed the similar coherent relationship between growth rate and $\delta^{18}$O for a speleothem from Dongge Cave, China, during 7500 years BP to 8500 years BP. Similar coherency was also found in speleothem record from Lynds Cave, Australia, which was interpreted to reflect relatively wet conditions, and coincide with the so-called mid-Holocene climatic optimum (*Xia et al.*, 2001).

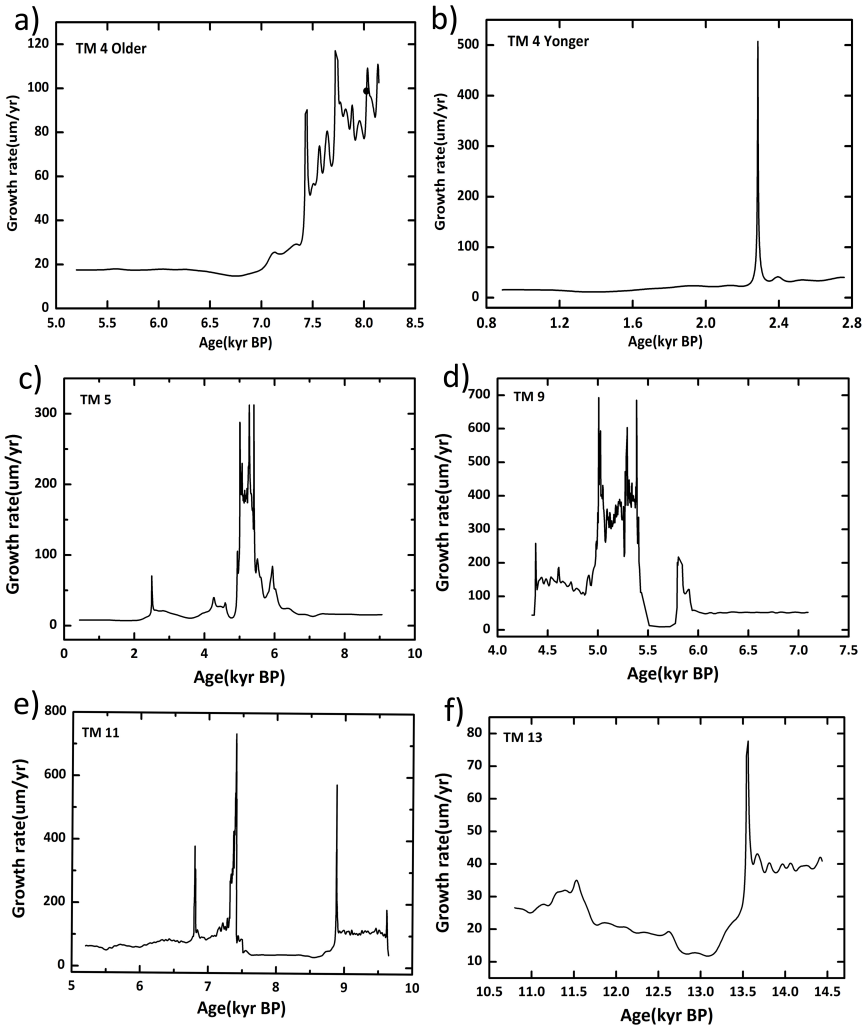


Figure 3.15: Growth rate versus time for stalagmites, a) TM4 younger portion, b) TM4 older portion, c) TM5, d) TM9, e) TM11, f)TM13

### 3.6.5 $\delta^{18}$O and $\delta^{13}$C record

Table 3.4 summarizes the $\delta^{18}$O and $\delta^{13}$C results of Tham Mai cave stalagmites. 604 samples are measured for TM4 younger portion. $\delta^{18}$O of TM4 younger portion has a mean of -9.68‰, ranging from -10.79‰ to -8.57‰. $\delta^{13}$C of TM4 younger portion has a mean of -11.19‰, ranging from -13.96‰ to -8.6‰. 418 samples are measured for TM4 older portion. $\delta^{18}$O of TM4 older portion has a mean of -10.72‰, ranging from -12.55‰ to -9.27‰. $\delta^{13}$C of TM4 older portion has a mean of -11.33‰, ranging from -13.78‰ to -9.5‰. 388 samples are measured for TM5. $\delta^{18}$O of TM5 portion has a mean of -9.9‰, ranging from -11.55‰ to -8.62‰. $\delta^{13}$C of TM5 has a mean of -10.78‰, ranging from -13.89‰ to -7.42‰. 432 samples are measured for TM9. $\delta^{18}$O of TM9 portion has a mean of -9.47‰, ranging from -10.97‰ to -8.38‰. $\delta^{13}$C of TM9 has a mean of -9.77‰, ranging from -11.18‰ to -7.83‰. 742 samples are measured for TM11. $\delta^{18}$O of TM11 portion has a mean of -9.99‰, ranging from -10.92‰ to -8.46‰. $\delta^{13}$C of TM11 has a mean of -10.32‰, ranging from -11.72‰ to -7.66‰. 392 samples are measured for TM13. $\delta^{18}$O of TM13 portion has a mean of -8.54‰, ranging from -10.95‰ to -7.10‰. $\delta^{13}$C of TM13 has a mean of -10.1‰, ranging from -12.12‰ to -8.20‰. $\delta^{18}$O and $\delta^{13}$C record for each slaglamite is showing in (Fig.3.15).

Table 3.6: Summary of Laos speleothems $\delta^{18}$O (‰) and $\delta^{13}$C (‰) results

| sample name | isotope samples | mean $\delta^{18}$O | range of $\delta^{18}$O | mean $\delta^{13}$C | range of $\delta^{13}$C |
|---|---|---|---|---|---|
| $TM4_{younger}$ | 604 | -9.68 | (-10.79,-8.57) | -11.19 | (-13.96,-8.6) |
| $TM4_{older}$ | 418 | -10.72 | (-12.55,-9.27) | -11.33 | (-13.78,-9.5) |
| TM5 | 388 | -9.9 | (-11.55,-8.62) | -10.78 | (-13.89,-7.42) |
| TM9 | 423 | -9.47 | (-10.97,-8.38) | -9.77 | (-11.18,-7.83) |
| TM11 | 742 | -9.99 | (-10.92,-8.46) | -10.32 | (-11.72,-7.66) |
| TM13 | 392 | -8.54 | (-10.95,-7.10) | -10.1 | (-12.12,-8.20) |

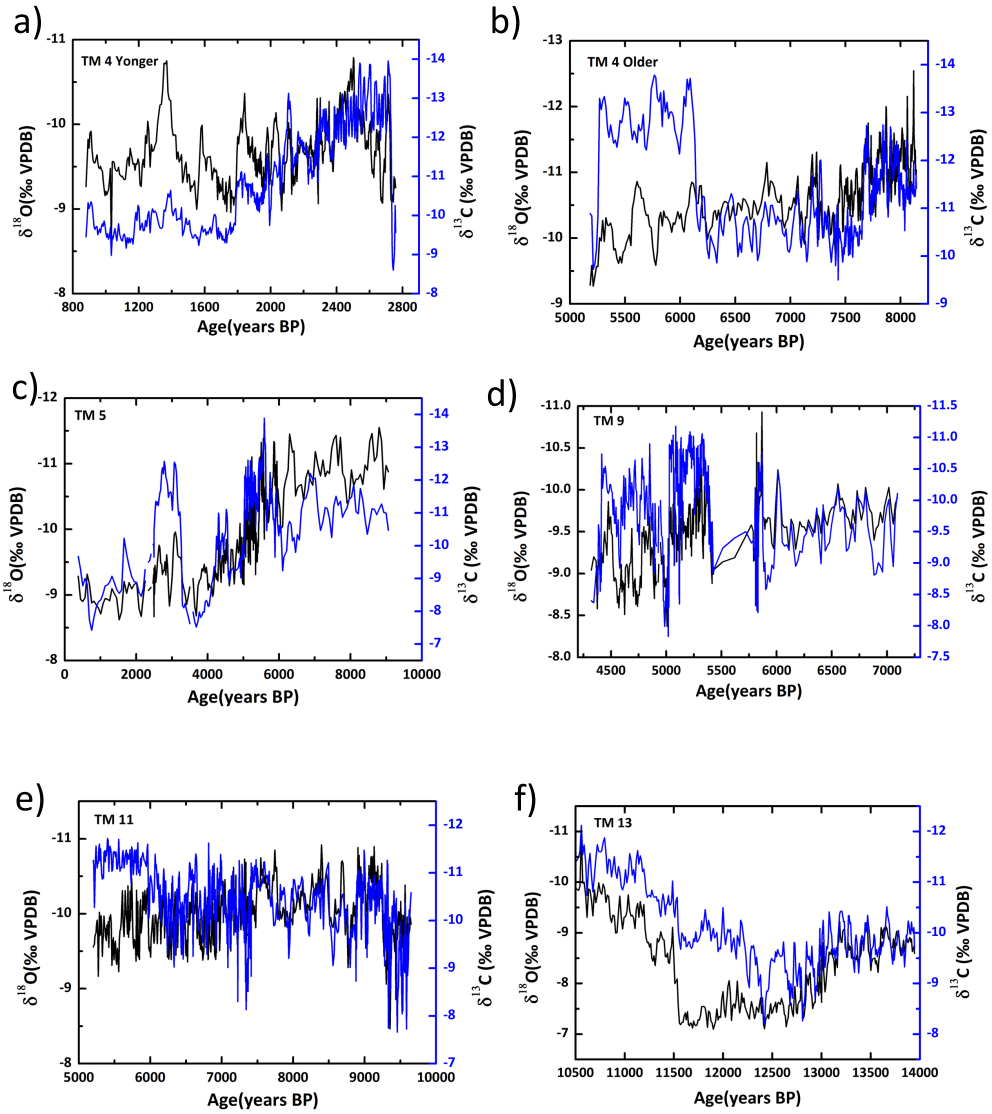


Figure 3.16: $\delta^{18}$O (black)and $\delta^{13}$C (blue) records for each stalagmite from Tham Mai cave, a) TM4 younger portion, b) TM4 older portion, c) TM5, d) TM9, e) TM11, f)TM13

**The $\delta^{18}$O record**

Several distinct features are characterized in the $\delta^{18}$O records (Fig.3.17). The Younger Dryas is characterized by an abrupt $\delta^{18}$O increase beginning ∼14 kyr BP and lasting until ∼12 kyr BP when $\delta^{18}$O values decrease by almost 4‰. The timing of the Younger Dryas is close to that observed in Dongge Cave and in Greenland ice cores within age uncertainties. This suggests that similar to the EAM, the SEAM weakened in sync with high latitude abrupt cooling events.

During the Holocene, the Tham Mai speleothem $\delta^{18}$O records are characterized by lower values during the early to mid-Holocene with increasing values towards the late Holocene. This is similar to trends seen throughout the Asian monsoon region, reflecting the strong insolation control on monsoon strength and ITCZ position (Fig.3.21). This general decrease in $\delta^{18}$O is interrupted by several heavy excursions between 10 kyr BP to 8 kyr BP. TM11 displays a heavier excursion at ∼9.2 kyr BP. The similar heavy $\delta^{18}$O excursion is also observed in the NGRIP ice core (*Johnsen et al.*, 2001), Dongge cave stalgmite $\delta^{18}$O (*Dykoski et al.*, 2005) and Qunf cave stalagmite records (*Fleitmann et al.*, 2003). TM5 and TM11 $\delta^{18}$O display a sharp 1-2 ‰ increase at ∼8.2 kyr BP (within age error), corresponding to 8.2 kyr BP event obsessed in Greenland, indicating that the SEAM also weakened in response to this event. In addition, another large increase in $\delta^{18}$O occurred at ∼3.5 kyr BP. This abrupt event is also seen in other records, such as Dongge cave, Heshang cave $\delta^{18}$O record and titanium record in the Cardiac Basin(*Haug et al.*, 2001). From centennial-scale, variation of $\delta^{18}$O throughout the Holocene is 0.5‰ to 1‰.

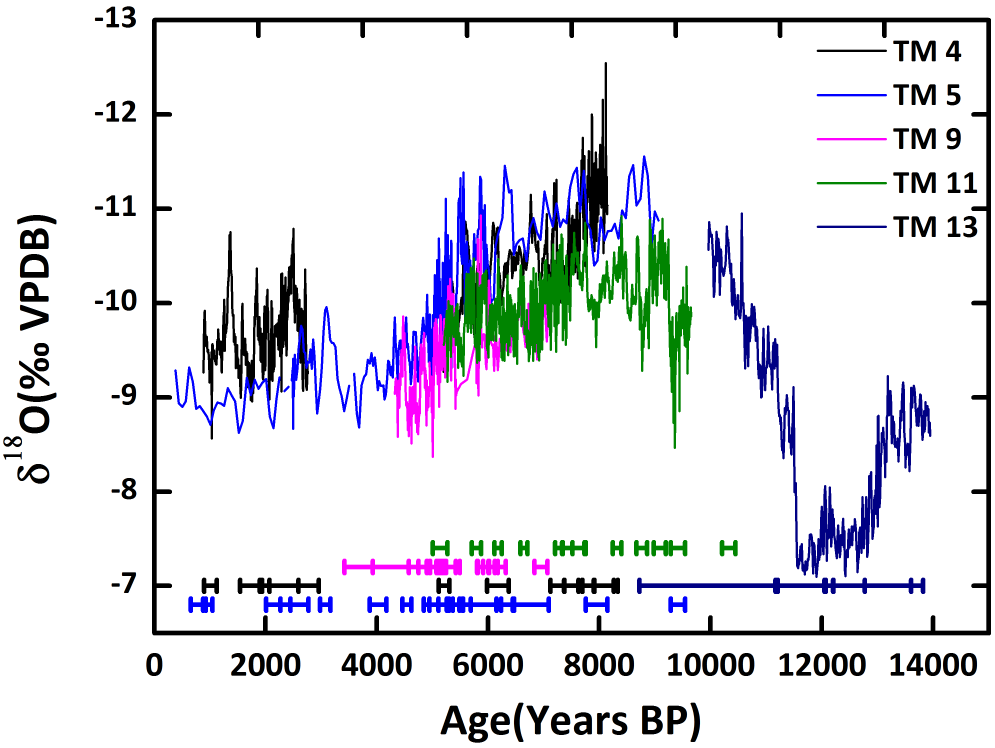


Figure 3.17: Five stalagmites $\delta^{18}$O records from Tham Mai cave, with error bars indicating $U-Th$ ages and errors. Note that $\delta^{18}$O plotted increasing downwards. Black is TM4 record, light blue is TM5, pink is TM9, green is TM11, dark blue is TM13

**The $\delta^{13}$C record**

From TM13 record, during the Younger Dryas, changes in Laos speleothem $\delta^{13}$C tracks the $\delta^{18}$O, indicating that the Younger Dryas was likely characterized by extremely dry conditions in Southeast Asia. $\delta^{13}$C records follow the trend of $\delta^{18}$O until the middle Holocene when the proxies begin to diverge, which is indicated in TM11. $\delta^{13}$C records display a diverse trend compared with $\delta^{18}$O from middle to late Holocene, indicating a wetter local environment (Fig.3.18). This may reflect increasing rainfall towards the Late Holocene as the ITCZ migrates southward in response to decreasing Northern Hemisphere summer insolation.

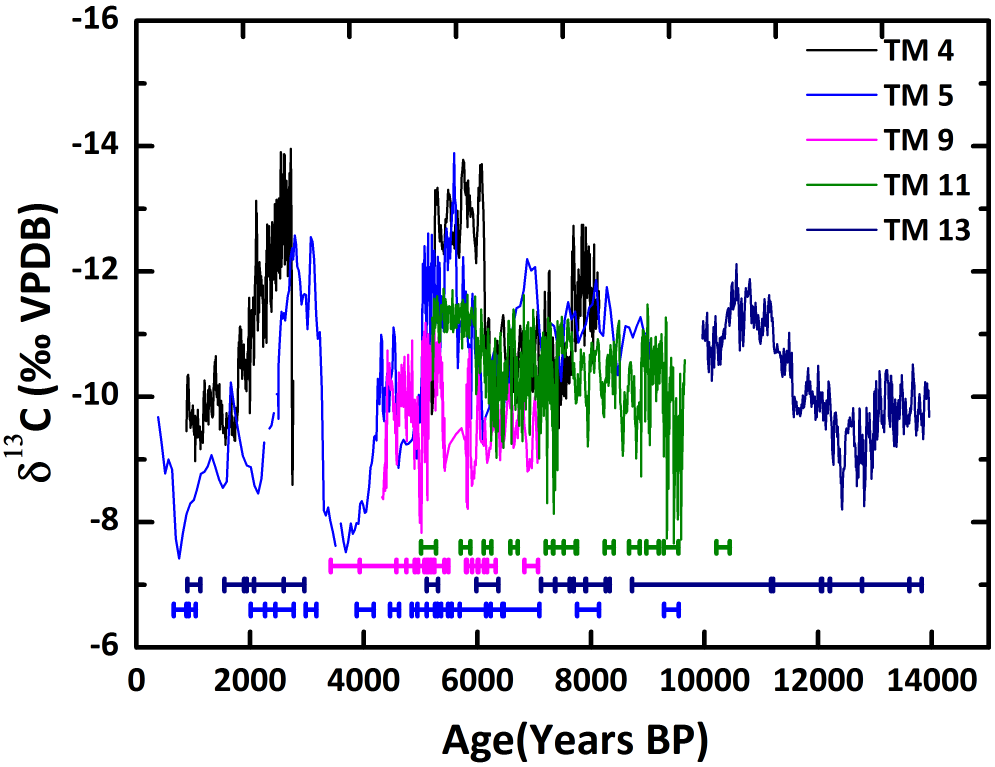


Figure 3.18: Five stalagmites $\delta^{13}$C records from Tham Mai cave, with error bars indicating $U-Th$ ages and errors. Note that $\delta^{13}$C plotted increasing downwards. Black is TM4 record, light blue is TM5, pink is TM9, green is TM11, dark blue is TM13

## 3.7 Discussion

Tham Mai speleothem $\delta^{18}$O record shows a clear response to the millennial scale Younger Dryas event, with $\delta^{18}$O values increasing by 3‰. This feature is similar to the feature observed in the Greenland ice core temperature record and other cave records in Aisan monsoon region (*Wang et al.*, 2001; *Dykoski et al.*, 2005; *Dong et al.*, 2010, e.g.). This indicates an in-phase weakening of the SEAM in response to a weakening of the Atlantic Meridional Overturning Circulation (AMOC), similar to numerous other Northern Hemisphere sites and opposite to the response in the Southern Hemisphere (*Ayliffe et al.*, 2013; *Griffiths et al.*, 2009, 2013).

In addition, A strong similarity in pattern is shown between Tham Mai speleothem $\delta^{18}$O record and bulk titanium record from the Cariaco Basin (*Haug et al.*, 2001), and an anti-correlation relationship in shown between Tham Mai speleothem $\delta^{18}$O and Liang-Luar cave $\delta^{18}$O from Flores, Indonesia(8-9N, 120-123E) (*Griffiths et al.*, 2009) (Fig.3.19). *Haug et al.* (2001) presented a bulk titanium record from the Cariaco Basin, which is a record of the degree of river runoff, and thus is affected by the amount of precipitation which is controlled by the position of ITCZ at this region. Liang-Luar cave, Flores is a record of the strength of Australian-Indonesian summer monsoon, which is also affected by ITCZ. Thus, these three records are likely connected through manifestation of ITCZ. The ITCZ controls the position of precipitation over the South American continent (*Haug et al.*, 2001) and also Indonesia (*Griffiths et al.*, 2009). Our record from Laos indicates that the ITCZ has a similar effect in SEAM.

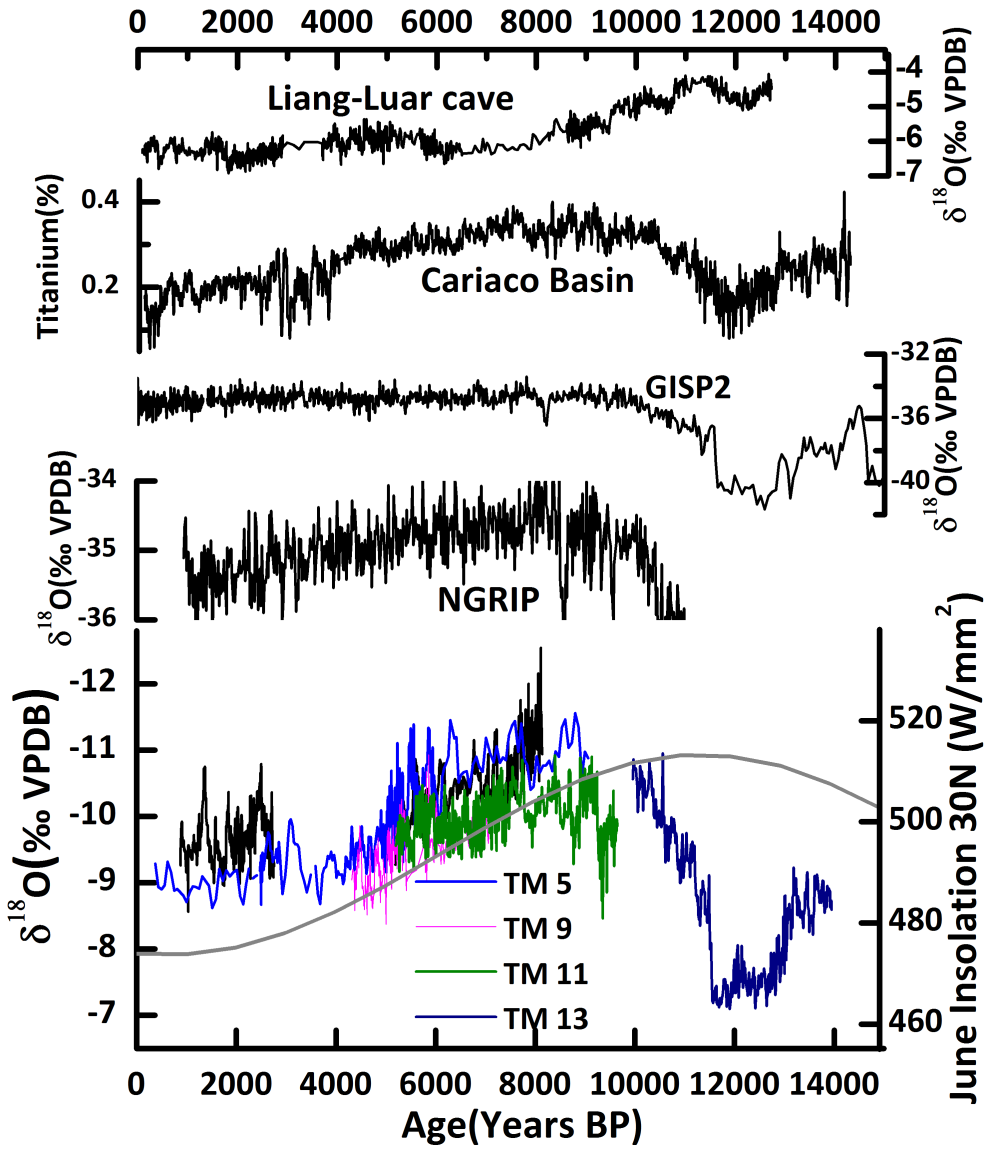


Figure 3.19: Comparison of speleothem $\delta^{18}$O records from Tham Mai cave, Laos and previously published a) speleothem $\delta^{18}$O record from Liang-Luar cave, Flores (*Griffiths et al.*, 2009), b) Titanium(%) record from the Cariaco Basin (*Haug et al.*, 2001), c) GISP2 Greenland ice core $\delta^{18}$O record(*GISP2*), d) NGRIP Greenland ice core $\delta^{18}$O record (*Johnsen et al.*, 2001)

Tham Mai speleothem $\delta^{18}$O record also shows strong similarities with other Asian monsoon records (e.g. *Wang et al.*, 2001; *Dykoski et al.*, 2005; *Hu et al.*, 2008; *Dong et al.*, 2010) with characteristically low values in the early Holocene followed by increasing values towards the

present, following the general trend of 30N summer solar insolation(Fig.3.21). This pattern has widely been interpreted to reflect a direct response to decreasing Northern Hemisphere summer insolation over the Holocene and a resulting decrease in summer monsoon intensity. However, speleothem $\delta^{18}$O is known to be influenced by a combination of factors, including moisture source region, transport history, upstream precipitation amount, local precipitation amount, and karst hydrology. Recent studies with isotope-enabled general circulation models (GCMs) have suggested that the conventional "amount effect" is not large enough to explain the amplitude and spatial patterns of speleothem $\delta^{18}$O variability observed in the Asian monsoon region (*Mann et al.*, 2009; *Pausata et al.*, 2011). *Pausata et al.* (2011) suggests instead of local monsoon intensity, the $\delta^{18}$O variability observed in Chinese speleothems actually reflect rainout over the Indian Ocean and subcontinent before the moisture reaches China.

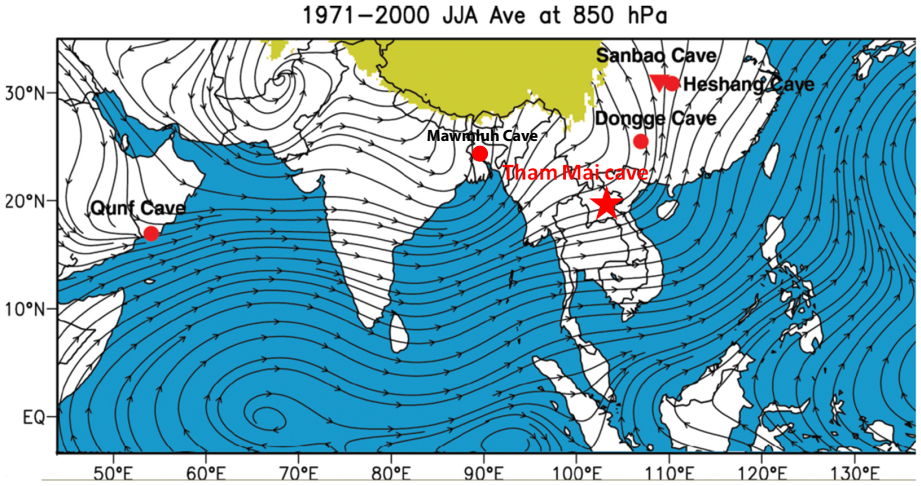


Figure 3.20: Generalised circulation pattern of the Asian summer monsoon over the period from 1971-2000 (NCAR/NCEP, kyr BP lnay et al., 1996). The red star indicates the location of Tham Mai cave. The locations of Qunf cave, Mawmluh cave, Dongge cave, and Heshang cave are depicted as red circles; Sanbao cave is shown as triangle

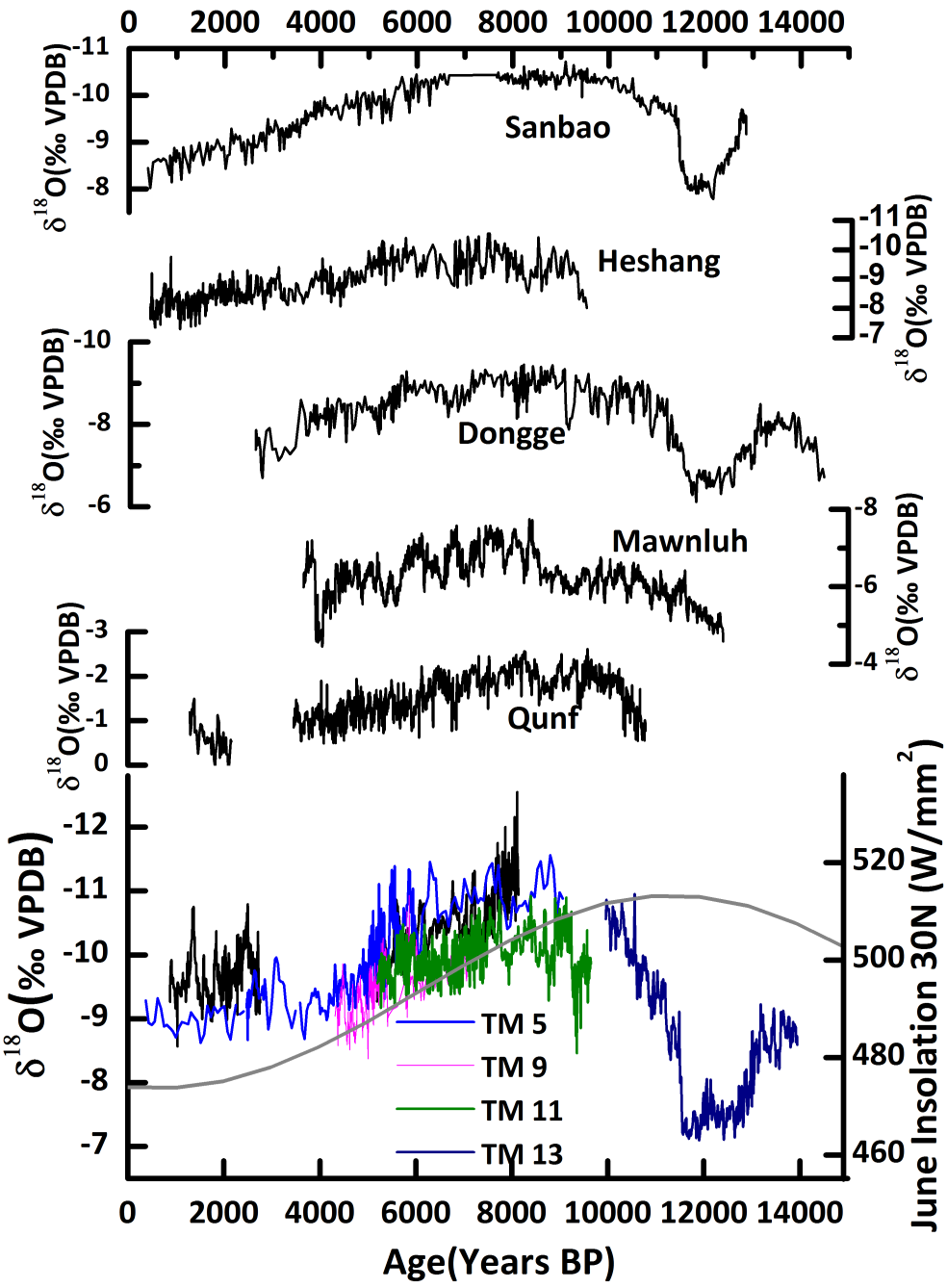


Figure 3.21: Comparison of speleothem $\delta^{18}$O records from Tham Mai cave, Laos and previously published speleothems $\delta^{18}$O records from Qunf cave,Oman (*Fleitmann et al.*, 2004), Mawmluh cave, India (*Berkelhammer et al.*, 2013), Dongge cave (*Dykoski et al.*, 2005), Heshang cave (*Hu et al.*, 2008), and Sanbao cave (*Dong et al.*, 2010) China. All records are plotted versus age (year BP). Northern Hemisphere June insolation (30N) is shown in grey

### 3.7.1 Investigating controls on speleothem $\delta^{18}$O

In order to best assist with Tham Mai cave $\delta^{18}$O record interpretation, we utilized the Holocene slice experiments conducted for 6 kyr BP and 0 kyr BP simulation results from Goddard Institute for Space Studies (GISS) ModelE, a fully coupled atmosphere-ocean GCM, to explore the interpretation of stalagmite $\delta^{18}$O records in the Asian monsoon region. These experiments use the previously described AR5 version of ModelE utilizing appropriate greenhouse gas concentrations and seasonal insolation values at each time slice. the mid- Holocene results are part of the CMIP5 coordinated experiment and are available on its archive. Each experiment was run for 500 years to equilibrium and we will analyze the last 100 years of each run. In addition, we compared Tham Mai cave $\delta^{18}$O and $\delta^{13}$C records to pursue possible local and regional climate responsibilities.

**Analysis of the Holocene results from the fully-coupled GISS ModelE2-R**

We first did model validation using the "time slice" control run of ModelE2-R and the MERRA nudged ModelE2 run (1979-2009) with the AR5 version of ModelE with a horizontal resolution of 2 x 2.5, 40 vertical layers in the atmosphere up to 0.1 hPa height. Model E2-R is fully-coupled to the 1 x 1.25, 32-layer Russell Ocean model, whereas ModelE2 utilizes prescribed Had1SSTs. Water isotope tracers are included in the atmosphere, land surface, sea ice, and ocean, and are tracked through the hydrologic cycle with appropriate fractionation factors applied during phase changes. Further details of ModelE are available in numerous publications (*Hansen et al.*, 2007; *Mann et al.*, 2009, e.g.).

To validate how well the ModelE control run, the MERRA nudged ModelE run, and IsoGSM simulate the modern climatology and oxygen isotope composition of modern precipitation in Laos, we have compared the mean monthly results with a gridded observational climate dataset (CRU TS3.10) and GNIP data (Fig.3.4). All models accurately capture the seasonal

cycles in T (r= 0.95 to 0.97), P (r = 0.91 to 0.96), and $\delta^{18}$O (r=0.67 to 0.79), though the summer precipitation is somewhat underestimated by each model.

**Asian monsoon paleo-precipitation and Isotopic changes**

To facilitate comparison, we compared the changes in past anomalies with present (0 kyr BP, pre-Industrial, control run) simulations. GISS ModelE2 results show both decreased (or barely changed) $\delta^{18}$O values and decreased precipitation amount in Indo-Pacific area at 6 kyr BP relative to the control run (Fig.3.22). This suggest that at 6 kyr BP, southeast Asia is dryer than today which is opposite than changes over India and East Asia. However, the speleothems record from our case study site Laos show a similar increasing $\delta^{18}$O values from middle Holocene to Late Holocene as other speleothems through out Asian monsoon regions. These results, therefore, suggest that speleothem records from the Asian monsoon area are not necessarily reflecting local precipitation, though do reflect the strong insolation control on monsoon strength, ITCZ position, and/or other coupled climate process

Given that the Indian Ocean is the dominant source of moisture to our study site and our Goddard Institute for Space Studies (GISS) ModelE 6k and 0k comparison results, the Tham Mai data supports the recent interpretation that the Chinese speleothem records are also primarily recording variations in the isotopic composition of moisture advected from the Indian Ocean (*Pausata et al.*, 2011).

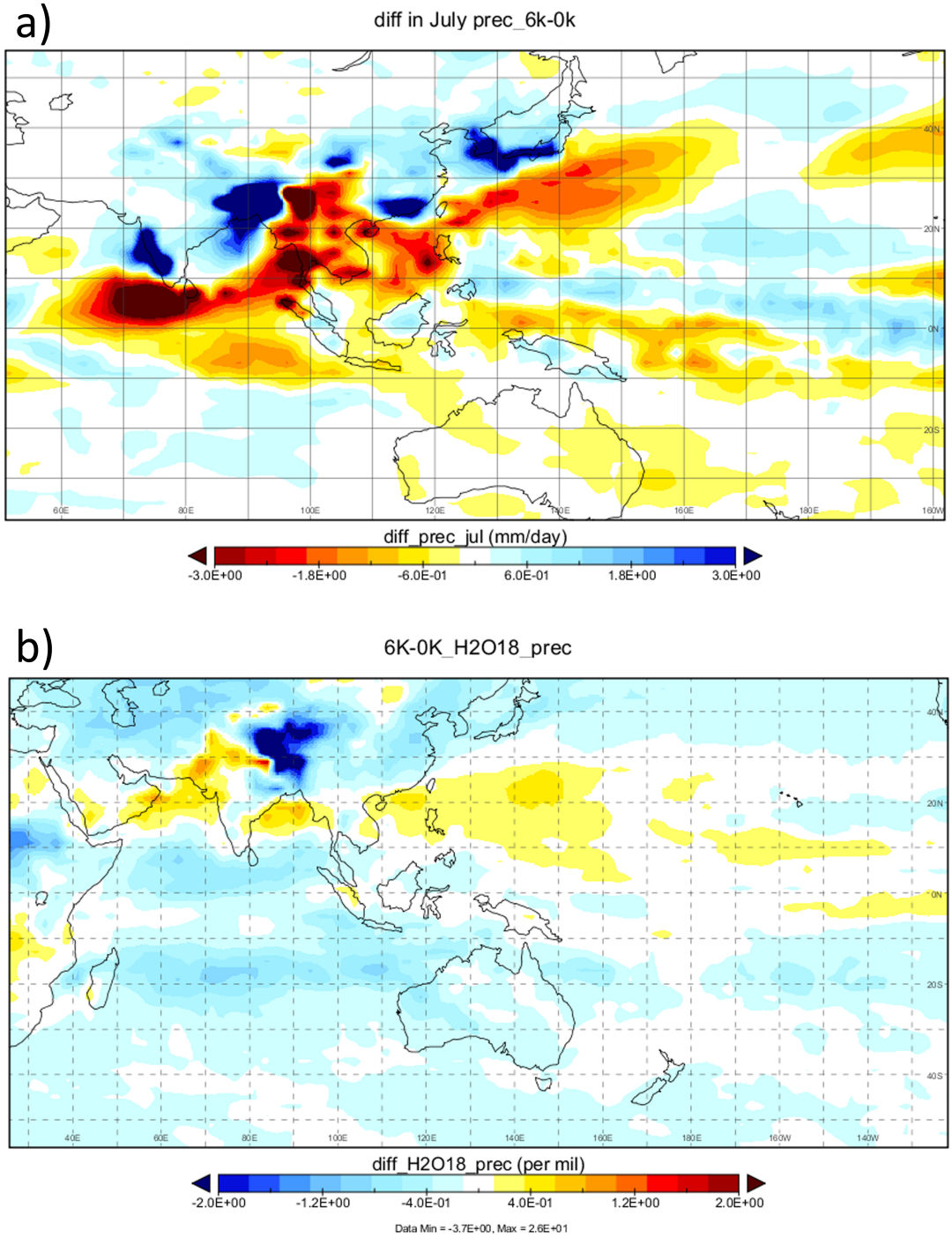


Figure 3.22: (a) GISS ModelE2 simulations 6K run - control run summer precipitation difference at each grid point. At 6K, southeast Asia is dryer than today which is opposite than changes over India and East Asia, (b) GISS ModelE2 simulations 6K run - control run precipitation $\delta^{18}$O difference at each grid point.

### 3.7.2 The linkage between $\delta^{18}$O and $\delta^{13}$C records

Speleothem $\delta^{13}$C is widely used as an indicator of local hydrologic variability, although several climatic and non-climatic factors can influence the carbon isotopic composition of calcite (*Baker et al.*, 1997; *Dorale et al.*, 1998; *Baldini et al.*, 2008). Usually, wetter local hydrologic conditions are associated with higher biogenic activity and/or higher percentage of C3 vegetation, which would lead to more negative stalagmite calcite $\delta^{13}$C value. TM11 and TM4 indicate that $\delta^{13}$C follows the $\delta^{18}$O increasing pattern.

$\delta^{13}$C and $\delta^{18}$O records from Tham Mai have several distinct features. $\delta^{13}$C record from TM13 shows broadly similar patterns with $\delta^{18}$O over the Younger Dryas ($R^2 = 0.59$), suggesting dry conditions at Tham Mai cave at this time. This indicates that, despite the complexity of $\delta^{13}$C, TM13 $\delta^{18}$O shifts could reflect a combination of decreased monsoon intensity and local rainfall amount during the Younger Dryas. TM4 older portion and TM11 show that this similar pattern between $\delta^{13}$C and $\delta^{18}$O continued until ∼6 kyr BP. TM11 indicates that the $\delta^{13}$C and $\delta^{18}$O records diverge in the Mid-Holocene, with low $\delta^{18}$O values suggestive of strong upstream rainout, but higher $\delta^{13}$C values suggestive of drier conditions. *Chawchai et al.* (2013) presented a multi-proxy sediment record from lake Kumphawapi in northeast Thailand. Their lake record suggests a dry local environmental condition ∼6500 years BP, which is consistent with our $\delta^{13}$C record recorded in TM11. One hypothesis is that the mid-Holocene insolation forcing led to increased precipitation over the tropical Indian ocean and Indian Monsoon region, while leaving SE Asia and perhaps much of China dry, thus explaining the low $\delta^{18}$O values yet high $\delta^{13}$C values at this time.

## 3.8 Conclusions

The speleothem record from Tham Mai Cave in Laos shows strong similarities to other records of Asian monsoon strength, including a strong insolation driven weakening since the mid-Holocene and abrupt decreases during the Younger Dryas, 9.2 and 8.2 kyr BP events. The centennial scale variation is generally within an amplitude of 0.5 to 1‰. Several $\delta^{18}$O events vary greater than 1‰ (e.g. the Younger Dryas, 9.2, 8.2 kyr BP). The general pattern of Tham Mai $\delta^{18}$O record and these $\delta^{18}$O events are in line with changes in the North Atlantic region and anti-correlated with $\delta^{18}$O record from Liang-Luar Cave, Flores.

Although several previous studies explained this coherent variability of stalagmites $\delta^{18}$O records through-out the Asian monsoon region, our GISS ModelE2 simulations study, toghther with the association shown between Tham Mai $\delta^{18}$O and $\delta^{13}$C records, suggest the Holocene evolution of Laos speleothem $\delta^{18}$O may be influenced by changes in moisture source region and/or upstream rainout and not simply monsoon strength or rainfall amount.

## 3.9 Acknowledgments

We thank Dachun Zhang for help with stable isotope analyses and Vasile Ersek, Alex Thomas,Tom Browning and Andrew Mason for help with U-Th dating at Oxford. We would also like to thank Dr. Joyce White, Mr. BounheuangBouasisengpaseuth, and the Lao PDR Ministry of Information and Culture for supporting our participation within the Middle Mekong Archaeology Project (MMAP: http://penn.museum/sites/mmap/). In addition, we thank Phousavanh (Phou) Vorasing, Sengphone Keophanhya, and Norseng Sayvongdouane from the MMAP team for assistance with fieldwork in 2010 and 2013. This work has been partially funded by a Faculty Seed Grant from the UCI Committee on Research, Computing, and Library Resources. We also thank the Henry R. Luce foundation for partial support of our January 2010 fieldwork during the 2010 MMAP season.

# Chapter 4

# Quantifying karst hydrology impact on stalagmite $\delta^{18}$O with forward modeling: an example from Tham Mai cave

## 4.1 Introduction

Speleothems have proven to be valuable archives of past climate variability since they can be precisely dated (e.g. *Cheng et al.*, 2000; *Richards and Dorale*, 2003; *Scholz and Hoffmann*, 2008), annually laminated (*Baker et al.*, 1993), and contain high-resolution climate proxies (e.g. *Wang et al.*, 2001, 2005; *Hu et al.*, 2008; *Dayem et al.*, 2010). Oxygen stable isotopes ($\delta^{18}$O) are the most widely utilized speleothem proxy for reconstructing past climate variability. In general, assuming that the $\delta^{18}$O signature of rainfall is directly transmitted through the karst system and preserved in cave drip water, the $\delta^{18}$O of speleothem is thus

affected by moisture source, rainfall amount, trajectory history and coupled climate modes, such as El Niño Southern Oscillation (ENSO), Indian Ocean Dipole (IOD), Pacific Decadal Oscillation (PDO) (e.g. *Yuan et al.*, 2004; *Wang et al.*, 2008; *Mann et al.*, 2009; *Dayem et al.*, 2010; *Pausata et al.*, 2011; *Chiang et al.*, 2015). However, precipitation $\delta^{18}$O ($\delta^{18}O_p$), the primary source of speleothem $\delta^{18}$O, is first modified via evaporation fractionation in the soil and shallow epikarst. Soil water $\delta^{18}$O is further modified by flow path, water storage, mixing within the soil, epikarst, and karst (e.g. *Fairchild et al.*, 2006; *Baker et al.*, 2013). $\delta^{18}$O signature of rainfall is thus transformed before the formation of speleothem.

Over glacial-interglacial time scales, speleothem $\delta^{18}$O signatures are dominated by the magnitude of temperature and ocean/atmospheric circulation. On orbital time scale, speleothem $\delta^{18}$O clearly contains a "first order" climate signal (*Baker and Bradley*, 2010). On orbital time scales, variability of the $\delta^{18}$O at four Chinese caves is 5‰ at Hulu cave (32.5N, 119.1E) (*Yuan et al.*, 2004), ∼5 to 6‰ at Dongge cave (25.3N,108.1E) (*Wang et al.*, 2001), ∼4‰ at Heshang cave (30.45N, 110.4E) (*Hu et al.*, 2008), and ∼4‰ at Xiaobailong cave (24.2N,103.3E) (*Cai et al.*, 2006) (summerized in *Dayem et al.* (2010)). This ∼3 to 5 ‰ amplitude variation should reserve the climate signal regardless of the complexity of cave hydrology.

However, at inter-annual to annual time scales, the magnitude of climate change is much smaller, thus the signal:noise ratio in speleothem in speleothem proxies is smaller. On an inter-annual time scale, variability of the $\delta^{18}$O at Heshang cave is ∼2‰ (*Hu et al.*, 2008), Wanxiang cave is ∼3‰ (*Zhang et al.*, 2008), and Tham Mai cave in Laos is ∼1.5‰. While cave drip water inherits $\delta^{18}$O signatures from precipitation above the cave, this signature is modified in the soil-karst system before it feeds the stalagmite. Once rain water gets to the karst aquifer, it may follow complex routes, due to the nature of karst aquifers. This will mix water from different routes and potentially of different ages. Finally, upon reaching a cave void site where a speleothem may form, the drip water $\delta^{18}$O may be further transformed

through non-equilibrium fractionation during calcite precipitation due to rapid degassing or evaporation (*Fairchild et al.*, 2006; *Baker and Bradley*, 2010). Thus, at inter-annual to annual time scales, the uncertainty introduced from cave hydrology is not negligible. In this case, we need to take the complexity introduced by cave hydrology into account before further interpreting speleothem $\delta^{18}$O as a climate proxy.

In addition, it has been noticed that in the cases when stalagmite $\delta^{18}$O time series have been replicated by stalagmites from similar climatic regions and even from one cave, a between sample $\delta^{18}$O variability of a order of $\sim$0.5‰ is observed upon the "first order" orbital scale climate signal (*Williams et al.*, 2005; *Baker and Bradley*, 2010). It is likely that this between sample $\delta^{18}$O variability is generated because of the complexity in karst process that transform $\delta^{18}$O between rain water and an individual stalagmite.

The objective of this chapter is to quantify the range of possible stalagmite $\delta^{18}$O variations introduced by hydrological variability over inter-annual to decadal time scale, and to advance our knowledge of the speleothem $\delta^{18}$O proxy record by comparing stalagmite $\delta^{18}$O with pseudo $\delta^{18}$O series generated by hydrological forward modeling approach. I use a lumped parameter model (KarstFor model, previously KarstHydroMod) developed by *Chris Bradley and Andy Baker and Catherine N. Jex and Melanie J. Leng* (2010) to generate pseudo stalagmite $\delta^{18}$O proxies. Using the existing simulation output from a spectrally nudged isotope-enabled general circulation model (IsoGSM), I derived six pseudo stalagmite $\delta^{18}$O proxies. The variation magnitude of these six pseudo proxies is compared with speleothem $\delta^{18}$O. As an example, I use speleothem $\delta^{18}$O from Tham Mai cave, Laos (20.75 N, 102.65 E) (*Yang et al.*, 2016). Speleothems from Tham Mai cave provide replicated $\delta^{18}$O records for the middle Holocene over $\sim$4300 years BP to $\sim$9000 years BP. The work from this chapter will also benefit future high resolution $\delta^{18}$O records interpretation from Tham Mai cave.

The ultlization of KarstFor model will help us in at least three ways: 1) enable us to assess the signal:noise ratio in speleothem $\delta^{18}$O time series, and help us understand to which extent

we can interpret a direct climate correlation with an individual stalagmite $\delta^{18}$O record; 2) identify non-stationary relationships between $\delta^{18}$O and climate and processes that produce low-frequency $\delta^{18}$O variability; 3) explain the observed between sample $\delta^{18}$O magnitude discrepancy for samples from the same cave or from a similar climatic region (*Baker et al.*, 2010).

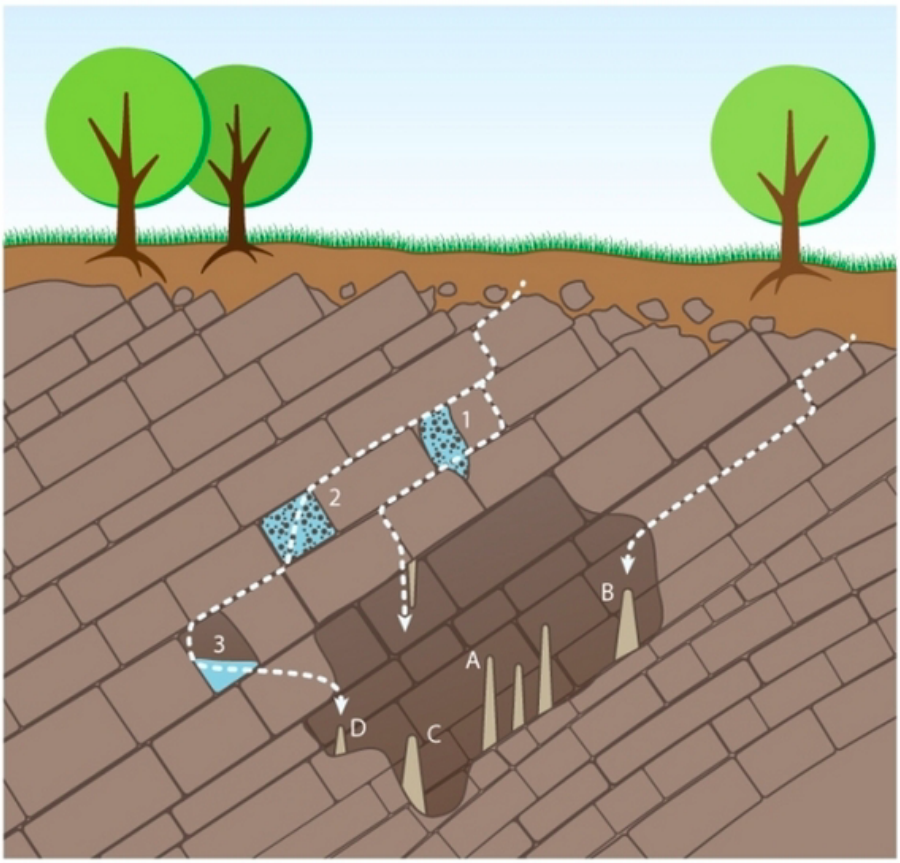


Figure 4.1: Possible flow paths that water can flow through the limestone bedrock to stalagmites in a cave. Four stalagmites (A,B,C and D) fed by different flow pathways are illustrated. Stalagmite A is fed by diffuse flow, through either the limestone matrix or through very fine fractures. Stalagmite B is fed by a larger proportion of the fracture flow, with a mixture of relatively fast fracture flow, as shown by the dotted line, tougher with slow diffuse flow from the overlying strata. Stalagmite C is fed by water taking a more complex flow route, including a mixture of water passing through an overlying cave which is full of sediment(labelled 1). Stalagmite D has the most complicated flow route. Stalagmite D fed by a mixture of water passing through two sediment filled caves (1 and 2), as well as the water passes through an active, water filled relatively small cave (3). Adapted from *Baker and Fairchild* (2012)

## 4.2 Motivation

### 4.2.1 Between sample $\delta^{18}$O discrepancy within one cave

Tham Mai cave is situated in NE Laos, contains numerous actively forming stalagmites, and has only one known entrance. Five speleothem records have been presented covering from ∼0.79 to 15.53 kyr BP with sub-decadal resolution. Four speleothems within this cave (TM4, TM5, TM9 and TM11) grew contemporaneously (∼4300 years BP to ∼9000 years BP) are used to do replication (Fig.4.2). These four speleothems replicated each other and show a remarkably similar $\delta^{18}$O pattern, despite the fact that they have different $\delta^{18}$O magnitude. The average $\delta^{18}$O of TM4 from 5182 to 8144 years BP is -10.7‰ ±0.5‰; the average $\delta^{18}$O of TM5 from 4319 to 9063 years BP is -10.14‰ ±0.56; the average $\delta^{18}$O of TM9 from 4319 to 7094 years BP is -10.16‰ ±0.56‰; and the $\delta^{18}$O of TM11 from 5192 to 9065 years BP is -10‰ ±0.32‰. The averaged $\delta^{18}$O magnitude discrepancy during the contemporary time period among these four speleothems is ∼1.2 ‰ (Fig.4.3). In order to interpret $\delta^{18}$O records from Tham Mai cave with a higher confidence, assuming these samples were deposited under a close to equilibrium condition, we need to investigate to what extend we can attribute this ∼1.2 ‰ as a result of the dynamics of karst water movement and storages.

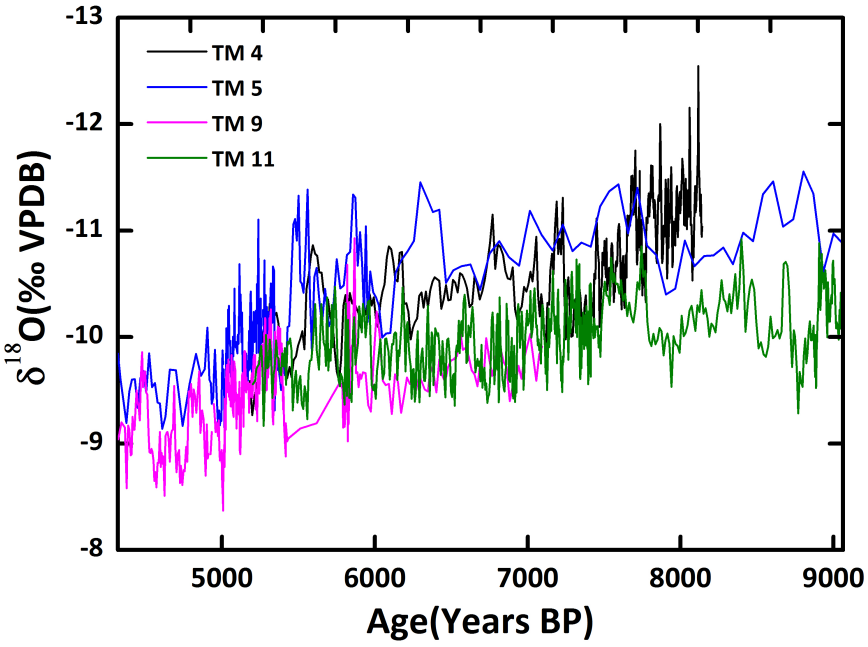


Figure 4.2: The $\delta^{18}$O records of TM4, TM5, TM9 and TM11 from 4300 years BP to 9000 years BP. A $\sim$1.2 ‰ absolute discrepancy is observed among these four speleothems.

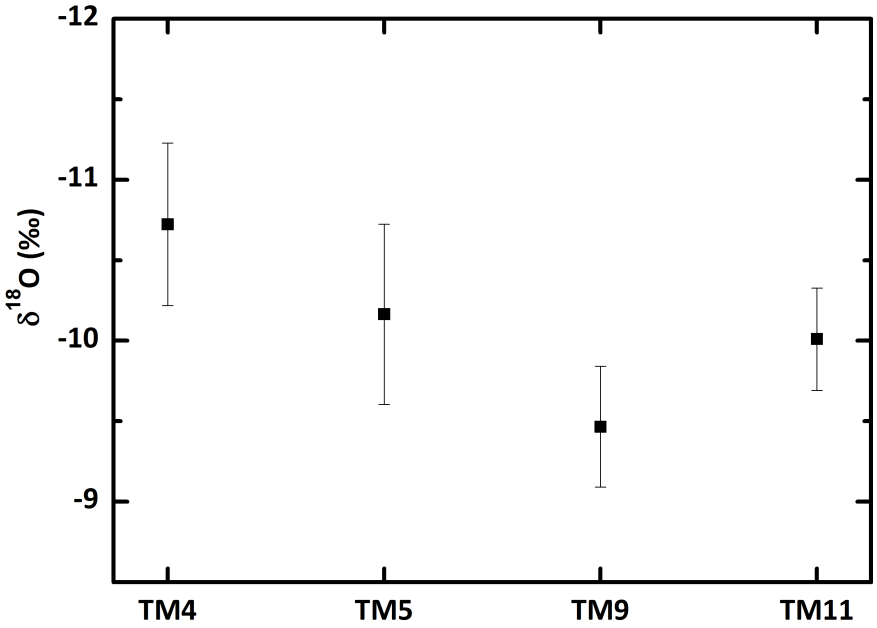


Figure 4.3: Average values with $2\sigma$ standard deviation for four replicated speleothem $\delta^{18}$O proxies from 4300 years BP to 9000 years BP

### 4.2.2 Inter-annual high resolution $\delta^{18}$O records

#### Tham Mai cave high resolution records

In order to study SEAM variability for the last 2 kyr BP, we construct inter-annual resolution speleothem $\delta^{18}$O record from Tham Mai cave. On an inter-annual time scale, It is likely that variations in SEAM are related to changes in regional climate modes, such as the Madden-Julian Oscillation (MJO), El Niño Southern Oscillation (ENSO), Indian Ocean Dipole (IOD), and Pacific Decadal Oscillation (PDO). We correlate MERRA nudged GISS ModelE2 precipitation amount-weighted $\delta^{18}$O at the grid point closest to Tham Mai cave spatially with Sea Surface Temperature (SSTs), Outgoing Longwave Radiation (OLR), sea-level pressure and 850 mb minus 200 mb zonal wind fields(U850-200) for the period 1979-2009 (Fig.4.4). Precipitation $\delta^{18}$O from the grid point closest to the case study site reveals a significant correlation with Pacific SSTs over the Niño-3.4 region and in the western and northern Indian Ocean, suggesting that the $\delta^{18}$O of annual rainfall may be influenced by ENSO and IOD (Fig.4.4). In addition, correlations with OLR, SLP, and vertical zonal wind shear (*Webster and Yang*, 1992) over the tropical Indo-Pacific also suggest a strong relationship with the Asian monsoon intensity and convection over the Indo-Pacific warm pool, , which likely contribute to "pre- fractionation" of moisture advected to our study site.

Overall, assuming these samples were deposited under equilibrium conditions, comparison with precipitation $\delta^{18}$O and reanalysis product data suggests that Tham Mai cave speleothem $\delta^{18}$O does contain a climate signal that can be related to coupled climate modes (e.g.ENSO and IOD) and atmospheric circulation.

However, our high resolution last 2000 years speleothem record from Tham Mai cave shows a complex phase (Fig.4.5). Regardless of the uncertainties from $U - Th$ dating, the complex phases in our records might indicate that rainfall anomalies in tropical Pacific Ocean is

controlled by several climate systems. These climate systems are superimposed and interact with each other. Although significant correlations between Tham Mai cave local precipitation $\delta^{18}$O, coupled climate modes (e.g. ENSO and IOD) and atmospheric circulation have been identified in Fig.4.4, this climate signal in precipitation $\delta^{18}$O is transformed before the deposition of speleothems as a result of variations in the hydrological routing of water from the surface to the cave (*Baker and Bradley*, 2010; *Chris Bradley and Andy Baker and Catherine N. Jex and Melanie J. Leng*, 2010; *Wackerbarth et al.*, 2010). While the overall variability of the $\delta^{18}$O from Tham Mai cave for last 2000 years is only ~1.5‰, a careful quantification on hydrological process contribution on $\delta^{18}$O variation is needed.

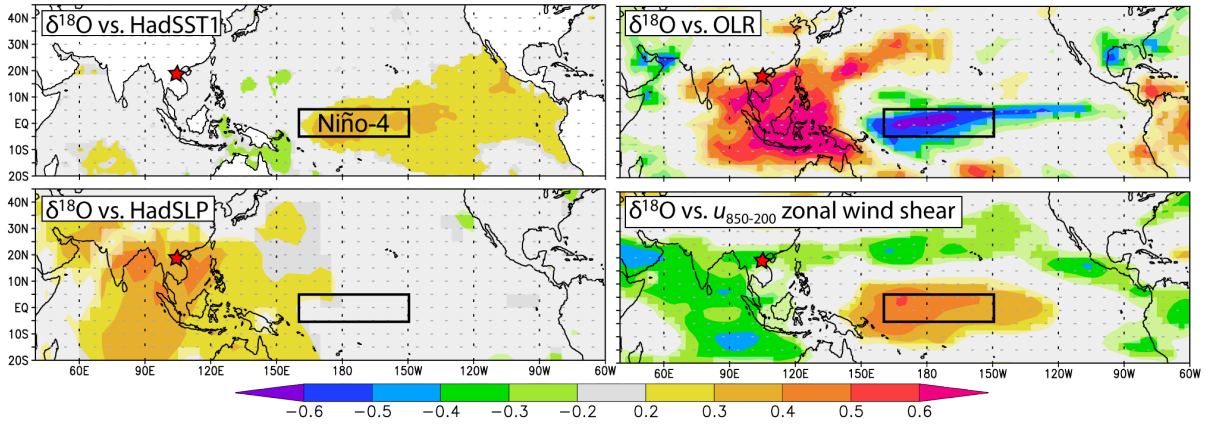


Figure 4.4: Field correlation maps between MERRA nudged GISS ModelE2 precipitation amount-weighted $\delta^{18}$O (1979-2009) at the grid point closest to our cave site (red star) and SSTs (upper left), outgoing longwave radiation (OLR) (upper right), sea-level pressure (lower left) and 850 mb minus 200 mb zonal wind fields (lower right) for the period 1979-2009. Colors represent significant r values at the 90% level. Plots for IsoGSM (1871-2010; not shown) show similar patterns.

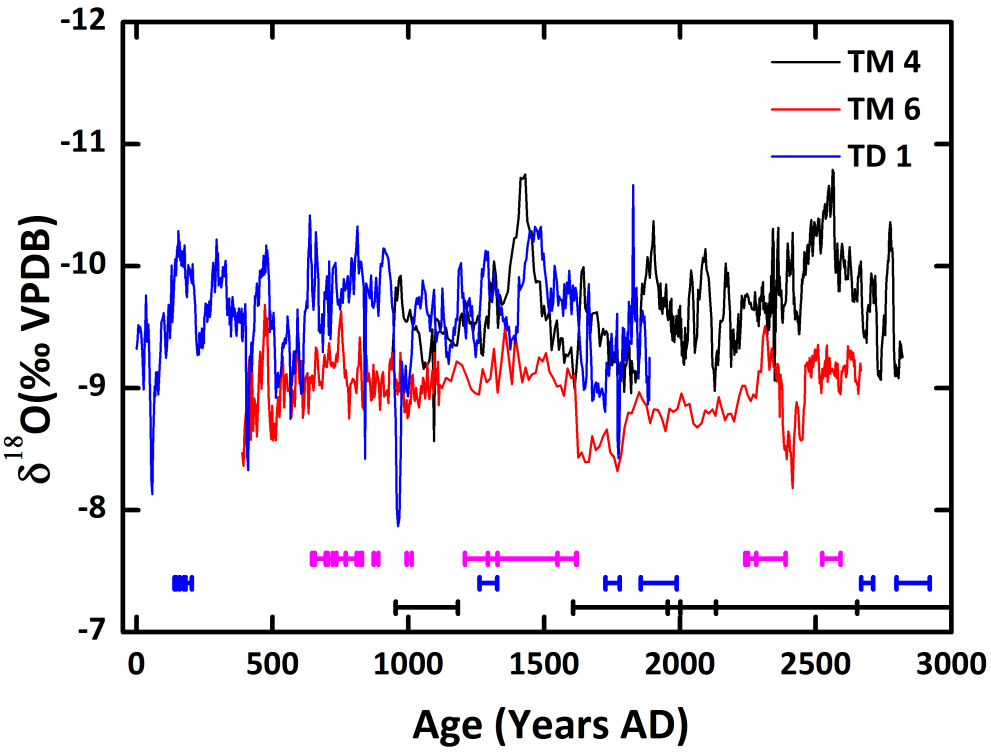


Figure 4.5: Three stalagmites $\delta^{18}$O records from Tham Mai cave for last 3000 years. Note that $\delta^{18}$O plotted increasing downwards. TD1 $\delta^{18}$O is plotted as measured $\delta^{18}$O subtracted -3‰ in order to have a similar magnitude with other two records. Black is TM4 record, red is TM6 record, and blue is TD1 record. Scanned images, $U - Th$ ages and age model of these speleothems are presented in Chapter 2 and Chapter 3.

**Chinese cave high resolution records**

*Zhang et al.* (2008) published a well-dated 1810-year long speleothem $\delta^{18}$O record from Wanxiang Cave, near the northern limit of the East Asian summer monsoon. This record shows numerous decadal-scale variations over the past two millennia that were closely linked with Northern Hemisphere temperatures, Alpine glacial retreat, solar variability, and Chinese cultural changes (*Zhang et al.*, 2008). In addition, this record revealed anomalously weak monsoon intensity during the Little Ice Age (LIA; A.D. ∼1350-1850) and anomalously strong monsoons during the Medieval Climate Anomaly (MCA; A.D. ∼900-1350). *Hu et al.* (2008) published another high annual resolution record from Heshang cave, China, which is also considered as a Asian monsoon rainfall record. Cave hydrological monitoring in these

two caves have demonstrated that they were deposited under a close to equilibrium condition, and hence stalagmite $\delta^{18}$O directly reflects infiltrating water $\delta^{18}$O composition. For these modern high resolution stalagmite samples, one way to calibrate speleothem high resolution records is to regress speleothem $\delta^{18}$O proxy with instrumental precipitation $\delta^{18}$O. Due to the temporal and spatial sparsity of existing instrumental $\delta^{18}O_p$ dataset GNIP (the Global Network for Isotopes in Precipitation), I compared these two speleothem records with IsoGSM $\delta^{18}O_p$ data from the closet grid point of cave sites. However, ∼annual resolution speleothem $\delta^{18}$O and IsoGSM precipitation $\delta^{18}$O at Wanxiang Cave and Heshang Cave does not show a correlation (Fig.4.6 and Fig.4.7). This discrepancy may be due to the complex cave hydrological influences on precipitation $\delta^{18}$O, though we also can not exclude the possibility that the model does not accurately capture precipitation $\delta^{18}$O at these two cave sites. In these circumstances, uncertainties introduced by soil, groundwater, and cave hydrology process are significant and need to be quantified before further interpretation.

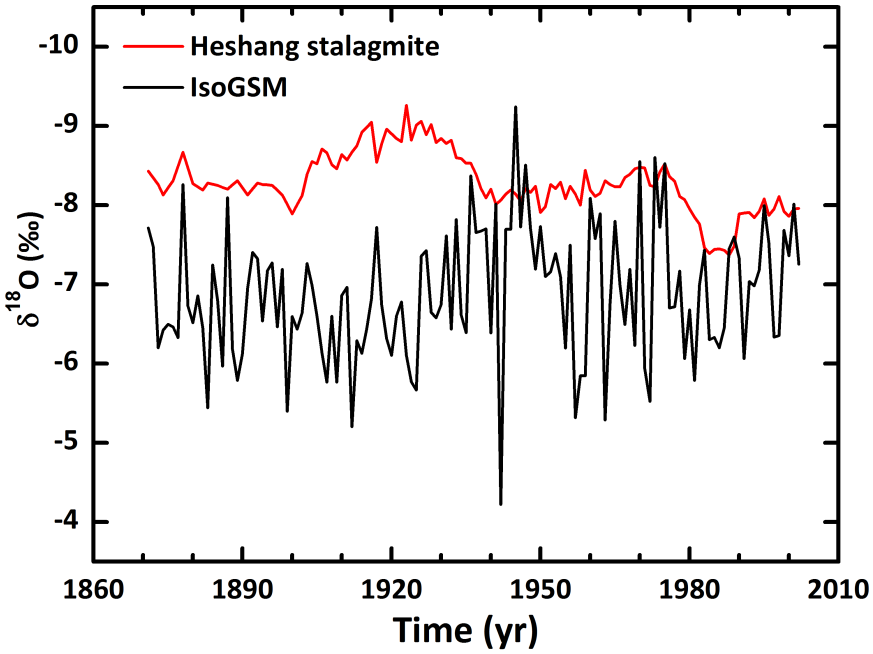


Figure 4.6: Comparison of Heshang cave speleothem $\delta^{18}$O with IsoGSM $\delta^{18}O_p$ from the grid point closest to Heshang cave site (*Hu et al.*, 2008).

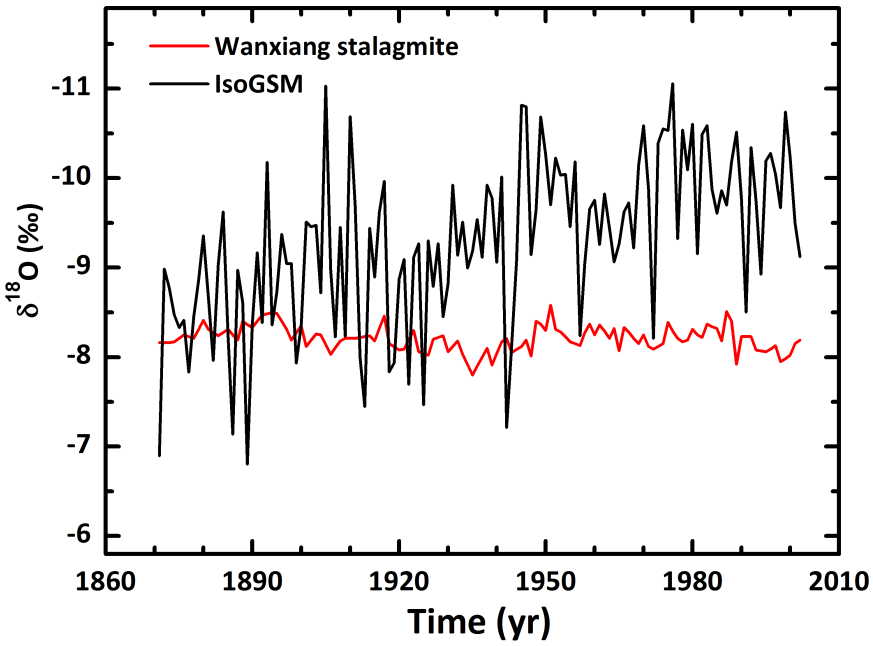


Figure 4.7: Comparison of Wanxiang cave speleothem $\delta^{18}$O with IsoGSM $\delta^{18}O_p$ from the grid point closest to Wanxiang cave site (*Zhang et al.*, 2008).

## 4.3 KarstFor model and complexity in karst hydrology

Recently, quantitative hydrological models have been developed to simulate this modification process (*Fairchild et al.*, 2006; *Baker et al.*, 2010; *Baker and Bradley*, 2010; *Chris Bradley and Andy Baker and Catherine N. Jex and Melanie J. Leng*, 2010). *Baker and Bradley* (2010) and *Baker et al.* (2013) presented a lumped parameter karst hydrology model (KarstFor model), which integrates climate, soil, and groundwater processes in order to identify potential stalagmite $\delta^{18}$O responses to changes in three inputs: precipitation, temperature, and precipitation $\delta^{18}$O. The input water (precipitation) was then entered into a linearly connected hydrological reservoirs. The model includes five water stores connected through fracture flow: soil, epikarst, karst store 1, karst store 2, and an overflow store. In KarstFor model, the primary hydrological control on drip-water $\delta^{18}$O is the relative size of each store in relation to water inflows and outflows. The $\delta^{18}$O composite of each store is simulated as a linear function of precipitation $\delta^{18}O_p$ and store $\delta^{18}$O at a time step. Evaporation fractional is only allowed in the soil store. The model has five water stores: soil, epikarst, karst store 1, karst store 2, and overflow store. The drainage rate of each store is proportional to the volume of water stored. The capacity of each reservoir and the initial water stored within the reservoir are represented by parameters and can be modified.

Six stalagmite pseudoproxies are generated from KarstFor model. The pseudoproxy time-series are influenced by varying precipitation $\delta^{18}$O, evapotranspiration, and mixing of water from different stores. Drip water source of Stal1 is Karst Store 2 $\delta^{18}$O. Drip water source of Stal2 is a mixture of 75% Epikarst Store $\delta^{18}$O and 25% precipitation of that month. Drip water source of Stal3 is a mixture of 50% Epikarst Store $\delta^{18}$O, 25% precipitation $\delta^{18}$O of that month, and 25% precipitation $\delta^{18}$O of previous month. Drip water source of Stal4 is Epikarst Store $\delta^{18}$O. Drip water source of Stal5 is Karst Store 1 $\delta^{18}$O. Drip water source of Stal6 is Overflow Store $\delta^{18}$O (Fig?). Stal1 and Stal6 $\delta^{18}$O series are generated by allowing calcite fractionation for each drip water $\delta^{18}$O series.

*Chris Bradley and Andy Baker and Catherine N. Jex and Melanie J. Leng* (2010) utilized the model to produce pseudo stalagmite proxies that agree with modern stalagmite $\delta^{18}$O for three sites (Gibraltar, NW Scotland, and Ethiopia). In addition, *Baker et al.* (2013) applied KarstFor model to quantify stalagmite $\delta^{18}$O response to glacial-interglacial transitions by using speleothem $\delta^{18}$O from Hulu cave, Naning, China as a case study. In this study, they conducted a series of model runs to determine the preferred parameter set, i.e. initial storage volume in each store and drainage rates followed by different stores. The size of each store and drainage rate are chosen to ensure that the overflow store occurred regularly. Since Hulu cave and Tham Mai cave are both located in the Asian monsoon domain and have similar modern climatology, we chose similar initial parameter values (i.e. store capacity and drainage rates) presented in (*Baker and Bradley*, 2010). To adapt their model setting to Tham Mai cave, we change several initial values, i.e. mean temperature (T = 20 $^{o}$C, karst and drip water $\delta^{18}$O (-8 ‰), stalagmite $\delta^{18}$O (-7 ‰). The initial value of mean temperature is the annual mean cave site temperature. The initial values of karst store/drip water/stalagmite $\delta^{18}$O are adapted with our drip water and modern glass plate calcite measurements during cave monitoring program 2010-2013.

The initial KarstFor model is writing in Fortran (*Baker et al.*, 2013) and converted the model into R. The R code is available as supplementary information after this chapter.

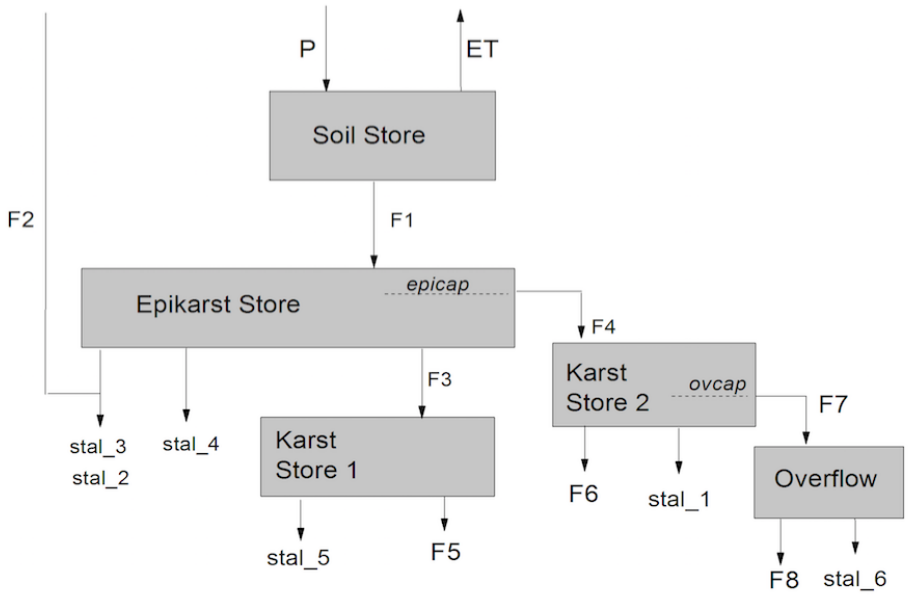


Figure 4.8: Conceptualisation of KarstFor model, a lumped parameter model *Chris Bradley and Andy Baker and Catherine N. Jex and Melanie J. Leng* (2010); *Baker et al.* (2013).The model has five water stores: soil, epikarst, karst store 1, karst store 2, and overflow store. F1 to F8 are water fluxes. Water flow from one store to another under certain constrains. Six stalagmite pseudo proxy are generated. Pseudo stalagmites are fed by drip waters from one or mixture of several stores. Adapted from (*Baker et al.*, 2013)

### 4.3.1 140 years IsoGSM input data series

As a case study and in order to quantify the "hydrological effect " at Tham Mai cave, We use 140 years (1680 month from 1871-2010) IsoGSM monthly dataset of precipitation, precipitation $\delta^{18}$O, evaporation, and temperature (Fig.4.9). IsoGSM is a multi-decadal, global, and three-dimensional precipitation isotope simulation, which has proven to be consistent with reanalysis data, especially National Centers for Environmental Prediction (NECP)/Department of Energy (DOE) (NCEP/DOE) Reanalysis 2(R2) (*Kanamitsu et al.*, 2002). The precipitation and temperature data are used to calculate water excess using Thornthwaite method (*Thornthwaite*, 1948; *Baker and Bradley*, 2010).

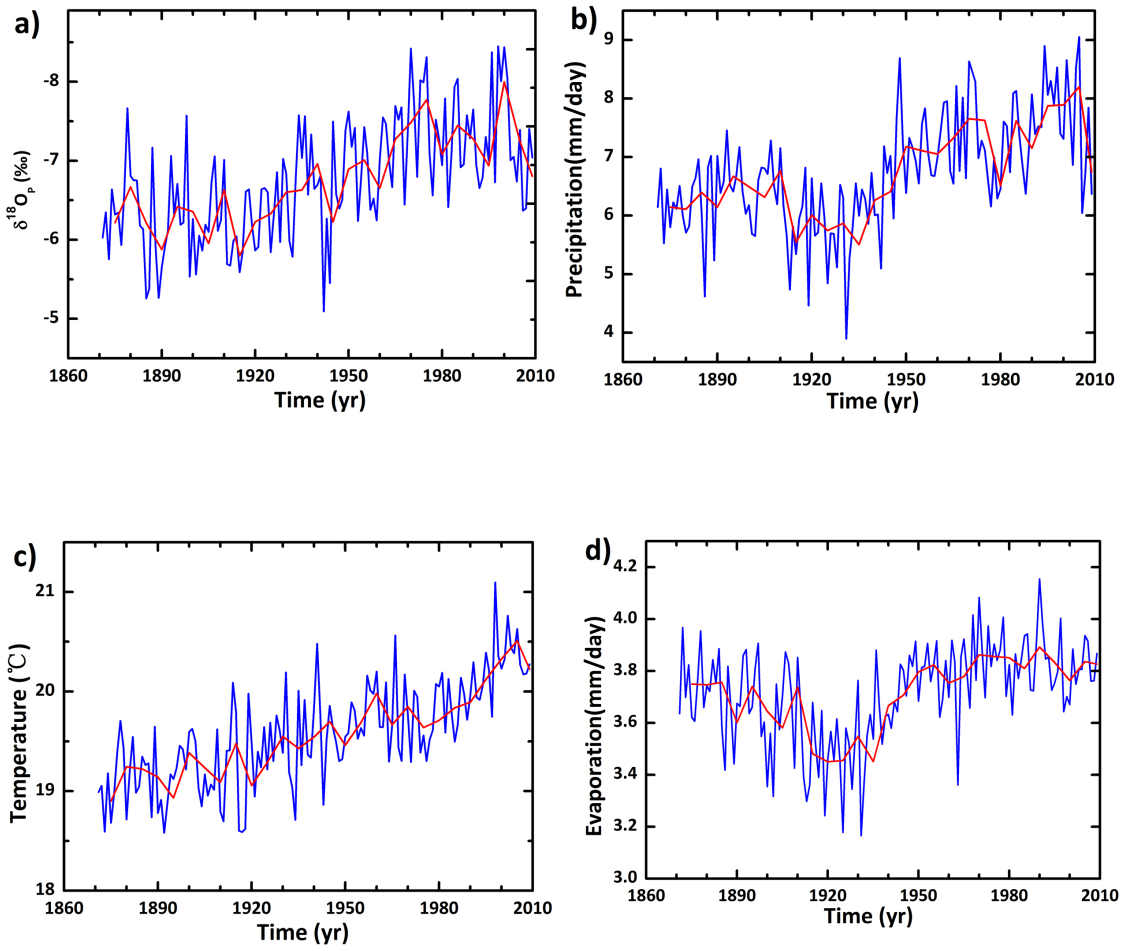


Figure 4.9: Input time series at the Tham Mai cave site from year 1871-2010: (a) $\delta^{18}O_p$, (b) precipitation, (c) surface temperature, (d) evaporation values. Blue lines indicate the 12-month and red lines the 60-month average values, respectively. Data is from IsoGSM

## 4.4 Results

Fig 4.10 shows six pseudo stalagmite $\delta^{18}$O proxies output. The pseudoproxy series vary markedly due to the differences in the inferred water flow path. Although Stal2, Stal3, Stal4, and Stal5 are varying in a similar fashion, the absolute difference among these stalagmite is $\sim$1.2 ‰. Stal2 has the most enriched $\delta^{18}$O. Stal2 is fed by a mixture of 75% Epikarrt Store water and 25% precipitation water. Stal4 has the most deleted $\delta^{18}$O signature. Stal4 is fed by water from Epikarst. Stal3 and Stal5 has similar absolute magnitude. Stal3 is fed by mixed water from four different origins. Stal5 is fed by water from the largest store(Karst Store 1), which is about 1.5 time bigger than Epikarst Store. Stal1 and Stal6 exhibit a sharp change in $\delta^{18}$O value around year 1951 and 1991, respectively. Stal1 and Stal6 are derived from each drip-water $\delta^{18}$O by allowing for calcite fractionation. This indicates that calcite fractionation before calcite precipitation may introduce sharp change in stalagmite $\delta^{18}$O proxy.

Fig 4.11 shows averaged value with $2\sigma$ standard deviation for six pseudo $\delta^{18}$O proxies. This graph summarizes the information from Fig 4.8. The absolute magnitude difference among these six pseudo stalagmites is 1.2‰, which is similar to the magnitude discrepancy among real speleothem records from Tham Mai cave (Fig 4.2 and Fig 4.3). Fig 4.12 and Fig 4.13 are similar to Fig 4.10 and Fig 4.11, but for time period 1979-2010.

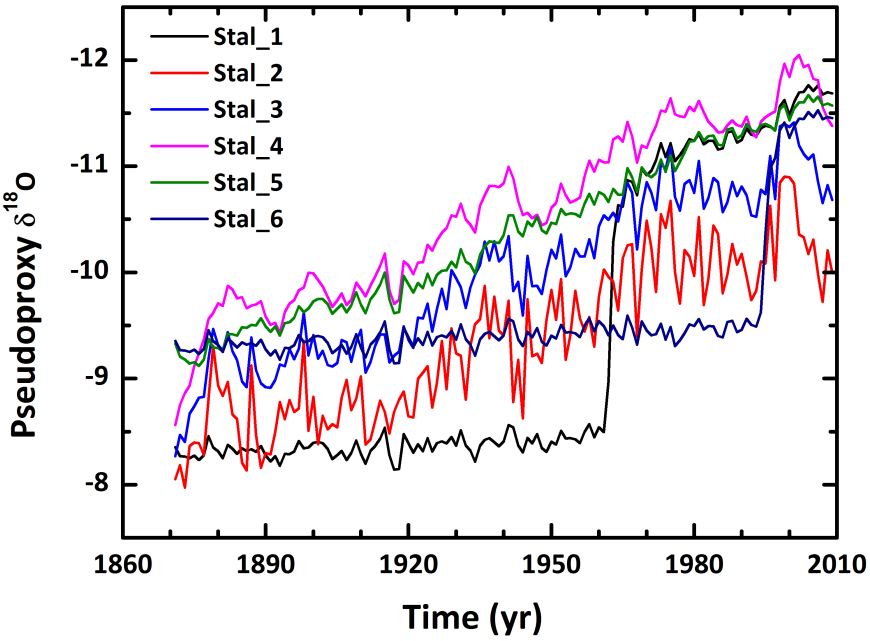


Figure 4.10: Six pseudo $\delta^{18}$O proxies from year 1871-2010, output from KarstFor model simulations. Black: Stal1,Red: Stal2, Blue:Stal3, Pink: Stal4, Green: Stal5, and Dark blue: Stal6

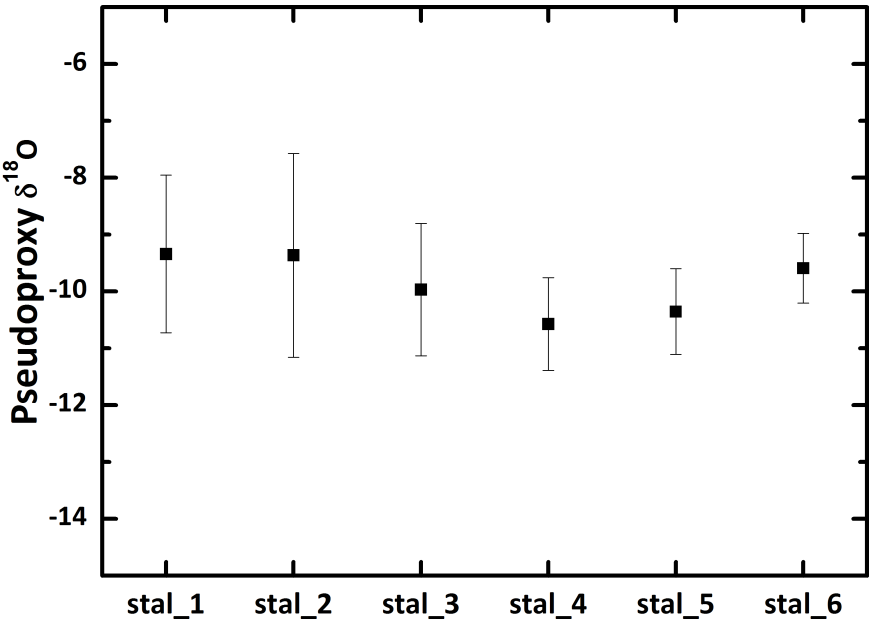


Figure 4.11: Average values with $2\sigma$ standard deviation for six pseudo $\delta^{18}$O proxies from year 1871-2010

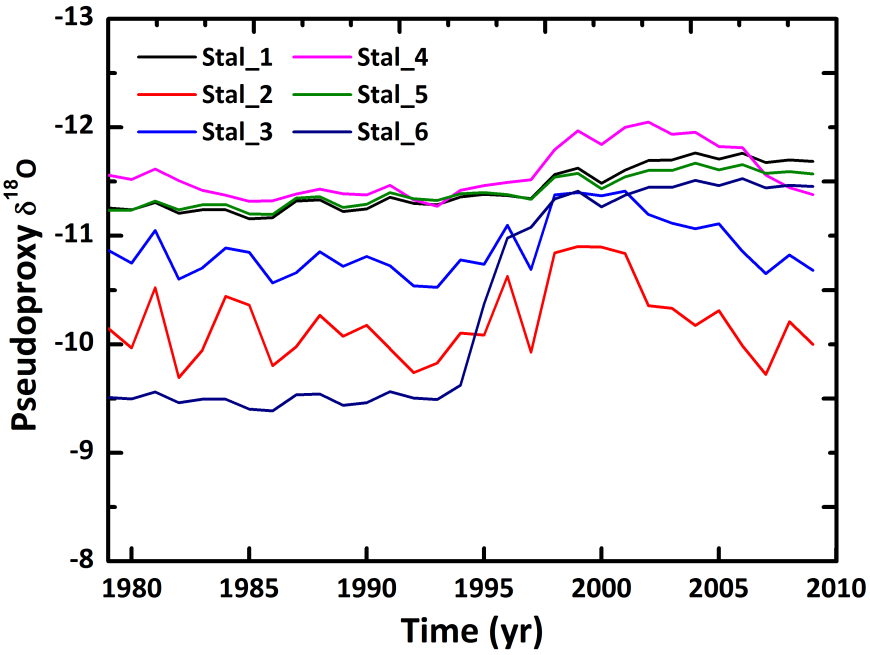


Figure 4.12: Six pseudo $\delta^{18}$O proxies from year 1979-2010, output from KarstFor model simulations. Black: Stal1,Red: Stal2, Blue:Stal3, Pink: Stal4, Green: Stal5, and Dark blue: Stal6

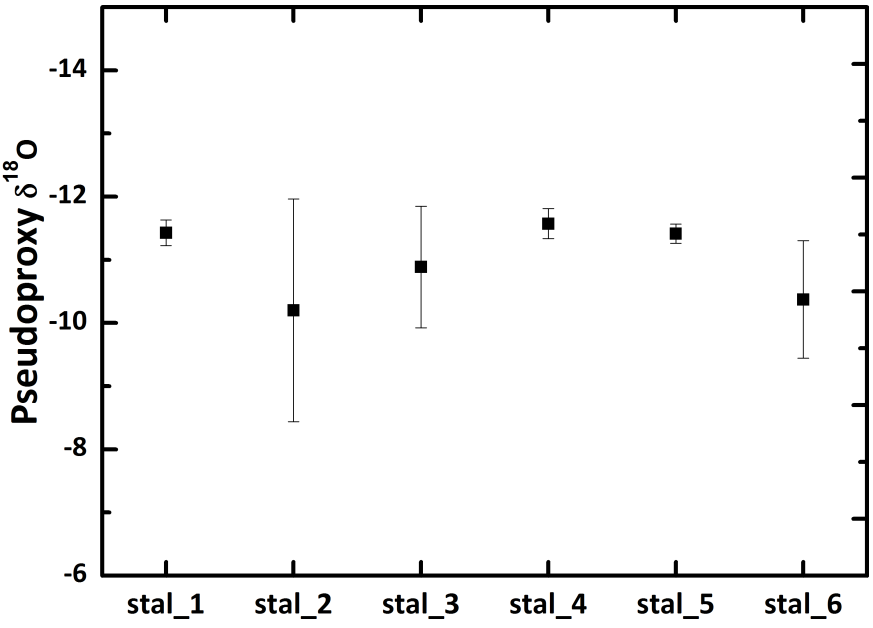


Figure 4.13: Average values with $2\sigma$ standard deviation for six pseudo $\delta^{18}$O proxies from year 1979-2010

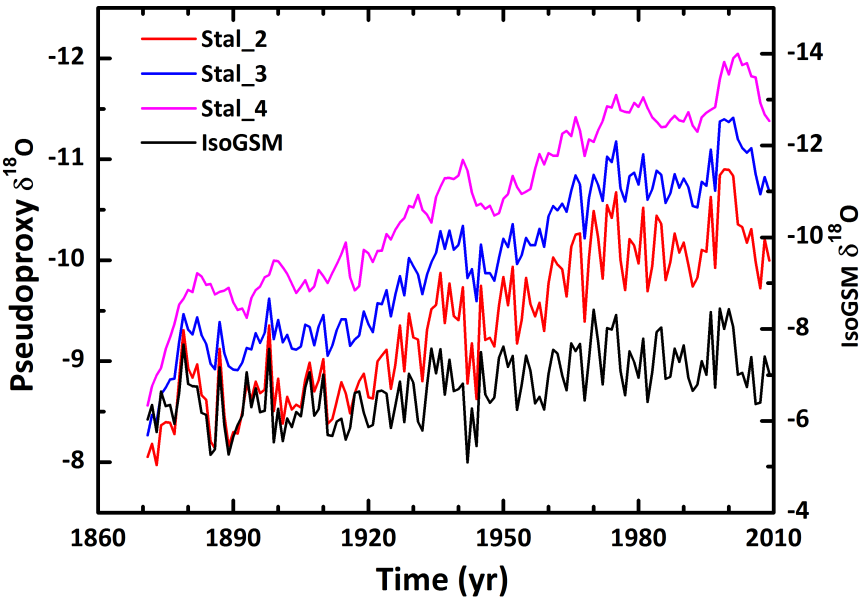


Figure 4.14: Three representative pseudo $\delta^{18}$O proxies rom KarstFor model simulations and IsoGSM $\delta^{18}$O from year 1871-2010. Black: IsoGMS, Red: Stal2, Blue: Stal3, Pink: Stal4

Fig 4.12 shows a comparison between three representative pseudo $\delta^{18}$O proxies rom KarstFor model simulations and IsoGSM $\delta^{18}$O from year 1871-2010. These four proxies covary with each other but have different magnitude of variation and absolute values. Pseudoproxy from Stal2 varies closely with IsoGSM $\delta^{18}$O, especially from 1871 to 1920.

## 4.5 Conclusion

In this chapter, we use KarstFor model to investigate and quantify sources of uncertainty in stalagmite $\delta^{18}$O. We used Tham Mai cave as a case study. Our four speleothems from Tham Mai cave which grew contemporaneously from ∼4300 years BP to ∼9000 years BP. Although these four speleothems covary with one another for the period of overlapping growth, these four speleothems have different mean $\delta^{18}$O over their period of overlap during ∼4300 years BP to ∼9000 years BP. The magnitude of mean $\delta^{18}$O discrepancy among these four speleothems is ∼1.2 ‰. We use the hydrological forward model (KarstFor) to quantitatively assess the extent to which variability between these four speleothems $\delta^{18}$O records can be attributed to

hydrological variability. Our model simulation results suggest that this ∼1.2 ‰ discrepancy can be generated due to hydrological variability within one cave. The incredible replication of speleothem $\delta^{18}$O records suggests that Tham Mai cave speleothems were deposited under isotopic equilibrium and preserved the "first order" of climate signal, at least during the Holocene time period.

In addition, our comparison with IsoGSM precipitation $\delta^{18}$O from the closest grid of Tham Mai cave and reanalysis data (SST, SLP, OLR, U850-200) suggests that Tham Mai cave speleothem $\delta^{18}$O does contain a climate signal that can be related to coupled climate modes(e.g.ENSO and IOD) and atmospheric circulation. However, this conclusion is based on the assumption that speleothems from Tham Mai cave were deposited under isotopic equilibrium and this climatic signal in speleothem $\delta^{18}$O is not blurred by local hydrological noise. In the case where high resolution cave records are available, such as Wanxiang, Heshang, and Tham Mai cave, sample specific factors become important. It is crucial to understand the interplay between climatic and local hydrological effects of speleothem $\delta^{18}$O. In the case of Tham Mai cave, our KarstFor modeling results suggest a 1.2 ‰ stalagmite $\delta^{18}$O variability that could be related to flow routing. Unfortunately, due to the relatively large $U - Th$ uncertainties,especially for TM6, we are not able to perform a direct comparison between Tham Mai cave speleothem $\delta^{18}$O and KarstFor pseudo proxies. Additional high resolution records are needed to better constrain climate versus last hydrological variability in $\delta^{18}$O. A direct comparison of pseudo proxy and stalagmite $\delta^{18}$O will help us untangle the mystery of cave hydrology, especially for places where long term cave monitoring is not available,such as Tham Mai cave.

## 4.6 Supplementary information

```
#test karrstfor on laos data, dataset from isogsm
#set values for initial store valumes, fluxes, isotope composition and cave temp.
setwd("~/Documents/HY_model")
SOILSTORXP=50.
SOILSTOR=50.
EPXSTORXP=100.
EPXSTOR=100.
EPICAP=400.
KSTSTOR2XP=50.
KSTSTOR2=50.
SOIL18OXP=-8.
KSTSTOR1XP=230.
KSTSTOR1= 230.
KSTSTOR118O = -8.
KSTSTOR118OXP = -8.
OVRFLOWXP=20
OVRFLOW=20
OVRFLOW18O=-8.
OVRFLOW18OXP=-8.
OVCAP=100
D18OXP=-8.
T1=20.
T2=20.
T3=20.
T4=20.
T5=20.
T6=20.
```

```
T7=20.
T8=20.
T9=20.
T10=20.
T11=20.
MEANT=20.
EPX18O=-7.
EPX18OXP=-7.
KSTSTOR218OXP=-7.
KSTSTOR218O=-7.
DRIP218O=-7.
P=-7.
R=-7.
STAL1D18O=-7.
STAL2D18O=-7.
STAL3D18O=-7.
STAL4D18O=-7.
STAL5D18O=-7.
STAL6D18O=-7
input = read.table("laos.txt",header=T)
attach(input)
HY_model_variables <- data.frame(
TT=NA,MM=NA,F1=NA,F3=NA,F4=NA,F5=NA,F7=NA,SOILSTOR=NA,
EPXSTOR=NA,KSTSTOR1=NA,KSTSTOR=NA,OVRFLOW=NA,STAL1D18O=NA,
STAL2D18O=NA,STAL3D18O=NA,STAL4D18O=NA,STAL5D18O=NA,STAL6D18O=NA)
#Reads the input file, which has the format 'number, month(1-12), PET, P, T, 18O.
for (i in 1:length(TT)){
    if (SOILSTORXP+PRP[i]-EVPT[i] < 0)
    {EVPT[i]=0}
```

```
57      else
        {SOILSTOR=SOILSTORXP+PRP[i]-EVPT[i]}
59      # Prevents any flux when surface is near-frozen. In this case, 0.0 degree C
        if(TEMPP[i] > 0)
61      {F1=SOILSTOR*0.2}
        else
63      {F1=0}
        #Increases epikarst store volume and generate overflow
65      EPXSTOR=EPXSTORXP+F1
        if(EPXSTOR > EPICAP)
67      {F4=EPXSTOR-EPICAP}
        else
69      {F4=0}
        # 0.08 term parameterised to maintain continuous F3 flux
71      F3=(EPXSTOR-F4)*0.008
        SOILSTOR=SOILSTOR-F1
73      EPXSTOR=EPXSTOR-F3-F4
        KSTSTOR1=KSTSTOR1XP+F3
75      F5=KSTSTOR1*0.005
        KSTSTOR1=KSTSTOR1-F5
77      KSTSTOR2=KSTSTOR2XP+F4
        if(KSTSTOR2 > OVCAP)
79      {F7=KSTSTOR2-OVCAP}
        else
81      {F7=0}
        KSTSTOR2=KSTSTOR2-F7
83      F6=KSTSTOR2*0.002
        KSTSTOR2=KSTSTOR2-F6
85      OVRFLOW=OVRFLOWXP+F7
```

```
F8=OVRFLOW*0.001
OVRFLOW=OVRFLOW-F8
E=PRP[i]+SOILSTORXP
if(E < 0.01)
{E=0.001}
else
{E=PRP[i]+SOILSTORXP}

f=SOILSTORXP/E
G=PRP[i]/E
# 0.03 term can be changed to enable evaporative fractionation in soil store
H=D18O[i]+(EVPT[i]*0.03)
SOIL18O=(f*SOIL18OXP)+(G*H)
if(SOIL18O > 0.0001)
{SOIL18O=SOIL18OXP}

A=F1
B=A+EPXSTORXP
C=(EPXSTORXP/B)*EPX18OXP
D=(A/B)*SOIL18O
EPX18O=C+D
B1=F3+KSTSTOR1XP
C1=(KSTSTOR1XP/B1)*KSTSTOR118OXP
D1=(F3/B1)*EPX18O
KSTSTOR118O=C1+D1
P=D18O[i]
R=D18OXP
DRIP118O=(EPX18O*0.50)+(P*.25)+(R*.25)
DRIP218O=(EPX18O*0.75)+(P*0.25)
```

```
115     if(F4 < 0.01)
        {KSTSTOR218O=KSTSTOR218OXP}
117     else
        {B2=F4+KSTSTOR2XP
119         C2=(KSTSTOR2XP/B2)*KSTSTOR218OXP
            D2=(F4/B2)*EPX18O
121         KSTSTOR218O=C2+D2}

123     if(F7 < 0.01)
        {OVRFLOW18O=OVRFLOW18OXP}
125     else
        {B3=F7+OVRFLOWXP
127         C3=(OVRFLOWXP/B3)*OVRFLOW18OXP
            D3=(F7/B3)*KSTSTOR218O
129         OVRFLOW18O=C3+D3}

131     # Caculates temperature dependent fractionation using Kim and O'Niell.
        #Other equations can be used.
133     #Also, monthly T averaging will be site specific.
        MEANT=(T1+T2+T3+T4+T5+T6+T7+T8+T9+T10+T11+TEMPP[i])/12
135     if(KSTSTOR2 < 0.01)
        {STAL1D18O=-99.9}
137     else
        {STAL1D18O=KSTSTOR218O+3.152+(-0.233*MEANT)}
139
        STAL2D18O=DRIP118O+3.152+(-0.233*MEANT)
141     STAL3D18O=DRIP218O+3.152+(-0.233*MEANT)
        if (EPXSTOR < 0.01)
143     {STAL4D18O=-99.9}
```

```
    else
145 {STAL4D18O=EPX18O+3.152+(-0.233*MEANT)}

147 if (KSTSTOR1 < 0.01)
    {STAL5D18O=-99.9}
149 else
    {STAL5D18O=KSTSTOR118O+3.152+(-0.233*MEANT)}
151
    if (OVRFLOW < 0.01)
153 {STAL6D18O=-99.9}
    else
155 {STAL6D18O=OVRFLOW18O+3.152+(-0.233*MEANT)}

157 # Output data for this timestep and update model terms

159 newrow=c(TT[i],MM[i],F1,F3,F4,F5,F7,
    SOILSTOR,EPXSTOR,KSTSTOR1,KSTSTOR2,OVRFLOW, STAL1D18O,
161 STAL2D18O,STAL3D18O,STAL4D18O,STAL5D18O,STAL6D18O )
    HY_model_variables = rbind(HY_model_variables,newrow)
163 T1=T2
    T2=T3
165 T3=T4
    T4=T5
167 T5=T6
    T6=T7
169 T7=T8
    T8=T9
171 T9=T10
    T10=T11
```

```
173     T11=TEMPP[i]
        EPX18OXP=EPX18O
175     EPXSTORXP=EPXSTOR
        SOILSTORXP=SOILSTOR
177     SOIL18OXP=SOIL18O
        KSTSTOR1XP=KSTSTOR1
179     KSTSTOR2XP=KSTSTOR2
        OVRFLOWXP=OVRFLOW
181     KSTSTOR118OXP=KSTSTOR118O
        KSTSTOR218OXP=KSTSTOR218O
183     OVRFLOW18OXP=OVRFLOW18O
        D18OXP=D18O[i]
185 }


187

write.table(HY_model_variables,file="output.txt",sep="␣")
```

# Chapter 5

# Inter-annual Controls on Oxygen Isotope Variability in Asian Monsoon Precipitation and Implications for Paleoclimate Reconstructions

## 5.1 Abstract

Asian monsoon precipitation $\delta^{18}O$ ($\delta^{18}O_p$ ) is known to vary in response to changes in monsoon strength, rainfall amount, moisture source region, and vapor transport history. To better interpret interannual $\delta^{18}O$ variability in high-resolution paleoclimate archives, such as speleothems and tree rings from this region, we utilize existing simulations from a spectrally nudged isotope-enabled general circulation model (IsoGSM) coupled with instrumental climate data to investigate the climatic controls on $\delta^{18}O_p$ at four key cave locations affected by the Asian monsoon: Qunf cave, Oman; Mawmluh cave, India; Tham Mai cave, Laos;

and Dongge cave, China. Comparison with instrumental climate data from 1979-2010 AD show that $\delta^{18}O_p$ at the four cave sites is unrelated to local precipitation amount, but instead reflects large-scale ocean-atmosphere processes. Spatial correlation with vertical wind shear indicates that $\delta^{18}O_p$ at all sites is significantly related to monsoon strength and Walker circulation. The spatial correlations with sea surface temperature (SST) and precipitation, suggest that the El Niño Southern Oscillation (ENSO) likely does play a role and that central Pacific type El Niño events influence precipitation $\delta^{18}O$ in Oman and northern Laos, in particular. A case study of Tham Mai cave reveals a moderate correlation with the NINO3.4 index (r=0.53) indicating that paleo-archives from this region may be useful for reconstructing past ENSO variability. Investigation of ENSO related moisture and $\delta^{18}O_p$ anomalies indicates that the positive anomalies over Southeast Asia during El Niño events may reflect increased contribution of high $\delta^{18}O$ precipitation from the Bay of Bengal.

## 5.2 Introduction

The Asian Monsoon (AM) is an important component of the global climate system that plays a major role in the transport of heat and moisture from the tropics to higher latitudes. Even small variations in the strength and/or timing of seasonal rainfall can have significant impacts on the billions of people living within the AM domain. Recent analyses of instrumental and reanalysis data have shown pronounced spatial and temporal variability in regional precipitation patterns across Asia (*Conroy and Overpeck*, 2011a; *Wang et al.*, 2001), yet our knowledge of the past regional behavior of the monsoon system, and the varying influence from modes of ocean-atmosphere circulation [e.g. Madden-Julian Oscillation (MJO), El Niño /Southern Oscillation (ENSO), Indian Ocean Dipole (IOD), Pacific Decadal Oscillation (PDO)], is significantly lacking. The increasing availability of high-resolution, oxygen-isotope ($\delta^{18}O$ ) based terrestrial paleoclimate records from across the AM region

offers a significant opportunity to improve our understanding of the physical links between regional AM variability and interannual to decadal scale coupled climate modes, such as ENSO. However, the factors influencing the $\delta^{18}O$ of precipitation ($\delta^{18}O_p$ ) are numerous and complex, and likely vary both in space and time; hence a more complete understanding of the climatic influences on $\delta^{18}O_p$ over different time-scales is needed for robust interpretation of $\delta^{18}O$ based paleoclimate records.

Numerous terrestrial and marine paleoclimate records of past AM variability have helped to broaden our understanding of decadal to orbital scale monsoon dynamics over the past several glacial-interglacial cycles (e.g. *Clemens and Prell*, 2003; *Wang et al.*, 2008; *Cheng et al.*, 2009; *Porter*, 2001). Recently, the most detailed records have been based on oxygen isotope variations preserved in cave calcite deposits or speleothems (e.g. *Wang et al.*, 2008). Assuming deposition under equilibrium conditions, the $\delta^{18}O$ of the calcite is dependent only on that of the drip-water, which is closely related to $\delta^{18}O_p$ , and cave temperature. In the tropics and AM region, the cave drip-water signal dominates and mainly reflects changing $\delta^{18}O_p$ , though some noise may be introduced through transport and mixing in the epikarst (*Baker and Bradley*, 2010). While orbital- to millennial-scale variations in speleothem $\delta^{18}O$ have been widely interpreted as proxies for local or regional precipitation amount and/or monsoon intensity (*Sinha et al.*, 2005; *Fleitmann et al.*, 2007; *Cheng et al.*, 2009), the precise mechanism responsible for the broadly consistent signals seen across the AM region, even in locales with very different modern precipitation patterns, is still highly debated (*Pausata et al.*, 2011; *Mann et al.*, 2009; *Dayem et al.*, 2010; *Clemens et al.*, 2010; *Chiang et al.*, 2015). Most studies invoke some combination of changing rainfall seasonality ( *Wang et al.*, 2001; *Clemens et al.*, 2010; *Chiang et al.*, 2015), rainfall amount (e.g. *Fleitmann et al.*, 2004; *Berkelhammer et al.*, 2010), and/or changes in the isotopic composition of incoming water vapor due to upstream processes such as rainout (*Pausata et al.*, 2011; *Mann et al.*, 2009) to explain the precessional cycles and millennial scale excursions in speleothem $\delta^{18}O$ in the AM region.

While speleothem $\delta^{18}O$ variability over orbital to millennial scales likely reflects large-scale monsoon variability, other recent studies suggest that higher-frequency $\delta^{18}O$ variability may be dominated by other factors, such as local precipitation amount (*Zhang et al.*, 2008; *Tan et al.*, 2010) or ENSO (*Myers et al.*, 2015; *Tan*, 2014). Previously, analysis of data from the Global Network for Isotopes in Precipitation (GNIP) have been conducted to investigate the climatic controls on $\delta^{18}O_p$ in the AM region. For instance, multiple regression analysis of monthly GNIP data indicates that the seasonal variations in $\delta^{18}O_p$ at sites across China are significantly related to precipitation amount and temperature, with southern sites in general more related to rainfall amount and northern sites more related to temperature (*Johnson and Ingram*, 2004). The magnitude of the observed effects are not large enough to explain the observed speleothem data, however, likely reflecting the fact that the seasonal cycle is not a good analogue for interannual scale variability. In a more recent analysis of GNIP data, it was determined that ENSO-driven changes in atmospheric-oceanic circulation are the dominant source of inter-annual $\delta^{18}O_p$ variability in the monsoon regions of China (*Tan*, 2014). Analysis of instrumental meteorological data indicated that this signal likely reflects the variation in the ratio of water vapor originating from distant oceans (relatively negative $\delta^{18}O_p$ ) versus the local ocean (relatively positive $\delta^{18}O_p$ ). Recent paleoclimate records based on $\delta^{18}O_p$ variations preserved in fast-growing speleothems or in tree-ring cellulose from the AM region have supported this latter interpretation, with significant relationships seen between proxy $\delta^{18}O$ and tropical Pacific SSTs during the instrumental period at some sites (*Myers et al.*, 2015; *Sano et al.*, 2012).

In order to robustly interpret these records and to investigate the influence of ENSO and other climate modes on $\delta^{18}O_p$ variability across the AM region, additional analysis of precipitation isotope systematics is needed. Due to the sparseness, short duration, and often discontinuous nature of available $\delta^{18}O_p$ data in the AM region, recent studies have utilized isotope enabled general circulation models (GCMs) to investigate the mechanisms of inter-annual $\delta^{18}O_p$ variability (e.g. *Conroy et al.*, 2013). Analysis of simulated $\delta^{18}O_p$ allows for

systematic investigation of the numerous parameters that are known to influence $\delta^{18}O_p$ variability, such as local precipitation amount (*Dansgaard*, 1964), the moisture source region (*Bhattacharya et al.*, 2003; *Griffiths et al.*, 2009; *Baker, Alexander J. and Sodemann, Harald and Baldini, James U. L. and Breitenbach, Sebastian F. M. and Johnson, Kathleen R. and van Hunen, Jeroen and Zhang, Pingzhong*, 2015), distillation during transport (*Hoffmann and Heimann*, 1997; *Yoshimura et al.*, 2003; *Vuille et al.*, 2005), recycling of water by land surface exchange processes (*Gat and Matsui*, 1991), and re-evaporation of precipitation in unsaturated air (*Worden et al.*, 2007).

To improve the interpretation of $\delta^{18}O$ records, especially but not limited to $\delta^{18}O$ from speleothems, we utilize the 20th century reanalysis nudged isotope incorporated global spectral model (IsoGSM) simulations of $\delta^{18}O_p$ (*Yoshimura et al.*, 2008) and observed climate data from the past 30 years to explore the relationship between $\delta^{18}O_p$ and multiple climatic factors within the AM region. We focus on four locations that, in addition to being strongly influenced by the AM, have key paleoclimate records based on speleothem $\delta^{18}O_p$ . These four sites are located in the Arabian peninsula (Oman), India, Southeast Asia (Laos), and China (Fig. 5.1). Spatial correlation analysis, time series analysis, and composite maps are used to reveal the relationship between $\delta^{18}O_p$ and climatic parameters over inter-annual timescales.

## 5.3 Study sites and climatology

### 5.3.1 Data description

The International Atomic Energy Association/World Meteorological Organization Global Network for Isotopes in Precipitation (GNIP) database is the most complete instrumental data source available for studying precipitation isotopic variations, but it is limited by sparse temporal and spatial resolution. We utilize interpolated data calculated from raw GNIP data

(*Bowen and Wilkinson*, 2002b; *Bowen and Revenaugh*, 2003) to estimate the monthly mean oxygen isotope composition of precipitation at our four study sites.

### 5.3.2 IsoGSM simulation data

IsoGSM is a water isotope-incorporated general circulation model with the spectral dynamical core (*Yoshimura et al.*, 2008)(Y08). We used the quasi-reanalysis product of IsoGSM nudged toward the NCEP/DOE Reanalysis 2 (R2) (*Kanamitsu et al.*, 2002) atmosphere. In this product, large scale atmospheric wind and temperature fields are constrained by the spectral nudging technique (*Yoshimura et al.*, 2008). The data contains all conventional atmospheric variables (wind, temperature, humidity, pressure, radiation, flux, etc.) and isotopic variables, i.e., isotopic ratio of atmospheric vapor, liquid and solid water storages (snow, soil moisture, river storage, etc.), and water fluxes (precipitation, evaporation, runoff, etc.) since 1979 to 2014 in 6-hourly intervals. In this study, we used a similar IsoGSM product nudged towards 20th century reanalysis data (*Compo et al.*, 2011) by *Yoshimura* (2015). In this product, similar with Y08, but for longer period, 1871-2010. We use these two IsoGSM products (*Yoshimura et al.*, 2008; *Yoshimura*, 2015) to explore the controlling interannual climatic factors of $\delta^{18}O_p$ .

We compare the observed (GNIP) and modeled (IsoGSM) isotope data with climatic data, including: i) instrumental precipitation data from the Global Precipitation Climatology Project (GPCP) data version 2.2; ii) outgoing longwave radiation (OLR) data from the National Oceanic and Atmospheric Administration (NOAA) (*Liebmann and Smith*, 1996); iii) wind shear, defined as the difference in zonal wind fields between 850hPa and 200hPa (U850-U200)., and obtained from the National Centers for Environmental Prediction-National Center for Atmospheric Research (NCEP-NCAR) reanalysis1 (*Kalnay et al.*, 1996); iv) vertically integrated atmosphere moisture transport, defined as the vertical integral of monthly mean

zonal and meridional moisture flux, and based on the reanalysis monthly data from NCEP-NCAR obtained from: http://www.cgd.ucar.edu/cas/catalog/newbudgets/index.html.

### 5.3.3 Site description and climatology

To investigate the mechanisms of interannual $\delta^{18}O_p$ variability in the AM region, we have chosen four cave sites for our study: Tham Mai Cave (20.75N, 102.65E, elevation 360 m), Laos; Dongge Cave (25.28N,108.08E, elevation 680 m), China; Mawmluh Cave (25.26N,91.71E, elevation 1290 m), India; and Qunf Cave (17.17N,54.3E, elevation 650 m), Oman. These study sites are all influenced by distinct monsoon sub-systems (Conroy and Overpeck), including the Indian summer monsoon (Qunf cave; Mawmluh Cave), East Asian summer monsoon (Dongge Cave), and Southeast Asian summer monsoon (Tham Mai Cave). Speleothem records have been obtained from each of these four caves, and millennial to orbital scale variations in $\delta^{18}O$ time-series have been interpreted as reflecting Asian monsoon intensity (e.g. *Fleitmann et al.*, 2003, 2007; *Berkelhammer et al.*, 2013; *Wang et al.*, 2005; *Dykoski et al.*, 2005; *Yang et al.*, 2016). Here we investigate the mechanisms underlying higher frequency variations (interannual to decadal scale) in $\delta^{18}O_p$ that may be recorded in fast growing speleothems, tree rings, and other archives from these regions.

Qunf cave in southern Oman is at the northern limit of the summer migration of the Intertropical Convergence Zone (ITCZ) and is influenced by the Indian summer monsoon. Approximately 90% of annual precipitation (400 to 500 mm at cave site) falls during the monsoon season from July to September. A high-resolution Holocene $\delta^{18}O$ record from Qunf cave has been interpreted to reflect the amount of monsoon precipitation from 10.3 to 2.7 and 1.4 to 0.4 kyr B.P., with more negative $\delta^{18}O$ values reflecting increased monsoon strength and vice versa (*Fleitmann et al.*, 2003). This record is dominated by orbital scale variability,

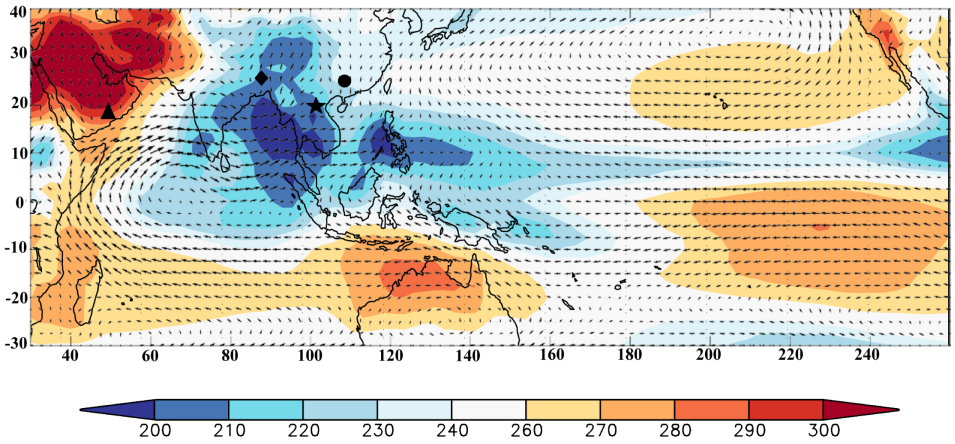


Figure 5.1: NCEP-NCAR JJAS 850 hPa wind vectors (m/s) and OLR averaged from 1979-2010 and location of the four cave sites: Tham Mai Cave, Laos (star), Dongge Cave, China (circle), Mawmluh Cave, India (diamand), and Qunf Cave, Oman (blue triangle).

with monsoon intensity closely tracking Northern Hemisphere summer insolation (NHSI), but it also records monsoon changes during more abrupt events such as the 8.2 kyr event.

Mawmluh Cave is located in Cherrapunji, Meghalaya, in northeastern India, and has an annual average precipitation of 11,000 mm, 70% of which falls during the summer monsoon months (June to September). In addition to monsoon precipitation, this location is highly sensitive to the northward propagating convective systems that originate in the Bay of Bengal. A speleothem $\delta^{18}O$ record that spans the period 3.6 to 12.5 kyr B.P. was interpreted as reflecting local precipitation amount related to ISM intensity via the 'amount effect' (*Berkelhammer et al.*, 2013). This is supported by the inverse relationship between monsoon precipitation amount and $\delta^{18}O_p$ identified in the IsoGSM simulations. However, *Berkelhammer et al.* (2013) also indicate that precipitation amount only accounts for 20% to 30% of the total $\delta^{18}O_p$ variability, thus other climate processes, such as shifts in the location of convective activity in the Bay of Bengal and seasonality, may also influence $\delta^{18}O_p$ at Mawmluh Cave. This speleothem record has now been replicated and extended back to 33.8 kyr B.P. (*Dutt et al.*, 2015). In addition, *Myers et al.* (2015) published a sub-annual resolution speleothem $\delta^{18}O$ record from Mawmluh Cave, which exhibits a significant corre-

lation with northern Pacific decadal variability and central equatorial Pacific SSTs. They suggested that variation in moisture transport during central Pacific type El Niño (CP El Niño ) events is a primary control on $\delta^{18}O_p$ in this region.

Tham Mai cave is located in the SEAM region of Northern Laos, near the interface of the ISM and EAM regions. The mean annual precipitation is 1195 mm, with 67% of precipitation occurring during the summer monsoon season (June to September). A speleothem $\delta^{18}O$ record spanning the period 0.85 to 14.36 kyr B.P. (*Yang et al.*, 2016) shows strong similarities with other Asian speleothem records (*Wang et al.*, 2005; *Hu et al.*, 2008; *Dong et al.*, 2010), and is interpreted as primarily reflecting Southeast Asian monsoon intensity. The record shows characteristically low values in the early Holocene followed by increasing values towards the present, indicating the strong influence of precessional forcing. Superimposed on this orbital scale variability is significant inter-annual to multi-decadal scale variability which may reflect other factors.

Dongge Cave is located in Guizhou province in southern inland China, in the East Asian monsoon region. Annual mean precipitation is 1753 mm, with 80% of the rainfall occuring during the summer monsoon months (May to October). A number of speleothem records have been published from Dongge Cave ranging from inter-annual to orbital scales (e.g. *Yuan et al.*, 2004; *Wang et al.*, 2005; *Dykoski et al.*, 2005; *Zhao et al.*, 2015). For example, *Dykoski et al.* (2005) produced a 16 kyr speleothem $\delta^{18}O$ record from Dongge that was interpreted as reflecting Asian monsoon intensity in response to orbital-scale variability in NHSI. Whether this record reflects local changes in the EAM or more regional shifts in the ISM is still a matter of debate, but recent studies have shown that Dongge Cave is located in a region of China where precipitation is predominantly sourced from the Indian Ocean and ISM regions; hence the $\delta^{18}O$ signal is likely dominated by ISM variability (e.g. *Yang et al.*, 2014; *Baker, Alexander J. and Sodemann, Harald and Baldini, James U. L. and Breitenbach, Sebastian F. M. and Johnson, Kathleen R. and van Hunen, Jeroen and Zhang, Pingzhong*, 2015).

## 5.4 Analyses and results

IsoGSM model validation *Yoshimura et al.* (2008) showed that IsoGSM simulated $\delta^{18}O_p$ agrees well with GNIP data for both annual and seasonal climatology, although they find that the amount of precipitation simulated in IsoGSM is systematically smaller than NCEP/DOE R2.

We first assess the skill of IsoGSM in simulating the $\delta^{18}O_p$ seasonal cycle. All four sites show strong seasonality in rainfall amount and $\delta^{18}O_p$ values, with summer monsoon moisture being significantly depleted in $\delta^{18}O_p$ with respect to boreal winter rainfall. IsoGSM monthly $\delta^{18}O_p$ values are significantly correlated with observed GNIP data for all sites (r >0.79, p < 0.01), though IsoGSM underestimates monthly $\delta^{18}O_p$ for some sites, especially for Qunf cave (Fig. 2). Each site shows a significant negative correlation (r>0.75, p < 0.01) between the climatology of monthly precipitation amount and modeled $\delta^{18}O_p$ values, with the maximum correlation occurring with a lag of 1-3 months (table S2). The maximum monthly precipitation for Tham Mai, Laos and Mawmluh Cave, India both occur in June, while precipitation peaks earlier for Qunf Cave, Oman ( April) and Dongge Cave, China ( May). The lowest $\delta^{18}O_p$ values exhibit a lag of 2-3 months behind maximum precipitation in both GNIP and IsoGSM data.

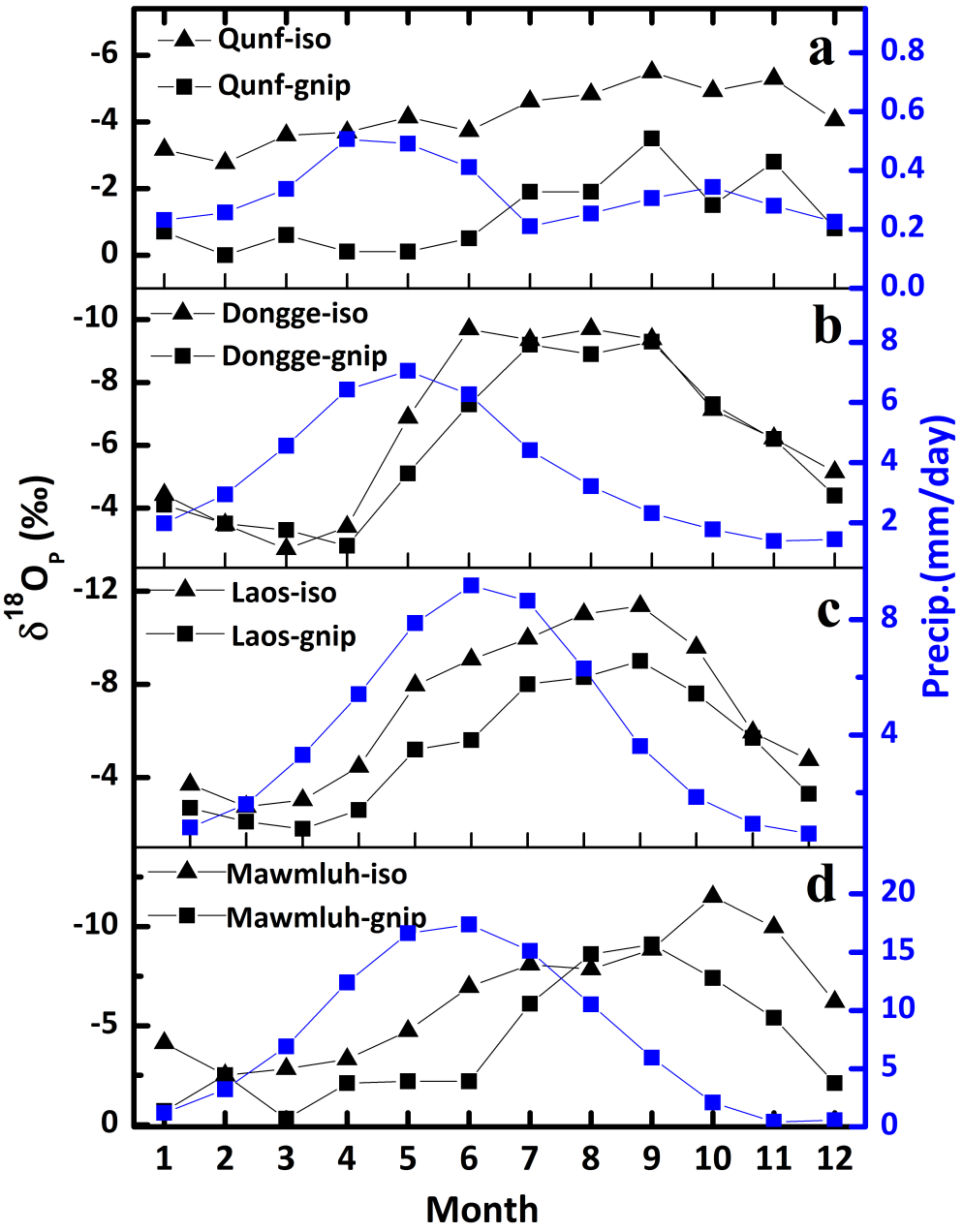


Figure 5.2: Monthly averages of GPCP precipitation (mm/day), GNIP $\delta^{18}O_p$ , and IsoGSM $\delta^{18}O_p$ for four sites averaged from 1979-2009. a) Qunf Cave, Oman, b) Dongge Cave, China c) Tham Mai Cave, Laos d) Mawmluh Cave, India.

### 5.4.1 Climatic controls on precipitation $\delta^{18}O_p$ variability

#### Precipitation amount

To investigate the timing and mechanisms of $\delta^{18}O_p$ variability on inter-annual timescales, we analyzed annual precipitation data from GPCP and $\delta^{18}O_p$ time series from IsoGSM from 1979-2009. The time series (Fig. 3) indicate that for all four cave locations, $\delta^{18}O_p$ is not significantly correlated with local precipitation amount (r ranges from 0-0.2). This suggests that the amount effect is not a major controlling factor for inter-annual $\delta^{18}O_p$ variability at these sites, and that other regional and broader climate process, such as ENSO, IOD, and monsoon strength must be considered.

A spatial correlation map with gridded GPCP data (Fig.4) shows that $\delta^{18}O_p$ at each site may be linked to non-local precipitation amount. Indeed, $\delta^{18}O_p$ at Qunf cave, Mawmluh Cave, and Tham Mai Cave all show a positive correlation (r= 0.4) with tropical central Pacific precipitation, indicating a potential link with ENSO. This positive correlation is particularly strong in the Niño 4 (5S-5N, 160E-150 W) and Niño 3.4 (5N - 5S, 120-170W) regions. These are the regions of central Pacific type ENSO events (CP El Niño ) (*Kao and Yu*, 2009). CP El Niño events manifest as positive SST and precipitation anomalies over the broad central Pacific region. Historical records have suggested that CP El Niño events, rather than those associated with the eastern equatorial Pacific (EP El Niño ), are more likely to be associated with Indian monsoon rainfall reduction (*Kumar et al.*, 2006; *Ashok and Yamagata*, 2009).

Tham Mai $\delta^{18}O_p$ also exhibits a negative correlation with precipitation over the broad Indo-Pacific warm pool region, indicating that increased convection over this region leads to more negative $\delta^{18}O_p$ over SE Asia. $\delta^{18}O_p$ of Dongge cave exhibits a negative correlation (r= -0.4 to -0.5) with precipitation in the central Indian Ocean and NE Bay of Bengal, suggesting

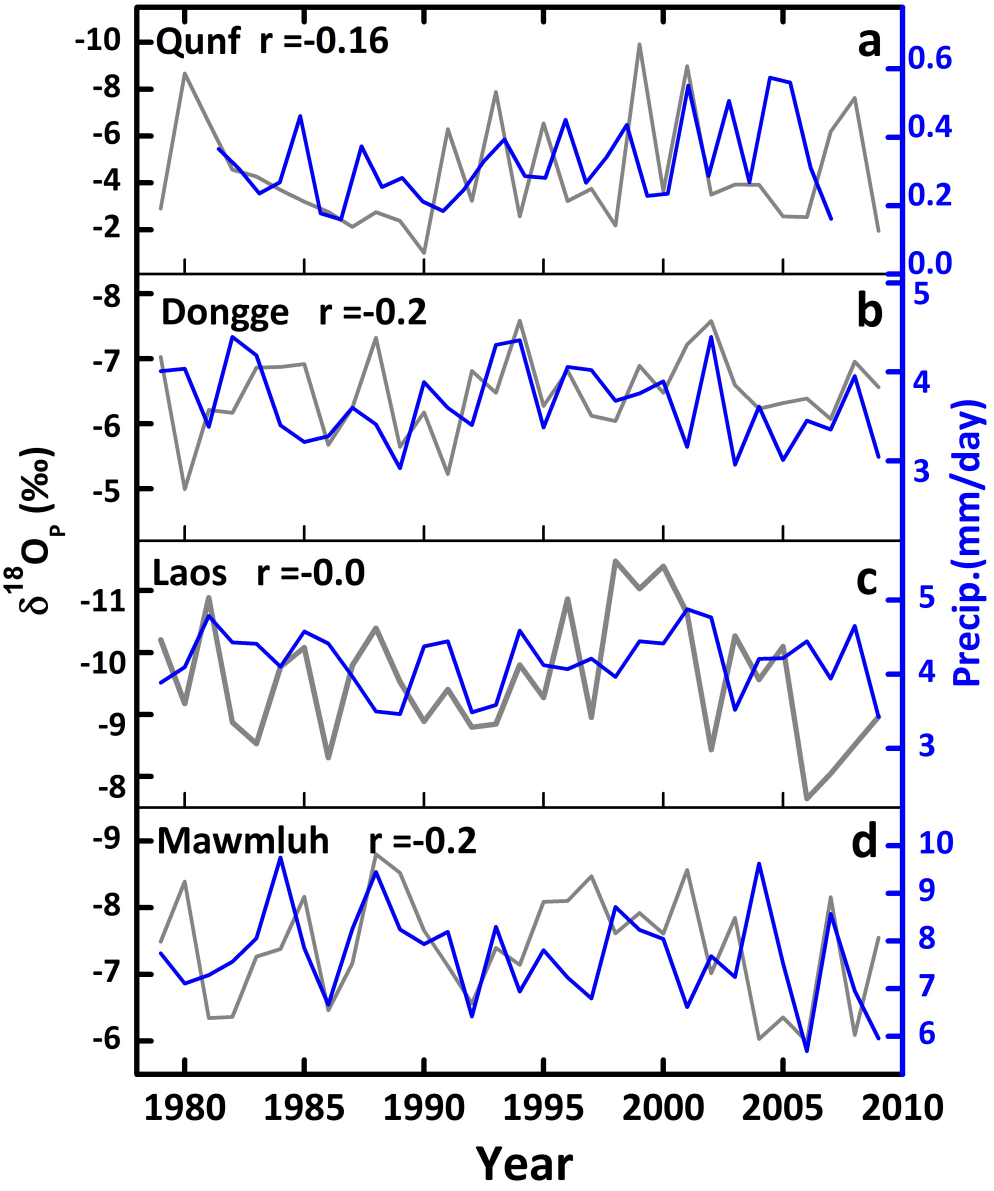


Figure 5.3: Time series of annual GPCP precipitation amount (mm/day) and IsoGSM $\delta^{18}O_p$ from the IsoGSM grid point closest to multiple sites in the Asian monsoon region from 1979-2009. a) Qunf Cave, Oman b) Dongge Cave c) Tham Mai cave, Laos d) Mawmluh cave, India. The correlation coefficients (r) between the two time series are shown for each location.

that $\delta^{18}O_p$ from the EAM region may be affected by upstream precipitation in the moisture source region which leads to depletion of $\delta^{18}O$ in water vapor transported to southern China.

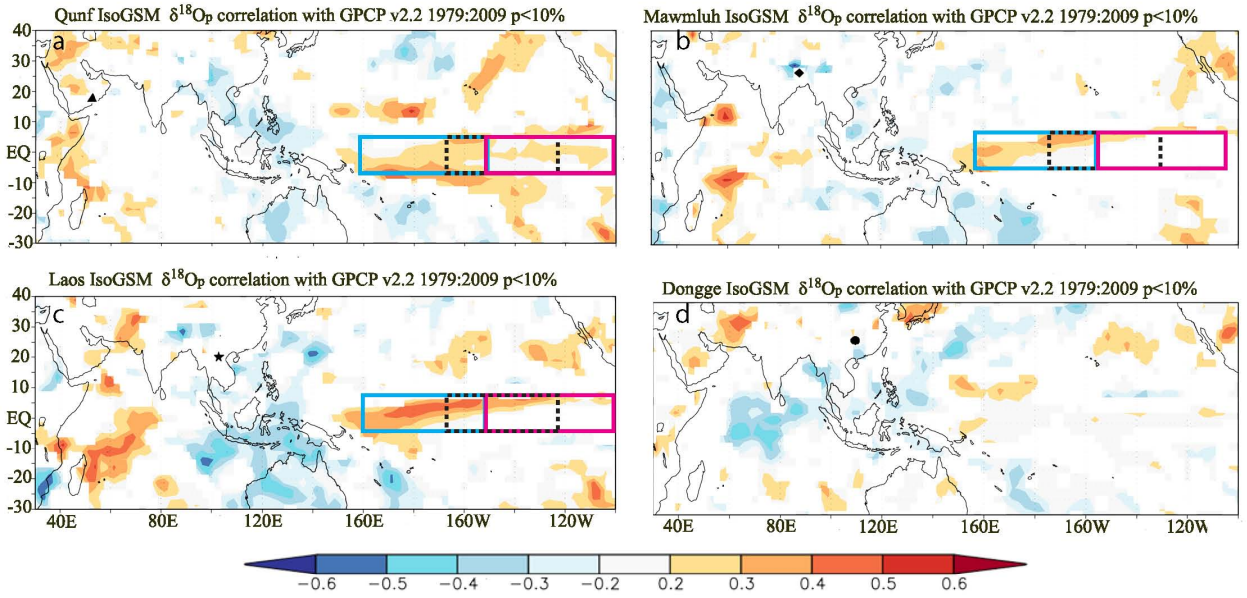


Figure 5.4: Correlation of GPCP with IsoGSM $\delta^{18}O_p$ extracted from grid point closest to four cave sites in the Asian Monsoon and tropical Indo-Pacific region and four potential isotopic influential climatic factors for the period 1979-2010. Colors represent significant r value at the 90% level. From top left to bottom right: a)Qunf Cave, Oman (triangle); b)Mawmluh Cave, India(diamond); c)Tham Mai Cave, Laos(star); d)Dongge Cave, China(circle). Light blue square is Niño 4 region(5S-5N, 160E-150 W), black dash square is Niño 3.4 region(5S-5N, 120-170W), and red square is Niño 3 region(5S- 5N, 90W-150W)

### Sea surface temperature

Spatial correlation maps between $\delta^{18}O_p$ and SST for each study site are shown in figure 5. $\delta^{18}O_p$ from IsoGSM of all four sites, especially Qunf, Mawmluh, and Tham Mai caves, show a positive correlation with Pacific SSTs over the Niño 4 and 3.4. region and in the western and southern Indian Ocean, suggesting that the $\delta^{18}O_p$ of annual rainfall may be influenced by ENSO and IOD. In particular, $\delta^{18}O_p$ of Qunf Cave has a strong positive correlation (r > 0.4) with broad central Pacific and southern Indian Ocean SST anomalies, patterns that bear resemblance to the typical spatial pattern of SST anomalies during CP El Niño events (*Kao and Yu*, 2009). This spatial correlation pattern between $\delta^{18}O_p$ and both Pacific Ocean and Indian Ocean SSTs is also present for the other three study sites, though the relationships

are not as strong. While Mawmluh, Tham Mai and Dongge cave $\delta^{18}O_p$ exhibit a positive correlation with SST anomalies in the tropical Pacific region, the relationship with SSTs in the Indian Ocean is significantly weaker.

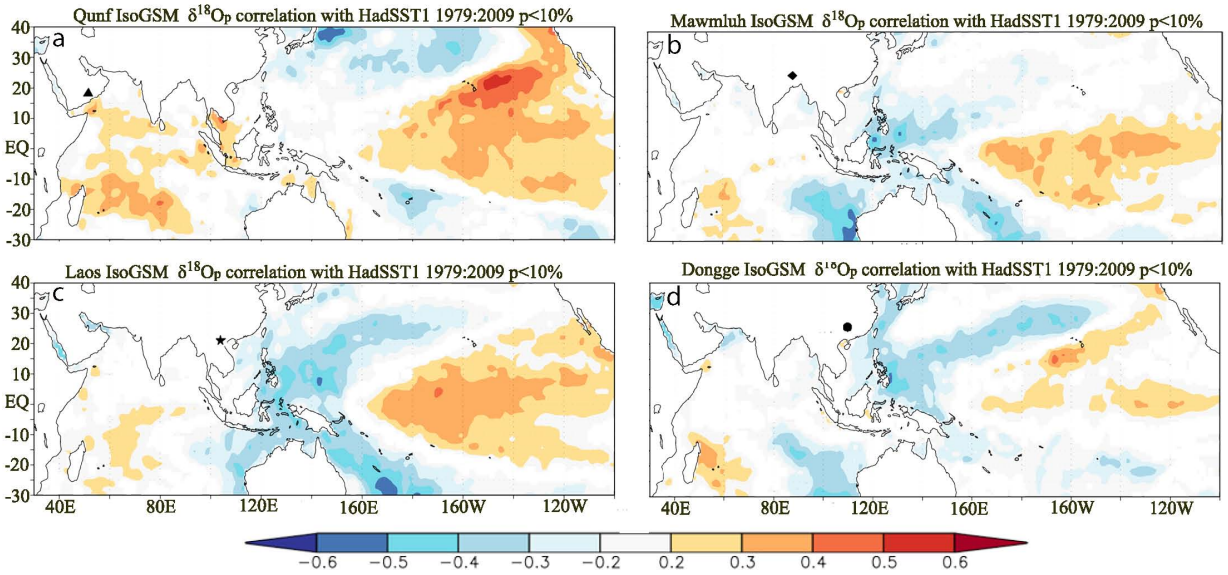


Figure 5.5: Correlation of HadSST1 with IsoGSM $\delta^{18}O_p$ extracted from grid point closest to four cave sites in the Asian Monsoon and tropical Indo-Pacific region and four potential isotopic influential climatic factors for the period 1979-2010. Colors represent significant r value at the 90% level. From top left to bottom right: a)Qunf Cave, Oman (triangle); b)Mawmluh Cave, India(diamond); c)Tham Mai Cave, Laos(star); d)Dongge Cave, China(circle).

### Sea level pressure

The AM is associated with large-scale changes in the seasonal SLP contrast between the Asian continent and the surrounding oceans (*Krishnamurti*, 1985; *Lau et al.*, 1988). The anomalous SLP configuration of the AM (i.e. high pressure over the ocean and low pressure over the land during summer) allows moisture transport from the Indian Ocean to the Asian continent. Spatial correlation maps between $\delta^{18}O_p$ and SLP data show that $\delta^{18}O_p$ values at all cave sites are positively correlated with SLP in the Bay of Bengal and Indian Ocean. The strongest relationships are seen for Tham Mai and Mawmluh ($r > 0.5$), indicating that the

$\delta^{18}O$ of water vapor reaching these cave sites is likely influenced by rainout over the Bay of Bengal and central/eastern Indian Ocean (Fig. 6). Indeed, close comparison between these two maps (Figs 6b and 6c) reveals very similar patters, with both cave sites showing strong correlations with Bay of Bengal, eastern Indian Ocean, and sub-tropical West Pacific SLP. These similarities suggest a common dynamical mechanism to explain the inter-annual $\delta^{18}O_p$ variability at these sites. By contrast, Dongge has a slightly weaker correlation with Bay of Bengal and tropical West Pacific SLP, whilst Qunf has the closest relationship with SLP over the western Indian Ocean. In general, negative SLP anomalies over the moisture source regions for all sites are associated with stronger surface convergence and intensification of convection which lead to strengthened low-level cyclonic circulation, heavier precipitation, and more negative $\delta^{18}O_p$ .

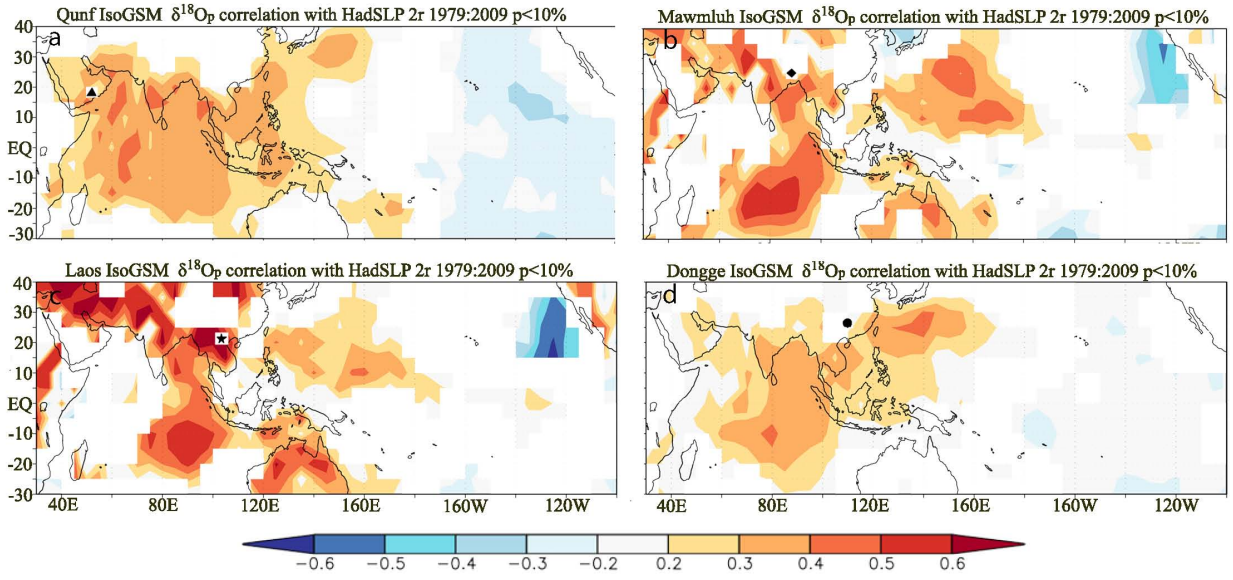


Figure 5.6: Correlation of HadSLP2 with IsoGSM $\delta^{18}O_p$ extracted from grid point closest to four cave sites in the Asian Monsoon and tropical Indo-Pacific region and four potential isotopic influential climatic factors for the period 1979-2010. Colors represent significant r value at the 90% level. From top left to bottom right: a)Qunf Cave, Oman (triangle); b)Mawmluh Cave, India(diamond); c)Tham Mai Cave, Laos(star); d)Dongge Cave, China(circle).

**Atmospheric circulation**

Webster and Yang (1992) proposed a broad scale monsoon index based on the magnitude of the mean summer vertical wind shear (VWS) between upper and lower tropospheric zonal flow over the 0-20N and 40-110E AM domain. An increase in both the upper level easterlies and the lower level westerlies can be observed during strong monsoon seasons, while a relaxation is more likely during weaker monsoon seasons (*Webster and Yang*, 1992). Significant negative correlations (r >0.3 to 0.6) between $\delta^{18}O_p$ and VWS (U850-200) values over the Indian Ocean are observed for Tham Mai cave, Qunf cave and Mawmluh cave locations (Fig. 7). In particular, Tham Mai $\delta^{18}O_p$ exhibits the strongest negative correlation (r >0.5) with VWS in the Eastern Indian Ocean, whilst $\delta^{18}O_p$ at Qunf and Dongge caves are only weakly to moderately correlated with VWS over the Northern Indian Ocean. Mawmluh Cave $\delta^{18}O_p$ also exhibits only a weak negative correlation with VWS over the Northwest Indian Ocean. In general though, it is clear that all cave sites show a positive correlation with VWS over the western Tropical Pacific region. In fact, the observed dipole pattern of negative correlations over the Indian Ocean and positive correlations over the Pacific Ocean at all sites is consistent with a strong linkage between a weaker Walker circulation, a weaker monsoon, and increased $\delta^{18}O_p$ at each locale, though the relationship appears strongest for Tham Mai, Laos.

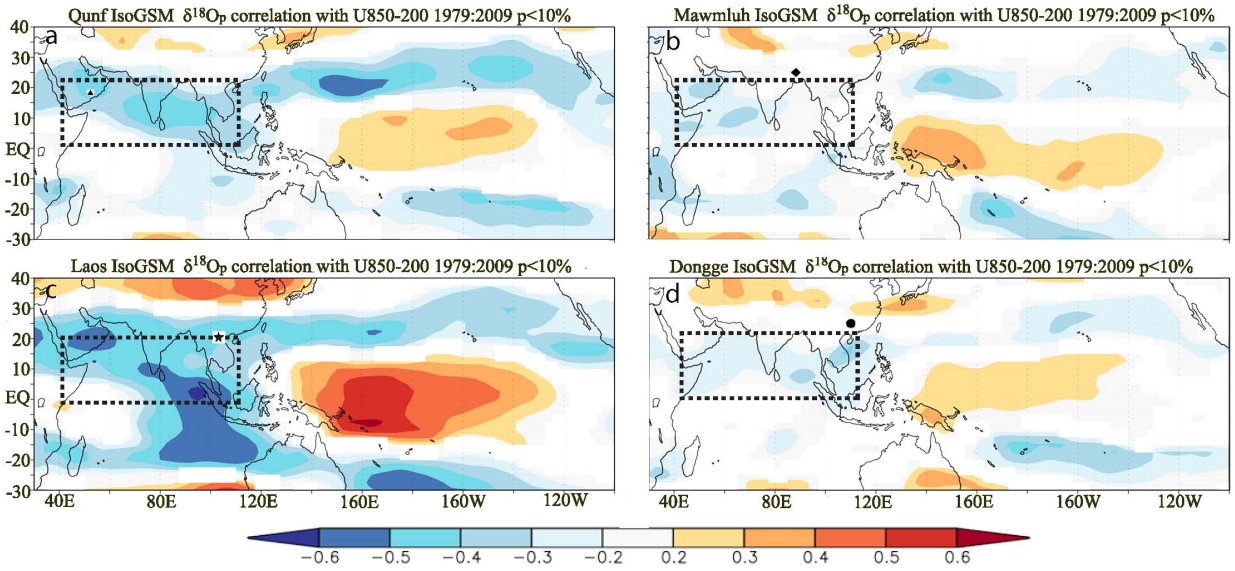


Figure 5.7: Correlation of NOAA U850-U200 wind shear with IsoGSM $\delta^{18}O_p$ extracted from grid point closest to four cave sites in the Asian Monsoon and tropical Indo-Pacific region and four potential isotopic influential climatic factors for the period 1979-2010. Colors represent significant r value at the 90% level. From top left to bottom right: a)Qunf Cave, Oman (triangle); b)Mawmluh Cave, India(diamond); c)Tham Mai Cave, Laos(star); d)Dongge Cave, China(circle). Box shown in part d is the region used for the Webster-Yang monsoon index (0-20N, 40-110 E).

### 5.4.2 Relationships between $\delta^{18}O_p$ , ENSO, IOD and AM

To further investigate how ENSO, IOD and AM affect $\delta^{18}O_p$ , we composite AM season (JJAS) $\delta^{18}O_p$ during two strong El Niño years (1982 and 1997 and examine $\delta^{18}O_p$ of the following years, 1983 and 1999 (Fig.8). The 1982 El Niño year was followed by a positive IOD year while the 1997 El Niño year was followed by a strong La Niña event. During composited El Niño years, Tham Mai Cave and Mawmluh Cave have positive $\delta^{18}O_p$ anomalies, whilst during the following La Niña and/or positive IOD year they have negative anomalies. A strong positive JJAS $\delta^{18}O_p$ anomaly over the Indo-Pacific warm pool region, together with a negative anomaly over the central equatorial Pacific, was exhibited during the composited El Niño years. Conversely, during the La Niña year, negative JJAS $\delta^{18}O_p$ anomalies were observed over the Indo-Pacific, while positive anomalies were observed over the Tropical West Pacific and South China Sea. The positive IOD event had a similar, but slightly weaker, effect on monsoon season $\delta^{18}O_p$ compared with that of the La Niña event.

Further investigation of ENSO/IOD effects on monsoon season moisture transport is facilitated by compositing AM season vertically integrated atmosphere moisture transport anomalies during El Niño , La Niña and positive IOD years (Fig. 9). A slight decrease in moisture from the central Indian Ocean and tropical Pacific (Fig. 9a: red boxes), together with increasing moisture from the Bay of Bengal, was exhibited during composited El Niño years. By contrast, a slight increase of moisture from the Indian Ocean and western tropical Pacific (Figs 9b and 9c; blue boxes), together with decreasing moisture from the Bay of Bengal (Figs 9b and 9c; red box), was observed during the La Niña and positive IOD year.

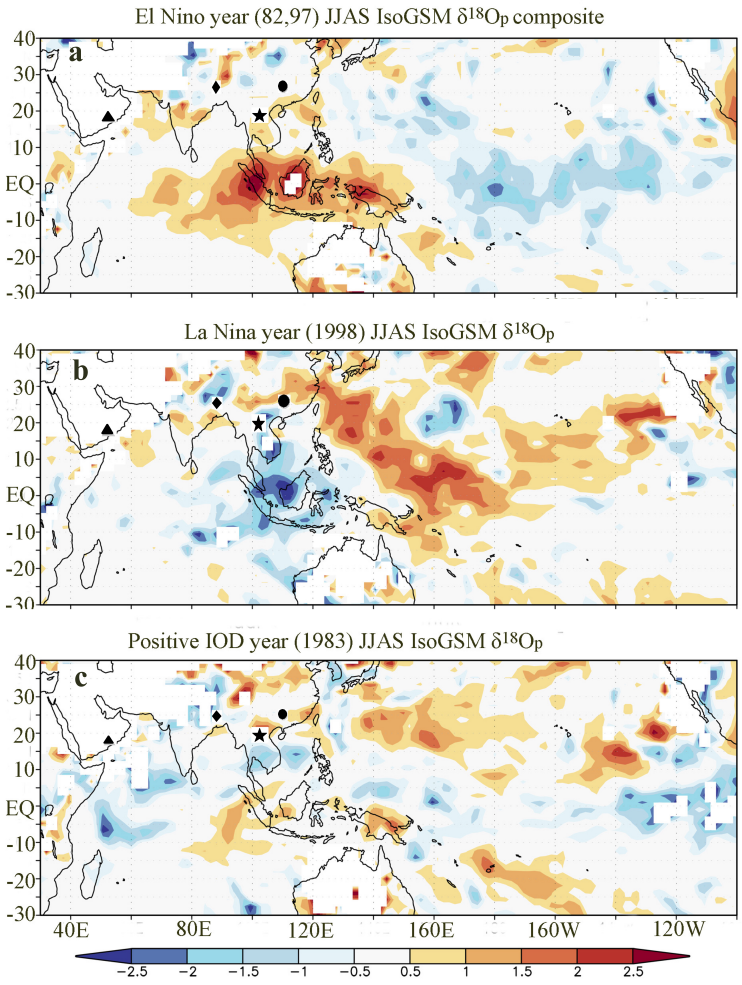


Figure 5.8: IsoGSM $\delta^{18}O_p$ anomaly composts of a) June-September 1982 and 1997 (two strong El Niño year); b) June-September 1998 (Strong La Niña year); c) June-September 1983 (Strong positive IOD year). Four cave locations: Qunf Cave, Oman (triangle), Mawmluh Cave, India(diamond), Tham Mai Cave, Laos(star), Dongge Cave, China(circle). JJAS $\delta^{18}O_p$ anomaly is calculated by using JJAS precipitation weighted $\delta^{18}O_p$ from specified year subtract the mean of JJAS precipitation weighted $\delta^{18}O_p$ 1979-2010.

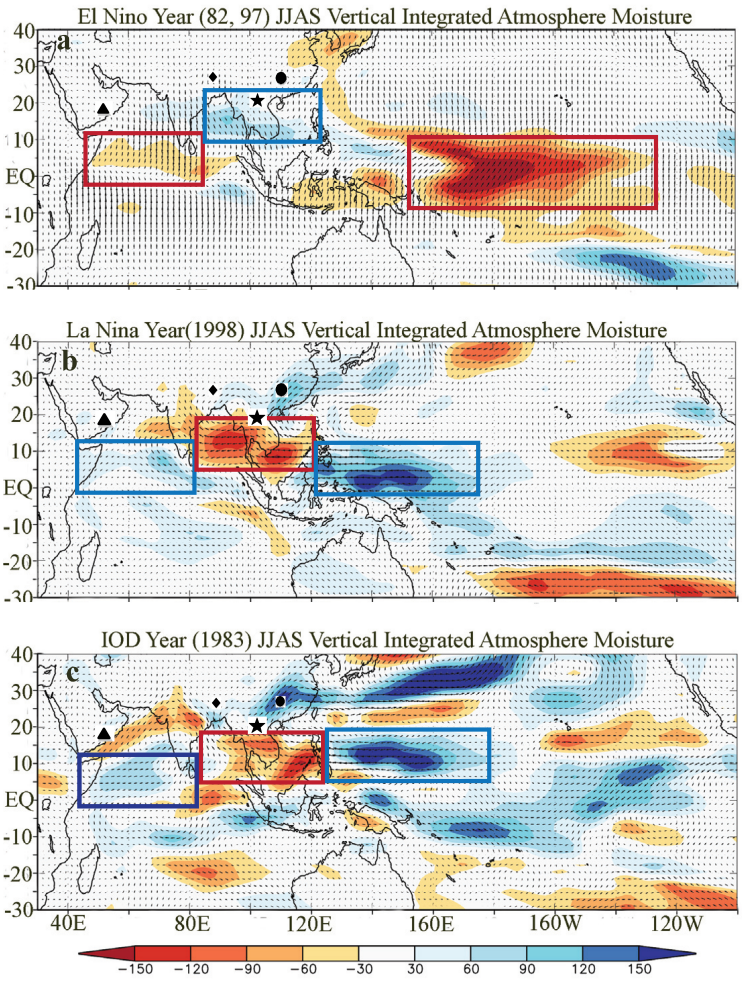


Figure 5.9: NCEP-NCAR vertical integrated atmosphere moisture transport (kg m-1 s-1) anomaly composts of a) June-September 1982 and 1997 (two strong El Niño year); b) 1998 (Strong La Niña year); c) of June-September 1983 (Strong positive IOD year). Different colors indicate amount of total water vapor flux anomaly, and vector indicate direction of total water vapor flux. Four cave locations: Qunf Cave, Oman (triangle), Mawmluh Cave, India (diamond), Tham Mai Cave, Laos (star), Dongge Cave, China (circle). JJAS Mosture transport anomaly is calculated by using JJAS moisture transport from specified year subtract the mean of JJAS moisture transport of 1979-2010.

## 5.5 Discussion and conclusions

Previous results have indicated that the dominant controls on $\delta^{18}O_p$ include local precipitation variability, regional hydrology, moisture source, atmospheric mixing and the degree of rainout during transit (*Lewis et al.*, 2010). Here we examine these range of effects in detail.

### 5.5.1 $\delta^{18}O_p$ – climate relationships

Both the time series analysis (Fig. 3) and spatial correlation maps (Fig. 4) suggest that local precipitation is not a dominant factor controlling the $\delta^{18}O_p$ at the four sites. *Berkelhammer et al.* (2013) suggested that summer monsoon precipitation amount has a significant relationship with $\delta^{18}O_p$ at Mawmluh cave, though they mention that this relationship is only significant when September and October are included in the monsoon rainfall season; this suggests that the timing of monsoon withdrawal is an important factor for $\delta^{18}O_p$ at this site. Contrary to this, here we use annual precipitation amount and annual weighted $\delta^{18}O_p$ , which may explain the lack of a strong correlation between local precipitation amount and $\delta^{18}O_p$ at Mawmluh site.

Results of this work also suggest that different sub-sectors of the AM share a similar moisture source. Indeed, the $\delta^{18}O_p$ at all four study sites, especially Qunf, Mawmluh and Tham Mai, exhibit a strong correlation with SLP and wind shear in the broad tropical Indian Ocean, indicating that this ocean basin is likely a major source of moisture for the broad AM region, in agreement with other recent studies (*Baker, Alexander J. and Sodemann, Harald and Baldini, James U. L. and Breitenbach, Sebastian F. M. and Johnson, Kathleen R. and van Hunen, Jeroen and Zhang, Pingzhong*, 2015). *Baker, Alexander J. and Sodemann, Harald and Baldini, James U. L. and Breitenbach, Sebastian F. M. and Johnson, Kathleen R. and van Hunen, Jeroen and Zhang, Pingzhong* (2015) used a Lagrangian model to diagnose

different precipitation moisture sources for several Chinese cave sites, and demonstrated that the Indian Ocean is the primary moisture source for the East Asian monsoon, while the Pacific Ocean is only a minor contributor to monsoonal precipitation. The observed correlations with SLP and VWS over the tropical Indo-Pacific suggest a strong role for IPWP convection in modulating EASM intensity. Increased convection and uplift of air masses over the IPWP also likely contributes to "pre- fractionation" of moisture advected to the study sites. This mechanism was also suggested by recent reconstructions of Southeast Asian rainfall $\delta^{18}O$ from the isotopes of tree-ring cellulose, which show that $\delta^{18}O$ of rainfall in the southern Indochina region is also strongly influenced by interannual-to-decadal scale shifts in Pacific SSTs (*Xu et al.*, 2011; *Zhu et al.*, 2012)

Employing the ECHAM-4 GCM fitted with isotopic tracers, *Vuille et al.* (2005) showed that there was a significant correlation (r =0.75) between VWS (U850-200) over the region 7.5N-2.5S and 45-20W, and the Niño 3.4 index. Several paleo-records from the AM domain have also shown a strong ENSO signal. For example, a 300-yr tree-ring cellulose $\delta^{18}O$ record from Vietnam (Sano 2012), which is highly correlated with another tree ring record from Laos (*Xu et al.*, 2011), exhibits a strong correlation with SSTs in the tropical Pacific (central) and Indian Oceans; this suggests the $\delta^{18}O_p$ of these locations is also tightly coupled with ENSO variability (*Xu et al.*, 2011; *Sano et al.*, 2012).

Our composite maps of JJAS $\delta^{18}O_p$ anomalies (Fig. 8) indicate a positive (negative) excursion in $\delta^{18}O_p$ during the El Niño years (La Niña and positive IOD year), which is characterized by increased (decreased) moisture transport from the Bay of Bengal and decreased (increased) moisture transport from the Indian Ocean (Fig. 9). This change in moisture source leads to a shorter vapor transport distance (and thus more positive $\delta^{18}O_p$ ) to the site of monsoon rainout during the El Niño year. By contrast, during the La Niña and positive IOD year, there is an observed increase in the moisture flux from the Indian Ocean and opposing decrease from the Bay of Bengal, indicating that most of the moisture transported

to SE Asia now travels a greater distance, and as a result becomes more depleted in $\delta^{18}O_p$ ). We infer these alternating shifts in moisture source and transport pathways to explain, at least in part, the positive correlation between $\delta^{18}O_p$ and ENSO in SE Asia.

Previous research indicates that VWS over the southern Indian Ocean, in particular the central and eastern parts of basin, is weaker during El Niño events compared with La Niña events (*Kuleshov et al.*, 2009; *Cherchi and Navarra*, 2013). This negative ENSO-monsoon relationship can be interpreted as a modulation of the Walker circulation (*Ju and Slingo*, 1995). For example, during the warm ENSO phase, the ascending limb of the Walker circulation over the western Pacific shifts eastward in response to SST warming of the eastern Pacific. This eastward propagation of lower-level convergence from the western Pacific is replaced by dry descending air, resulting in decreased ISM rainfall (and thus more positive $\delta^{18}O_p$ )(*Goswami*, 1998; *Lau and Wang*, 2006; *Collins et al.*, 2010). This negative ENSO-monsoon relationship may also explain the observed positive $\delta^{18}O_p$ at our study sites during the El Niño year. Of all the study sites examined in the study, the $\delta^{18}O_p$ data from northern Laos (Tham Mai Cave) appears to have the strongest negative correlation with U850-200 VWS (Fig. 7). Tham Mai sits at the interface between the ISM and EASM zones, yet the majority of moisture is sourced from the Indian Ocean and Bay of Bengal. Hence, the effects of ENSO on vapor source and transport fractionation during the monsoon season are particularly pronounced at Tham Mai Cave.

### 5.5.2 Different modes of ENSO influence on $\delta^{18}O_p$ in the Asian monsoon region

*Yu and Kao* (2007) discussed two types of ENSO in the tropical Pacific Eastern Pacific (EP) El Niño and Central Pacific (CP) El Niño based on surface observations and subsurface ocean assimilation data. CP El Niño events typically have SST and surface wind anomalies that are

confined to the central Pacific (Niño 4 and Niño 3.4 region). Moreover, because these types of ENSO are more likely to generate warming in southern Indian Ocean, they generally have stronger teleconnnections with the southern Indian Ocean (*Kao and Yu*, 2009). Conversely, EP El Niño events are generally characterized by SST anomalies centered in the eastern tropic Pacific (Niño 3 region) (*Kao and Yu*, 2009). Recent studies have looked at the different effects of these two ENSO "flavors" on $\delta^{18}O$ -based paleo-records. For example, *Myers et al.* (2015) published a sub-annual resolution speleothem $\delta^{18}O$ record from Mawmluh Cave, India, which exhibits a significant correlation with northern Pacific decadal variability and central equatorial Pacific SSTs. They suggested that variations in moisture transport during CP El Niño events is a primary control on $\delta^{18}O_p$ in this region.

The correlation maps between $\delta^{18}O_p$ at all sites and SSTs (Fig. 5), largely resembles the pattern of SST variability associated with CP El Niño events (*Kao and Yu*, 2009), with the strongest correlation being located in the broad central Pacific Ocean and Southern Indian Ocean regions. Moreover, correlation patterns between $\delta^{18}O_p$ and precipitation (Fig. 4) at, in particular, Qunf and Tham Mai caves, are very similar in nature to the precipitation anomalies observed during CP El Niño events. These patterns are characterized by a dipole-like structure within the tropical Pacific, with the largest anomalies being located in the far western and eastern Pacific. Therefore, whilst there are spatially varying influences of the two types of El Niño on the different subsectors of Asian Monsoon $\delta^{18}O_p$ , our spatial correlation map does indicate that, overall, sections of the AM region may be affected by CP El Niño modes.

Close inspection of the average composite $\delta^{18}O_p$ during El Niño and La Niña years (see table S1 and Fig S1 ) shows that Dongge, Tham Mai and Mawmluh cave sites all exhibit more negative $\delta^{18}O_p$ values during the La Niña year, more positive values during the El Niño year, and intermediate values during the neutral years. Qunf Cave does not share this pattern, but instead has more positive $\delta^{18}O_p$ (-4.3) during the CP- El Niño mode compared with neutral

average $\delta^{18}O_p$ (-4.7); this, again confirms a CP El Niño signal in Qunf $\delta^{18}O_p$ . Although, given that we only examined annual spatial correlations and composites, and in light of the ongoing debates on the different methods of identifying the two types of El Niño (*Ashok et al.*, 2007; *Yeh et al.*, 2009; *Yu et al.*, 2012), we cannot exclude the CP El Niño effects on other sites. Hence, further analysis on differentiating the two types of El Niño influence on AM region $\delta^{18}O_p$ is still needed.

### 5.5.3 Interpretation of $\delta^{18}O$ based paleo-records from Tropical Indo-Pacific

As discussed above, the Indo-Pacific region (including Tham Mai Cave) is particularly sensitive to moisture source variations and atmosphere circulation changes. To help place the modern $\delta^{18}O_p$ systematics into the context of the paleo record, we use Tham Mai Cave as a case study to further investigate the interpretation of other $\delta^{18}O$ -based paleo-records from the AM region. To do so, we examined the IsoGSM and instrumental climate data from the grid point closest to Tham Mai Cave.

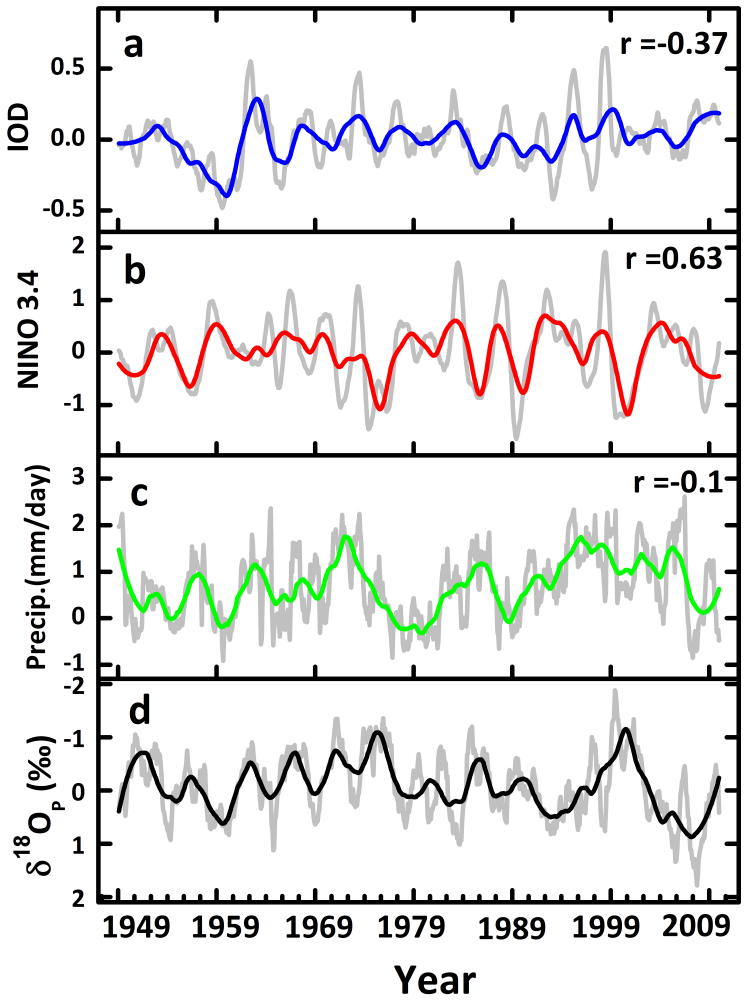


Figure 5.10: Monthly $\delta^{18}O_p$ (d) and precipitation (c) anomalies from the IsoGSM grid point closest to Tham Mai cave, Laos. HadISST Nino 3.4 index (b) and HadISST IOD index, (a) are shown for comparison. Grey lines are monthly data with seasonal cycle removed and bold, colored lines are 5-year running means. Correlation coefficients (r) are given for precipitation, Niño 3.4, and IOD versus $\delta^{18}O_p$ .

The Tham Mai annual $\delta^{18}O_p$ time series from 1979-2010 (Fig. 10, black line) is weakly correlated with local precipitation anomalies (r= -0.21, p<0.01) and significantly correlated with the Niño 3.4 index (r = 0.63, p<0.01). By contrast, the correlation between Tham Mai $\delta^{18}O_p$ anomalies and the IOD index is around zero, though this value becomes significant at -0.35 when a lag of 12 months is imposed (Fig. 11).

After smoothing each series with a 5-year running average, the correlation between Tham Mai $\delta^{18}O_p$ and the Niño 3.4 index also increased to 0.63, whilst the correlation with the IOD

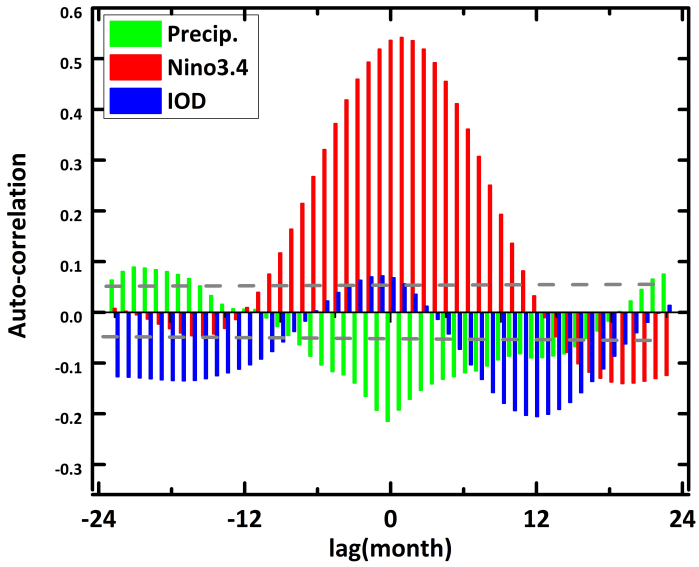


Figure 5.11: Cross correlation between monthly HadISST Niño 3.4 index(red), HadISST IOD index(blue), Laos local precipitation anomaly(green) and $\delta^{18}O_p$ anomaly extracted from Iso GSM from 1948-2009. The dash line is approximate critical values (at the 5% level).

index increased to 0.37. The correlation between $\delta^{18}O_p$ and local precipitation, however, actually decreased to -0.1. Hence, the interannual variability of Tham Mai $\delta^{18}O_p$ is likely affected by ENSO and IOD cycles. Meanwhile, analysis of the longer time series data from 1871-2010 (Fig. 12) shows an increasing trend of precipitation since 1925 (this turning point is identified by spline regression, see text S2), with superimposed decadal scale variability. Prior to this, the $\delta^{18}O_p$ and precipitation data display a general decreasing trend from 1900 to 1925. These lower-frequency phase relationships are consistent with an amount effect or monsoon intensity control on precipitation $\delta^{18}O_p$ at this site ($r = -0.57$, $p<0.001$). Therefore, the $\delta^{18}O_p$ in northern Laos may be affected by different factors that operate on different time scales and frequencies. For example, in northern Laos, the low frequency trends may reflect monsoon strength, while the inter-annual to decadal-scale variability may reflect coupled ocean-atmosphere modes that influence the precipitation $\delta^{18}O_p$ , but not necessarily the amount of precipitation.

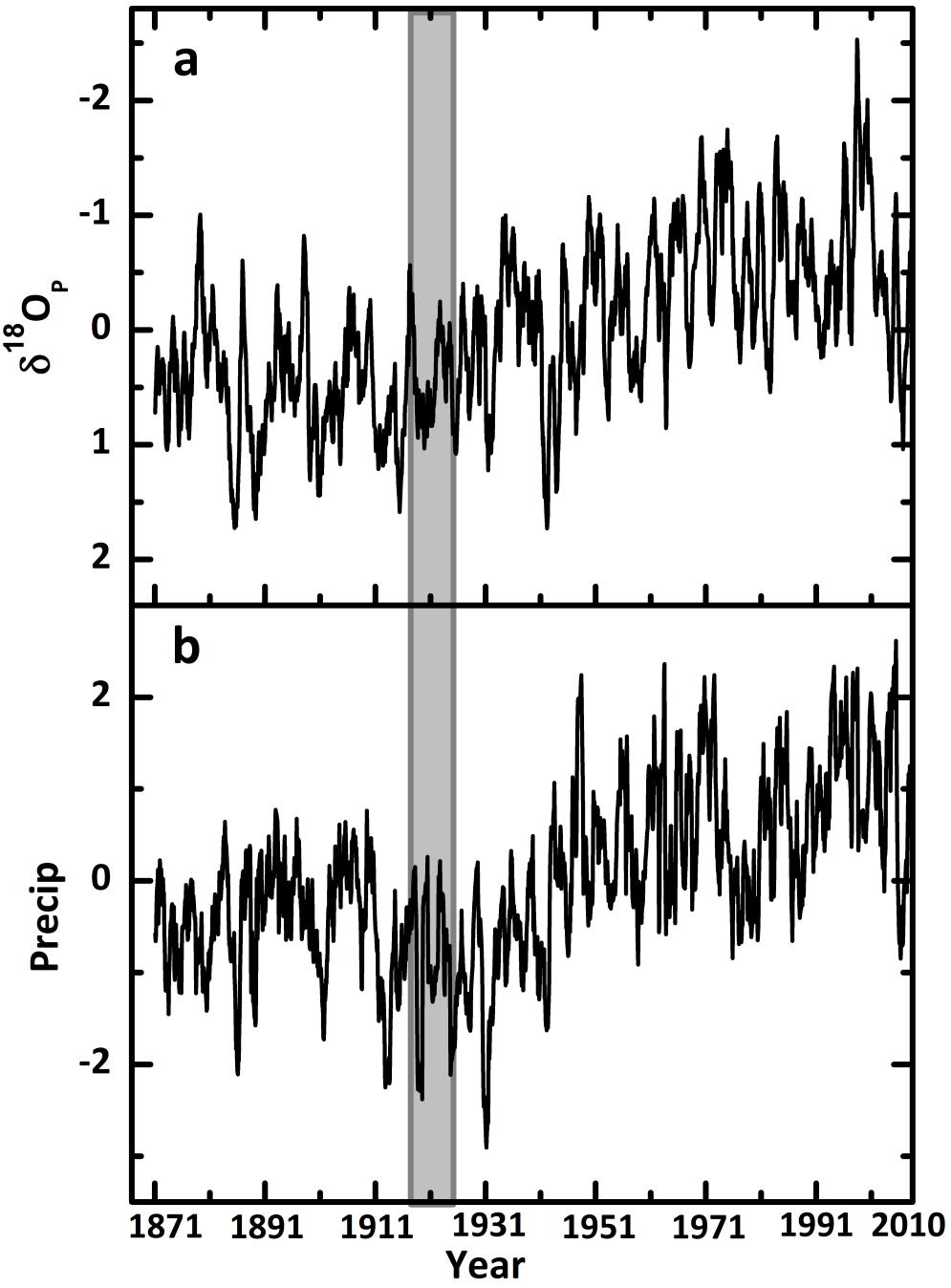


Figure 5.12: 12-Month moving averaged IsoGSM $\delta^{18}O_p$ (A) and precipitation (mm/day)(B) from 1871 to 2010).

Based on the results presented, we can conclude that changes in $\delta^{18}O_p$ values over the AM region reflects monsoon intensity and/or convective precipitation over the Indian Ocean, Bay of Bengal, and/or tropical Indo-Pacific region, while local precipitation only has a small contribution. The strong correlation between Tham Mai $\delta^{18}O_p$ (from the grid point closest

to the cave) and Pacific SST over the Niño 3.4 region, and the western and northern Indian Ocean, suggest that the $\delta^{18}O_p$ of annual rainfall may be influenced by ENSO and IOD. The strong association between $\delta^{18}O_p$ , ENSO, IOD and monsoon strength is potentially due to the change of moisture source and trajectory. The southeast Asian and east Asian monsoon regions receive more moisture from Bay of Bengal and less from Indian Ocean during El Niño years, while the opposite is true for La Niña years.

## 5.6 Acknowledgments

We would like to thank Jin-Yi Yu for useful discussions regarding interpretation of our results. This research was supported by funding from University of California, Irvine,and NSF grant AGS-1405472. This research was also supported by a grant from the Center of Research, College of Science and Health, Willam Paterson University of New Jersey.

## 5.7 Supplementary information

### 5.7.1 Two type of El Niño signal in Indo-Pacific $\delta^{18}O_p$

We investigate the composite average $\delta^{18}O_p$ during two types El Niño and La Niña year. Composite average of El Niño and La Niña year $\delta^{18}O_p$ shows that during El Niño years, Dongge, Tham Mai and Mawmluh caves have more negative $\delta^{18}O_p$ compared with La Niña years and neutral ENSO years. In addition, composite average of Central Pacific (CP) type El Niño year (*Yu and Kao*, 2007) $\delta^{18}O_p$ at Qunf cave shows that during CP El Niño year, Qunf cave has more positive $\delta^{18}O_p$ (-4.3) compared with neutral average $\delta^{18}O_p$ (-4.7), indicating a CP El Niño signal in Qunf $\delta^{18}O_p$ . Moreover, composite $\delta^{18}O_p$ at Qunf cave for the years following La Niña years (-5.2) is significantly lighter ($p<0.01$) than neutral year $\delta^{18}O_p$ . This is consistent with the results of *Tan* (2014), which indicates the light value of $\delta^{18}O_p$ correspond to La Niña year or the years in which La Niña occurred in the second half of the year.

### 5.7.2 Detrending and regression process on Tham Mai IsoGSM and precipitation time series

We first fit both precipitation and $\delta^{18}O_p$ monthly data from 1871-2010 with linear model and obtained the residual of the fitted model. The seasonal cycle was removed using a moving average. The mean was removed by subtracting each monthly data from the overall monthly overall mean. The mathematic equation of detrending process can be shown as following:

$$Y_{i,j+12} = B * (X_{i,j} + X_{i,j+1}..... + X_{i,j+11}) \tag{5.1}$$

where i is from 1 to 12, and j is from 1 to1680, B is column vector of 1/12 with length of 12. The overall mean is removed by $Y_{ij} = Y_{ij} - mean(Y_i)$.

However, it is also clear that precipitation has a break point at around year 1910-1930, so that a simple linear model is obviously not the best model to fit the data. Thus, we fit the data with a B-spline model with one knot. we used Akaike information criterion (AIC) and Mean Square Error (MSE) to find the location of best knot. The best knot occurred at 1925 AD, with MSE equals to 0.514 and AIC equals to 3583. The fitted B-spline on precipitation is showing Figure12. We also compare the results of simple linear model with the result of B-spline model. AIC of simple 10536 and MSE is 5.69. Thus, we concluded that the B-spline model is a better choice for precipitation.

Table 5.1: Composite $\delta^{18}O_p$ and GPCP precip.[1] amount(mm/day) for El Niño, La Niña, and neutral ENSO year between 1979-2010.

| | Qunf | Dongge | Lao | Mawmluh |
|---|---|---|---|---|
| El Niño $\delta^{18}O_p$ ave | -4.47 | -6.26 | -9.38 | -7.13 |
| La Niña $\delta^{18}O_p$ ave | -4.33 | -6.77 | -9.91 | -7.79 |
| Neutral $\delta^{18}O_p$ ave | -4.7 | -6.48 | -9.53 | -7.30 |
| El Niño precip. ave | 0.26 | 3.49 | 3.98 | 7.3 |
| La Niña precip. ave | 0.33 | 3.6 | 4.25 | 8.18 |
| Neutral precip. ave | 0.35 | 3.62 | 4.25 | 7.72 |

1: precip. stands for precipitation

**Table S2.** Monthly $\delta^{18}O_p$ from IsoGSM and GNIP, GPCP averaged from1979-2010 for four sites, and correlations(R) between $\delta^{18}O_p$ and GPCP .

| | Mawnluh | | | Laos | | | Dongge | | | Qunf | | |
|---|---|---|---|---|---|---|---|---|---|---|---|---|
| month | gpcp | isogsm | gnip | gpcp | isogsm | gnip | gpcp | isogsm | gnip | gpcp | isogsm | gnip |
| jan | 1.2 | -4.1 | -0.7 | 0.8 | -3.7 | -2.7 | 2.0 | -4.4 | -4.1 | 0.2 | -3.2 | -0.7 |
| feb | 3.2 | -2.5 | -2.5 | 1.6 | -2.8 | -2.1 | 2.9 | -3.5 | -3.5 | 0.3 | -2.8 | 0.0 |
| mar | 6.9 | -2.8 | -0.3 | 3.3 | -3.0 | -1.8 | 4.6 | -2.7 | -3.3 | 0.3 | -3.6 | -0.6 |
| april | 12.4 | -3.3 | -2.1 | 5.4 | -4.5 | -2.6 | 6.4 | -3.4 | -2.8 | 0.5 | -3.7 | -0.1 |
| may | 16.6 | -4.7 | -2.2 | 7.9 | -8.0 | -5.2 | 7.1 | -6.9 | -5.1 | 0.5 | -4.1 | -0.1 |
| jun | 17.4 | -7.0 | -2.2 | 9.2 | -9.1 | -5.6 | 6.3 | -9.7 | -7.3 | 0.4 | -3.7 | -0.5 |
| july | 15.1 | -8.1 | -6.1 | 8.7 | -10.0 | -8.0 | 4.4 | -9.4 | -9.2 | 0.2 | -4.6 | -1.9 |
| aug | 10.5 | -7.9 | -8.6 | 6.3 | -11.0 | -8.3 | 3.2 | -9.7 | -8.9 | 0.3 | -4.8 | -1.9 |
| sep | 5.9 | -8.8 | -9.1 | 3.6 | -11.4 | -9.0 | 2.3 | -9.4 | -9.3 | 0.3 | -5.5 | -3.5 |
| oct | 2.1 | -11.5 | -7.4 | 1.8 | -9.6 | -7.6 | 1.8 | -7.1 | -7.3 | 0.3 | -4.9 | -1.5 |
| nov | 0.4 | -10.0 | -5.4 | 0.9 | -5.9 | -5.7 | 1.4 | -6.2 | -6.2 | 0.3 | -5.3 | -2.8 |
| dec | 0.6 | -6.2 | -2.1 | 0.6 | -4.8 | -3.3 | 1.4 | -5.2 | -4.4 | 0.2 | -4.1 | -0.8 |
| R(p<0.001) | gpcp | | gnip | gpcp | | gnip | gpcp | | gnip | gpcp | | gnip |
| IsoGSM | -0.74(lag=2) | | 0.79 | -0.76(lag=3) | | 0.97 | -0.87(lag=3) | | 0.95 | 0.61(lag=2) | | 0.88 |
| GNIP | -0.75(lag=2) | | | -0.79(lag=3) | | | 0.87(lag=2) | | | 0.4(lag=1) | | |

Figure 5.13: Monthly $\delta^{18}O_p$ from IsoGSM and GNIP, GPCP averaged from 1979-2010 for four sites, and correlations(R) between $\delta^{18}O_p$ and GPCP.

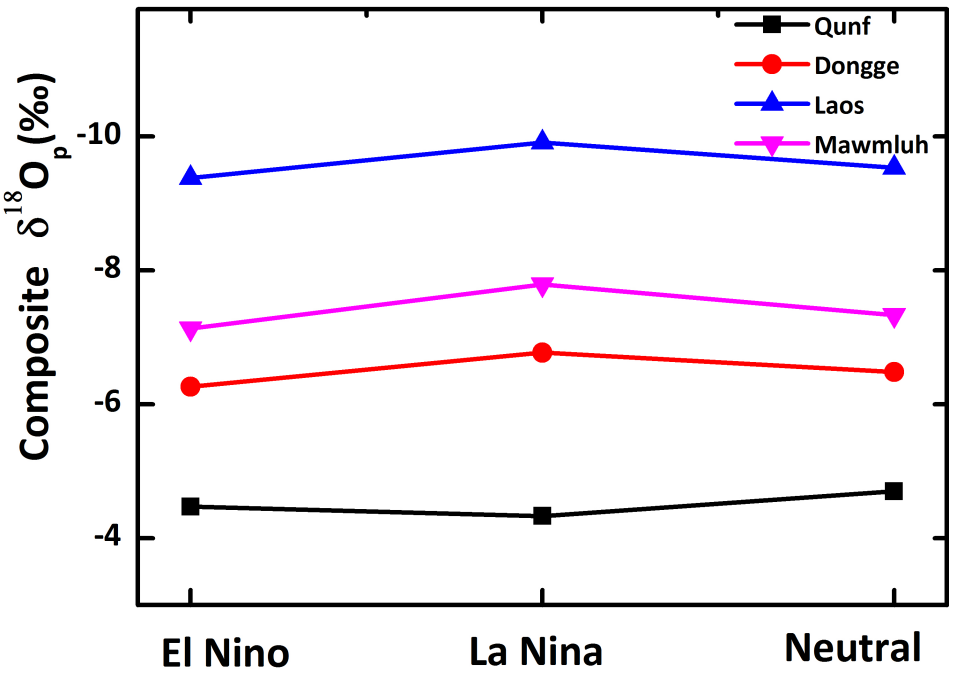


Figure 5.14: Composite $\delta^{18}O_p$ of El Niño , La Niña , and neutral ENSO year between1979-2010 for Tham Mai (red), Mawmluh (green), Dongge (red), and Qunf (black) caves.

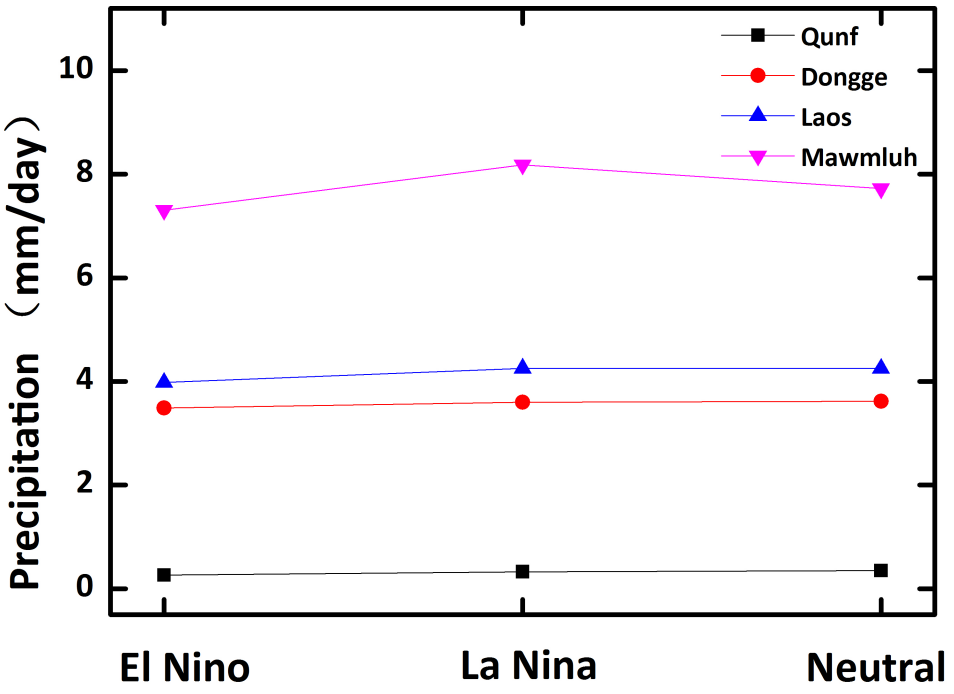


Figure 5.15: Composite precipitation of El Niño , La Niña , and neutral ENSO year between1979-2010 for Tham Mai (red), Mawmluh (green), Dongge (red), and Qunf (black) caves.

# Chapter 6

# Conclusions and Future Work

The overall aim of this research presented in this thesis were to 1) develop a record of SEAM over the past 14,000 years on inter-annual to decadal timescales; 2) explore the mechanisms that control precipitation and speleothem $\delta^{18}$O on interannual to orbital timescales in Laos; 3) quantify the noise from cave hydrological process on speleothem $\delta^{18}$O signature. In chapter 2 and 3, I present the results of the calcite $\delta^{18}$O time series, $U-Th$ dating techniques and results. Our speleothem $\delta^{18}$O record has been compared with other speleothem records across AM region, Greenland Ice core, Cariaco Basin $^{14}C$ record to explore the mechanisms that control speleothem $\delta^{18}$O over orbital scale. In chapter 4, I utilized previously developed KarstFor model to quantify the noise from cave hydrological process on speleothem $\delta^{18}$O. In chapter 5, I utilized existing simulations from IsoGSM to explore the mechanism that control precipitation $\delta^{18}$O on inter-annual timescales. Our understanding of speleothem records, especially in SEAM region, is still being developed, and the results presented in this dissertation will be of broad interest across Earth science, including to isotope geochemists, paleoclimatologists, and climate modelers. Potential continuations of the work presented in this dissertation include:

- **Speleothem $\delta^{18}$O records**

  The findings in this dissertation demonstrate that speleothems from Tham Mai cave, Laos are well-suited for reconstructing past hydrologic variability. Further researches on Laos speleothem records include 1) extend current speleothem records to further back in time; 2) collect modern calcite and construct high resolution modern speleothem records. 3) speleothems from other caves in Laos are needed. These will help to 1) extend our current records beyond Younger Dryas; 2) explore controlling mechanism of AM from glacial to inter-glacial time period; 3) enhance the robustness of our current record interpretations by multi-cave replication; 4) validate KarstFor model results by comparing pseudo speleothem $\delta^{18}$O generated by the model with high resolution speleothem $\delta^{18}$O records.

- **Multi-proxy comparisons**

  Seasonal and interannual variations in trace element concentration (e.g. Mg, Sr, Ba, U, P, S) are a widespread feature of calcite speleothems from a variety of climatic regimes (*Fairchild et al.*, 2001) and also hold great potential as high resolution paleoclimate proxies, especially when used in conjunction with stable isotopes (Fairchild and Treble. 2009; Johnson, et al. 2006). Elemental variations observed in speleothems, while ultimately controlled by temperature and rainfall, are directly modified by soil, epikarst, cave, and crystal growth processes. Recently, a number of speleothem records and process- based modern calibration studies have shown strong hydrological control on speleothem trace element composition through processes related to water-rock interaction, degassing, and calcite precipitation in the epikarst (e.g. *Griffiths et al.*, 2010). While it is critical to calibrate these proxies in the modern cave system, when combined with $\delta^{18}$O records they provide a powerful tool that allows reconstruction of both local hydrology and large-scale climate features.

- **Continous cave monitoring**

  In order to obtain robust paleoclimate records, detailed studies of modern cave systems are required to determine the modern environmental controls on speleothem geochemistry (Fairchild et al., 2006). While preliminary cave monitoring and dripwater collection began in December 2010 at Tham Mai Cave, we still need to expand upon these activities. Continuous work on monitoring cave temperature, relative humidity, drip rate, and cave air pCO2 will give more confidence on speleothem records interpretations. Monthly dripwater samples, drip rates, and modern calcites are needed. Cave monitoring work will allow us to assess the role of seasonal variations in surface rainfall and temperature, cave hydrology, ventilation, and cave micro-climate on speleothem isotopes. In addition, cave monitoring will help constrain and validate forward modeling work.

- **Forward modeling**

  The result presented in Chapter 4 highlight the possibilities of using Forwarding models to quantify hydrological process induced uncertainties on speleothem $\delta^{18}$O. Future studies could seek to integrate Isotope enabled GCMs data with forward modeling to address the net climatic signal in speleothem $\delta^{18}$O conveyed by precipitation $\delta^{18}$O. For Tham Mai cave, further constraints on initial parameters still needs to be completed. To determine the preferred parameter set, a possible approach is do a series of model runs with different sets of initial parameters (i.e., drainage functions and initial storage volumes in each store). In addition, higher resolution modern speleothems records, ideally annual resolution speleothems covering same time period with model $\delta^{18}O_p$ and/or cave monitoring $\delta^{18}$O, are needed to validate the forward model. Furthermore, further complexity can be added to the existing KarstFor model, e.g. isotopically fractionation due to evaporation fro soil and a more complex groundwater or underflow behavior from the reservoir(*Baker and Bradley*, 2010).

# Bibliography


Abram, N. J., M. K. Gagan, Z. Liu, W. S. Hantoro, M. T. McCulloch, and B. W. Suwargadi (2007), Seasonal characteristics of the Indian Ocean Dipole during the Holocene epoch, *Nature*, *445*(7125), 299–302, doi:{10.1038/nature05477}.

Ashok, K., and T. Yamagata (2009), Climate change: The El Niño with a difference, *Nature*, *461*(7263), 481–484.

Ashok, K., S. K. Behera, S. A. Rao, H. Weng, and T. Yamagata (2007), El Niño Modoki and its possible teleconnection, *Journal of Geophysical Research: Oceans*, *112*(C11), doi: 10.1029/2006JC003798, c11007.

Atkinson, T. (1977), Carbon dioxide in the atmosphere of the unsaturated zone: An important control of groundwater hardness in limestones, *Journal of Hydrology*, *35*(1–2), 111 – 123, doi:http://dx.doi.org/10.1016/0022-1694(77)90080-4.

Atkinson, T. C. (1983), Growth mechanisms of speleothems in castleguard cave, columbia icefields, alberta, canada, *Arctic and Alpine Research*, *15*(4), 523–536, doi:10.2307/1551238.

Ayliffe, L. K., M. K. Gagan, J.-x. Zhao, R. N. Drysdale, J. C. Hellstrom, W. S. Hantoro, M. L. Griffiths, H. Scott-Gagan, E. S. Pierre, J. A. Cowley, and B. W. Suwargadi (2013), Rapid interhemispheric climate links via the australasian monsoon during the last deglaciation, *Nat Commun*, *4*.

Baker, A., and C. Bradley (2010), Modern stalagmite $^{18}O$: Instrumental calibration and forward modelling, *Global and Planetary Change*, *71*(3–4), 201 – 206, doi:http://dx.doi.org/10.1016/j.gloplacha.2009.05.002.

Baker, A., and I. J. Fairchild (2012), Drip water hydrology and speleothems, *Nature Education Knowledge*, *3(10):16*.

Baker, A., D. Genty, W. Dreybrodt, W. L. Barnes, N. J. Mockler, and J. Grapes (1998), Testing theoretically predicted stalagmite growth rate with recent annually laminated samples: Implications for past stalagmite deposition, *Geochimica et Cosmochimica Acta*, *62*(3), 393–404, doi:http://dx.doi.org/10.1016/S0016-7037(97)00343-8.

Baker, A., A. Asrat, I. J. Fairchild, M. J. Leng, L. Thomas, M. Widmann, C. N. Jex, B. Dong, P. van Calsteren, and C. Bryant (2010), Decadal-scale rainfall variability in

ethiopia recorded in an annually laminated, holocene-age, stalagmite, *The Holocene*, *20*(6), 827–836.

Baker, A., C. Bradley, S. J. Phipps, M. Fischer, I. J. Fairchild, L. Fuller, C. Spötl, and C. Azcurra (2012), Millennial-length forward models and pseudoproxies of stalagmite delta;$^{18}$o: an example from nw scotland, *Climate of the Past*, *8*(4), 1153–1167, doi: 10.5194/cp-8-1153-2012.

Baker, A., C. Bradley, and S. J. Phipps (2013), Hydrological modeling of stalagmite $^{18}O$ response to glacial-interglacial transitions, *Geophysical Research Letters*, *40*(12), 3207–3212, doi:10.1002/grl.50555.

Baker, A., P. Smart, R. Edwards, and D. Richards (1993), Annual growth banding in a cave stalagmite, *Nature*, *364*(6437), 518–520.

Baker, A., W. Barnes, and P. Smart (1997), Variations in the discharge and organic matter content of stalagmite drip waters in Lower Cave, Bristol, *Hydrological processes*, *11*(11), 1541–1555.

Baker, Alexander J. and Sodemann, Harald and Baldini, James U. L. and Breitenbach, Sebastian F. M. and Johnson, Kathleen R. and van Hunen, Jeroen and Zhang, Pingzhong (2015), Seasonality of westerly moisture transport in the East Asian summer monsoon and its implications for interpreting precipitation $^{18}$O, *Journal of Geophysical Research: Atmospheres*, *120*(12), 5850–5862, doi:{10.1002/2014JD022919}.

Baldini, J. U. L., F. McDermott, D. L. Hoffmann, D. A. Richards, and N. Clipson (2008), Very high-frequency and seasonal cave atmosphere P-CO2 variability: Implications for stalagmite growth and oxygen isotope-based paleoclimate records, *Earth and planetary science letters*, *272*(1-2), 118–129, doi:{10.1016/j.epsl.2008.04.031}.

Bar-Matthews, M., A. Ayalon, A. Kaufman, and G. J. Wasserburg (1999), The eastern mediterranean paleoclimate as a reflection of regional events: Soreq cave, israel, *Earth and Planetary Science Letters*, *166*(1–2), 85 – 95.

Beck, J. W., D. A. Richards, R. Lawrence, Edwards, B. W. Silverman, P. L. Smart, D. J. Donahue, S. Hererra-Osterheld, G. S. Burr, L. Calsoyas, A. J. Timothy, Jull, and D. Biddulph (2001), Extremely large variations of atmospheric 14c concentration during the last glacial period, *Science*, *292*(5526), 2453–2458, doi:10.1126/science.1056649.

Berkelhammer, M., A. Sinha, L. Stott, H. Cheng, F. Pausata, and K. Yoshimura (2013), *An Abrupt Shift in the Indian Monsoon 4000 Years Ago*, pp. 75–88, American Geophysical Union, doi:10.1029/2012GM001207.

Berkelhammer, M., A. Sinha, M. Mudelsee, H. Cheng, R. L. Edwards, and K. Cannariato (2010), Persistent multidecadal power of the Indian Summer Monsoon, *Earth and planetary science letters*, *290*(1-2), 166–172, doi:{10.1016/j.epsl.2009.12.017}.

Bhattacharya, S. K., K. Froehlich, P. K. Aggarwal, and K. M. Kulkarni (2003), Isotopic variation in Indian Monsoon precipitation: Records from Bombay and New Delhi, *Geophysical Research Letters*, *30*(24), doi:10.1029/2003GL018453, 2285.

Bollasina, M., and S. Nigam (2009), Indian ocean sst, evaporation, and precipitation during the south asian summer monsoon in ipcc-ar4 coupled simulations, *33*(7-8), 1017–1032, doi:10.1007/s00382-008-0477-4.

Bowen, G. J., and J. Revenaugh (2003), Interpolating the isotopic composition of modern meteoric precipitation, *Water Resources Research*, *39*(10), doi:10.1029/2003WR002086, 1299.

Bowen, G. J., and B. Wilkinson (2002a), Spatial distribution of 18o in meteoric precipitation, *Geology*, *30*(4), 315–318, doi:10.1130/0091-7613(2002)030⟨0315:SDOOIM⟩2.0.CO;2.

Bowen, G. J., and B. Wilkinson (2002b), Spatial distribution of $^{18}O$ in meteoric precipitation, *Geology*, *30*(4), 315–318, doi:10.1130/0091-7613(2002)030$⟨$0315:SDOOIM$⟩$2.0.CO;2.

Buckley, B. M., K. Duangsathaporn, K. Palakit, S. Butler, V. Syhapanya, and N. Xaybouangeun (2007), Analyses of growth rings of pinus merkusii from lao p.d.r., *Forest Ecology and Management*, *253*(1–3), 120 – 127, doi:http://dx.doi.org/10.1016/j.foreco.2007.07.018.

Buckley, B. M., K. J. Anchukaitis, D. Penny, R. Fletcher, E. R. Cook, M. Sano, L. C. Nam, A. Wichienkeeo, T. T. Minh, and T. M. Hong (2010), Climate as a contributing factor in the demise of angkor, cambodia, *Proceedings of the National Academy of Sciences*, *107*(15), 6748–6752, doi:10.1073/pnas.0910827107.

Burns, S., A. Matter, N. Frank, and A. Mangini (1998), Speleothem-based paleoclimate record from northern Oman, *Geology*, *26*(6), 499–502.

Cai, Y., Z. An, H. Cheng, R. L. Edwards, M. J. Kelly, W. Liu, X. Wang, and C.-C. Shen (2006), High-resolution absolute-dated indian monsoon record between 53 and 36 ka from xiaobailong cave, southwestern china, *Geology*, *34*(8), 621–624, doi:10.1130/G22567.1.

Chawchai, S., A. Chabangborn, M. Kylander, L. Löwemark, C.-M. Mörth, M. Blaauw, W. Klubseang, P. Reimer, S. Fritz, and B. Wohlfarth (2013), Lake kumphawapi – an archive of holocene palaeoenvironmental and palaeoclimatic changes in northeast thailand, *Quaternary Science Reviews*, *68*, 59 – 75, doi:http://dx.doi.org/10.1016/j.quascirev.2013.01.030.

Cheng, H., R. Edwards, J. Hoff, C. Gallup, D. Richards, and Y. Asmerom (2000), The half-lives of uranium-234 and thorium-230, *Chemical Geology*, *169*(1–2), 17 – 33, doi:{http://dx.doi.org/10.1016/S0009-2541(99)00157-6}.

Cheng, H., D. Fleitmann, R. L. Edwards, X. Wang, F. W. Cruz, A. S. Auler, A. Mangini, Y. Wang, X. Kong, S. J. Burns, and A. Matter (2009), Timing and structure of the 8.2 kyr BP event inferred from delta(18)O records of stalagmites from China, Oman, and Brazil, *Geology*, *37*(11), 1007–1010, doi:{10.1130/G30126A.1}.

Cherchi, A., and A. Navarra (2013), Influence of ENSO and of the Indian Ocean Dipole on the Indian Summer Monsoon variability, *Climate Dynamics*, *41*(1), 81–103, doi:10.1007/s00382-012-1602-y.

Cherdyntsev, V., I. Kazachevskii, and K. YA (1965), Age of carbonate determined from the isotopes of thorium and uranium, *Geochem Int*, *2*, 749–756.

Chiang, J. C., I. Y. Fung, C.-H. Wu, Y. Cai, J. P. Edman, Y. Liu, J. A. Day, T. Bhattacharya, Y. Mondal, and C. A. Labrousse (2015), Role of seasonal transitions and westerly jets in east asian paleoclimate, *Quaternary Science Reviews*, *108*, 111 – 129, doi:http://dx.doi.org/10.1016/j.quascirev.2014.11.009.

Chiang, J. C. H. (2009), The Tropics in Paleoclimate, *Annual review of earth and planetary sciences*, *37*, 263–297, doi:{10.1146/annurev.earth.031208.100217}.

Chris Bradley and Andy Baker and Catherine N. Jex and Melanie J. Leng (2010), Hydrological uncertainties in the modelling of cave drip-water $^{18}$O and the implications for stalagmite palaeoclimate reconstructions, *Quaternary Science Reviews*, *29*(17–18), 2201 – 2214.

Clemens, S. C., and W. L. Prell (2003), A 350,000 year summer-monsoon multi-proxy stack from the Owen Ridge, Northern Arabian Sea, *Marine Geology*, *201*(1–3), 35 – 51, doi:http://dx.doi.org/10.1016/S0025-3227(03)00207-X.

Clemens, S. C., and W. L. Prell (2007), The timing of orbital-scale indian monsoon changes, *Quaternary Science Reviews*, *26*(3–4), 275 – 278, doi:http://dx.doi.org/10.1016/j.quascirev.2006.11.010.

Clemens, S. C., W. L. Prell, and Y. Sun (2010), Orbital-scale timing and mechanisms driving Late Pleistocene Indo-Asian summer monsoons: Reinterpreting cave speleothem $^{18}$O, *Paleoceanography*, *25*(4), doi:10.1029/2010PA001926, pA4207.

Collins, S. L., J. E. Fargione, C. L. Crenshaw, E. Nonaka, J. R. Elliott, Y. Xia, and W. T. Pockman (2010), Rapid plant community responses during the summer monsoon to nighttime warming in a northern Chihuahuan Desert grassland, *Journal of Arid Environments*, *74*(5), 611 – 617, doi:http://dx.doi.org/10.1016/j.jaridenv.2009.10.005.

Compo, G. P., J. S. Whitaker, P. D. Sardeshmukh, N. Matsui, R. J. Allan, X. Yin, B. E. Gleason, R. S. Vose, G. Rutledge, P. Bessemoulin, S. Brönnimann, M. Brunet, R. I. Crouthamel, A. N. Grant, P. Y. Groisman, P. D. Jones, M. C. Kruk, A. C. Kruger, G. J. Marshall, M. Maugeri, H. Y. Mok, Ø. Nordli, T. F. Ross, R. M. Trigo, X. L. Wang, S. D. Woodruff, and S. J. Worley (2011), The twentieth century reanalysis project, *Quarterly Journal of the Royal Meteorological Society*, *137*(654), 1–28, doi:10.1002/qj.776.

Conroy, J. L., and J. T. Overpeck (2011a), Regionalization of present-day precipitation in the greater monsoon region of Asia, *Journal of Climate*, *24*(15), 4073–4095, doi:10.1175/2011JCLI4033.1.

Conroy, J. L., and J. T. Overpeck (2011b), Regionalization of present-day precipitation in the greater monsoon region of asia*, *Journal of Climate*, *24*(15), 4073–4095, doi:10.1175/2011JCLI4033.1.

Conroy, J. L., K. M. Cobb, and D. Noone (2013), Comparison of precipitation isotope variability across the tropical Pacific in observations and SWING2 model simulations, *Journal of Geophysical Research: Atmospheres*, *118*(11), 5867–5892, doi:10.1002/jgrd.50412.

Cook, E. R., K. J. Anchukaitis, B. M. Buckley, R. D. D'Arrigo, G. C. Jacoby, and W. E. Wright (2010), Asian Monsoon Failure and Megadrought During the Last Millennium, *Science*, *328*(5977), 486–489, doi:{10.1126/science.1185188}.

Cosma, C., and T. Jurcuţ (1996), *Radonul şi mediul înconjurător*, Editura Dacia, Cluj-Napoca .

Cruz, F. W., S. J. Burns, I. Karmann, W. D. Sharp, M. Vuille, A. O. Cardoso, J. A. Ferrari, P. L. Silva Dias, and O. Viana (2005), Insolation-driven changes in atmospheric circulation over the past 116,000 years in subtropical brazil, *Nature*, *434*(7029), 63–66.

Dansgaard, W. (1964), Stable isotopes in precipitation, *Tellus*, *16*, 436–468.

Dayem, K. E., P. Molnar, D. S. Battisti, and G. H. Roe (2010), Lessons learned from oxygen isotopes in modern precipitation applied to interpretation of speleothem records of paleoclimate from eastern asia, *Earth and Planetary Science Letters*, *295*(1–2), 219 – 230, doi:http://dx.doi.org/10.1016/j.epsl.2010.04.003.

Deininger, M., J. Fohlmeister, D. Scholz, and A. Mangini (2012), Isotope disequilibrium effects: The influence of evaporation and ventilation effects on the carbon and oxygen isotope composition of speleothems –a model approach, *Geochimica et Cosmochimica Acta*, *96*, 57–79, doi:http://dx.doi.org/10.1016/j.gca.2012.08.013.

Dong, J., Y. Wang, C. Hai, H. Ben, R. Lawrence, X. Kong, J. Wu, S. Chen, D. Liu, X. Jiang, and K. Zhao (2010), A high-resolution stalagmite record of the Holocene East Asian monsoon from Mt Shennongjia, central China, *The Holocene*, *20*(2), 257–264.

Dorale, J., R. Edwards, E. Ito, and L. Gonzalez (1998), Climate and vegetation history of the midcontinent from 75 to 25 ka: A speleothem record from Crevice Cave, Missouri, USA, *Science*, *282*(5395), 1871–1874.

Drysdale, R., G. Zanchetta, J. Hellstrom, R. Maas, A. Fallick, M. Pickett, I. Cartwright, and L. Piccini (2006), Late Holocene drought responsible for the collapse of Old World civilizations is recorded in an Italian cave flowstone, *Geology*, *34*(2), 101–104, doi:{10.1130/G22103.1}.

DUPLESSY, J. C., J. LABEYRIE, C. LALOU, and H. V. NGUYEN (1970), Continental climatic variations between 130,000 and 90,000 years bp, *Nature*, *226*(5246), 631–633.

Dutt, S., A. K. Gupta, S. C. Clemens, H. Cheng, R. K. Singh, G. Kathayat, and R. L. Edwards (2015), Abrupt changes in Indian summer monsoon strength during 33,800 to 5500years B.P., *Geophysical Research Letters*, *42*(13), 5526–5532, doi:10.1002/2015GL064015, 2015GL064015.

Dykoski, C., R. Edwards, H. Cheng, D. Yuan, Y. Cai, M. Zhang, Y. Lin, J. Qing, Z. An, and J. Revenaugh (2005), A high-resolution, absolute-dated Holocene and deglacial Asian monsoon record from Dongge Cave, China, *Earth and planetary science letters*, *233*(1-2), 71–86, doi:{10.1016/j.epsl.2005.01.036}.

Edwards, R., J. Chen, T. Ku, and G. Wasserburg (1987), Precise timing of the last interglacial period from mass-spectrometric determination of 230Th in corals, *Science*, *236*(4808), 1547–1553, doi:{10.1126/science.236.4808.1547}.

Fairchild, I., A. Baker, A. Borsato, S. Frisia, R. Hinton, F. McDermott, and A. Tooth (2001), Annual to sub-annual resolution of multiple trace-element trends in speleothems, *Journal of the geological society*, *158*(Part 5), 831–841.

Fairchild, I., C. Smith, A. Baker, L. Fuller, C. Spotl, D. Mattey, F. McDermott, and EIMP (2006), Modification and preservation of environmental signals in speleothems, *Earth-science reviews*, *75*(1-4), 105–153, doi:{10.1016/j.earscirev.2005.08.003}.

Fairchild, I. J., and A. Baker (2012), *Speleothem Science: From process to past environment*, Blackwell Publishing ltd.

Fischer, M. J., and P. C. Treble (2008), Calibrating climate-18o regression models for the interpretation of high-resolution speleothem 18o time series, *Journal of Geophysical Research: Atmospheres*, *113*(D17), n/a–n/a, doi:10.1029/2007JD009694, d17103.

Fleitmann, D., S. J. Burns, U. Neff, A. Mangini, and A. Matter (2003), Changing moisture sources over the last 330,000 years in Northern Oman from fluid-inclusion evidence in speleothems, *Quaternary Research*, *60*(2), 223 – 232, doi:http://dx.doi.org/10.1016/S0033-5894(03)00086-3.

Fleitmann, D., S. J. Burns, U. Neff, M. Mudelsee, A. Mangini, and A. Matter (2004), Palaeoclimatic interpretation of high-resolution oxygen isotope profiles derived from annually laminated speleothems from Southern Oman, *Quaternary Science Reviews*, *23*(7–8), 935 – 945, doi:http://dx.doi.org/10.1016/j.quascirev.2003.06.019, isotopes in Quaternary Paleoenvironmental reconstruction.

Fleitmann, D., S. J. Burns, A. Mangini, M. Mudelsee, J. Kramers, I. Villa, U. Neff, A. A. Al-Subbary, A. Buettner, D. Hippler, and A. Matter (2007), Holocene ITCZ and Indian monsoon dynamics recorded in stalagmites from Oman and Yemen (Socotra), *Quaternary Science Reviews*, *26*(1–2), 170 – 188, doi:http://dx.doi.org/10.1016/j.quascirev.2006.04.012.

Fleitmann, D., P. Treble, F. Cruz, and K. M. Cobb (2008), White paper on 'Speleothem-based cimate proxy records', http://www.ncdc.noaa.gov/paleo/reports/, Terieste, Italy.

Frisia, S., I. J. Fairchild, J. Fohlmeister, R. Miorandi, C. Spötl, and A. Borsato (2011), Carbon mass-balance modelling and carbon isotope exchange processes in dynamic caves, *Geochimica et Cosmochimica Acta*, *75*(2), 380 – 400, doi:http://dx.doi.org/10.1016/j.gca.2010.10.021.

Frisia, S. and Borsato, A. (2010), *Developements in Sedimentology*, chap. Carbonates in Continental Settings, pp. 269–318, Elsevier, Amsterdam.

Gagan, M., E. Hendy, S. Haberle, and W. Hantoro (2004), Post-glacial evolution of the Indo-Pacific Warm Pool and El Nino-Southern Oscillation, *Quaternary international*, *118*, 127–143, doi:{10.1016/S1040-6182(03)00134-4}.

Gat, J. R. (1996), Oxygen and hydrogen isotopes in the hydrologic cycle, *Annual Review of Earth and Planetary Sciences*, *24*(1), 225–262, doi:10.1146/annurev.earth.24.1.225.

Gat, J. R., and E. Matsui (1991), Atmospheric water balance in the Amazon basin: An isotopic evapotranspiration model, *Journal of Geophysical Research: Atmospheres*, *96*(D7), 13,179–13,188, doi:10.1029/91JD00054.

Genty, D., and Y. Quinif (1996), Annually laminated sequences in the internal structure of some belgian stalagmites; importance for paleoclimatology, *Journal of Sedimentary Research*, *66*(1), 275–288.

Genty, D., D. Blamart, R. Ouahdi, M. Gilmour, A. Baker, J. Jouzel, and S. Van-Exter (2003), Precise dating of dansgaard-oeschger climate oscillations in western europe from stalagmite data, *Nature*, *421*(6925), 833–837.

Genty, D., A. Baker, M. Massault, C. Proctor, M. Gilmour, E. Pons-Branchu, and B. Hamelin (2001), Dead carbon in stalagmites: Carbonate bedrock paleodissolution vs. ageing of soil organic matter. Implications for C-13 variations in speleothems, *Geochimica et cosmochimica acta*, *65*(20), 3443–3457.

GISP2 (), *The Greenland Summit Ice Cores, National Snow and Ice Data Center, University of Colorado at Bouder,and the World Data Center-A for Paleoclimatology, National Geophysical Data Center, Boulder Colorado, 1997. (CD-ROM).*

Goswami, B. N. (1998), Interannual variations of Indian Summer Monsoon in a GCM: External conditions versus internal feedbacks, *Journal of Climate*, *11*(4), 501–522, doi:10.1175/1520-0442(1998)011$⟨$0501:IVOISM$⟩$2.0.CO;2.

Griffiths, M. L., R. N. Drysdale, M. K. Gagan, J. x. Zhao, L. K. Ayliffe, J. C. Hellstrom, W. S. Hantoro, S. Frisia, Y. x. Feng, I. Cartwright, E. S. Pierre, M. J. Fischer, and B. W. Suwargadi (2009), Increasing Australian-Indonesian monsoon rainfall linked to early Holocene sea-level rise, *Nature Geosci*, *2*(9), 636–639.

Griffiths, M. L., R. N. Drysdale, H. B. Vonhof, M. K. Gagan, J. xin Zhao, L. K. Ayliffe, W. S. Hantoro, J. C. Hellstrom, I. Cartwright, S. Frisia, and B. W. Suwargadi (2010b), Younger dryas–holocene temperature and rainfall history of southern indonesia from 18o

in speleothem calcite and fluid inclusions, *Earth and Planetary Science Letters*, *295*(1–2), 30 – 36, doi:http://dx.doi.org/10.1016/j.epsl.2010.03.018.

Griffiths, M. L., R. N. Drysdale, M. K. Gagan, J. C. Hellstrom, I. Couchoud, L. K. Ayliffe, H. B. Vonhof, and W. S. Hantoro (2013), Australasian monsoon response to dansgaard–oeschger event 21 and teleconnections to higher latitudes, *Earth and Planetary Science Letters*, *369–370*, 294 – 304, doi:http://dx.doi.org/10.1016/j.epsl.2013.03.030.

Griffiths, M. L., R. N. Drysdale, M. K. Gagan, S. Frisia, J.-x. Zhao, L. K. Ayliffe, W. S. Hantoro, J. C. Hellstrom, M. J. Fischer, Y.-X. Feng, and B. W. Suwargadi (2010), Evidence for Holocene changes in Australian-Indonesian monsoon rainfall from stalagmite trace element and stable isotope ratios, *Earth and planetary science letters*, *292*(1-2), 27–38, doi:{10.1016/j.epsl.2010.01.002}.

Guilyardi, E. (2006), El Nino-mean state-seasonal cycle interactions in a multi-model ensemble, *Climate dynamics*, *26*(4), 329–348, doi:{10.1007/s00382-005-0084-6}.

Hansen, J., M. Sato, R. Ruedy, P. Kharecha, A. Lacis, R. Miller, L. Nazarenko, K. Lo, G. A. Schmidt, G. Russell, I. Aleinov, S. Bauer, E. Baum, B. Cairns, V. Canuto, M. Chandler, Y. Cheng, A. Cohen, A. Del Genio, G. Faluvegi, E. Fleming, A. Friend, T. Hall, C. Jackman, J. Jonas, M. Kelley, N. Y. Kiang, D. Koch, G. Labow, J. Lerner, S. Menon, T. Novakov, V. Oinas, J. Perlwitz, J. Perlwitz, D. Rind, A. Romanou, R. Schmunk, D. Shindell, P. Stone, S. Sun, D. Streets, N. Tausnev, D. Thresher, N. Unger, M. Yao, and S. Zhang (2007), Climate simulations for 1880–2003 with giss modele, *29*(7-8), 661–696, doi:10.1007/s00382-007-0255-8.

Harmon, R. S., D. C. Ford, and H. P. Schwarcz (1977), Interglacial chronology of the rocky and mackenzie mountains based upon 230th–234u dating of calcite speleothems, *Canadian Journal of Earth Sciences*, *14*(11), 2543–2552, doi:10.1139/e77-220.

Haug, G., K. Hughen, D. Sigman, L. Peterson, and U. Rohl (2001), Southward migration of the intertropical convergence zone through the Holocene, *Science*, *293*(5533), 1304–1308.

Hellstrom, J. (2006), U–th dating of speleothems with high initial 230th using stratigraphical constraint, *Quaternary Geochronology*, *1*(4), 289 – 295, doi:http://dx.doi.org/10.1016/j.quageo.2007.01.004.

Hendy, C. (1971), The isotopic geochemistry of speleothems—i. the calculation of the effects of different modes of formation on the isotopic composition of speleothems and their applicability as palaeoclimatic indicators, *Geochimica et Cosmochimica Acta*, *35*(8), 801 – 824, doi:http://dx.doi.org/10.1016/0016-7037(71)90127-X.

Hoffmann, G., and M. Heimann (1997), Water isotope modeling in the Asian monsoon region, *Quaternary International*, *37*, 115 – 128, doi:http://dx.doi.org/10.1016/1040-6182(96)00004-3.

Hope, G. (2001), Environmental change in the Late Pleistocene and later Holocene at Wanda site, Soroako, South Sulawesi, Indonesia, *Palaeogeography palaeoclimatology palaeoecology*, *171*(3-4), 129–145, doi:{10.1016/S0031-0182(01)00243-7}.

Hopley, D., J.-x. Zhao, and L. Collins (2011), *Encyclopedia of Earth Sciences Series*, pp. 1128–1132, Springer Netherlands, doi:10.1007/978-90-481-2639-2{_}161.

Hu, C., G. Henderson, J. Hang, S. Xie, Y. Sun, and K. Johnson (2008), Quantification of Holocene Asian monsoon rainfall from spatially separated cave records, *Earth and Planetary Science Letters*, pp. 221–32.

Hughen, K., J. Overpeck, L. Peterson, and S. Trumbore (1996), Rapid climate changes in the tropical Atlantic region during the last deglaciation, *Nature*, *380*(6569), 51–54.

Hwang, Y.-T., D. M. W. Frierson, B. J. Soden, and I. M. Held (2011), Robust responses of the hydrological cycle to global warming (vol 19, pg 5686, 2006), *Journal of climate*, *24*(5), 1559–1560, doi:{10.1175/2010JCLI4045.1}.

Ivanovich, M., and R. Harmon (), Uranium Series Disequilibrium. Applications to Environmental Problems., *Clarendon Press, Oxford*, p. 541.

Ivanovich, M. (1982), Uranium Series Disequilibrium, p. 7476.

Johnsen, S. J., D. Dahl-Jensen, N. Gundestrup, J. P. Steffensen, H. B. Clausen, H. Miller, V. Masson-Delmotte, A. E. Sveinbjörnsdottir, and J. White (2001), Oxygen isotope and palaeotemperature records from six greenland ice-core stations: Camp century, dye-3, grip, gisp2, renland and northgrip, *Journal of Quaternary Science*, *16*(4), 299–307, doi:10.1002/jqs.622.

Johnson, K., and B. Ingram (2004), Spatial and temporal variability in the stable isotope systematics of modern precipitation in China: implications for paleoclimate reconstructions, *Earth and planetary science letters*, *220*(3-4), 365–377, doi:{10.1016/S0012-821X(04)00036-6}.

Johnson, K., B. Ingram, W. Sharp, and P. Zhang (2006), East Asian summer monsoon variability during Marine Isotope Stage 5 based on speleothem delta O-18 records from Wanxiang Cave, central China, *Palaeogeography palaeoclimatology palaeoecology*, *236*(1-2), 5–19, doi:{10.1016/j.palaeo.2005.11.041}.

Jones, B. (2009), Cave pearls—the integrated product of abiogenic and biogenic processes, *Journal of Sedimentary Research*, *79*(9), 689–710, doi:10.2110/jsr.2009.071.

Ju, J., and J. Slingo (1995), The Asian summer monsoon and ENSO, *Quarterly Journal of the Royal Meteorological Society*, *121*(525), 1133–1168, doi:10.1002/qj.49712152509.

Kalnay, E., M. Kanamitsu, R. Kistler, W. Collins, D. Deaven, L. Gandin, M. Iredell, S. Saha, G. White, J. Woollen, Y. Zhu, A. Leetmaa, R. Reynolds, M. Chelliah, W. Ebisuzaki, W. Higgins, J. Janowiak, K. C. Mo, C. Ropelewski, J. Wang, R. Jenne, and D. Joseph (1996), The NCEP/NCAR 40-year reanalysis project, *Bulletin of the American Meteorological Society*, *77*(3), 437–471, doi:10.1175/1520-0477(1996)077$\langle$0437:TNYRP$$2.0.CO;2$.

Kanamitsu, M., W. Ebisuzaki, J. Woollen, S.-K. Yang, J. J. Hnilo, M. Fiorino, and G. L. Potter (2002), NCEP–DOE AMIP-II Reanalysis (R-2), *Bulletin of the American Meteorological Society*, *83*(11), 1631–1643, doi:10.1175/BAMS-83-11-1631.

Kao, H.-Y., and J.-Y. Yu (2009), Contrasting Eastern-Pacific and Central-Pacific Types of ENSO, *Journal of Climate*, *22*(3), 615–632, doi:10.1175/2008JCLI2309.1.

Kim, Sang-Tae and O'Neil, James R. (1997), Equilibrium and nonequilibrium oxygen isotope effects in synthetic carbonates, *Geochimica et Cosmochimica Acta*, *61*(16), 3461–3475, doi:{http://dx.doi.org/10.1016/S0016-7037(97)00169-5}.

Krishnamurti, T. N. (1985), Summer monsoon experiment—a review, *Monthly Weather Review*, *113*(9), 1590–1626, doi:10.1175/1520-0493(1985)113$⟨$1590:SMER$⟩$2.0.CO;2.

Kuleshov, Y., C.-M. Fabrice, L. Qi, I. Chouaibou, C. Hoareau, and F. Roux (2009), Tropical cyclone genesis in the Southern Hemisphere and its relationship with the ENSO, *Annales Geophysicae*, *27*, 2523–2538, doi:10.5194/angeo-27-2523-2009.

Kumar, K. K., B. Rajagopalan, M. Hoerling, G. Bates, and M. Cane (2006), Unraveling the mystery of Indian monsoon failure during El Niño, *Science*, *314*(5796), 115–119.

Lau, K. M., G. J. Yang, and S. H. Shen (1988), Seasonal and intraseasonal climatology of summer monsoon rainfall over Eeat Asia, *Monthly Weather Review*, *116*(1), 18–37, doi:10.1175/1520-0493(1988)116$⟨$0018:SAICOS$⟩$2.0.CO;2.

Lau, N.-C., and B. Wang (2006), Interactions between the Asian monsoon and the El Niño/Southern Oscillation, in *The Asian Monsoon*, Springer Praxis Books, pp. 479–512, Springer Berlin Heidelberg, doi:10.1007/3-540-37722-0_12.

Lewis, S. C., A. N. LeGrande, M. Kelley, and G. A. Schmidt (2010), Water vapour source impacts on oxygen isotope variability in tropical precipitation during Heinrich events, *Climate of the past*, *6*(3), 325–343, doi:{10.5194/cp-6-325-2010}.

Li, J., S.-P. Xie, E. R. Cook, G. Huang, R. D'Arrigo, F. Liu, J. Ma, and X.-T. Zheng (2011), Interdecadal modulation of El Nino amplitude during the past millennium, *Nature climate change*, *1*(2), 114–118, doi:{10.1038/NCLIMATE1086}.

Liebmann, B., and C. Smith (1996), Description of a complete (interpolated) outgoing longwave radiation dataset, *BULLETIN OF THE AMERICAN METEOROLOGICAL SOCIETY*, *77*(6), 1275–1277.

Liu, Z., X. Wen, E. Brady, B. Otto-Bliesner, G. Yu, H. Lu, H. Cheng, Y. Wang, W. Zheng, Y. Ding, R. Edwards, J. Cheng, W. Liu, and H. Yang (2014), Chinese cave records and the East Asia Summer Monsoon, *Quaternary Science Reviews*, *83*, 115 – 128.

Lohmann, G., A. Wackerbarth, P. M. Langebroek, M. Werner, J. Fohlmeister, D. Scholz, and A. Mangini (2013), Simulated european stalagmite record and its relation to a quasi-decadal climate mode, *Climate of the Past*, (9), 89–98, doi:10.5194/cp-9-89-2013.

Magee, J., G. Miller, N. Spooner, and D. Questiaux (2004), Continuous 150 ky monsoon record from Lake Eyre, Australia: Insolation-forcing implications and unexpected Holocene failure, *Geology*, *32*(10), 885–888, doi:{10.1130/G20672.1}.

Mann, M. E., G. A. Schmidt, S. K. Miller, and A. N. LeGrande (2009), Potential biases in inferring Holocene temperature trends from long-term borehole information, *Geophysical Research Letters*, *36*(5), doi:10.1029/2008GL036354, l05708.

Matthew S. Lachniet (2009), Climatic and environmental controls on speleothem oxygen-isotope values, *Quaternary Science Reviews*, *28*(5–6), 412 – 432.

McDermott, F. (2004), Palaeo-climate reconstruction from stable isotope variations in speleothems: a review, *Quaternary science reviews*, *23*(7-8), 901–918, doi:{10.1016/j.quascirev.2003.06.021}.

McGregor, H., and M. Gagan (2004), Western Pacific coral delta(18)O records of anomalous Holocene variability in the El Nino-Southern Oscillation, *Geophysical research letters*, *31*(11), doi:{10.1029/2004GL019972}.

Meckler, A. N., M. O. Clarkson, K. M. Cobb, H. Sodemann, and J. F. Adkins (2012), Interglacial hydroclimate in the tropical west pacific through the late pleistocene, *Science*, *336*(6086), 1301–1304, doi:10.1126/science.1218340.

Merryfield, W., and G. Boer (2005), Variability of upper Pacific Ocean overturning in a coupled climate model, *Journal of climate*, *18*(5), 666–683, doi:{10.1175/JCLI-3282.1}.

Mickler, P. J., L. A. Stern, and J. L. Banner (2006), Large kinetic isotope effects in modern speleothems, *Geological Society of America Bulletin*, *118*(1-2), 65–81, doi:10.1130/B25698.1.

Mickler, Patrick J. and Banner, Jay L. and Stern, Libby and Asmerom, Yemane and Edwards, R. Lawrence and Ito, Emi (2004), Stable isotope variations in modern tropical speleothems: Evaluating equilibrium vs. kinetic isotope effects 1, *Geochimica et Cosmochimica Acta*, *68*(21), 4381–4393, doi:{http://dx.doi.org/10.1016/j.gca.2004.02.012}.

Myers, C. G., J. L. Oster, W. D. Sharp, R. Bennartz, N. P. Kelley, A. K. Covey, and S. F. Breitenbach (2015), Northeast Indian stalagmite records Pacific decadal climate change: Implications for moisture transport and drought in india, *Geophysical Research Letters*, *42*(10), 4124–4132, doi:10.1002/2015GL063826, 2015GL063826.

Oster, J. L., I. P. Montañez, T. P. Guilderson, W. D. Sharp, and J. L. Banner (2010), Modeling speleothem 13c variability in a central sierra nevada cave using 14c and 87sr/86sr, *Geochimica et Cosmochimica Acta*, *74*(18), 5228 – 5242, doi:http://dx.doi.org/10.1016/j.gca.2010.06.030.

P. D., C., and P. R. A (2008), *The Asian Monsson: Cause, History and Effects*, Cambridge University Press, Cambridge, United Kingdom.

Paeth, H., A. Scholten, P. Friederichs, and A. Hense (2008), Uncertainties in climate change prediction: El Nino-Southern Oscillation and monsoons, *Global and planetary change*, *60*(3-4), 265–288, doi:{10.1016/j.gloplacha.2007.03.002}.

Partin, J. W., K. M. Cobb, J. F. Adkins, B. Clark, and D. P. Fernandez (2007), Millennial-scale trends in west pacific warm pool hydrology since the last glacial maximum, *Nature*, *449*(7161), 452–455.

Pausata, F. S. R., D. S. Battisti, K. H. Nisancioglu, and C. M. Bitz (2011), Chinese stalagmite $^{18}O$ controlled by changes in the Indian monsoon during a simulated Heinrich event, *Nature Geosci*, *4*(7), 474–480.

Porter, S. C. (2001), Chinese loess record of monsoon climate during the last glacial–interglacial cycle, *Earth-Science Reviews*, *54*(1–3), 115 – 128, doi:http://dx.doi.org/10.1016/S0012-8252(01)00043-5, recent research on loess and palaeosols, pure and applied.

Richards, D., and J. Dorale (2003), Uranium-series chronology and environmental applications of speleothems, in *Uranium-series geochemistry*, *REVIEWS IN MINERALOGY & GEOCHEMISTRY*, vol. 52, pp. 407–460, MINERALOGICAL SOC AMERICA, 1015 EIGHTEENTH ST, NW, SUITE 601, WASHINGTON, DC 20036-5274 USA.

Robinson, L. F., G. M. Henderson, and N. C. Slowey (2002), U–th dating of marine isotope stage 7 in bahamas slope sediments, *Earth and Planetary Science Letters*, *196*(3–4), 175 – 187, doi:http://dx.doi.org/10.1016/S0012-821X(01)00610-0.

Rosholt, J., and A. PS (1962), Evelutation of the $Pa^{231}/U - Th^{230}/U$ method for dating pleistocene carbonate rocks, *US Geol Surv Pro Paper*, *450-E*, 108–111.

Rozanski, K., L. Araguás-Araguás, and R. Gonfiantini (1993), *Isotopic Patterns in Modern Global Precipitation*, pp. 1–36, American Geophysical Union, doi:10.1029/GM078p0001.

Ruddiman, W. F. (2006), What is the timing of orbital-scale monsoon changes?, *Quaternary Science Reviews*, *25*(7–8), 657 – 658, doi:http://dx.doi.org/10.1016/j.quascirev.2006.02.004.

Rudzka, D., F. McDermott, D. Baldini, L.M. adn Fleitmann, and A. Moreno (2011), The coupled $^{13}C$ -radiocarbon systematics of three late glacial/early holocene speleothems; insights into soil and cave processes at climatic transitions, *Geochimica et Cosmochimica Acta*, *75*, 4321–4339 4321–4339 4321–4339.

Sano, M., C. Xu, and T. Nakatsuka (2012), A 300-year Vietnam hydroclimate and ENSO variability record reconstructed from tree ring $^{18}O$, *Journal of Geophysical Research: Atmospheres*, *117*(D12), doi:10.1029/2012JD017749, d12115.

Sasowsky, I., J. Mylroie, C. Spötl, A. Mangini, S. Bums, N. Frank, and R. Pavuza (2004), *Speleothems from the High-Alpine Spannagel Cave, Zillertal Alps (Austria)*, pp. 243–256, Springer US, doi:10.1007/978-1-4419-9118-8{_}13.

Scholz, D., and D. Hoffmann (2008), 230th/u-dating of fossil corals and speleothems, *Quaternary Science Journal*, *57*(1-2), 52–76.

Scholz, D., and D. L. Hoffmann (2011), Stalage – an algorithm designed for construction of speleothem age models, *Quaternary Geochronology*, *6*(3–4), 369 – 382, doi:http://dx.doi.org/10.1016/j.quageo.2011.02.002.

Scholz, D., D. L. Hoffmann, J. Hellstrom, and C. B. Ramsey (2012), A comparison of different methods for speleothem age modelling, *Quaternary Geochronology*, *14*, 94 – 104, doi:http://dx.doi.org/10.1016/j.quageo.2012.03.015.

Scholz, D., C. Mühlinghaus, and A. Mangini (2009), Modelling $^{13}$C and $^{18}$O in the solution layer on stalagmite surfaces, *Geochimica et Cosmochimica Acta*, *73*(9), 2592–2602, doi:{http://dx.doi.org/10.1016/j.gca.2009.02.015}.

Shakun, J. D., S. J. Burns, D. Fleitmann, J. Kramers, A. Matter, and A. Al-Subary (2007), A high-resolution, absolute-dated deglacial speleothem record of indian ocean climate from socotra island, yemen, *Earth and Planetary Science Letters*, *259*(3–4), 442 – 456, doi:http://dx.doi.org/10.1016/j.epsl.2007.05.004.

Shen, C.-C., H.-T. Lin, M.-F. Chu, E.-F. Yu, X. Wang, and J. A. Dorale (2006), Measurements of natural uranium concentration and isotopic composition with permil-level precision by inductively coupled plasma-quadrupole mass spectrometry, *Geochemistry geophysics geosystems*, *7*, doi:{10.1029/2006GC001303}.

Sinha, A., K. G. Cannariato, L. D. Stott, H.-C. Li, C.-F. You, H. Cheng, R. L. Edwards, and I. B. Singh (2005), Variability of Southwest Indian summer monsoon precipitation during the Bølling-Ållerød, *Geology*, *33*(10), 813–816, doi:10.1130/G21498.1.

Sinha, A., K. G. Cannariato, L. D. Stott, H. Cheng, R. L. Edwards, M. G. Yadava, R. Ramesh, and I. B. Singh (2007), A 900-year (600 to 1500 a.d.) record of the indian summer monsoon precipitation from the core monsoon zone of india, *Geophysical Research Letters*, *34*(16), doi:10.1029/2007GL030431, l16707.

Solomon, S., D. Qin, M. Manning, Z. Chen, M. Marquis, K. Averyt, M. Tignor, and H. Miller (2007), *The physical sicence basis. In: Contribution of working group I to the fourth assessment reprot of the intergovernmental panel on climate change*, Cambridge University Press, Cambridge, United Kingdom.

Southon, J., A. L. Noronha, H. Cheng, R. L. Edwards, and Y. Wang (2012), A high-resolution record of atmospheric 14c based on hulu cave speleothem {H82}, *Quaternary Science Reviews*, *33*, 32 – 41, doi:http://dx.doi.org/10.1016/j.quascirev.2011.11.022.

Stott, L., A. Timmermann, and R. Thunell (2007), Southern hemisphere and deep-sea warming led deglacial atmospheric CO(2) rise and tropical warming, *Science*, *318*(5849), 435–438, doi:{10.1126/science.1143791}.

Tan, L., Y. Cai, Z. An, R. L. Edwards, H. Cheng, C.-C. Shen, and H. Zhang (2010), Centennial- to decadal-scale monsoon precipitation variability in the semi-humid region, northern China during the last 1860 years: Records from stalagmites in Huangye Cave, *The Holocene*, doi:10.1177/0959683610378880.

Tan, M. (2014), Circulation effect: response of precipitation $^{18}O$ to the ENSO cycle in monsoon regions of China, *Climate Dynamics*, *42*(3-4), 1067–1077, doi:10.1007/s00382-013-1732-x.

Thornthwaite, C. W. (1948), An approach toward a rational classification of climate, *Geographical Review*, *38*(1), 55–94.

van der Kaars, S. (2001), Pollen distribution in marine sediments from the south-eastern Indonesian waters, *Palaeogeography palaeoclimatology palaeoecology*, *171*(3-4), 341–361, doi:{10.1016/S0031-0182(01)00253-X}.

Vuille, M., M. Werner, R. S. Bradley, and F. Keimig (2005), Stable isotopes in precipitation in the Asian monsoon region, *Journal of Geophysical Research: Atmospheres*, *110*(D23), doi:10.1029/2005JD006022, d23108.

Wackerbarth, A., D. Scholz, J. Fohlmeister, and A. Mangini (2010), Modelling the 18o value of cave drip water and speleothem calcite, *Earth and Planetary Science Letters*, *299*(3–4), 387 – 397, doi:http://dx.doi.org/10.1016/j.epsl.2010.09.019.

Wang, B., R. Wu, and K.-M. Lau (2001), Interannual variability of the Asian Summer Monsoon: Contrasts between the Indian and the Western North Pacific–East Asian Monsoons, *Journal of Climate*, *14*(20), 4073–4090, doi:10.1175/1520-0442(2001)014$\langle$4073:IVOTAS$\rangle$2.0.CO;2.

Wang, Y., H. Cheng, R. Edwards, Y. He, X. Kong, A. Zs, J. Wu, M. Kelly, C. Dykoski, and X. Li (2005), The Holocene Asian monsoon: links to solar changes and North Atlantic climate, *Science*, pp. 854–7.

Wang, Y., H. Cheng, L. R. Edwards, X. Kong, X. Shao, S. Chen, J. Wu, X. Jiang, X. Wang, and Z. An (2008), Millennial- and orbital-scale changes in the East Asian monsoon over the past 224,000[thinsp]years, *Nature*, *451*(7182), 1090–1093.

Wang, Y., H. Cheng, R. Edwards, Z. An, J. Wu, C. Shen, and J. Dorale (2001), A high-resolution absolute-dated Late Pleistocene monsoon record from Hulu Cave, China, *Science*, *294*(5550), 2345–2348.

Webster, P., and S. Yang (1992), Monsoon and ENSO: Selectively interactive systems, *Quarterly Journal of the Royal Meteorological Society*.

Williams, P., D. King, J.-X. Zhao, and K. Collerson (2005), Late pleistocene to holocene composite speleothem 18o and 13c chronologies from south island, new zealand—did a global younger dryas really exist?, *Earth and Planetary Science Letters*, *230*(3–4), 301 – 317, doi:http://dx.doi.org/10.1016/j.epsl.2004.10.024.

Worden, J., D. Noone, and K. Bowman (2007), Importance of rain evaporation and continental convection in the tropical water cycle, *Nature*, *445*(7127), 528–532.

Xia, Q., J. xin Zhao, and K. Collerson (2001), Early–mid holocene climatic variations in tasmania, australia: multi-proxy records in a stalagmite from lynds cave, *Earth and Planetary Science Letters*, *194*(1–2), 177 – 187, doi:http://dx.doi.org/10.1016/S0012-821X(01)00541-6.

Xu, C., M. Sano, and T. Nakatsuka (2011), Tree ring cellulose $^{18}O$ of Fokienia hodginsii in northern Laos: A promising proxy to reconstruct ENSO?, *Journal of Geophysical Research: Atmospheres*, *116*(D24), doi:10.1029/2011JD016694, d24109.

Yadava, M., R. Ramesh, and G. Pant (2004), Past monsoon rainfall variations in peninsular India recorded in a 331-year-old speleothem, *Holocene*, *14*(4), 517–524, doi:{10.1191/0959683604hl728rp}.

Yancheva, G., N. R. Nowaczyk, J. Mingram, P. Dulski, G. Schettler, J. F. W. Negendank, J. Liu, D. M. Sigman, L. C. Peterson, and G. H. Haug (2007), Influence of the intertropical convergence zone on the East Asian monsoon, *Nature*, *445*(7123), 74–77, doi:{10.1038/nature05431}.

Yang, H., K. R. Johnson, M. L. Griffiths, A. N. LeGrande, V. Ersek, and G. M. Henderson (2016), Hydrologic variability during the Younger Dryas and Holocene based on speleothems from Laos, in preparation.

Yang, X., J. Liu, F. Liang, D. Yuan, Y. Yang, Y. Lu, and F. Chen (2014), Holocene stalagmite $^{18}O$ records in the East Asian monsoon region and their correlation with those in the Indian monsoon region, *The Holocene*.

Yeh, S.-W., J.-S. Kug, B. Dewitte, M.-H. Kwon, B. P. Kirtman, and F.-F. Jin (2009), El Niño in a changing climate, *Nature*, *461*(7263), 511–514.

Yoshimura, K. (2015), Stable water isotopes in climatology,meteorology,and hydrology:a review, *Journal of the Meteorological Society of Japan. Ser. II*, *93*(5), 513–533.

Yoshimura, K., T. Oki, N. Ohte, and S. Kanae (2003), A quantitative analysis of short-term $^{18}O$ variability with a Rayleigh-type isotope circulation model, *Journal of Geophysical Research: Atmospheres*, *108*(D20), doi:10.1029/2003JD003477, 4647.

Yoshimura, K., M. Kanamitsu, D. Noone, and T. Oki (2008), Historical isotope simulation using Reanalysis atmospheric data, *Journal of Geophysical Research: Atmospheres*, *113*(D19), doi:10.1029/2008JD010074, d19108.

Yu, J.-Y., and H.-Y. Kao (2007), Decadal changes of ENSO persistence barrier in SST and ocean heat content indices: 1958–2001, *Journal of Geophysical Research: Atmospheres*, *112*(D13), doi:10.1029/2006JD007654, d13106.

Yu, J.-Y., Y. Zou, S. T. Kim, and T. Lee (2012), The changing impact of El Niño on US winter temperatures, *Geophysical Research Letters*, *39*(15), doi:10.1029/2012GL052483, l15702.

Yuan, D., H. Cheng, R. L. Edwards, C. A. Dykoski, M. J. Kelly, M. Zhang, J. Qing, Y. Lin, Y. Wang, J. Wu, J. A. Dorale, Z. An, and Y. Cai (2004), Timing, duration, and transitions of the last interglacial Asian monsoon, *Science*, *304*(5670), 575–578.

Zhang, P., H. Cheng, R. L. Edwards, F. Chen, Y. Wang, X. Yang, J. Liu, M. Tan, X. Wang, J. Liu, C. An, Z. Dai, J. Zhou, D. Zhang, J. Jia, L. Jin, and K. R. Johnson (2008), A test of climate, sun, and culture relationships from an 1810-year chinese cave record, *Science*, *322*(5903), 940–942, doi:10.1126/science.1163965.

Zhao, K., Y. Wang, L. R. Edwards, H. Cheng, D. Liu, and X. Kong (2015), A high-resolved record of the Asian Summer Monsoon from Dongge Cave, China for the past 1200 years, *Quaternary Science Reviews*, *122*, 250–257, doi:http://dx.doi.org/10.1016/j.quascirev.2015.05.030.

Zhou, T., B. Wu, A. A. Scaife, S. Brönnimann, A. Cherchi, D. Fereday, A. M. Fischer, C. K. Folland, K. E. Jin, J. Kinter, J. R. Knight, F. Kucharski, S. Kusunoki, N. C. Lau, L. Li, M. J. Nath, T. Nakaegawa, A. Navarra, P. Pegion, E. Rozanov, S. Schubert, P. Sporyshev, A. Voldoire, X. Wen, J. H. Yoon, and N. Zeng (2009), The clivar c20c project: which components of the asian–australian monsoon circulation variations are forced and reproducible?, *33*(7-8), 1051–1068, doi:10.1007/s00382-008-0501-8.

Zhu, M., L. Stott, B. Buckley, and K. Yoshimura (2012), 20th century seasonal moisture balance in Southeast Asian montane forests from tree cellulose $^{18}O$, *Climatic Change*, *115*(3-4), 505–517, doi:10.1007/s10584-012-0439-z.